UNIVERSITÀ DEGLI STUDI DI PADOVA

SEDE AMMINISTRATIVA: UNIVERSITÀ DEGLI STUDI DI PADOVA

DIPARTIMENTO DI GEOSCIENZE

SCUOLA DI DOTTORATO DI RICERCA IN: SCIENZE DELLA TERRA
CICLO: XXVI

GLOBAL CLIMATE CHANGE AND BIOTA: EVIDENCE FROM FORAMINIFERA DURING THE MIDDLE EOCENE CLIMATIC OPTIMUM

Direttore della Scuola: Ch.mo Prof. Massimiliano Zattin

Supervisore: Dr. Luca Giusberti

Co-supervisori: Dr. Ellen Thomas, Ch.mo Prof. Mark Pagani, Ch.mo Prof. Valeria Luciani

Dottorando: Flavia Boscolo Galazzo

Summary

The Paleogene represents one of the more climatically dynamic periods in the Earth History. The early Eocene peak of global warming was followed by a long-term cooling trend over the middle–late Eocene (49 to 34 Ma) eventually leading to the establishment of a continental Antarctic ice-sheet by the early Oligocene (Miller et al., 1987; Zachos et al., 2001). This crucial climatic transition was significantly interrupted by a prominent and transient (~500 kyr) global warming event: the Middle Eocene Climatic Optimum (MECO), which occurred at the top of Chron C18r at ca. 40 Ma (Bohaty et al., 2009). The MECO is worldwide recorded by pronounced changes in $\delta^{13}C$ and $\delta^{18}O$ values in marine carbonates and coeval oscillations in the carbonate compensation depth. The pace and pattern of warming strongly differentiate the MECO from early-middle Eocene hyperthermals.

Although it represents one of the larger climatic disruptions of the Paleogene, the MECO and its paleoenvironmental and biotic repercussions are still poorly known and constrained.

The final aim of my Ph.D. project was to gain a deeper understanding of the paleoenvironmental and paleoceanographic perturbations associated with the MECO, including the degree of affection of deep-sea biota through the study of benthic foraminiferal fauna.

To pursue these aims, the project has been focused on two mid-latitude locations with comparable paleodepths but significantly different background paleoceanographic conditions: a hemipelagic section deposited in the central-western Tethys (Alano section, northeastern Italy) and ODP Site 1263 in the South-Eastern Atlantic (Walvis Ridge). The first goal of the Ph.D. project was to reconstruct benthic foraminiferal changes across the MECO of the Alano section, detected by previous bio-magnetostratigraphic and geochemical studies (Spofforth et al., 2010). In the context of a multi-disciplinary investigation on the MECO of the Alano section, I carried out a taxonomic and quantitative analysis to investigate benthic foraminiferal assemblage changes and infer changes in export productivity and sea-floor conditions.

The second goal of the Ph.D. project was the study of MECO at Site 1263 based on an integrated approach using geochemical tools widely employed in paleoceanographic and paleoclimatic reconstructions in conjunction with benthic foraminiferal assemblage study. Specifically, I generated TEX_{86} and surface to bottom oxygen and carbon isotopic records running mono-generic samples of mixed-layer dwellers planktic foraminfera, bulk carbonate and monospecific samples of benthic foraminifera. As for the Alano section, benthic foraminiferal assemblage has been studied through a taxonomic investigation and a quantitative analysis.

On the whole, the investigations carried out suggest that the repercussions of MECO warming on the environment and biota greatly varied geographically. In the central-western Tethys, a

progressive eutrophication during the MECO induced a restructuring of benthic foraminiferal fauna, with opportunistic-stress tolerant taxa becoming dominant in the MECO aftermath in coincidence with the deposition of an organic rich interval.

The multi-proxy reconstruction carried out at Site 1263, indicate that large paleoceanographic changes (e.g., circulation, productivity, stratification changes) did not occur during the MECO at this pelagic site. Benthic foraminiferal assemblages do not show major faunal changes, but the MECO warming was paralleled by a marked decline in foraminiferal accumulation rates. This indicate a decrease in the transfer of organic matter into the ocean interior, likely as an effect of warming which affected pelagic food webs and eventually the flux of organic matter to the sea-floor. The results presented in this thesis suggest that it is not possible generalize upon the effects of past climatic perturbations; it is the combination of regional features with the global climate which generates environmental thresholds and impacts. A multi-site and multi-proxy approach is thus needed in studying past climate perturbations to gain a comprehensive reconstruction of their impacts and dynamics.

Riassunto

Il Paleogene rappresenta uno dei periodi climaticamente più dinamici della storia della Terra. Alla fase di più intenso riscaldamento globale raggiunta nell'Eocene inferiore (*Early Eocene Climatic Optimum*, EECO; Zachos et al., 2001) fece seguito, nell'Eocene medio-superiore (49-39 Ma), un prolungato trend di raffreddamento climatico che alla fine portò all'instaurarsi del regime "*icehouse*" con la comparsa di calotte glaciali permanenti in Antartide, alla base dell'Oligocene (Miller et al., 1987; Zachos et al., 2001). Questa fase cruciale di transizione climatica fu interrotta da un importante evento di riscaldamento globale durato circa cinquecentomila anni: il *Middle Eocene Climatic Optimum* (MECO) verificatosi circa 40 milioni di anni fa, al top del Chron C18r (Bohaty et al., 2009). Il MECO è riconoscibile a livello globale nel *record* sedimentario marino da pronunciati cambiamenti nei valori isotopici del $\delta^{13}C$ e $\delta^{18}O$ e da fluttuazioni della profondità di compensazione dei carbonati (CCD; Bohaty et al., 2009). Il MECO si differenzia dagli eventi ipertermali dell'Eocene inferiore-medio per la differente durata e modalità di riscaldamento.

Il mio progetto di dottorato è finalizzato ad indagare in dettaglio le perturbazioni paleoambientali e paleoceanografiche associate al MECO, valutando nello specifico le ripercussioni di questo evento sul biota marino profondo (foraminiferi bentonici).

Per perseguire quest'obiettivo il progetto si è focalizzato su due siti caratterizzati da paleobatimetrie confrontabili e situati entrambi alle medie latitudini: una sezione emipelagica depostasi nella Tetide centro-occidentale (sezione di Alano; Italia nordorientale) e il Site ODP 1263, nell'Atlantico sudorientale (Walvis Ridge).

La prima parte del dottorato è stata incentrata sulla ricostruzione delle modificazioni della fauna a foraminiferi bentonici nel MECO della sezione di Alano, precedentemente identificato da studi bio-magnetostratigrafici e geochimici (Spofforth et al., 2010). Nel più ampio contesto di un'indagine multidisciplinare riguardante il MECO di Alano, ho eseguito uno studio tassonomico e quantitativo delle associazioni a foraminiferi bentonici, allo scopo di analizzarne i cambiamenti e valutare le variazioni nel flusso di materia organica e delle condizioni al fondo.

La seconda parte del dottorato è stata interamente dedicata allo studio del MECO del Site 1263. Per lo studio del Site 1263 ho utilizzato un approccio integrato, affiancando allo studio delle associazioni a foraminiferi bentonici l'uso di metodologie geochimiche ampiamente utilizzate in paleoceanografia e paleoclimatologia: TEX_{86}, misure di $\delta^{13}C$ e $\delta^{18}O$ (queste ultime eseguite su gusci di foraminiferi planctonici e bentonici oltre che sul *bulk sample*).

Nel complesso, lo studio svolto ha evidenziato come le ripercussioni del MECO sull'ambiente e il biota marino profondo siano state caratterizzate da un'ampia variabilità geografica. Nella Tetide

centro-occidentale una progressiva eutrofizzazione associata al MECO provocò una ristrutturazione transitoria della fauna a foraminiferi bentonici, dominata da taxa opportunisti nell'intervallo immediatamente successivo all'evento e in coincidenza con la deposizione di livelli ricchi in materia organica.

L'approccio *multi-proxy* utilizzato nello studio del Site 1263 ha invece evidenziato l'assenza di grandi modificazioni paleoambientali o paleoceanografiche (es. cambiamenti della circolazione oceanica o nella produttività primaria) associate al MECO. Nei sedimenti del Site 1263 non si osservano infatti significative modificazioni della fauna a foraminiferi bentonici. I tassi di accumulo dei foraminiferi bentonici (BFAR) e planctonici (CFAR) subiscono invece un marcato calo, indicativo di una diminuzione del flusso di materia organica dalla superficie al fondo, probabilmente indotta dall'aumento di temperatura e dalla conseguente alterazione della catena trofica pelagica.

I risultati presentati in questa tesi suggeriscono che non è possibile generalizzare sugli effetti ambientali e biotici causati da perturbazioni climatiche del passato che, per quanto globali, si manifestano nel momento in cui alterano specifici equilibri locali e innescano il superamento di soglie ambientali. Nello studio di perturbazioni climatiche del passato è quindi fondamentale avere a disposizione *record* provenienti da aree geografiche diverse utilizzando un approccio integrato, così da ottenere una ricostruzione la più possibile completa delle dinamiche e degli effetti prodotti da tali eventi.

TABLE OF CONTENTS

Chapter III

Chapter IV

Chapter V

A middle Eocene micropaleontological trick: the case of Tethyan <u>Planorotalites</u> pag. 121

CHAPTER I
Introduction

1.1. Research context and aims

Since the last two centuries Earth is experiencing a fast rate increase in emission of greenhouse gases due to anthropogenic burning of fossil-fuels and consequent input of carbon into the atmosphere manly in the form of carbon dioxide (CO_2) with levels almost reaching 400 parts per million (ppm) (398.35 ppm as of May 2nd 2013, Mauna Loa Observatory). The direct, widely acknowledged effect is a global increase in Earth's average surface temperature (e.g., Solomon et al., 2007; Pagani et al., 2010). Global temperatures of the past decade have not yet exceeded peak interglacial values but are warmer than during ~75% of the Holocene. The United States Intergovernmental Panel on Climate Change model projections for 2100 exceeds the full distribution of Holocene temperature under all plausible greenhouse gas emission scenarios (Marcott et al., 2013). Nowadays, global change researchers' efforts are focused in the achievement of a better understanding and forecast how global climate and ecosystems will respond to this rate of changes.

However, due to the potential effect of positive feedback mechanisms enhancing Earth-system climate sensitivity, these responses can be nonlinear and predict their timing and magnitude can be challenging (Zachos et al., 2008).

Earth's deep past offers the intriguing occasion to study time intervals in which pCO_2 was much higher than now and/or rapidly changing (e.g., Pagani et al., 2005; Pagani et al., 2010). In the last decade, the study of sedimentary sections encompassing the early Eocene and the so-called "hyperthermal" events, greatly improved our knowledge about the climate and climate dynamics of the greenhouse world of the late Paleocene-early Eocene.

The study of proxy records (e.g., fossil, geochemical, sedimentological) across the hyperthermals have highlighted impacts of different nature and magnitude on the environments and biota, showing their critical importance to investigate past abrupt climatic changes (e.g., Paytan et al., 2007; McInerney and Wing, 2011; Stassen et al., 2012; Winguth, et al., 2012; Foster et al., 2013).

This thesis follows this research line and focuses on the study of a large climatic perturbation called the Middle Eocene Climatic Optimum (MECO; Bohaty and Zachos, 2003), a global and transient warming event occurred about 40 Ma ago.

Goal of this study was to investigate the environmental and biotic changes associated with the MECO, with the broader final aim to contribute to our understanding of ecosystems alterations related to transient warming events.

I dealt with two case-studies using both a micropaleontological and multi-proxy approach.

A multi-proxy approach is indeed increasingly emerging within this research field as the ocean and global climate are closely coupled systems, and the study of past climate perturbations improves with an approach which integrates faunal data with paleoclimatic and paleoceanographic data.

In the first case-study, I focused on deep-sea benthic foraminifera, as key organisms in the study of past climatic perturbations.

Benthic foraminifera are among the more abundant eukaryotic organisms at depths greater than 1000 m and the most abundant benthic organisms preserved in the deep-sea fossil record (Gooday et al., 1992; 1998; Gooday, 2003). Benthic foraminifera ecology give us insights not only on ocean sea-floor conditions but indirectly also on surface waters, being affected by the amount, type and periodicity of the organic matter coming from the surface (e.g., Gooday et al., 2003).

Through the study of benthic foraminifera is possible to simultaneously evaluate changes in sea-floor oxygenation, export productivity, and the degree of stress of the community itself (e.g., Jorissen et al., 2007). Such features make them important tools to reconstruct perturbations affecting the sea-floor and deep-sea biota.

An integrated approach has been used for my second case-study: the analysis of benthic foraminiferal fauna has been coupled with a multi-proxy geochemical study, in order to place the faunal data within a paleoceanographic context and provide a more refined reconstruction of the repercussions associated with the MECO.

2. Materials

This research project has been focused on two mid-latitude locations with comparable paleodepths but significantly different background paleoceanographic conditions: a hemipelagic section deposited in the central-western Tethys (Alano section, northeastern Italy) and ODP Site 1263 in the South-Eastern Atlantic. Both these sedimentary successions have continuous records of the MECO and the intervals below and above it (Bohaty et al., 2009; Spofforth et al., 2010), being suitable to detail changes related to the event as well as the recovery to pre-event conditions.
The Alano section was deposited in a marginal-marine basin, not too far from land (Spofforth et al., 2010; Agnini et al., 2011), whereas Site 1263 lies in an open ocean setting, beneath the eastern part of the South Atlantic subtropical gyre. The selected localities hence represent two (paleo) oceanographic end-members, an ideal combination for studying the MECO repercussions on the marine ecosystem with and without the influence of land proximity.

3. Thesis outline

In **Chapter 2** I present and discuss the results of the micropaleontological analysis carried out at of the Alano section. Within the solid biomagnetostratigraphic frame reported by Agnini et al. (2011), the MECO of the Alano section has been the focus of multi-disciplinary investigations which included geochemical, sedimentological and calcareous plankton proxies (Luciani et al., 2010; Spofforth et al., 2010; Toffanin et al., 2011). In this context, I performed a detailed quantitative study of benthic foraminiferal assemblages across the stratigraphic interval spanning the MECO at Alano, (documenting for the first time) biotic and environmental sea-floor changes during this climatic perturbation. The results of this research have been interpreted in the context of the multi-disciplinary data already available, providing a surface to bottom reconstruction of the paleoenvironmental and biotic repercussions of the MECO in a central-western Tethys setting.
In **Chapter 3** I present and discuss the results of the geochemical analysis performed at Site 1263, together with data on foraminiferal accumulation rates.
The MECO at Site 1263 was firstly documented by Bohaty et al. (2009); however, an integrated study of paleoceanographic changes related to the MECO in this area was missing. The present study represents one of the first multi-proxy investigations of the MECO in an open ocean setting. Specifically, I aimed to reconstruct the water column surface to bottom temperature change during the event, changes in water column stratification and surface and export productivities. To detail the expression of the MECO in the South-East Atlantic, a specific suite of geochemical proxies,

including both inorganic and organic proxies, was selected. In particular, I calculated TEX_{86} based on the relative abundance of extracted GDGTs molecules and generated surface to bottom oxygen and carbon isotopic records. The isotopic records were obtained running mono-generic samples of mixed-layer and subsurface dwellers planktic foraminifera, bulk carbonate and monospecific samples of benthic foraminifera.

Surface and export productivities changes were inferred from benthic foraminiferal accumulation rate (BFAR) and coarse fraction accumulation rate (CFAR) and compared with $\delta^{13}C$ surface to bottom records.

At Site 1263 I also performed a detailed investigation of benthic foraminiferal fauna changes associated with the MECO: I present and discuss the results in **Chapter 4.**

The faunal data are interpreted in the context of the paleoceanographic reconstruction outlined in Chapter 3. In **Chapter 5** I discuss the taxonomy and abundance pattern of a problematic small-sized, low-trochospiral foraminifera occurring in the interval encompassing the MECO at Alano and Monte Cagnero sections (northeastern and central Italy, respectively).

References

Agnini, C., Fornaciari, E., Giusberti, L., Grandesso, P., Lanci, L., Luciani, V.,Muttoni, G., Rio, D., Stefani, C., Pälike, H., Spofforth, D.J.A., 2011. Integrated bio-magnetostratigraphy of the Alano section (NE Italy): a proposal for defining the Middle–Late Eocene boundary. Geological Society of American Bulletin, 123 (5/6), 841–872.

Bohaty, S.M., Zachos, J.C., 2003. A significant Southern Ocean warming event in the late middle Eocene. Geology, 31, 1017–1020.

Bohaty, S.M., Zachos, J.C., Florindo, F., Delaney, M.L., 2009. Coupled greenhouse warming and deep-sea acidification in the Middle Eocene. Paleoceanography, 24, PA2207, http://dx.doi.org/10.1029/2008PA001676.

Foster L.C., Schmidt D.N., Thomas E., Arndt S., Ridgwell A., 2013. Surviving rapid climate change in the deep sea during the Paleogene hyperthermals. Proceedings of the National Academy of Sciences, doi/10.1073/pnas.1300579110.

Gooday, A.J., 2003. Benthic foraminifera (Protista) as tools in deepwater palaeoceanography: environmental influences on faunal characteristics. Advances in Biology, 46, 1–90.

Gooday, A.J., Levin, L.A., Linke, P., Heeger, T., 1992, The role of benthic foraminifera in deep-sea food webs and carbon cycling. In: Rowe, G.T., and Pariente, V., (Eds.). Deep-sea food chains and the global carbon cycle. Dordrecht, Kluwer Academic Publishers, 63–91.

Gooday, A.J., Bett, B.J., Shires, R., Lambshead, P.J.D., 1998, Deep-sea benthic foraminiferal diversity in the NE Atlantic and NW Arabian Sea: A synthesis. Deep-Sea Research Part II, Topical Studies in Oceanography, 45, 165–201.

Jovane, L., Florindo, F., Coccioni, R., Dinare's-Turell, J., Marsili, A., Monechi, S., Roberts, A.P., Sprovieri, M., 2007. The middle Eocene climatic optimum event in the Contessa Highway section, Umbrian Apennines, Italy. Geological Society of American Bulletin, 119, 413–427.

Luciani, V., Giusberti, L., Agnini, C., Fornaciari, E., Rio, D., Spofforth, D.J.A., Pälike, H., 2010. Ecological and evolutionary response of Tethyan planktonic foraminifera to the middle Eocene climatic optimum (MECO) from the Alano section (NE Italy). Palaeogeography, Palaeoclimatology, Palaeoecology, 292, 82–95.

Marcott, S.A., Shakun, J.D., Clark, P.U., Mix, A.C., 2013. A Reconstruction of Regional and Global Temperature for the Past 11,300 Years. Science, 339, 1198-1201.

McInerney, F.A., Wing S.L., 2011. The Paleocene-Eocene thermal maximum: a perturbation of carbon cycle, climate, and biosphere with implications for the future. Annual Review of Earth and Planetary Sciences, 39, 489–516.

Pagani, M., Zachos, J.C., Freeman, K.H., Tipple, B., Bohaty, S., 2005. Marked decline in atmospheric carbon dioxide concentrations during the Paleogene. Science, 309, 600–603.

Pagani, M., Liu, Z., LaRiviere, J., Ravelo, A.C., 2010. High Earth-system climate sensitivity determined from Pliocene carbon dioxide concentrations. Nature Geosciences, 3, 27-30.

Paytan, A., Averyt, K., Faul, K., Gray, E., Thomas, E., 2007. Barite accumulation, ocean productivity, and Sr/Ba in barite across the Paleocene-Eocene Thermal Maximum. Geology, 35, 1139–1142.

Solomon, S., Qin, D., Manning, M., Marquis, M., Averyt, K., Tignor, M.M.B., LeRoy Miller, H., Jr., Chenet, Z., IPCC Climate Change 2007: The Physical Science Basis (Cambridge Univ. Press, 2007).

Spofforth, D.J.A., Agnini, C., Pälike, H., Rio, D., Fornaciari, E., Giusberti, L., Luciani, V., Lanci, L., Muttoni, G., 2010. Organic carbon burial following the Middle Eocene Climatic Optimum (MECO) in the central-western Tethys. Paleoceanography, 25, PA3210.

Stassen, P., Thomas, E., Speijer, R.P., 2012. The progression of environmental changes during the onset of the Paleocene-Eocene thermal maximum (New Jersey Coastal Plain). Austrian Journal of Earth Sciences, 105/1, 154-160.

Toffanin, F., Agnini, C., Fornaciari, E., Rio, D., Giusberti, L., Luciani, V., Spofforth, D.J.A., Pälike, H., 2011. Changes in calcareous nannofossil assemblages during the Middle Eocene Climatic Optimum: clues from the central-western Tethys (Alano section, NE Italy). Marine Micropaleontology, 81, 22–31.

Winguth, A.M.E., Thomas, E., Winguth, C., 2012. Global decline in ocean ventilation, oxygenation, and productivity during the Paleocene-Eocene Thermal Maximum: Implications for the benthic extinction. Geology, 40, 263–266.

Zachos, J.C., Dickens, G.R., Zeebe, R.E., 2008. An early Cenozoic perspective on greenhouse warming and carbon-cycle dynamics. Nature, 451, 279-283.

CHAPTER II

Paleoenvironmental changes during the Middle Eocene Climatic Optimum (MECO) and its aftermath: The benthic foraminiferal record from the Alano section (NE Italy)

F. Boscolo Galazzo[a], L. Giusberti[a], V. Luciani[b], E. Thomas[c,d,e]

Published in Palaeogeography, Palaeoclimatology, Palaeoecology 378 (2013), 22–35

a Department of Geosciences, University of Padova, Via G. Gradenigo 6, Italy

b Department of Physics and Earth Sciences, University of Ferrara, Via G. Saragat 1, Italy

c Department of Geology and Geophysics, Yale University, New Haven, CT, USA

d Department of Earth and Environmental Sciences, Wesleyan University, Middletown, CT, USA

e School of Earth Sciences, University of Bristol, UK

Abstract

The Middle Eocene Climatic Optimum (MECO) was one of the most severe, short-term global climate perturbations of the Cenozoic that occurred at ca. 40 Ma and was characterized by a gradual 4–6 °C temperature increase of intermediate and deep-waters. We investigated the response to the MECO of the deep-sea ecosystem in the central-western Tethys, through a quantitative study of bathyal benthic foraminiferal assemblages in the expanded and continuous Alano section (northeastern Italy), for which data on stratigraphy, lithology, isotope and trace element geochemistry, and calcareous microplankton were available. During the gradual warming of MECO (lasting between 350 and 650 kyr) marine export productivity increased, causing a significant but transient restructuring of benthic foraminiferal faunas, which changed gradually from assemblages typical for oligo-mesotrophic sea floor conditions to assemblages indicative of more eutrophic conditions. Just after the peak MECO conditions, which lasted less than 100 kyr, a prolonged phase of environmental instability (~500 kyr) occurred, marked by even more highly increased export productivity leading to bottom-water oxygen depletion, as reflected in deposition of organic-rich sediments and multiple peaks of bi-triserial opportunistic benthic foraminiferal taxa, including buliminids, bolivinids and uvigerinids. The high productivity may have been caused by a strong influx of nutrient-bearing fresh water into the basin, due to the increased vigour of the hydrological cycle during the warm period, and this increased fresh-water influx might have been a factor in enhancing water column stratification, thus exacerbating the hypoxic conditions, which persisted about 400–500 kyr. After deposition of the organic-rich layers the environmental perturbation ended, and benthic foraminiferal assemblages recovered while conditions became very similar to what they were before the MECO. The environmental disturbance during and directly after the MECO thus strongly but transiently affected benthic foraminiferal assemblages in the central western Tethys.

1. Introduction

The Eocene was a crucial time in the Earth's Cenozoic climate evolution. The highest temperatures of the Cenozoic were reached in the early Eocene (Early Eocene Climatic Optimum or EECO, ~52–50 Ma), followed by long-term high-latitude and deep-water cooling, which continued through the middle and late Eocene (Zachos et al., 2001; Katz et al., 2008; Zachos et al., 2008; Bijl et al., 2010). During this cooling, the Earth has been said to be in the so-called “doubthouse” climate state, between the “greenhouse” conditions of the early Paleogene (high temperatures and pCO_2 levels, no polar ice sheets reaching sea level; e.g., Pagani et al., 2005) and the “icehouse”

regime, starting with the development of the Antarctic continental ice sheet in the earliest Oligocene (Miller et al., 1987; Zachos et al., 1996; Coxall et al., 2005; Miller et al., 2005; Lear et al., 2008). During the "doubthouse" conditions, small, ephemeral ice sheets may have been present on the Antarctic continent but did not reach sea level (Miller et al., 2005), while sea ice may have been present in the Arctic Ocean (Stickley et al., 2009). The long transition to globally cooler climates was interrupted by transient warming events (e.g., Tripati et al., 2005; Sexton et al., 2006; Edgar et al., 2007), the most prolonged and intense of which was the Middle Eocene Climatic Optimum (MECO; Bohaty and Zachos, 2003). The MECO interrupted the cooling trend of the middle-late Eocene at ~40.6–40.0 Ma (Bohaty et al., 2009). It was first identified in Southern Ocean sediment cores as a transient oxygen isotopic excursion (~−1.0‰) (Bohaty and Zachos, 2003), then recognized and more precisely dated in isotopic records from different areas (Jovane et al., 2007; Bohaty et al., 2009). The ~500–750 kyr MECO warming (as expressed in an oxygen isotope excursion, OIE) started gradually, followed by a short interval of maximum warming (<100 kyr; Bohaty et al., 2009; Edgar et al., 2010), then ended by rapid cooling to pre-event values, within 200 kyr (Bohaty et al., 2009). The $\delta^{18}O$ records indicate warming of ~4–6 °C of both surface and deep waters (Bohaty et al., 2009; Edgar et al., 2010). High-latitude sea-surface temperatures (SSTs) ranged as high as 28 °C during the peak of the event, as estimated from organic-biomarker proxies (Bijl et al., 2010). The 500–750 kyr long duration and the pattern of gradual warming followed by rapid cooling clearly differentiate the MECO from late Paleocene through early Eocene hyperthermals with durations of 40–170 kyr, and either symmetrical beginning and ending, or a rapid start with gradual recovery (Bohaty et al., 2009; Bowen and Zachos, 2010; Galeotti et al., 2010; Stap et al., 2010; Zachos et al., 2010). The MECO also differs from these earlier hyperthermals because the latter characteristically show global negative carbon isotope excursions (CIE) coeval with the OIE indicating warming, the CIEs reflecting the emission of isotopically negative carbon compounds in the ocean–atmosphere (e.g., review in Lunt et al., 2011; McInerney and Wing, 2011). These hyperthermals thus are considered equivalent to global warming caused by anthropogenic carbon emissions, and are associated with deep-sea ocean acidification and carbonate dissolution (e.g., Zachos et al., 2005; Hoenisch et al., 2012). In contrast, MECO carbon isotope records vary geographically and bathymetrically (e.g., Spofforth et al., 2010). Oceanic $\delta^{13}C$ records show considerable geographic variability, but have generally rising $\delta^{13}C$ values across MECO, with a brief, ~0.5‰ negative CIE during peak warming of MECO only, clearly postdating the early, gradual warming (Bohaty et al., 2009, fig. 4; Edgar et al., 2010). Despite the lack of CIE coeval with the warming, i.e., evidence for large-scale emission of isotopically negative carbon compounds into the atmosphere, there is evidence for 2–3 times increased atmospheric CO_2 levels during

MECO from organic biochemical proxies (Bijl et al., 2010). Evidence for ocean acidification is less clear, because no records of direct dissolution proxies have been published (e.g., clay layers, fractionation of foraminifera). The occurrence of low carbon accumulation rates during MECO at sites located at depths of more than about 3400 m in the South Atlantic and Indian Oceans, however, has been interpreted as reflecting acidification (Bohaty et al., 2009). In conclusion, the MECO warming thus has been considered due to increased atmospheric CO_2 levels as the result of emission of carbon compounds with not markedly negative isotopic composition, so that their emission would not be seen in a significant, negative CIE, e.g., CO_2 from decarbonation during metamorphism and/or volcanic activity (Bohaty et al., 2009). Despite the fact that extreme warming events of the Paleogene deeply affected the biota, as e.g., the Paleocene–Eocene Thermal Maximum (PETM; e.g., Sluijs et al., 2007; McInerney and Wing, 2011), surprisingly few studies have been devoted to the biotic response to the MECO in ocean drilling sections, an exception being the study on siliceous plankton in the southern Indian Ocean (Witkowski et al., 2012). At these locations there was a significant increase in biosiliceous sedimentation associated with the MECO, as well as rapid assemblage changes in autotrophic and heterotrophic siliceous microfossil groups. MECO has been recognized in Italian sections, representing deposition in the western Tethys Ocean, having been first recognized in the Contessa section (paleodepth 800–1000 m), for which litho- and biomagnetostratigraphic data were presented (Jovane et al., 2007). Bulk $\delta^{13}C$ values show a positive excursion of ~0.6 per mille during MECO, but $\delta^{18}O$ records are diagenetically strongly overprinted so there is no direct evidence for warming. More detailed records have become available on the expanded and continuous Alano di Piave section (north-eastern Italy), for which Spofforth et al. (2010) presented lithological, trace metal geochemistry and stable isotope records. A detailed magnetobiostratigraphy of the full Alano di Piave section was published by Agnini et al. (2011), showing the longer-term time frame, and placing the MECO in higher Chron C18r and Chron C18n2n, within nannofossil zones CP14a and NP16. The paleodepth during MECO was middle bathyal (600–1000 m; Agnini et al., 2011). A detailed record of MECO planktonic foraminiferal biotic events in this section was presented by Luciani et al. (2010), and of calcareous nannofossil events by Toffanin et al. (2011), making this section the only one for which detailed biotic records of carbonate microfossil assemblages across the MECO have been described. At Alano, features of the MECO as described from deep-sea sections (Bohaty et al., 2009) have been recognized, including the gradual onset of the MECO at ~40.5 Ma, with progressively lower oxygen isotopic values (upper part of magnetochron C18r), minimum $\delta^{18}O$ values representing peak warming at the base of C18n.2n (~40.13 Ma), and recovery of the $\delta^{18}O$ values to background values over less than 100 kyr (Spofforth et al., 2010). The Alano section shows a negative $\delta^{13}C$ excursion in bulk

carbonate associated with the MECO gradual warming as shown in bulk $\delta^{18}O$ values. Directly above the sediment interval reflecting MECO peak warming, however, the Alano section differs from the deep sea sections, because there are two intervals with a high organic carbon content and a trace element signature indicative of low oxygen conditions (Spofforth et al., 2010). This interval has a positive $\delta^{13}C$ excursion in bulk carbonate, now correlated with the excursion in the Contessa section (Jovane et al., 2007). This positive CIE has been interpreted as an indication of enhanced marine productivity, which may have led to sequestration of CO_2 from the ocean–atmosphere system in carbon-rich sediments, at least on a regional scale (Spofforth et al., 2010). Both planktonic foraminifera and calcareous nannofossils reflect major environmental disturbance during MECO (Luciani et al., 2010; Toffanin et al., 2011), but no detailed records are available on the benthic foraminifera, thus the sea floor environment. We therefore performed a quantitative study of the MECO benthic foraminiferal assemblages in order to characterize changes in the benthic ecosystem of a bathyal environment during a yet poorly understood climatic perturbation. Through the integration of benthic foraminiferal data with published planktonic biotic and geochemical data we aim to better constrain the environmental and ecological changes across the Middle Eocene Climatic Optimum from a central-western Tethys perspective.

2. Setting, lithology and biochronostratigraphy

A continuous and expanded middle to upper Eocene section of grey marls crops out along the Calcino torrent riverbed, close to the village of Alano di Piave (Venetian Prealps, northeastern Italy). The section consists of 120–130 m monotonous grey marls, with intercalated silty–sandy tuff layers and biocalcarenitic–calciruditic beds (Agnini et al., 2011), and spans the upper part of Chron C18r (~41.5 Ma) to the base of Chron C16r (~36.5 Ma). The marls were deposited at middle-bathyal paleodepth (Agnini et al., 2011) in the Belluno Basin, a paleogeographic unit which originated in the Jurassic as the result of regional rifting and subsequent collapse of Triassic shallow-water carbonate platforms (e.g., Winterer and Bosellini, 1981). Hemipelagic sedimentation persisted until the late Eocene in the south-western sector of the Belluno Basin (Cita, 1975; Trevisani, 1997), which was surrounded by the structural high of the Lessini Shelf to the west (Bosellini, 1989) and of the Friuli Platform to the east (Fig. 1),with the section about 100–150 kmaway fromthe nearest land during sediment deposition. Because of its excellent exposure, abundant calcareous plankton and stratigraphical completeness, the Alano section has been proposed as candidate for the Global Stratotype Section and Point (GSSP) of the Priabonian (Agnini et al., 2011). This study focuses on the interval from 10 to 32 m above the base of the

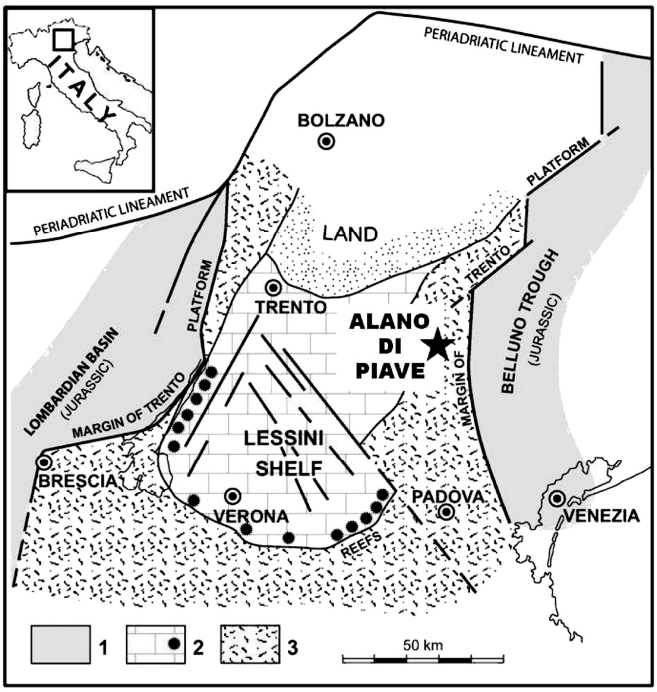

Fig. 1. Main paleogeographic elements of the Southern Alps during the Paleogene (modified from Bosellini, 1989) and location of Alano section (star). Legend: 1) deep-water mudstones of the Jurassic basins; 2) Paleogene lagoon and shelf edge reefs; 3) Palaeogene pelagic claystones and marlstones.

section, which falls in planktonic foraminiferal Zones E10–11, E12 and lower E13 (Berggren and Pearson, 2005) or P12 to lower P14 (Berggren et al., 1995), and calcareous nannofossil Zone NP16 (Martini, 1971) or CP 14a (Okada and Bukry, 1980), as described by Agnini et al. (2011). Between 17 and 25 m, the dominant marly facies is interrupted by a ~8 m thick sapropel-like interval, which consists of laminated, dark grey to-black, marlstones (Fig. 2). This interval is characterized by an increase of the total organic carbon content (TOC) as well as sulphur, and pyrite is common (Spofforth et al., 2010). Redox-sensitive trace element patterns indicate low-oxygen conditions. The sapropel-like level can be subdivided into two subunits (ORG1 and ORG2; Spofforth et al., 2010), separated by a 2 m-thick, lighter coloured and organic poor, marly interval (~19 to ~21 m, Fig. 2). In this section, the base of the gradual $\delta^{18}O$ negative excursion is at 13 m (~40.5 Ma), and the OIE reaches its peak (ca. −3.4‰) between 16.90 and 17 m, just below the base of the lower sapropel-like subunit (ORG1). The $\delta^{13}C$ and CaCO3 records mirror this pattern and, after a gradual decrease, reach minimum values of ~0.2‰ (from 1‰) and 20% (from 60%) respectively at ~16.90–17 m (Fig. 2). This brief interval, with minimum isotopic and carbonate values, has been interpreted as the peak of MECO. The interval overlying the MECO isotopic excursion (between ca. 17 and 25 m; Fig. 2) includes the ORG1 and ORG2 horizons, and is defined as “post-MECO interval” (Luciani et al., 2010). Agnini et al. (2011) estimate that the duration of the MECO and the post-MECO interval

together was about 800–900 kyr (see also Spofforth et al., 2010). In the post-MECO interval, $\delta^{18}O$ values rapidly increase, and by 25 m recover to pre-event values. Within the 17–25 m interval, the $\delta^{13}C$ record is complex and strongly correlated with lithological changes. Two positive excursions between 19 and 21 m are similar in magnitude (1.25‰), and coincide with the elevated TOC levels in intervals ORG1 and ORG2 (up to 3%; Fig. 2), interrupted by a negative excursion to near pre-event values.

3. Materials and methods

3.1. Benthic foraminifera

Benthic foraminifera were extracted from the marlstones using our standard method, disaggregation with 10–30% concentration hydrogen peroxide, for 1–2 h, followed by washing over ≥63 and ≥450 μm sieves. When necessary, samples were additionally soaked in a surface-tension-active solution. Finally, some samples were gently sonicated in order to break up clumps of residue. Quantitative analysis of benthic foraminiferal assemblages was performed on 39 samples from the 22 m interval described above. Sample spacing is 40 cm over the interval corresponding to the $\delta^{18}O$ isotopic shift, and on average 80 and 100 cm below and above this interval. Quantitative study was based on representative splits of residues (using a micro-splitter Jones, Geneq Inc.), counting at least 280 specimens larger than 63 μm and < 450 μm (Appendix 2). The use of the small-size fraction is time-consuming and presents difficulties in taxonomic determination, but we preferred to avoid the loss of small taxa, which are important for paleoecological investigations (e.g., Thomas 1985; Schroeder et al., 1987; Boltovskoy et al., 1991; Thomas et al., 1995; Giusberti et al., 2009). More than 250 taxa were identified at specific or higher taxonomic level, mainly following Hagn (1956), Braga et al. (1975), Grünig and Herb (1980), Grünig (1984, 1985), Parisi and Coccioni (1988), Barbieri (1990), and Ortiz and Thomas (2006). Additional analyses were carried out on the ≥450 μm size fraction: specimens were identified and counted (Appendix 2.1), and absolute and relative abundance was calculated. The most representative taxa were photographed using SEM (scanning electron microscope). Relative abundance of the common taxa (>5%) was calculated (Figs. 3, 4), together with faunal indices commonly used in paleoenvironmental reconstruction: the Fisher α diversity index and the dominance (using the PAST package; Hammer et al., 2001), the absolute abundance (N/g: number of benthic foraminifera per gram of sediment), the infaunal–epifaunal ratio (mainly following Corliss, 1985; Jones and Charnock, 1985; Corliss and Chen, 1988; Kaminski and Gradstein, 2005), the relative abundance of bi-triserial taxa and the

agglutinated-calcareous ratio. Bi-triserial taxa percentage was calculated as the sum of all the buliminids minus the relative abundance of *Bolivinoides crenulata*, since this species shows a very different trend in abundance than the other bi-triserial taxa (Figs. 2, 3). The comparison of changes in relative and absolute abundance allows evaluating of the importance of the "fixed sum" problem (Thomas et al., 1995). Relative abundance and faunal indices were calculated excluding fragments of astrorhizids, an informal group in which we lumped all fragments of tubular, branching forms such as *Rhabdammina* and *Rhizammina*. In the residues it is difficult to estimate the number of individuals of these taxa, because only small fragments of these fragile forms (which are usually rare) were found. In order to avoid the loss of their signal completely, the absolute abundance of astrorhizid fragments was calculated. Infaunal/epifaunal ratio and bi-triserial taxa percentages were calculated excluding "small trochospiral hyaline" and indeterminable trochospiral hyaline (ITH) specimens (see Appendix A). STH and ITH were excluded in calculating relative abundance. Deep-water benthic foraminiferal communities are dominantly influenced by two environmental parameters: the food supply (quantity, quality and periodicity of the flux of food particles to the sea floor) and the oxygenation of bottom and/or pore waters (e.g., Lutze and Coulbourn, 1984; Corliss and Chen, 1988; Herguera and Berger, 1991; Loubere, 1991; Sen Gupta and Machain-Castillo, 1993; Alve, 1995; Jorissen et al., 1995; Loubere, 1996; Bernhard et al., 1997; Bernhard and Sen Gupta, 1999; Loubere and Fariduddin, 1999a,b; Morigi et al., 2001; Gooday, 2003; Jorissen et al., 2007). Benthic foraminifera are able to adapt to a wide spectrum of trophic conditions (e.g., Murray, 2006, 2013), but many taxa have an optimum range with respect to organic input, under which they may become dominant faunal elements (e.g., Loubere, 1991; Gooday, 1996; Loubere, 1996; Loubere and Fariduddin, 1999a,b; Fontanier et al., 2002; Jorissen et al., 2007). The C_{org} flux to the sea-floor directly influences the oxygenation at the sediment–water interface through oxidative degradation of organic matter: an excess of organic matter leads to lower oxygen availability to benthic communities (e.g., Valiela, 1984; Jorissen et al., 1995; Murray, 2006). Benthic foraminifera, as unicellular organisms, are in general able to tolerate oxygen depletion better than metazoans, and the more resistant taxa take advantage of a food-enriched environment where there is less competition (e.g., Phleger and Soutar, 1973; Koutsoukos et al., 1990; Sen Gupta and Machain-Castillo, 1993; Alve, 1995; Jorissen et al., 1995; Van der Zwaan et al., 1999). In most environments there thus is a strong, negative correlation between food supply and oxygen levels (TROX model, Jorissen et al., 1995). Interspecific competition influences the structure of benthic foraminiferal assemblages in terms of abundance and species composition: the most diverse assemblages, combining epifaunal to fairly deep infaunal components, occur in environments which are neither extreme in food supply nor in oxygenation. At lower food levels there is not sufficient

food to sustain infaunal populations although pore water oxygenation is good and would allow them to thrive, and at very high food supply the oxygen levels in pore waters (and finally in bottom waters) become too low to allow foraminifera to survive. Knowledge of these relationships in the modern oceans helps to interpret fossil benthic foraminiferal assemblages, in order to gain information about past environmental changes. We are, however, limited in our understanding of past benthic foraminiferal assemblages by our limited knowledge of recent faunas. Even for many living species the relation between test morphology and microhabitat has not been observed directly, but is extrapolated from data on other taxa (e.g., Jorissen, 1999). This is necessarily so for extinct taxa. In addition, many foraminifera move vertically through the sediment (e.g., Gooday and Rathburn, 1999; Fontanier et al., 2002). In one of the few statistical studies evaluating the correlation between test morphology and microhabitat, it is argued that the assignment of modern foraminifera to microhabitats may be accurate only about 75% (Buzas et al., 1993). Comparisons between past and recent environments thus need careful evaluation.

4. Results

Benthic foraminiferal assemblages at the Alano section are strongly dominated by calcareous forms throughout the studied interval (~85–98% of the assemblage; Fig. 2). There is a marked increase in the relative abundance of the agglutinated taxa in 2 samples just below the base of ORG1, and within samples from ORG2. The preservation of benthic foraminifera varies from good, in the lower and upper part of the section, to moderate, especially within the two ORG beds in which tests are filled by pyrite. In these intervals foraminifera are very rare in some samples.

4.1. Paleobathymetry

According to Agnini et al. (2011), the lower-middle portion of the Alano section, including the studied interval, was deposited at middle bathyal depth (600–1000 m, using depth distributions as in van Morkhoven et al., 1986). This estimate was based on the evaluation of P/B values (>90) and on the occurrence of paleobathymetric index taxa, including the presence of *Nuttallides truempyi*, *Cibicidoides barnetti* (indicative of depths > ~500–600 m), combined with taxa as *Hanzawaia ammophila* and *Oridorsalis umbonatus* (e.g., Ortiz and Thomas, 2006). The occurrence of common bi- and triserial taxa agrees with a middle bathyal depth assignment (Agnini et al., 2011).

4.2. Faunal changes across the Middle Eocene Climatic Optimum

Benthic foraminiferal assemblages show marked changes across the studied section, especially directly after the MECO, within the two ORG intervals and the directly overlying interval. Based on quantitative analysis, six main benthic foraminiferal assemblages (A to F; Fig. 2) were identified as described below.

4.2.1. Assemblage A: pre-MECO interval (5 samples, 10.00–12.80 m)

Samples below the onset of the MECO are characterized by fluctuating, moderately high faunal diversity (Fisher α ~24) and absolute abundance around 350 specimens/g (Fig. 2). Infaunal taxa are more abundant (75%) than epifaunal, and consist of bi-triserial taxa (on average 33%, Table 1) and very small, weakly ornamented *Bolivinoides crenulata* (on average 15%; Figs. 2, 3). Epifaunal taxa are represented mainly by *Nuttallides* spp. and *Cibicidoides* spp. (Figs. 3, 4). Preservation is moderately good, $CaCO_3$% is high (~45%) and the planktonic foraminiferal F-index is low, (Fig. 2;

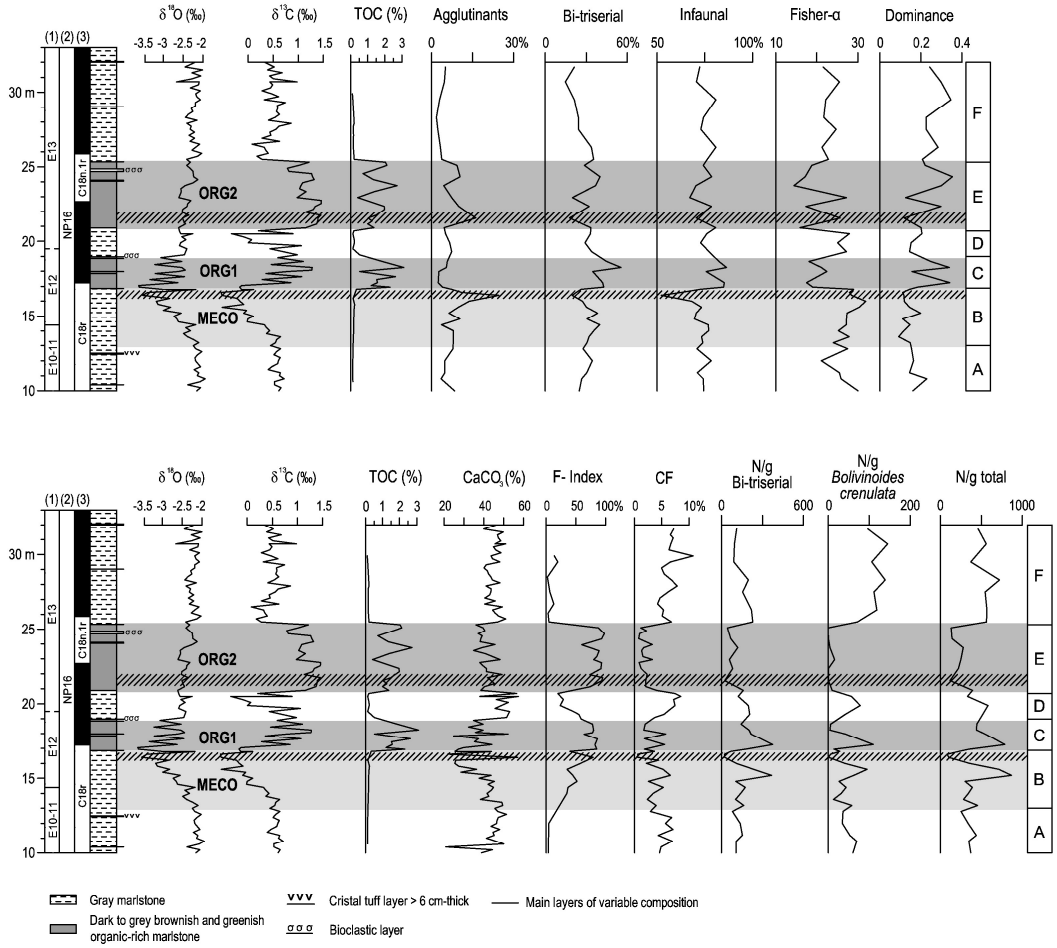

Fig. 2. Faunal and geochemical variations across the MECO at Alano plotted against bio-magnetostratigraphy, lithology and recognized benthic foraminiferal assemblages (A to F). Agglutinants = agglutinated to agglutinated and calcareous-hyaline ratio; Bi-triserial = cumulative relative abundance of the buliminids minus *Bolivinoides crenulata*; Infaunal = infaunal to infaunal and epifaunal ratio; Fisher-α and Dominance diversity indices; N/g Bi-triserial = number of bi-triserial benthic foraminifera per gram minus *Bolivinoides crenulata* in the ≥63 b 450 μm size fraction; N/g *Bolivinoides crenulata* = number of *Bolivinoides crenulata* per gram in the ≥63 b 450 μm size fraction and N/g total = number of benthic foraminifera per gram (faunal density) in the ≥63 b 450 μm size fraction. Stable isotopes ($\delta^{18}O$ and $\delta^{13}C$), total organic carbon (TOC%) and CaCO3% are from Spofforth et al. (2010). Fragmentation index and coarse fraction (F-index and CF) are from Luciani et al. (2010). Biostratigraphy after Agnini et al. (2011) following: (1) planktonic foraminiferal zones of Berggren and Pearson (2005) and (2) calcareous nannofossil zones of Martini (1971). Polarity/Chron (3) after Agnini et al. (2011). The hatched bands indicate intervals of marked carbonate dissolution.

Table 1). At ~11 m, *B. crenulata* begins an upward decrease (both relative and absolute abundance), paralleled by a gradual increase in relative abundance of the other bi-triserial taxa (Fig. 3).

4.2.2. Assemblage B: MECO interval (11 samples, 13.20–16.80 m)

With the onset of MECO, the relative abundance of bi-triserial taxa increases upwards, reaching 40% (Fig. 2, Table 1). The genera *Bulimina* and *Uvigerina* increase in abundance to 13%

and 8%, respectively. Among buliminids, *Bulimina* stalacta, *Bulimina* cf. *midwayensis*, the *Bulimina trinitatensis–impendens* group, *Bulimina* cf. *alazanensis*, and the *Bulimina* cf. *elongata* group become more common, as does the small, hispid, Uvigerina farinosa (Figs. 3, 4; Plate I). The foraminiferal assemblage becomes more diverse and structured, so that the Fisher-α index gradually increases to ~30 at the top of the interval (~15.60 m), with a richer agglutinated fauna (8%), mainly represented by large *Plectina dalmatina* and *Tritaxia szaboi* (Plate I). Among epifaunals, large, heavily calcified *Cibicidoides* spp., *Nuttallides truempyi* and the *Osangularia pteromphalia–mexicana* group are common (Figs. 3, 4; Plate II). *Plectina dalmatina*, *T. szaboi* and *Cibicidoides eocaenus* dominate the fraction ≥450 μm. The total N/g and bi-triserial absolute abundance fluctuate throughout (Fig. 2). Close to the maximum $\delta^{18}O$ negative values (peak MECO) at the top of the interval, N/g peaks to the highest values (~900 specimens/g; ca. 15.40 m). The MECO acme at Alano (16.40–16.90 m) coincides with a drop in $CaCO_3$ (~30%), coarse fraction and peak F index values (80; Fig. 2), thus increased dissolution. Preservation of tests deteriorates, N/g drops to minimum values, and bi-triserial relative abundance and infaunal/epifaunal ratio markedly decrease (to ~24% and 57% respectively; Fig. 2). Agglutinated taxa peak at 25%, together with *Cibicidoides* spp. (~15%; Figs. 2, 3).

4.2.3. Assemblage C: post-MECO-ORG1 interval (5 samples, 16.95–18.65 m)

Within ORG1 (TOC ~2–3%; $CaCO_3$ ~35%), preservation of both benthic and planktonic foraminifera deteriorates, the F-index of planktonic foraminifera is around 80, and tests show signs of dissolution (Fig. 2). Both benthic and planktonic foraminifera are frequently filled with pyrite. The benthic foraminiferal assemblage changes dramatically: infaunal morphotypes become dominant, with percentages close to 85%. Bi-triserial taxa reach their highest values (around 50%), whereas the relative and absolute abundance of *Bolivinoides crenulata* decreases at the top of the interval, after a series of fluctuations (Figs. 2, 3). Benthic foraminiferal absolute abundance is high (~500 specimens/g), while Fisher α decreases (~20; Fig. 2, Table 1). The ORG1 interval is characterized, from the bottom to the top, by a series of peaks of different buliminids (Fig. 3): *Uvigerina* spp. and *Uvigerina chirana* (together ~20%), *Bolivina antegressa* (15%), small *Bolivina* spp. (~30%), *B. crenulata* (~13%) and *Bulimina* cf. *semicostata* (~35%) (Plate I, Appendix A). The ORG1 interval is lithologically heterogeneous: it is interrupted at 17.98 m (sample COL113B) by a thin, greenish layer with a lower TOC% content (Fig. 2). In this layer, the benthic foraminiferal assemblage differs from that in underlying and overlying samples, because the percentage of bi-triserial taxa and the infaunal/epifaunal ratio drop to values similar to that of the pre-MECO interval

(40% and 70% respectively; Fig. 2), although the absolute abundance of these taxa is still high. *Bolivinoides crenulata* shows a slight increase, to up to 8% (Fig. 3).

4.2.4. Assemblage D: marly interval between ORGs (4 samples, 19.30–20.50 m).

The faunal composition of Assemblage D resembles that in the pre-MECO interval, and in sample COL113B (ORG1 at 17.98 m). General preservation of both benthic and planktonic foraminifera improves (F-index ~ 35, CaCO3 ~ 50%; Fig. 2, Table 1), the infaunal/epifaunal value drops to ~75%, and bi-triserial taxa, despite the high absolute abundance, are ~40% and mainly represented by small bolivinids (Fig. 3). *Bolivinoides crenulata* attains a percentage around 15%, total N/g is on average 450 specimens/g and Fisher α is ~22 (Figs. 2, 3).

4.2.5. Assemblage E: post-MECO ORG2 interval (7 samples, 20.90–25.10 m).

Within the ORG2 interval CaCO3 drops again (41%), the preservation of foraminifera is markedly worse than in interval ORG1, dissolution is more marked, and the F-index is slightly higher (Fig. 2, Table 1). ORG2 is similar toORG1 in its high percentages of bi-triserial taxa and infaunal morphotypes (Fig. 2, Table 1). As in ORG1, buliminids peak (Figs. 3, 4) such as *Bulimina alazanensis* (17%), as do some biserial species, such as *Bolivina antegressa* (double peak of 26 and 29%), *Bolivina nobilis–Bolivina gracilis* transitional forms (21%), and to a lesser extent *Uvigerina* spp. (7%) (Plate I; Appendix A). Typical for this interval are increases in small osangulariids (peak to 13%; Fig. 3 and Plate II), *Oridorsalis umbonatus* (Fig. 3; Plate II) and calcareous uniserial taxa. ORG2 mainly differs fromORG1 by its markedly lower absolute abundance of benthic foraminifera (from 500 to ca. 200 specimens/g on average; Fig. 2, Table 1). Bi-triserial and infaunal taxa are less abundant in ORG2 than in ORG1, fluctuating between 20–35 and 70–80% respectively, and faunal diversity fluctuates strongly in the lower-middle portion, whereas in the upper part it remains more or less stable, around 15 (Fig. 2). Higher Fisher α values are recorded in 2 samples at 21.55 and 22.95 m (samples COL470B and 610B). In the lower one the high faunal diversity (Fig. 2) is associated with increased agglutinated foraminiferal abundance (mainly plectinids, Fig. 4), the upper one corresponds to a grey-greenish, organic poor marly layer. Both these samples have a lower percentage of bi-triserial taxa and infaunal/epifaunal ratio (Fig. 2), and COL610B shows a slight increase in abundance of *Bolivinoides crenulata* (both relative and absolute abundance, Figs. 2, 3).

4.2.6. Assemblage F: recovery phase after the post-MECO interval (7 samples;25.50–31.70 m)

Assemblage F coincides with the full recovery to pre-event values in $\delta^{18}O$ and $\delta^{13}C$ records, as well as in $CaCO_3$ (45%) and TOC percentages. The preservation of foraminifera is good, and the F-index has very low values (Fig. 2, Table 1). Assemblage F is characterized by an increase in N/g (>500 specimens/g) reflecting the highest faunal density of the studied interval (Table 1), mainly specimens of *Bolivinoides crenulata* (100–150 specimens/g). The relative abundances of B. *crenulata* and other bi-triserial taxa are high (20–30% and 40%, respectively). *Bolivinoides crenulata* continues to increase in abundance up to the top of the assemblage, whereas the other buliminids decrease markedly. Bi-triserial taxa are mainly represented by very small, smooth-walled or weakly costate bolivinids and by very small and smooth-walled *Bulimina*, mainly the *Bulimina* cf. *elongata* group (average 13%; Fig. 3).

Assemblage	Fisher α	Dominance	N/g	Infaunal%	Bi-Triserial%	F-index	$CaCO_3$%
F	19	0.184	550	~75	~30	9	45
E	~ 20	0.063	190	73	34	86	41
D	22	0.075	455	77	38	35	49
C	20	0.084	515	83	51	79	36
B	27	0.048	375	70	35	48	41
A	24	0.067	350	74	33	4	44
ST.DEV.	2.77	0.04	119.56	4.03	6.77	31.35	4.03

Table. 1. Typical values of parameters for the recognized benthic foraminiferal assemblages.

5. Discussion

5.1. Pre-MECO and MECO (assemblages A, B): toward increased food availability at the sea floor

In the Alano section, pre-MECO background conditions (assemblage A) are characterized by a fairly abundant and diversified infauna, with abundant small bolivinids including *Bolivinoides crenulata* (Figs. 2, 3). The abundance of bi-triserial taxa indicates a high and continuous food supply to the sea-floor (e.g., Gooday and Rathburn, 1999; Loubere and Fariduddin, 1999b; Morigi et al., 2001; Gooday, 2003). The common occurrence of buliminids in assemblage A, however, probably cannot be ascribed to very high productivity in the surface waters. The scarce epifaunal community, and the low diversity and low abundance assemblage, coupled with absence of evidence for hypoxic conditions (Spofforth et al., 2010), suggest that there was a low to moderate flux of organic matter to the seafloor, as supported by calcareous plankton communities indicating generally oligotrophic surface waters (Luciani et al., 2010; Toffanin et al., 2011). The apparent mismatch between benthic foraminifera indicative of a higher organic supply than suggested by indicators of productivity in overlying waters can be explained by the presence of an additional, lateral supply of more refractory organic matter (e.g., as in the present bay of Biscay, Fontanier et al., 2005), especially in view of the paleogeographic setting of the Alano section, i.e., the vicinity of land and the shelf areas surrounding the Belluno basin. This setting may have allowed a supply of terrigenous material containing refractory organic matter (e.g., Ortiz and Thomas, 2006). Some infaunal taxa are able to use such refractory organic matter (e.g. Fontanier et al., 2002, 2005). Bolivinids specifically are characterized by tolerance to a wide spectrum of trophic and oxygen conditions (e.g. Kitazato and Ohga, 1995; Silva et al., 1996; Bernhard et al., 1997). We therefore argue that benthic foraminiferal data from the pre-MECO interval may indicate relatively oligotrophic surface waters, under which the sea floor habitat was influenced by continental-derived, refractory organic matter. With the beginning of the MECO, the relative abundance of bi- and triserial taxa started to increase (assemblage B), suggesting a gradual increase in supply of less refractory organic material from increased primary productivity in overlying surface waters. The relative abundance of bi-triserial taxa, indicative of a continuous food supply (e.g. Lutze and Coulbourn, 1984), increased together with faunal diversity. Within the samples just below the maximum negative OIE (i.e. peak MECO), peak values in benthic foraminiferal absolute abundance were reached (Fig. 2). Such an increase in benthic foraminiferal absolute abundance may indicate the supply of larger amounts or less refractory organic matter to the benthos (Herguera and Berger, 1991; Jorissen et al., 1995; Thomas et al., 1995; Gooday, 2003; Jorissen et al., 2007). Among bi-

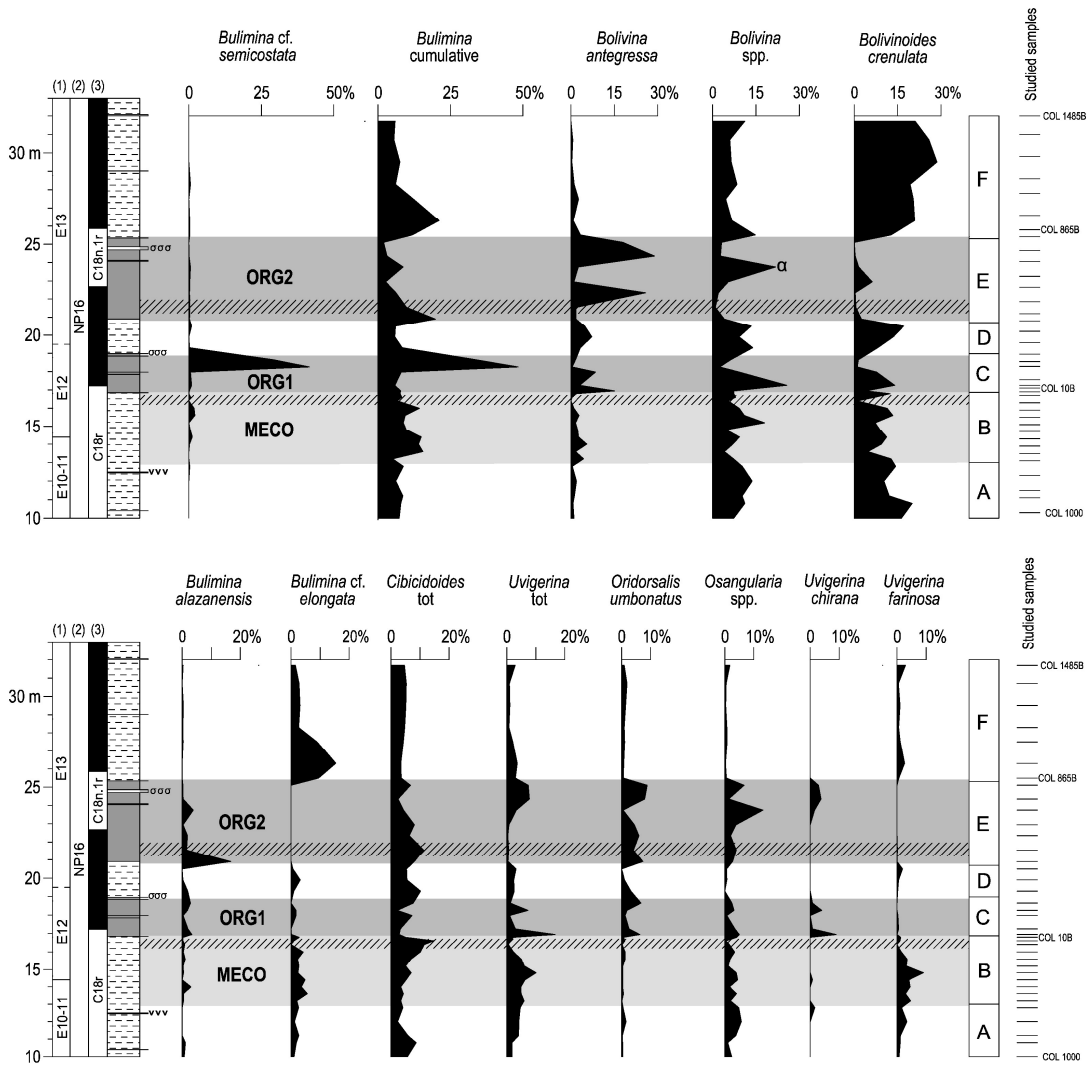

Fig. 3. Relative abundance of selected benthic foraminifera across the MECO in the Alano section plotted against bio-magnetostratigraphy, lithology and the recognized assemblages (A to F). The letter α indicates the ORG2 peak of *Bolivina nobilis–gracilis* transitional forms. Biostratigraphy after Agnini et al. (2011) following: (1) planktonic foraminiferal zones of Berggren and Pearson (2005) and (2) calcareous nannofossil zones of Martini (1971). Polarity/Chron (3) after Agnini et al. (2011). The hatched bands indicate intervals of marked carbonate dissolution.

triserial taxa, small and hispid uvigerinids such as *Uvigerina farinosa* increased in abundance (Fig. 3). These forms resemble living *Uvigerina* species typical for deep-sea high productivity areas (Loubere, 1991, 1996, 1997; Loubere and Fariduddin, 1999b). N/g can be influenced by the abundant presence of small individuals and decreased sedimentation rates (Thomas, 2003; Giusberti et al., 2009), but that is not the case here: in assemblage B, the abundance of the coarse fraction and the mean size of benthic foraminiferal tests increase, and sedimentation rates increase (Spofforth et al., 2010). The N/g values in assemblage B increase, coupled with a gradual increase in influx of detrital material (Spofforth et al., 2010), and a shift from oligotrophic to more eutrophic-dominated calcareous planktonic communities (Luciani et al., 2010; Toffanin et al., 2011). This increased influx of terrestrial detrital sediments may have resulted from increased weathering resulting from

the increasingly vigorous hydrological cycle during warm climates (Pierrehumbert, 2002). The increased delivery of highly weathered, inorganic terrestrial material may have provided more nutrients, resulting in higher surface productivity (Luciani et al., 2010; Spofforth et al., 2010; Toffanin et al., 2011). The latter led to intensified export productivity to the sea floor and thus a higher supply of labile, more nutritious fresh phytal material to the benthos. The high faunal diversity across the MECO (Fig. 2, Table 1) indicates that the higher flux of labile organic matter, though able to sustain a richer infaunal and epifaunal community, did not result in poorly oxygenated conditions (e.g, Jorissen et al., 1995; Levin et al., 2001; Gooday, 2003). Overall, the benthic foraminiferal data provide evidence for a transition from more oligotrophic conditions with lateral supply of terrestrial organic matter to a fully mesotrophic environment favouring exploitation of both infaunal and epifaunal ecological niches, thus establishment of a more complex and vertically structured benthic foraminiferal community (e.g., Jorissen et al., 1995; Van der Zwaan et al., 1999). An exception to the increase in biserial-triserial taxa was the decrease in abundance of the biserial species *Bolivinoides crenulata* during the onset of the MECO, although with, strong fluctuations (Figs. 2, 3). This species thus shows a trend in abundance opposite to that of the other bi-triserial taxa. Possibly, this taxon could outcompete other infaunal taxa at a higher abundance of refractory organic matter and lesser abundance of freshly produced phytal material. Alternatively, it could not compete well under higher temperatures, as it also decreased in abundance during a hyperthermal event at the early/middle Eocene boundary in middle bathyal section Agost, Spain (Ortiz et al., 2008). The MECO peak-warming at Alano coincided with a marked drop in the preservation of foraminiferal tests, which show pitting, thus signs of dissolution, a drop in N/g values, coarse fraction and in $CaCO_3$%, thus overall carbonate dissolution (Fig. 2). As a result of dissolution, bi-triserial taxa strongly declined in absolute abundance, and peak values in Fisher α diversity declined, while the relative abundance of the dissolution-resistant *Cibicidoides* spp. and agglutinated taxa increased (Figs. 2, 3). The presence of a dissolution interval during MECO at the relatively shallow setting of the Alano section (600–1000 m) probably does not reflect a global rise in the lysocline. Bohaty et al. (2009) did not observe severe dissolution even at depths greater than 3000 m, where the mass accumulation of $CaCO_3$ declined, and at shallower depths even the mass accumulation rates of $CaCO_3$ remained unchanged. Our data thus indicate that the lysocline shallowed considerably during MECO at a regional scale in the western Tethys, while much less shallowing occurred in the Atlantic and Pacific oceans. Further paleoceanographic studies on the Eocene Tethys are needed in order to test in which regions there is evidence for a rising lysocline.

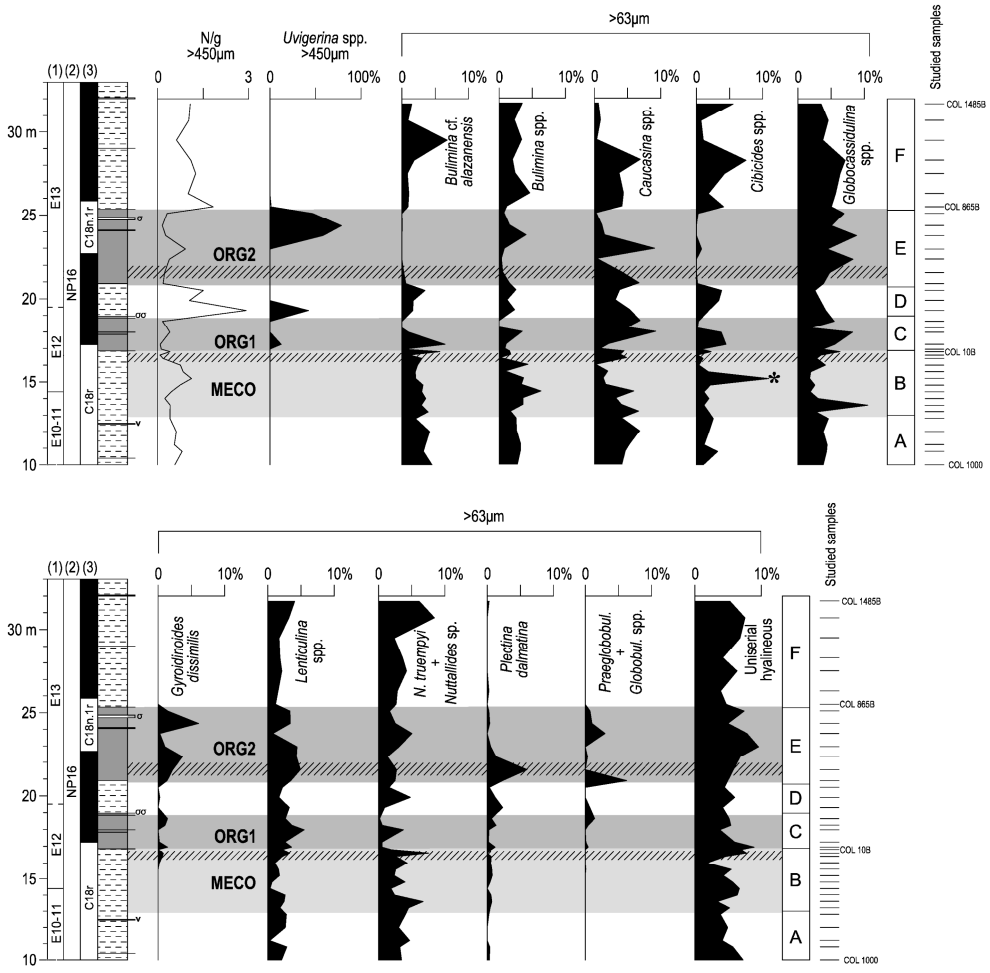

Fig. 4. N/g = number of benthic foraminifera per gram (faunal density), relative abundance of *Uvigerina* spp. heavy costate forms in the ≥450 µm size fraction and relative abundance of common benthic foraminiferal taxa in the ≥63 ≤ 450 µm size fraction plotted against bio-magnetostratigraphy, lithology, stable isotopes ($\delta^{18}O$ and $\delta^{13}C$), $CaCO_3$% and total organic carbon (TOC%; from Spofforth et al., 2010). The asterisk * indicates the sample COL480A (15.20 m), in which anomalous high abundance of *Cibicides* spp. is associated with the presence of numerous resedimented specimens of shallow-water taxa belonging to the genera *Amphistegina*, *Asterigerina* and *Asterigerinata*. Biostratigraphy after Agnini et al. (2011) following: (1) planktonic foraminiferal zones of Berggren and Pearson (2005) and (2) calcareous nannofossil zones of Martini (1971). Polarity/Chron (3) after Agnini et al. (2011). The hatched bands indicate intervals of marked carbonate dissolution.

5.2. Post-MECO ORG1 (assemblage C): eutrophication and hypoxia at the sea-floor

Striking paleoceanographic changes occurred at Alano immediately after the peak temperatures of MECO were reached. Within this interval, relatively high benthic foraminiferal absolute abundance, high percentage and N/g of mostly small bi-triserial taxa (Figs. 2, 3), suggest that the dissolution affecting the assemblage was minor and did not compromise the overall ecological signal (Table 1). Benthic foraminiferal assemblage C has high N/g values, a lower diversity (Fisher alpha) than its predecessor faunas, due to the strong dominance of infaunal morphotypes (*Bulimina*,

Bolivina and *Uvigerina*), with high percentages of bi-triserial taxa (Figs. 2, 3, 4), suggesting a eutrophic sea-floor environment with a high, continuous flux of organic matter (e.g., Lutze and Coulbourn, 1984; Jorissen et al., 1995; Morigi et al., 2001; Gooday, 2003). In the modern oceans, these genera dominate assemblages under high food and low oxygen conditions (e.g., Sen Gupta and Machain-Castillo, 1993; Alve and Bernhard, 1995; Bernhard and Sen Gupta, 1999), such as those during deposition of the Neogene and Quaternary Mediterranean sapropels (e.g., Katz and Thunell, 1984; Jorissen, 1999; Schmiedl et al., 2003; Morigi, 2009). Buliminids are tolerant to hypoxic conditions and able to take advantage from the large amounts of organic matter and low interspecific competition that generally characterize oxygen-poor environments (e.g., Sen Gupta and Machain-Castillo, 1993; Alve, 1995; Bernhard et al., 1997; Van der Zwaan et al., 1999; Gooday, 2003). Assemblage C thus may indicate oxygen depletion at the sea floor, or at least within pore waters close to the seafloor to which infaunal taxa are exposed. Oxygen levels probably fell below the tolerance of the more oxiphilic species (e.g., Van der Zwaan et al., 1999; Gooday, 2003; Jorissen et al., 2007), but remained above the threshold for infaunal taxa (≤1 ml/l; Murray, 2001). The entire interval is bioturbated and benthic foraminifera occur throughout, thus the interval is not characterized by anoxia, but the geological record is always time-averaged, so that we cannot exclude that brief (e.g., millennial or submillennial) episodes of anoxia occurred, but directly followed by recolonization of the benthos. The hypoxic conditions may have been exacerbated by increased fresh water influx into the basin due to the increased vigour of the hydrological cycle during the warm peak of MECO (e.g., Pierrehumbert, 2002). The striking change in the benthic foraminiferal composition during the transition from assemblage B to assemblage C can be explained as caused by a food-enriched, somewhat oxygen depleted sea-floor environment, which favoured a fairly diversified "high productivity", stress-tolerant fauna. Sedimentological and geochemical proxies support this hypothesis, because the high TOC% values, common occurrence of pyrite, low Mn/Al and high S% indicate oxygen-poor conditions at or just below the sea-floor (Spofforth et al., 2010). The benthic foraminiferal evidence indicates, however, that the hypoxic conditions were not stable: within assemblage C, peaks of different species of buliminids occur (Fig. 3). For example, the sample dominated by *Bolivinoides crenulata* (COL40B-17.25 m) and other bolivinids abundant in the underlying assemblages, indicates a lower flux of organic matter and a better oxygenation at the sediment/water interface, than the surrounding samples (Fig. 3). Similar instability is shown in the occurrence of the light-coloured, marly layer within ORG1 (sample COL113B-17.98 m), also dominated by *B. crenulata* (Figs. 2, 3), and with a lower infaunal/epifaunal ratio and bi-triserial taxa percentage, suggestive of a significant lowering of the flux of organic matter and temporary re-oxygenation at the sediment/water interface. Geochemical

and sedimentological proxies agree with this interpretation (Spofforth et al., 2010). We thus speculate that a strong competition for resources at and just below the sediment/water interface influenced the composition of the benthic assemblages, favouring peaks of diverse taxa depending on the degree of organic flux and oxygen depletion, thus motion of redox boundaries through the sediment column (e.g., Van der Zwaan et al., 1999; Fontanier et al., 2005; Jorissen et al., 2007). In conclusion, we infer that variable and fluctuating C_{org} flux regimes characterized ORG1 deposition, indicating an unstable paleoenvironment with variable surface waters productivity.

5.3. Marly interval between ORGs (assemblage D): improved bottom water oxygenation and decreasing surface productivity

The benthic assemblages in this organic poor interval indicate re-oxygenation linked to a significant decrease in surface water productivity, and potentially some cooling, as indicated by the abundance of *Bolivinoides crenulata* and the decrease of the eutrophic, low-oxygen tolerant taxa, particularly in the middle-upper part of the interval (Figs. 2, 3). High infaunal/epifaunal values persist and a high abundance of bi-triserial taxa (relative and absolute) coupled with high total N/g values (Fig. 2) occur at the base of this interval. These data, along with maximum values of absolute and relative abundance of heavily costate *Uvigerina* spp. in the ≥450 μm fraction (Fig. 4; Plate I), indicate that the flux of organic matter was still high, and relatively continuous. The high diversity, however, suggests that higher oxygen levels returned at the sediment/water interface, as corroborated by sedimentological evidence. The persistent high total N/g (Fig. 2) may be caused by an increase in abundance of small specimens, and/or by the decreased sedimentation rate of detrital input (Spofforth et al., 2010). Benthic assemblages agree with the interpretation of changes in calcareous plankton indicating an overall decrease of eutrophication (Luciani et al., 2010; Toffanin et al., 2011).

5.4. Post-MECO ORG2 (assemblage E): increased hypoxia at the sea-floor

During the deposition of ORG2 surface water productivity increased again, leading to a higher C_{org} flux to the sea floor as indicated by increase of bi-triserial taxa (Figs. 2, 3), and the dark colour of the marls due to high TOC. Benthic foraminiferal preservation declined in assemblage E, while F-index values increased (Fig. 2), indicating increased carbonate dissolution, even somewhat higher than in ORG1.

Plate I

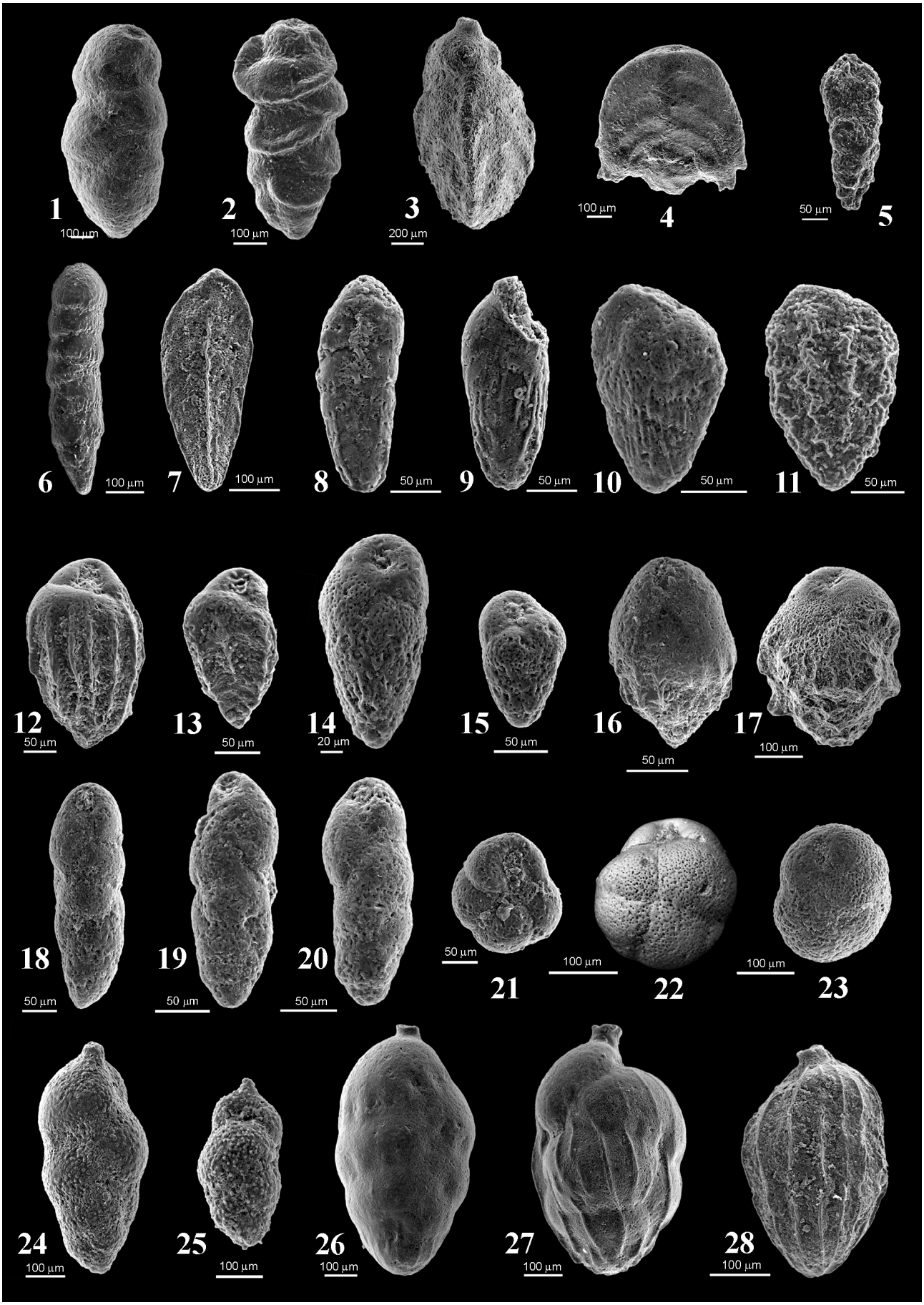
1
100 µm
2
100 µm
3
200 µm
100 µm
4
50 µm
5
6
100 µm
7
100 µm
8
50 µm
9
50 µm
10
50 µm
11
50 µm
12
50 µm
13
50 µm
14
20 µm
15
50 µm
16
50 µm
17
100 µm
18
50 µm
19
50 µm
20
50 µm
50 µm
21
100 µm
22
100 µm
23
24
100 µm
25
100 µm
26
100 µm
27
100 µm
28
100 µm

Plate II

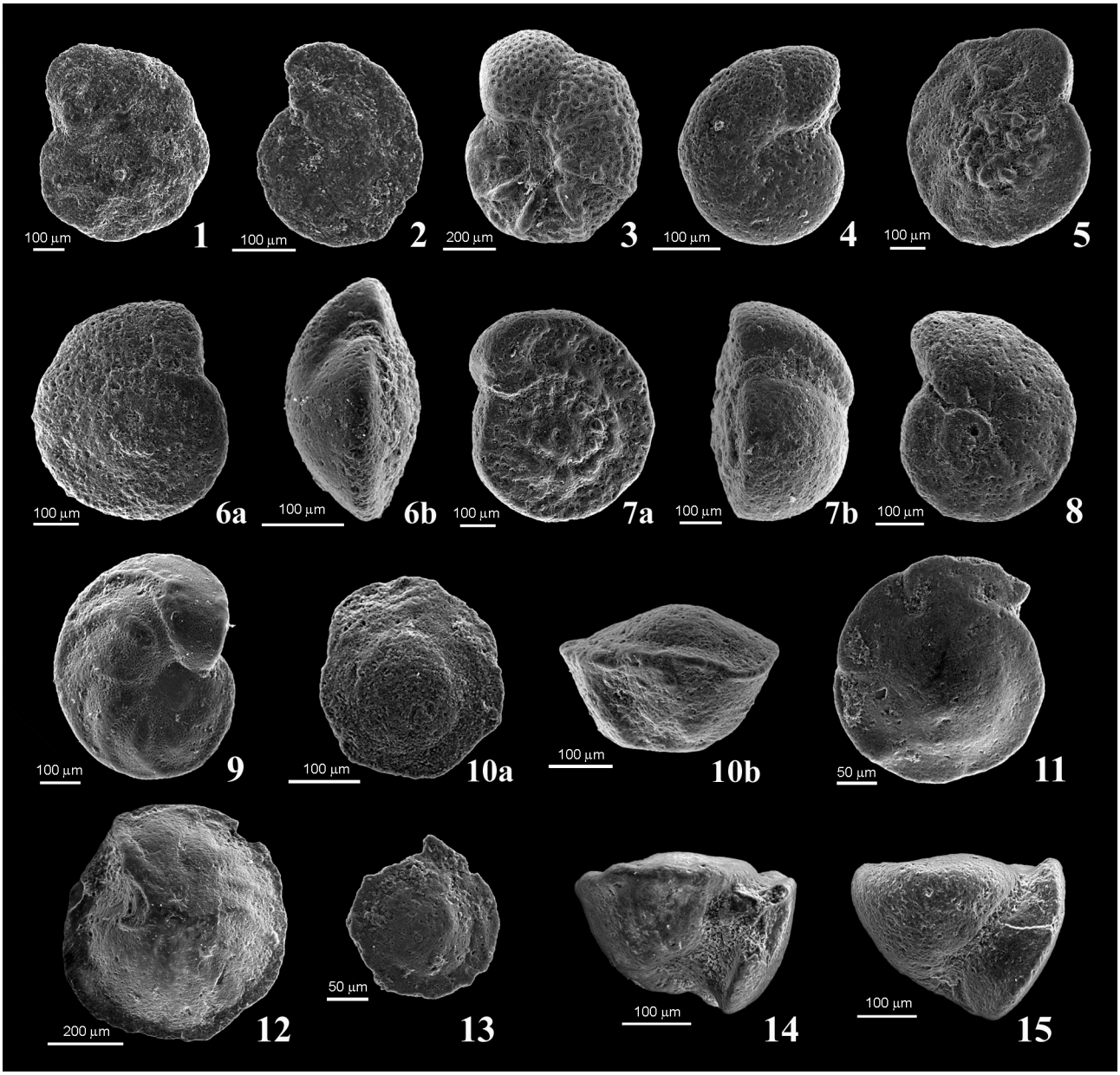

Plate I. Fig. 1 *Plectina dalmatina* (Schubert, 1911) COL140B-18.25 m; Fig. 2 *Plectina* sp. COL10B-16.95 m; Fig. 3 *Tritaxia szaboi* (Hantken, 1875) COL440A-14.80 m; Fig. 4 *Vulvulina eocaena–haeringensis* group COL865B-25.50 m; Fig. 5 *Eobigenerina variabilis* (Vašiček, 1947) COL520A-15.60 m; Fig. 6 *Rectouvigerina mexicana* (Cushman, 1926) COL470B-21.55 m; Fig. 7 *Bolivina antegressa* Subbotina, 1953 COL945B-26.30 m; Fig. 8 *Bolivina nobilis–gracilis* transitional forms COL690B-23.75 m; Fig. 9 *Bolivina nobilis–gracilis* transitional forms COL690B-23.75 m; Fig. 10 *Bolivina* sp. smooth/slightly costate group; Fig. 11 *Bolivinoides crenulata* (Cushman, 1936) COL945B-26.30 m; Fig. 12 *Bulimina alazanensis* Cushman, 1927 COL405-20.90 m; Fig. 13 *Bulimina* cf. *alazanensis* Cushman, 1927 COL520A-15.60 m; Fig. 14 *Bulimina* cf. *semicostata* Nuttall, 1930 COL140B-18.25 m; Fig. 15 *Bulimina* cf. *semicostata* Nuttall, 1930 COL140B-18.25 m; Fig. 16 *Bulimina stalacta* Cushman and Parker, 1936 COL560A-16.00 m; Fig. 17 *Bulimina trinitatensis–impendens* group COL470B-21.55 m; Fig. 18 *Bulimina* cf. *elongata* d'Orbigny, 1846 group COL440A-14.80 m; Fig. 19 *Bulimina* cf. *elongata* d'Orbigny, 1846 group COL945B-26.30 m; Fig. 20 *Bulimina* cf. *elongata* d'Orbigny, 1846 group COL945B-26.30 m; Fig. 21 *Caucasina* sp. COL1065B-27.50 m; Fig. *22 Globocassidulina subglobosa* (Brady, 1881) COL140B-18.25 m; Fig. 23 *Globocassidulina punctata* Berggren and Miller, 1986 COL80A-11.20 m; Fig. 24 *Uvigerina chirana* Cushman and Stone, 1947 COL10B-16.95 m; Fig. 25 *Uvigerina farinosa* Hantken, 1875 COL440A-14.80m; Fig. 26 *Uvigerina* sp. A COL10B-16.95 m; Fig. 27 *Uvigerina* sp. C COL10B-16.95 m; Fig. 28 *Uvigerina* sp. heavy costate form COL245B-19.30 m.

Plate II. Fig. 1 *Reticulophragmium* cf. *acutidorsatum* (Hantken, 1868) COL825B-25.10 m; Fig. 2 *Haplophragmoides walteri* (Grzybowski, 1898) COL945B-26.30 m; Fig. 3 *Anomalinoides capitatus* (Gümbel, 1868) COL520A-15.60 m; Fig. 4 *Anomalinoides spissiformis* Cushman and Stainforth, 1945 COL305B-19.90 m; Fig. 5 *Cibicidoides ungerianus* (d'Orbigny, 1846) COL440A-14.80 m; Fig. 6a *Cibicidoides eocaenus* (Gümbel, 1868) spiral view COL1000-10.00 m; Fig. 6b *Cibicidoides eocaenus* (Gümbel, 1868) lateral view COL365B-20.50 m; Fig. 7a *Cibicidoides grimsdalei* (Nuttall, 1930) spiral view COL945B-26.30 m; Fig. 7b *Cibicidoides grimsdalei* (Nuttall, 1930) spiral view COL945B-26.30 m; Fig. 8 *Cibicidoides micrus* Bermúdez, 1949 COL500A-15.40 m; Fig. 9 *Hanzawaia ammophila* Gümbel, 1868 COL40B-17.25 m; Fig. 10a *Nuttallides truempyi* (Nuttall, 1930) spiral view COL1000-10.00 m. Fig. 10b *Nuttallides truempyi* (Nuttall, 1930) lateral view COL440A-14.80 m; Fig. 11 *Oridorsalis umbonatus* (Reuss, 1851) spiral view COL750B-24.35 m; Fig. 12 *Osangularia pteromphalia-mexicana* group umbilical view COL440A-14.80 m; Fig. 13 *Osangularia* sp. spiral view COL690B-23.75 m; Fig. 14 *Gyroidinoides dissimilis* (Cushman and Renz, 1947) COL140B-18.25 m; Fig. 15 *Gyroidinoides soldanii* d'Orbigny, 1826 COL520-15.60 m.

The dissolution does not seem to have significantly altered the benthic foraminiferal signal in most samples, as shown by the constant presence of small specimens (e.g., bolivinids, osangulariids, *Globocassidulina* spp.; Figs. 3, 4). Sample COL470B (+21.55 m) is an exception, and has poor preservation associated with high faunal diversity, low faunal density and bi-triserial abundance, and a high agglutinated/hyaline value (Figs. 2, 3). The high faunal diversity is caused by removal of the small and dominant buliminids by dissolution, thus emphasizing the abundance of other taxa, mostly agglutinants (Figs. 2, 4). The benthic foraminiferal signal might have been affected by carbonate dissolution, but overall assemblage E indicates more severely oxygen-depleted conditions during ORG2 deposition than during ORG1. The lowermost portion of this interval (COL405B-20.90 m) is characterized by a high abundance of *Bulimina alazanensis* (Fig. 3), a typical taxon of modern oceans "high productivity" assemblages (Loubere, 1991, 1996, 1997; Loubere and Fariduddin, 1999b). High primary productivity leading to lowered oxygen conditions is indicated by the taxonomic composition of the foraminiferal assemblage, which is dominated by very small bolivinids such as *Bolivina antegressa* and *Bolivina nobilis–Bolivina gracilis* group, associated with abundant small *Osangularia* spp. (Fig. 3). *Osangularia* is common in many Cretaceous black shales, and considered an opportunistic taxon able to rapidly recolonize when oxygenation improves slightly (e.g., Friedrich et al., 2005). The small bolivinids are morphologically similar to those dominating assemblages in the oxygen minimum zones (OMZs) in the present Pacific and Indian Oceans (e.g., *Bolivina argentea* and *Bolivina seminuda*; Sen Gupta and Machain-Castillo, 1993; Bernhard et al., 1997). Small calcareous benthic foraminifera typically dominate assemblages in oxygen-depleted environments (e.g., Koutsoukos et al., 1990). *Bolivina* in hypoxic sediments may be small as the result of physiological adaptation for facilitating gas exchange (e.g., Bernhard et al., 2010), and the small size minimizes oxygen consumption with respect to the surface-to-volume ratio (Bradshaw, 1961; Kuhnt and Wiedmann, 1995; Friedrich, 2009). In addition, opportunistic benthic foraminifera tend to reproduce fast (thus at an early age and small size) under low oxygen conditions, due to the low competition at high food availability (Phleger and Soutar, 1973; Koutsoukos et al., 1990; Friedrich, 2009). The low oxygen conditions due to high surface primary productivity may have been exacerbated by increased fresh water flux into the basin due the increased vigour of the hydrological cycle during warm climates (e.g., Pierrehumbert, 2002). We thus argue that only the most opportunistic taxa could thrive to form the low-diversity high-dominance Assemblage E (e.g., Koutsoukos et al., 1990; Jorissen et al., 1995; Van der Zwaan et al., 1999). Geochemical proxies also indicate more markedly hypoxic conditions during ORG2 than during ORG1 at Alano (Spofforth et al., 2010), as also suggested by the highest abundance of the deep infaunal *Praeglobobulimina*, *Globobulimina* species in the studied section.

Lower N/g in the assemblage might have been caused by hypoxia, but could also have been influenced by enhanced dissolution caused by pore water acidification due to excessive organic decay and pyrite oxidation (e.g., Green et al., 1993; Aller and Blair, 2006; Sprong et al., 2012). Different degrees of preservation in ORG2 suggest the occurrence of brief re-oxygenation episodes of varying duration and intensity (e.g., Green et al., 1993; Diester-Haass et al., 1998). Such episodes of reventilation could have been associated with less productive surface waters, such as reflected in sample COL610B (22.95 m), an organic poor, light-coloured layer with common *Bolivinoides crenulata*, high Fisher α, low dominance and bi-triserial percentage (Figs. 2, 3). In conclusion, the structure and composition of assemblage E reflect high productivity and low oxygen conditions, under unstable water column stratification, leading to variability in the degree of oxygenation and flux of organic matter at the sea floor.

5.5. Recovery phase above post-MECO (assemblage F): rapid sea-floor re-oxygenation and return to background conditions

Directly above ORG2, benthic foraminifera abruptly return to a higher faunal density (Table 1) and became dominated by *Bolivinoides crenulata*, together with small and little ornamented bi-triserial taxa such as *Bulimina* cf. *elongata* and *Bulimina* cf. *alazanensis* (Appendix A), which are more abundant in assemblage F than in the pre-MECO interval (Figs. 2, 3, 4). When oxygenation recovered, and possibly waters cooled assisting in recovery of oxygenation, *B. crenulata* and other bi-triserial taxa took advantage of the increased oxygen availability and the organic matter stored in the sediments, reaching higher abundances than in assemblage A. If sedimentation was continuous, the abrupt disappearance of taxa typical for hypoxic conditions just above the uppermost dark marls testifies to a very rapid return to well-oxygenated bottom waters, as well as normally productive surface waters for the region. Such rapid reoxygenation may have been assisted by decreasing density gradients in the water column due to the decrease in fresh-water supply at the end of the MECO warm period, as well as by the decreasing temperatures.

6. Summary and conclusions

(1) Benthic foraminiferal assemblages indicate that in the Alano section in western Tethys environments gradually changed toward more eutrophic conditions at the onset of the MECO, culminating with the deposition of the two sapropelic intervals after the end of peak-MECO warming, in agreement with the observed marked increase in abundance of eutrophic–opportunistic

taxa of calcareous plankton in these intervals (Luciani et al., 2010; Spofforth et al., 2010; Toffanin et al., 2011).

(2) The marine productivity may have gradually increased as a response to increase in fresh-water run-off during increased vigour of the hydrological cycle during MECO warming, which augmented influx of nutrients from increased weathering, thus higher nutrient availability, leading to increased surface and export productivity, and increased the quality and quantity of organic matter reaching the sea-floor.

(3) Micropaleontological, geochemical, isotopic and sedimentological data all indicate that the environment at the Alano section was unstable and perturbed throughout the post-MECO interval when two layers of organic-rich sedimentwere deposited, probably under hypoxic conditions (Luciani et al., 2010; Spofforth et al., 2010; Toffanin et al., 2011).

(4) Benthic foraminiferal data present evidence that this instability was expressed in an increase in surface productivity during deposition of the organic rich layers, thus increasing the C_{org} flux which led to lower bottom water oxygenation and increased organic matter preservation. Such changes in surface-water productivity could be explained by an intermittently strengthened hydrological cycle leading to overall increased but variable delivery of nutrients.

(5) A transient interval of lowered surface productivity interrupted the deposition of organic rich sediment, as shown by a decrease in abundance of planktonic and benthic foraminiferal taxa. Benthic foraminifera indicate that the reduced primary productivity was coupled to improved bottom water oxygenation, possibly during cooler, less humid conditions.

(6) Biotic, sedimentological and geochemical data suggest that after this transient interval, hypoxic conditions returned during deposition of the second organic rich layer, due to increasing surface water productivity caused by renewed fresh water influx carrying nutrients. Benthic foraminiferal assemblages indicate a more stressed, more-oxygen depleted sea-bottom environment than during the deposition of the first organic-rich layer.

(7) The deposition of the organic rich layers was local or regional, but its occurrence just after the MECO peak warming may suggest a connection, possibly through passing of an environmental threshold. The rapid increase in temperature during the MECO-peak warming could have caused

increased discharge of nutrient-rich freshwaters into the basin, thus highly increased productivity, especially because the Alano section was located relatively close to the end of the basin, limiting bottom-surface water exchange.

(8) Benthic foraminiferal data combined with the record of calcareous plankton (Luciani et al., 2010; Toffanin et al., 2011), provide clear evidence that the increased productivity caused the positive carbon isotope excursion during deposition of the organic rich layers at Alano, because of the burial of isotopically light organic matter (Luciani et al., 2010; Spofforth et al., 2010).

(9) The Alano record thus may support the hypothesis by Bohaty et al. (2009) that increased organic carbon burial could have acted to sequester an excess of CO_2 from the ocean–atmosphere system in a relatively short time interval (Spofforth et al., 2010), possibly in combination with organic carbon burial in other marginal basins (Beniamovski et al., 2003).

(10) The MECO and post-MECO intervals were not associated with extinctions or permanent changes in the structure and composition of the benthic foraminiferal communities in the middle bathyal setting in western Tethys.

(11) Studies of the biotic effects of MECO are needed at more locations in order to provide a more global perspective of the event, allowing a better understanding of the benthic foraminiferal response to this transient warm period of Earth history.

Appendix A. Taxonomic list of benthic foraminiferal taxa recognized in the Alano di Piave section.

Agglutinant taxa

Ammobaculites agglutinans = *Spirolina agglutinans* d'Orbigny, 1846.
Ammodiscus cretaceus = *Operculina cretacea* Reuss, 1845.
Ammodiscus glabratus Cushman & Jarvis, 1928.
Ammodiscus peruvianus Berry, 1928.
Ammodiscus tenuissimus Grzybowski, 1898.
Ammomarginulina aubertae Gradstein & Kaminski, 1989.
Ammosphaeroidina pseudopauciloculata = *Cystamminella pseudopauciloculata* Mjatliuk, 1966.
Arenobulimina sp.
Bathysiphon spp.
Bigenerina spp.
Clavulina parisiensis d'Orbigny, 1826.
Clavulina spp.
Clavulinids. Juvenile specimens.
Cylindroclavulina eocaena Gümbel, 1868 *sensu* Grünig (1985; pl. 4, figs. 3-4).
Cylindroclavulina spp.
Conotrochammina cf. *wangaia* Finlay, 1940.
?*Conotrochammina* sp.
?"*Cribrostomoides*" *trinitatensis* Cushman & Jarvis, 1928.
Dorothia spp.
Dorothia spp. Juvenile specimens
Eobigenerina variabilis = *Bigenerina variabilis* Vašiček, 1947 in Cetean et al. (2011)
Eobigenerinid. Large-sized specimens.
Glomospira charoides = *Trochammina squamata* var. *charoides* Jones & Parker, 1860.
Glomospira spp.
Glomospirella sp.
Haplophragmoides horridus = *Haplophragmium horridum* Grzybowski, 1901.
Haplophragmoides walteri = *Trochammina walteri* Grzybowski, 1898.
Haplophragmoides cf. *walteri* = *Trochammina* cf. *walteri* Grzybowski, 1898.
Haplophragmoides spp. (It includes also coarsely agglutinated specimens).
?*Haplophragmoides.*
Hormosina trinitatensis = *Hormosina globulifera* Brady var. *trinitatensis* Cushman & Renz, 1946.
Karreriella chapapotensis = *Textularia chapapotensis* Cole, 1928.
Karreriella chapapotensis = *Textularia chapapotensis* Cole, 1928 *sensu* Tjalsma & Lohmann 1983. Specimens figured in Tjalsma & Lohamann (1983) have more inflated and elongate chambers if compared with the holotype figured in Cole (1928).
Karreriella cf. *cubensis* Cushman & Bermúdez, 1937.
Karreriella hantekeniana Cushman, 1936.
Karreriella subglabra = *Gaudryina subglabra* Gümbel, 1868.
Karreriella a spp.

Karrerulina coniformis = Gaudryina coniformis Grzybowski, 1898.
Karrerulina conversa = Gaudryina conversa Grzybowski, 1901.
Karrerulina horrida = Karreriella horrida Mjatlyuk, 1970.
Karrerulina spp.
Lituotuba lituiformis = Trochammina lituiformis Brady, 1879.
Marssonella traubi Hagn, 1956.
Marssonella spp.
?*Martinottiella* spp.
Plectina dalmatina = Gaudryina dalmatina Schubert, 1911 *sensu* Mathelin & Sztrakós (1993). Common specimens with collapsed or deformed chambers occur within sapropelic intervals.
Pectina dalmatina = Gaudryina dalmatina Schubert, 1911 juvenile specimens
Plectina spp. Common specimens with collapsed or deformed chambers occur within sapropelic intervals.
Psammosphera sp.
Pseudobolivinids.
?Pseudobolivinids.
Ramulina sp.
Recurvoides anormis Mjatliuk, 1970.
Recurvoides spp.
Reophax duplex = Reophax duplex var. α Grzybowski, 1896.
Reophax spp.
Reophacids.
Reticulophragmium acutidorsatum = Haplophragmium acutidorsatum Hantken, 1868.
Reticulophragmium cf. *acutidorsatum = Haplophragmium acutidorsatum* Hantken, 1868.
Reticulophragmium spp.
Saccammina placenta = Reophax placenta Grzybowski, 1898.
Saccammina grzybowsky = Reophax grzybowskii Schubert, 1902.
Spiroplectammina dalmatina-pectinata group *sensu* Grünig (1985). It includes:

- *Spiroplectammina dalmatina = Textularia dalmatina* De Witt Puyt (1941)
- *Spiroplectammina pectinata = Vulvulina pectinata* Hantken (1875)

Spiroplectammina navarroana Cushman, 1932.
Spiroplectammina spectabilis = Spiroplecta spectabilis Grzybowski, 1898.
Spiroplectammina cf. *spectabilis = Spiroplecta* cf. *spectabilis* Grzybowski, 1898.
Spiroplectammina spp.
Subreophax spp.
? *Textularia.*
Textularidae indet.
Tritaxia szaboi = Clavulina szaboi Hantken, 1875. Usually it occurs in the >450µm fraction.
Tritaxia szaboi juvenile specimens= *Clavulina szaboi* Hantken, 1875.
Tritaxilina pupa = Gaudryina pupa Gümbel, 1868.
Tritaxilina sp.
Trochammina sp.
? *Trochammina* sp. *sensu* Grünig (1985).
? *Trochammina.*

Trochamminids.
Trochamminoides subcoronatus = *Trochammina subcoronata* Grzybowski, 1896.
Trochamminoides spp.
Vulvulina haeringensis-eocaena group includes the following species:

- *Vulvulina haeringensis* =*Venilina haeringensis* Gümbel, 1868
- *Vulvulina eocaena* Montagne, 1941

Vulvulina spp.
Agglutinant sp. A. Biserial forms similar to textulariids.
Agglutinant sp. B. Specimens similar to *Cylindroclavulina eocaena sensu* Grünig (1985) but much more compressed.
Agglutinant sp. C. Forms similar to karrerulinids.
Agglutinant sp. D. Indeterminate uniserial species.

Porcellaneous taxa

Miliolids.
Spiroloculina sp. A. Not keeled forms with numerous whorls.

Calcareous-hyaline taxa

Allomorphina macrostoma Karrer, 1892.
Angulogerina muralis = *Uvigerina muralis* Terquem, 1882.
Anomalinoides alazanensis = *Anomalina alazanensis* Nuttall, 1932.
Anomalinoides capitatus = *Rotalia capitata* Gümbel, 1868.
Anomalinoides capitatus ?juvenile forms. Small-sized specimens characterized by less dense perforations and flush sutures between the early chambers of the last whorl.
Anomalinoides spissiformis = *Anomalina alazanensis* Nuttall var. *spissiformis* Cushman & Stainforth, 1945.
Anomalinoides spp.
Angulogerina spp.
Aragonia aragonensis = *Textularia aragonensis* Nuttall, 1930.
Astacolus spp.
Baggina cf. *marielina* Cushman & Bermúdez, 1937. Some specimens were found within one sample in the >450 µm fraction (COL550B-22.35 m).
Bagginids.
Bolivina antegressa Subbotina, 1953 *sensu* Grünig, 1985.
Bolivina nobilis-gracilis transitional forms. Transitional forms between *B. nobilis* Hantken (1875) and *B. gracilis* Cushman & Applin (1926) as described in Grünig & Herb (1980) and Grünig (1985). We found these forms only within one sample from ORG2 interval (at 23.75 m).
Bolivina spp. smooth.
Bolivina spp. heavy costate forms.
Bolivinoides crenulata = *Bolivina crenulata* Cushman, 1936.
Bulimina alazanensis Cushman, 1927.

Bulimina alazanensis-truncana transitional forms. Specimens with less marked triangular outline and slightly inflated chambers which we consider transitional forms between typical *B. alazanensis* Cushman (1927) and *B. truncana* Gümbel (1868).
Bulimina cf. *alazanensis* Cushman, 1927. Small specimens with a distinctly triangular outline, chambers not visible, lateral sides slightly concave. Ornamentation consists of a single longitudinal rib in the mid of each side, running from the basal end to the base of the last chamber and of a couple of ribs which profile each margin.
Bulimina cf. *elongata* group. In this group we lumped together *Bulimina* specimens similar to *B. elongata* d'Orbigny 1846, characterized by a strong morphological variability. Specimens belonging to this group often show differences in the position and shape of the aperture that we are not able to discern under stereoscopic microscope but which became evident only under SEM. For this reason we preferred to allocate all these specimens within this heterogeneous group. These forms are characterized by very small dimension, test elongate and slightly perforate, with numerous chambers often rather inflated in the last whorl. In some cases the tests are twisted on their major axis.
Bulimina cf. *midwayensis* = *Bulimina arkadelphiana* Cushman & Parker var. *midwayensis* Cushman & Parker, 1936.
Bulimina sculptilis Cushman, 1923.
Bulimina sculptilis var. *laciniata* Cushman & Parker, 1937.
Bulimina cf. *semicostata* Nuttall, 1930. Very small forms which differ from typical *B. semicostata* for a stouter and less triangular test with a rather rounded initial apex. Aperture located in the middle of an inflated and overhanging last chamber. Our specimens resemble *Bulimina semicostata* as figured in Kahio (1991).
Bulimina stalacta Cushman & Parker, 1936.
Bulimina sp. with thin costae.
Bulimina trinitatensis-impendes group *sensu* Barbieri et al. (2003). It includes:

- *Bulimina trinitatensis* Cushman & Jarvis, 1928
- *Bulimina impendens* Parker & Bermúdez, 1937

Bulimina tuxpamensis Cole, 1928.
Bulimina spp.
Buliminella spp.
Buliminids.
?*Cassidulina* cf. *armosa* Bandy, 1949.
Cassidulina spp.
Caucasina sp. Specimens with a low trochospiral coil of about two whorls, without a highly spired triserial stage. Chambers nine to ten in number, sutures slightly depressed, loop shape aperture extending up the face of the last chamber.
Chilostomella sp. Rare specimens were found only whitin >450 µm fraction.
Cibicides cf. *westi* Howe, 1939.
Cibicides westi Howe var. *arguta* Bykova, 1954.
Cibicides spp.
Cibicidoides barnetti = *Cibicides barnetti* Bermúdez, 1949.

Cibicidoides barnetti = *Cibicides barnetti* Bermúdez, 1949. Sapropel morphotype. It differs from the typical *C. barnetti* in having more developed seams on the dorsal side, less convex umbilical side and a more pronounced keel.
Cibicidoides eocaenus = *Rotalia eocaena* Gümbel, 1868 *sensu* Van Morkhoven et al. (1986).
Cibicidoides grimsdalei = *Cibicides grimsdalei* Nuttall, 1930.
Cibicidoides havanensis Cushman & Bermúdez, 1937. Very rare specimens were found only within >450 µm fraction.
Cibicidoides hettneri Petters & Sarmiento, 1956.
Cibicidoides mexicanus = *Cibicides mexicana* Nuttall, 1932.
Cibicidoides micrus = *Cibicides micrus* Bermúdez, 1949.
Cibicidoides cf. *robertsonianus* Brady var. *haitiensis* Coryell & Rivero, 1940.
Cibicidoides cf. *subspiratus* = *Cibicides subspirata* Nuttall, 1930. Our specimens differ from typical material in having a well developed keel only in the first half of the last whorl.
Cibicidoides ungerianus = *Rotalina ungeriana* d'Orbigny, 1846.
?*Cibicidoides* sp. A. Very small specimens with several chambers and curved sutures.
?*Cibicidoides* spp. small?
Cibicidoides spp.
?*Coryphostoma* spp.
Dentalina spp.
Dentalinid.
Ellipsoglandulina sp.
Ellipsoidella sp.
Epistominella spp.
Eponides abatissae Selli var. *multicameratus* Petters & Gandolfi, 1948.
Eponides cf. *abatissae* Selli var. *multicameratus* Petters & Gandolfi, 1948. Specimens with less numerous chambers and a more convex umbilical side.
Eponides spp.
Fursenkoina spp.
?*Fursenkoina.*
Globobulimina spp.
Globocassidulina inexculta = *Cassidulina inexculta* Franzenau, 1890.
Globocassidulina punctata Berggren & Miller, 1986.
Globocassidulina subglobosa = *Cassidulina subglobosa* Brady, 1881. Transitional forms to typical *G. globosa* Hantken 1875 were observed in the studied material.
?*Globorotalites* spp.
Gyroidinoides altiformis = *Gyroidina soldanii* d'Orbigny var. *altiformis* Stewart & Stewart, 1930.
Gyroidinoides dissimilis = *Gyroidina dissimilis* Cushman & Renz, 1947.
Gyroidinoides gyrardanus = *Rotalina girardana* Reuss, 1851.
Gyroidinoides cf. *octocameratus* = *Gyroidina soldanii* d'Orbigny subspecies *octocamerata* Cushman & Hanna, 1927.
Gyroidinoides soldanii d'Orbigny, 1826.
Gyroidinoides subangulatus = *Gyroidina soldanii* d'Orbigny var. *subangulata* Plummer, 1927.
Gyroidinoides spp.
Gyroidinids.

Hanzawaia ammophila = Rotalia ammophila Gümbel, 1868.
Hanzawaia cushmani = Cibicides cushmani Nuttall, 1930.
Hemirobulina spp.
?Hemirobulina sp.
Indeterminate hyalineous.
Indeterminate trochosphiral hyalineous (ITH). ITH group includes all the broken pieces of big-size trochospiral forms or indeterminable big-size trochospiral forms affected by strong dissolution. Common in the sapropelic intervals.
Lagena hexagona Williamson var. *lata* Goddard, 1907.
Lenticulina granulata = Robulina granulata Hantken, 1875.
Lenticulina spp. with costae.
Lenticulina spp. smooth.
Marginulinopsis fragaria = Marginulina fragaria Gümbel, 1868.
Nodosarella spp.
Nodosaria – Chrysalogonium group. It includes the following genera:
• *Nodosaria* spp.
• *Pyramidulina* spp.
• *Chrysalogonium* spp.
Nonion havanense Cushman & Bermúdez, 1937.
Nonion spp.
Nonionella spp.
Nonionids.
?*Nuttallides decorata = Pseudoparrella*? *decorata* Phleger & Parker, 1951.
Nuttallides truempyi = Eponides truempyi Nuttall, 1930.
Oridorsalis umbonatus = Rotalina umbonata Reuss, 1851.
Oridorsalis spp.
Osangularia pteromphalia-mexicana group. It includes:

- *Osangularia pteromphalia* Güembel, 1868
- *Osangularia mexicana = Pulvinulinella culter* Parker & Jones var. *mexicana* Cole, 1927

Osangularia pteromphalia-mexicana group (sapropel morphotype). We found these forms only within the sapropelic intervals. They are characterized by an almost flat dorsal side and a very convex umbilical side; dorsal side with thickened spiral and chambers sutures and an excavated area over each chamber. A narrow, thin keel surrounds the periphery.
Osangularia cf. *plummerae* Brotzen, 1940.
Osangularia spp. Small-sized *Osangularia* mostly occurring within the sapropelic intervals.
Paleopolymorphina spp.
Parafrondicularia spp.
Planularia spp.
Planulina spp.
Plectofrondicularia spp.
Pleurostomella spp.
Indeterminate pleurostomellids.
Polymorphinids
?*Praebulimina* sp.

Praeglobobulimina pupoides = *Bulimina pupoides* d'Orbigny, 1846.
Pullenia cretacea Cushman, 1936.
Pullenia eocaena Cushman & Siegfus, 1939.
Pullenia quinqueloba Reuss, 1852.
Pullenia spp.
Rectouvigerina mexicana = *Siphogenerina mexicana* Cushman, 1926.
?*Rectouvigerina ?mexicana* = *Siphogenerina mexicana* Cushman, 1926. Broken specimens with missing last chambers and early stage of the test very similar to *Rectouvigerina mexicana*.
?Rectouvigerina spp.
Saracenaria spp.
Siphogenerinoides cf. *eleganta* = *Siphogenerina* cf. *eleganta* Plummer, 1926.
Siphonella spp.
Small low trochospiral hyalineous (STH). Very small-sized, low trochospiral forms with test diameter between 63 and ca. 80 μm, common in the sapropelic intervals. They are undetermined even at generic level due to their small size and bad preservation of the tests.
?*Sporobuliminella* spp.
Stilostomellids.
Tappanina selmensis = *Bolivinita selmensis* Cushman, 1933.
Trifarina sp. A. Small forms characterized by blunt margins and slightly inflated lateral sides. Aperture on a short neck bordered by a thin lip.
Trifarina sp. B. Elongate forms with concave lateral sides.
Trifarina sp. C. Species with thin costae.
Turrilina sp.
Unilocular hyalineous.
Uniserial hyalineous.
Uvigerina chirana Cushman & Stone, 1947.
Uvigerina farinosa Hantken, 1875.
Uvigerina sp. A. Smooth specimens with few and scattered costae only in the first chambers.
Uvigerina sp. B. Specimens with few and thin costae throughout the test until the base of the neck.
Uvigerina sp. C. Species with rather developed costae throughout the test with the exception of the last chamber. It differs from *U. eocaena* Gümbel (1870) for the rounded apex and less pronounced costae.
Uvigerina cf. *hourcqi* Graham Klasz & Rerat, 1965.
Uvigerina spp. with costae
Uvigerina spp. heavy costate forms. Large-sized specimens >450 μm with pronounced and continuous costae throughout the test occur within some samples of the ORGs intervals.
Uvigerina spp.
?Uvigerina.
Small undetermined uvigerinids.
? *Vaginulina* sp.
Valvulineria filiaeprincipis Hagn, 1956.
Valvulineria wittpuyti Bellen, 1941.
Valvulineria spp.
Valvulinerids

References

Agnini, C., Fornaciari, E., Giusberti, L., Grandesso, P., Lanci, L., Luciani, V.,Muttoni, G., Rio, D., Stefani, C., Pälike, H., Spofforth, D.J.A., 2011. Integrated bio-magnetostratigraphy of the Alano section (NE Italy): a proposal for defining the Middle–Late Eocene boundary. Geological Society of American Bullettin 123 (5/6), 841–872. http://dx.doi.org/10.1130/B30158.1.

Aller, R.C., Blair,N.E., 2006. Carbon remineralization in theAmazon-Guiana tropical mobile mud belt: a sedimentary incubator. Continental Shelf Research 26, 2241–2259.

Alve, E., 1995. Benthic foraminiferal distribution and recolonization of formerly anoxic environments in Drammensfjord, southern Norway. Marine Micropaleontology 25, 169–186.

Alve, E., Bernhard, J.M., 1995. Vertical migratory response of benthic foraminifera to controlled oxygen concentrations in an experimental mesocosm. Marine Ecology Progress Series 116, 137–151.

Barbieri, R., 1990. L'Eocene medio e superiore del Bacino di Tripolitania (Libia nord occidentale): biostratigrafia e paleoecologia. Bollettino della Società Paleontologica Italiana 29 (3), 253–271.

Barbieri, R., Benjamini, C., Monechi, S., and Reale, V., 2003. Stratigraphy and benthic foraminiferal events across the middle–late Eocene transition in the western Negev, Israel. In: Prothero, D.R., Ivany, L.C., and Nesbitt, E.A., (Eds.), From Greenhouse to Icehouse: The Marine Eocene–Oligocene Transition: New York, Columbia University Press, pp. 453–470.

Beniamovski, V.N., Alekseev, A.S., Ovechkina, M.N., Oberhänsli, H., 2003. Middle to Upper Eocene disoxic–anoxic Kuma Formation (northeast Peri-Tethys): biostratigraphy and paleoenviroments. In:Wing, S.L., Gingerich, P.D., Schmitz, B., Thomas, E. (Eds.), Causes and Consequences of Globally Warm Climates in the Early Paleogene: Boulder, Colorado, Geological Society of America Special Paper, 369, pp. 95–112.

Berggren, W.A., Pearson, P.N., 2005. A revised tropical to subtropical Paleogene planktonic foraminiferal zonation. Journal of Foraminiferal Research 35, 279–298.

Berggren, W.A., Kent, D.V., Swisher III, C.C., Aubry, M.-P., 1995. A revised Cenozoic geochronology and chronostratigraphy. In: Berggren, W.A., et al. (Ed.), Geochronology, Time Scales and Global Stratigraphic Correlation: Society for Sedimentary Geology Special Publication, 54, pp. 129–212.

Bernhard, J.M., Sen Gupta, B.K., 1999. Foraminifera of oxygen-depleted environments. In: Sen Gupta, B.K. (Ed.), Modern Foraminifera. Kluwer Academic Press, pp. 201–216.

Bernhard, J.M., Sen Gupta, B.K., Borne, P.F., 1997. Benthic foraminiferal proxy to estimate dysoxic bottom water oxygen concentrations, Santa Barbara Basin, US Pacific continental margin. Journal of Foraminiferal Research 27, 301–310.

Bernhard, J.M., Goldstein, S.T., Bowser, S.S., 2010. An ectobiont-bearing foraminifera, *Bolivina pacifica*, that inhabits microxic pore waters: cell-biological and paleoceanographic insight. Environmental Microbiology 12 (8), 2107–2119.

Bijl, P.K., Houben, A.J.P., Schouten, S., Bohaty, S.M., Sluijs, A., Reichart, G.-J., Sinninghe Damsté, J.S., Brinkhuis, H., 2010. Transient middle Eocene atmospheric CO_2 and temperature variations. Science 330, 819–821.

Bohaty, S.M., Zachos, J.C., 2003. A significant Southern Ocean warming event in the late middle Eocene. Geology 31, 1017–1020.

Bohaty, S.M., Zachos, J.C., Florindo, F., Delaney, M.L., 2009. Coupled greenhouse warming and deep-sea acidification in the Middle Eocene. Paleoceanography 24 (PA2207). http://dx.doi.org/10.1029/2008PA001676.

Boltovskoy, E., Scott, D.B., Medioli, F.S., 1991. Morphological variations of benthic foraminiferal tests in response to changes in ecological parameters, a review. Journal of Paleontology 65, 175–185.

Bosellini, A., 1989. Dynamics of Tethyan carbonate platform. In: Crevello, P.D., James, L.W., Sarg, J.F., Read, J.F. (Eds.), Controls on Carbonate Platform and Basin Platform: Society for Sedimentary Geology (SEPM) Special Publication, vol. 44, pp. 3–13.

Bowen, G.J., Zachos, J.C., 2010. Rapid carbon sequestration at the termination of the Palaeocene–Eocene Thermal Maximum. Nature Geoscience 3, 866–869.

Bradshaw, J.S., 1961. Laboratory experiments on the ecology of foraminifera. Contributions from the Cushman Foundation of Foraminiferal Research, 12 87–106.

Braga, G., De Biase, R., Grünig, A., Proto Decima, F., 1975. Foraminiferi bentonici del Paleocene ed Eocene della sezione di Possano. In: Bolli, H.M. (Ed.), Monografia Micropaleontologica sul Paleocene e l'Eocene di Possagno: Provincia di Treviso, Italia: Schweizerische Palaeontologische Abhandlungen, 97, pp. 87–199.

Buzas, M.A., Culver, S.J., Jorissen, F.J., 1993. A statistical evaluation of the microhabitats of living (stained) infaunal benthic foraminifera. Marine Micropaleontology 29, 73–76.

Cetean, C.G., Setoyama, E., Kaminski, M.A., Neagu, T.R., Bubík, M., Filipescu, and Tyszka, S.J., 2011. Eobigenerina, a cosmopolitan deep-water agglutinated foraminifer, and remarks on late Paleozoic to Mesozoic species formerly assigned to Pseudobolivina and Bigenerina. In: Kaminski M.A., Flipescu S. (Eds.), Proceedings of the Eighth International Workshop on Agglutinated Foraminifera. Grzybowski Foundation Special Publication 16, 19-27.

Cita, M.B., 1975. Stratigrafia della Sezione di Possagno. In: Bolli, H.M. (Ed.), Monografia Micropaleontologica sul Paleocene e l'Eocene di Possagno: Provincia di Treviso, Italia: Schweizerische Palaeontologische Abhandlungen, 97, pp. 9–33.

Corliss, B.H., 1985. Microhabitats of Benthic Foraminifera within deep-sea sediments. Nature 314, 435–438.

Corliss, B.H., Chen, C., 1988. Morphotype patterns of Norwegian Sea deep-sea benthic foraminifera and ecological implications. Geology 16, 716–719.

Coxall, H.K., Wilson, P.A., Palike, H., Lear, C.H., Backman, J., 2005. Rapid stepwise onset of Antarctic glaciation and deeper calcite compensation in the Pacific Ocean. Nature 433 (7021), 53–57.

Diester-Haass, L., Robert, C., Chamley, H., 1998. Paleoproductivity and climate variations during sapropel deposition in the eastern Mediterranean Sea. In: Robertson, A.H.F., Emeis, K.-C., Richter, C., Camerlenghi, A. (Eds.), Proceedings of the Ocean Drilling Program, Scientific Results, 160, pp. 227–248.

Edgar, K.M., Wilson, P.A., Sexton, P.F., Suganuma, Y., 2007. No extreme bipolar glaciations during the main Eocene calcite compensation shift. Nature 448, 908–911.

Edgar, K.M., Wilson, P.A., Sexton, P.F., Gibbs, S.J., Roberts, A.P., Norris, R.D., 2010. New biostratigraphic, magnetostratigraphic and isotopic insights into the Middle Eocene Climatic Optimum in low latitudes. Palaeogeography, Palaeoclimatology, Palaeoecology

297, 670–682.

Fontanier, C., Jorissen, F.J., Licari, L., Alexandre, A., Anschutz, P., Carbonel, P., 2002. Live benthic foraminiferal faunas from the Bay of Biscay: faunal density, composition, and microhabitats. Deep-Sea Research I 49, 751–785.

Fontanier, C., Jorissen, F.J., Chaillou, G., Anschutz, P., Grémare, A., Griveaud, C., 2005. Live foraminiferal faunas from a 2800 m deep lower canyon station from the Bay of Biscay: faunal response to focusing of refractory organic matter. Deep-Sea Research I 52, 1189–1227.

Friedrich, O., 2009. Benthic foraminifera and their role to decipher paleoenvironment during mid-Cretaceous Oceanic Anoxic Events the “anoxic benthic foraminifera paradox”. Revue de Micropaleontologie 177, 2–18.

Friedrich, O., Nishi,H., Pross, J., Schmiedel, G., Hemleben, C., 2005. Millennial-to centennial scale interruptions of the Oceanic Anoxic Event 1b (early Albian, mid Cretaceous) inferred from benthic foraminiferal repopulation events. Palaios 20, 64–77.

Galeotti, S., Krishnan, S., Pagani, M., Lanci, L., Gaudio, A., Zachos, J.C., Monechi, S., Morelli, G., Lourens, L., 2010. Orbital chronology of Early Eocene hyperthermals from the Contessa Road section, central Italy. Earth and Planetary Science Letters 290, 192–200.

Giusberti, L., Coccioni, R., Sprovieri, M., Tateo, F., 2009. Perturbation at the sea floor during the Paleocene-Eocene Thermal Maximum: evidence from benthic foraminifera at Contessa Road, Italy. Marine Micropaleontology 70, 102–119.

Gooday, A.J., 1996. Epifaunal and shallow infaunal foraminiferal communities at three abyssal NE Atlantic sites subject to differing phytodetritus input regimes. Deep-Sea Research I 43, 1395–1421.

Gooday, A.J., 2003. Benthic foraminifera (Protista) as tools in deepwater palaeoceanography: environmental influences on faunal characteristics. Advances in Biology 46, 1–90.

Gooday, A.J., Rathburn, A.E., 1999. Temporal variability in living deep-sea benthic foraminifera. Earth-Science Reviews 46, 187–212.

Green, M.A., Aller, R.C., Aller, J.Y., 1993. Carbonate dissolution and temporal abundances of Foraminifera in Long Island Sound sediments. Limnology and Oceanography 38 (2), 33l–345l.

Grünig, A., 1984. Phenotypic variation in *Spiroplectammina, Uvigerina* and *Bolivina*. Benthos 1983. Second Symposium on Benthic Foraminifera (Pau, April 1983), pp. 249–255.

Grünig, A., 1985. Systematical description of Eocene foraminifera of Possagno (Northern Italy), Sansoain (Northern Spain) and Biarritz (Aquitaine, France). Memorie di Scienze Geologiche 37, 251–302.

Grünig, A., Herb, R., 1980. Paleoecology of late Eocene benthonic foraminifera from Possagno (Treviso-Northern Italy). Cushman Foundation Special Publication 18. 68–85.

Hagn, H., 1956. Geologische und Paläontologische untersuchungen im Tertiär des Monte Brione und seiner umgebung (Gardasee, Ober-Italien). Palaeontographica Abteilung A 107, 67–210.

Hammer, Ø., Harper, D.A.T., Ryan, P.D., 2001. PAST: Paleontological Statistics Software Package for Education and Data Analysis. Palaeontologia Electronica 4 (1) (9 pp., http://palaeoelectronica.org/2001_1/past/issue1_01.htm).

Herguera, J.C., Berger, W.H., 1991. Paleoproductivity from benthic foraminiferal abundance: glacial to postglacial changes in the west equatorial Pacific. Geology 19, 1173–1176.

Hoenisch, B., Ridgwell, A., Schmidt, D.N., Thomas, E., Gibbs, S.J., Sluijs, A., Zeebe, R., Kump, L., Martindale, R.C., Greene, S.E., Kiessling, W., Ries, J., Zachos, J.C., Royer, D.L., Barker, S., Marchitto Jr., T.M., Moyer, R., Pelejero, C., Ziveri, P., Foster, G.L., Williams, B., 2012. The geological record of ocean acidification. Science 335, 1058–1063.

Jones, R.W., Charnock, M.A., 1985. "Morphogroups" of agglutinated foraminifera. Their life positions and feeding habits and potential applicability in (paleo)ecological studies. Revue de Paléobiologie 4, 311–320.

Jorissen, F.J., 1999. Benthic foraminiferal successions across late Quaternary Mediterranean sapropels. In: Rohling, E.J. (Ed.), Fifth decade of Mediterranean paleoclimate and sapropel studies: Marine Geology, 153, pp. 91–101.

Jorissen, F.J., De Stigter, H.C., Widmark, J.G.V., 1995. A conceptual model explaining benthic foraminiferal microhabitats. Marine Micropaleontology 26, 3–15.

Jorissen, F.J., Fontanier, C., Thomas, E., 2007. Paleoceanographical proxies based on deep-sea benthic foraminiferal assemblage characteristics. In: Hillaire-Marcel, C., de Vernal, A. (Eds.), Developments in Marine Geology. : Proxies in Late Cenozoic Paleoceanography, vol. 1. Elsevier, Amsterdam, pp. 264–325.

Jovane, L., Florindo, F., Coccioni, R., Dinare's-Turell, J., Marsili, A., Monechi, S., Roberts, A.P., Sprovieri, M., 2007. The middle Eocene climatic optimum event in the Contessa Highway section, Umbrian Apennines, Italy. Geological Society of American Bulletin 119, 413–427. http://dx.doi.org/10.1130/B25917.1.

Kaiho K., 1991. Global changes of Paleogene aerobic/anaerobic benthic foraminifera and deep-sea circulation. Palaeogeography, Palaeoclimatology, Palaeoecology 83 (1-3), 65-85.

Kaminski, M.A. 1984. Shape variation in Spiroplectammina spectabilis (Grzybowski). Acta Palaeontologica Polonica 29, 29-49.

Kaminski, M.A., Gradstein, F.M., 2005. Atlas of Paleogene Cosmopolitan Deep-water Agglutinated Foraminifera. Gryzbowski Foundation Special Publication 10. 547 (+pp. vii).

Katz, M., Thunell, R., 1984. Benthic foraminiferal biofacies associated with middle Miocene to early Pliocene oxygen-deficient conditions in the eastern Mediterranean. Journal of Foraminiferal Research 14 (3), 187–202.

Katz, M.E., Miller, K.G., Wright, J.D., Wade, B.S., Browning, J.V., Cramer, B.S., Rosenthal, Y., 2008. Stepwise transition from the Eocene greenhouse to the Oligocene icehouse. Nature Geoscience 1, 329–334.

Kitazato, H., Ohga, T., 1995. Seasonal changes in deep-sea benthic foraminiferal populations: results of long-term observations at Sagami Bay, Japan. In: Sakai, H., Nozaki, Y. (Eds.),

Biogeochemical Processes and Ocean Flux Studies in the Western Pacific. Terra Scientific, Tokyo, pp. 331–342.

Koutsoukos, E.A.M., Leary, P.M., Hart, M.B., 1990. Latest Cenomanian–earliest Turonian low-oxygen tolerant benthonic foraminifera: a case study from the Sergipe Basin (N.E. Brazil) and the westernAnglo-Paris Basin (southern England). Palaeogeography, Palaeoclimatology, Palaeoecology 77, 145–177.

Kuhnt,W.,Wiedmann, J., 1995. Cenomanian–Turonian source rocks: paleobiogeographic and paleoenvironmental aspects. In: Huc, A.Y. (Ed.), Paleogeography, Paleoclimate and Source Rocks: American Association of PetroleumGeologists, Studies in Geology, pp. 213–232.

Lear, C.H., Bailey, T.R., Pearson, P.N., Coxall, H.K., Rosenthal, Y., 2008. Cooling and ice growth across the Eocene–Oligocene transition. Geology 36 (3), 251–254.

Levin, L.A., Etter, R.J., Rex, M.A., Gooday, A.J., Smith, C.R., Pineda, J., Stuart, C.T., Hessler, R.R., Pawson, D., 2001. Environmental influences on regional deep-sea species diversity. Annual Review of Ecology and Systematics 132, 51–93.

Loubere, P., 1991. Deep sea benthic foraminiferal assemblage response to a surface ocean productivity gradient: a test. Paleoceanography 6, 193–204.

Loubere, P., 1996. The surface ocean productivity and bottom water oxygen signals in deep water benthic foraminiferal assemblages. Marine Micropaleontology 28, 247–261.

Loubere, P., 1997. Benthic foraminiferal assemblage formation, organic carbon flux and oxygen concentrations on the outer continental shelf and slope. Journal of Foraminiferal Research 27, 93–100.

Loubere, P., Fariduddin, M., 1999a. Quantitative estimation of global patterns of surface ocean biological productivity and its seasonal variation on timescales from centuries to millennia. Global Biogeochemical Cycles 13, 115–133. http://dx.doi.org/10.1029/1998GB900001.

Loubere, P., Fariduddin, M., 1999b. Benthic foraminifera and the flux of organic carbon to the seabed. In: Sen Gupta, B.K. (Ed.), Modern Foraminifera. Kluwer, Dordrecht, pp. 181–199.

Luciani, V., Giusberti, L., Agnini, C., Fornaciari, E., Rio, D., Spofforth, D.J.A., Pälike, H., 2010. Ecological and evolutionary response of Tethyan planktonic foraminifera to the middle Eocene climatic optimum (MECO) from the Alano section (NE Italy). Palaeogeography, Palaeoclimatology, Palaeoecology 292, 82–95. http://dx.doi.org/10.1016/j.palaeo.2010.03.029.

Lunt, D., Ridgwell, A., Sluijs, A., Zachos, J., Hunter, S., Haywood, A., 2011. A model for orbital pacing of methane hydrate destabilization during the Palaeogene. Nature Geoscience 4, 775–778.

Lutze, G.F., Coulbourn, W.T., 1984. Recent benthic foraminifera from the continental margin of Northwest Africa; community structure and distribution. Marine Micropaleontology 8, 361–401.

Martini, E., 1971, Standard Tertiary and Quaternary calcareous nannoplankton zonation. In: Farinacci, A. (Ed.), Proceedings of the 2nd Planktonic Conference, 2, Ed. Tecnoscienza, Roma, pp. 739–785.

Mathelin J.C. and Sztràkos K., 1993. L'Eocène de Biarritz (Pyrénées Atlantiques, SW France). Stratigraphie et paléoenvironment. Monographie des foraminifères. Cahiers de Micropaléontologie 8 (1/2), 5-182.

McInerney, F.A., Wing, S.L., 2011. The Paleocene -Eocene thermal maximum: a perturbation of carbon cycle, climate, and biosphere with implications for the future. Annual Review of Earth and Planetary Sciences 39, 489–516. http://dx.doi.org/10.1146/annurev-earth-040610-133431.

Miller, K.G., Fairbanks, R.G., Mountain, G.S., 1987. Tertiary oxygen isotope synthesis, sea level history, and continental margin erosion. Paleoceanography 2 (1), 1–19.

Miller, K.G., Wright, J.D., Browning, J.V., 2005. Visions of ice sheets in a greenhouse world. Marine Geology 217, 215–231.

Morigi, C., 2009. Benthic environmental changes in the Eastern Mediterranean Sea during sapropel S5 deposition. Palaeogeography, Palaeoclimatology, Palaeoecology 273, 258–271.

Morigi, C., Jorissen, F.J., Gervais, A., Guichard, S., Borsetti, A.M., 2001. Benthic foraminiferal faunas in surface sediments off NWAfrica: relationship with organic flux to the ocean floor. Journal of Foraminiferal Research 31, 350–368.

Murray, J.W., 2001. The niche of benthic foraminifera, critical thresholds and proxies. Marine Micropaleontology 41, 1–7.

Murray, J.W., 2006. Ecology and Applications of Benthic Foraminifera. Cambridge University Press 426 (+pp. xi).

Murray, J.W., 2013. Living benthic foraminifera: biogeographic distributions and the significance of rare morphospecies. Journal of Micropalaeontology 32, 1–58.

Okada, H., Bukry, D., 1980. Supplementary modification and introduction of code numbers to the low-latitude coccolith biostratigraphic zonation (Bukry, 1973; 1975). Marine Micropaleontology 5, 321–325.

Ortiz, S., Thomas, E., 2006. Lower-middle Eocene benthic foraminifera from the Fortuna Section (Betic Cordillera, south-eastern Spain). Micropaleontology 52 (2), 97–150.

Ortiz, S., Gonzalvo, C., Molina, E., Rodriguez-Tovar, F.J., Uchman, A., Vandenberghe, N., Zeelmaekers, E., 2008. Palaeoenvironmental turnover across the Ypresian –Lutetian transition at the Agost section, Southastern Spain: In search of a marker event to define the Stratotype for the base of the Lutetian Stage. Marine Micropaleontology 69, 297–313.

Pagani,M., Zachos, J.C., Freeman, K.H., Tipple, B., Bohaty, S., 2005.Marked decline in atmospheric carbon dioxide concentrations during the Paleogene. Science 309, 600–603. Parisi, G., Coccioni, R., 1988. Deep-water benthic foraminifera at the Eocene–Oligocene boundary in the Massignano section (Ancona, Italy). International Subcommission on Paleogene Stratigraphy, E/O Meeting (Ancona, October 1987) Special Publication II 3, pp. 97–109.

Phleger, F.B., Soutar, A., 1973. Production of benthic foraminifera in three east Pacific oxygen minima. Micropaleontology 19, 110–115.

Pierrehumbert, R.T., 2002. The hydrologic cycle in deep-time climate problems. Nature 419, 191–198.

Schmiedl, G., Mitschele, A., Beck, S., Emeis, K.C., Hemleben, C., Schulz, H., Sperling, M., Weldeab, S., 2003. Benthic foraminiferal record of ecosystemvariability in the eastern Mediterranean Sea during times of sapropel S5 and S6 deposition. Palaeogeography, Palaeoclimatology, Palaeoecology 190, 139–164.

Schroeder, C.J., Scott, D.B., Medioli, F.S., 1987. Can smaller benthic foraminifera be ignored in paleoenvironmental analyses? Journal of Foraminiferal Research 17, 101–105.

Sen Gupta, B.K., Machain-Castillo, M.L., 1993. Benthic foraminifera in oxygen-poor habitats. Marine Micropaleontology 20, 3–4.

Sexton, P.F.,Wilson, P.A., Norris, R.D., 2006. Testing the Cenozoic multisite composite $\delta^{18}O$ and $\delta^{13}C$ curves: new monospecific Eocene records from a single locality, Demerara Rise (Ocean Drilling Program Leg 207). Paleoceanography 21 (2), PA2019.

Silva, K.A., Corliss, B.H., Rathburn, A.E., Thunell, R.C., 1996. Seasonality of living benthic foraminifera from the San Pedro basin, California borderland. Journal of Foraminiferal Research 26, 71–93.

Sluijs, A., Bowen, G.J., Brinkhuis, H., Lourens, L.J., Thomas, E., 2007. The Paleocene–Eocene Thermal Maximum super greenhouse: biotic and geochemical signatures, age models and mechanisms of global change. In: Williams, M., Haywood, A.M., Gregory, F.J., Schmidt, D.N. (Eds.), Deep-time Perspectives on Climate Change: Marrying the Signal from Computer Models and Biological Proxies: The Micropaleontological Society, Special Publication, pp. 323–349.

Spofforth, D.J.A., Agnini, C., Pälike, H., Rio, D., Fornaciari, E., Giusberti, L., Luciani, V., Lanci, L., Muttoni, G., 2010. Organic carbon burial following the Middle Eocene Climatic Optimum (MECO) in the central-western Tethys. Paleoceanography 25, PA3210.

Sprong, J., Kouwenhoven, T.J., Bornemann, A., Schulte, P., Stassen, P., Steurbaut, E., Youssef, M., Speijer, R.P., 2012. Characterization of the Latest Danian Event by means of benthic foraminiferal assemblages along a depth transect at the southern Tethyan margin (Nile Basin, Egypt). Marine Micropaleontology 86–87, 15–31.

Stap, L., Lourens, L.J., Thomas, E., Sluijs, A., Bohaty, S., Zachos, J.C., 2010. High-resolution deep-sea carbon and oxygen isotope records of Eocene Thermal Maximum 2 and H2. Geology 38, 208–210.

Stickley, C.E., St John, K., Koc, N., Jordan, R.W., Passchier, S., Pearce, R.B., Learns, L.E., 2009. Evidence for middle Eocene Arctic sea ice from diatoms and ice-rafted debris. Nature 460, 376–379.

Thomas, E., 1985. Late Eocene to Holocene deep-sea benthic foraminifers from the central equatorial Pacific Ocean. In: Mayer, L., et al., eds., Initial Reports of the Deep Sea Drilling Project, Washington D.C., U.S. Government Printing Office, v. 85, pp. 141–165.

Thomas, E., 2003. Extinction and food at the sea floor: a high resolution benthic foraminiferal record across the Initial Eocene Thermal Maximum, Southern Ocean Site 690. In: Wing, S., Gingerich, P., Schmitz, B., Thomas, E. (Eds.), Causes and Consequences of Globally Warm Climates of the Paleogene: The Geological Society of America Special Paper, vol. 369, pp. 319–332.

Thomas, E., Booth, L., Maslin, M., Shackleton, N.J., 1995. Northeastern Atlantic benthic foraminifera during the last 45,000 years: changes in productivity seen from the bottom up. Paleoceanography 10, 545–562. http://dx.doi.org/10.1029/94PA03056.

Tjalsma, R.C. and Lohmann, G.P., 1983. Paleocene-Eocene bathyal and abyssal benthic foraminifera from the Atlantic Ocean. Micropaleontology Special Publication 4, 1-90.

Toffanin, F., Agnini, C., Fornaciari, E., Rio, D., Giusberti, L., Luciani, V., Spofforth, D.J.A., Pälike, H., 2011. Changes in calcareous nannofossil assemblages during the Middle Eocene Climatic Optimum: clues from the central-western Tethys (Alano section, NE Italy). Marine Micropaleontology 81, 22–31.

Trevisani, E., 1997. Stratigrafia sequenziale e paleogeografia delmargine orientale del Lessini Shelf durante l'Eocene superiore (Prealpi Venete, provincie di Vicenza e Treviso). Studi Trentini di Scienze Naturali. Acta Geologica 71 (1994), 145–168.

Tripati, A., Backman, J., Elderfield, H., Ferretti, P., 2005. Eocene bipolar glaciation associated with global carbon cycle changes. Nature 436, 341–346.

Valiela, I., 1984. Marine Ecological Process. Springer, New York (546 pp.).

Van Morkhoven, F.P.C.M., Berggren, W.A., Edwards, A.S., 1986. Cenozoic Cosmopolitan deep-sea benthic foraminifera. Bullettin des Centres de Recherches Exploration-Production Elf-Aquitane, Mèmoire 11, 11–421.

Van der Zwaan, G.J., Duijnstee, I.A.P., Den Dulk, M., Ernst, S.R., Kouwenhoven, N.T., 1999. Benthic foraminifers: proxies or problems? A review of paleoecological concepts. Earth Science Reviews 46, 213–236.

Winterer, E.L., Bosellini, A., 1981. Subsidence and sedimentation on Jurassic passive continental margin, Southern Alps, Italy. American Association of Petroleum Geologists Bulletin 65, 394–421.

Witkowski, J., Bohaty, S.M.,McCartney, K., Harwood, D.M., 2012. Enhanced siliceous plankton productivity in response to middle Eocene warming at Southern Ocean ODP Sites 748 and 749. Palaeogeography, Palaeoclimatology, Palaeoecology 326–328, 78–94.

Zachos, J.C., Quinn, T.M., Salamy, K.A., 1996. High resolution (104 years) deep sea foraminiferal stable isotope records of the Eocene–Oligocene climate transition. Paleoceanography 11 (3), 251–266.

Zachos, J.C., Pagani, M., Sloan, L.C., Thomas, E., Billups, K., 2001. Trends, rhythms, and aberrations in global climate 65 Ma to present. Science 292, 686–693.

Zachos, J.C., Röhl, U., Schellenberg, S.A., Sluijs, A., Hodell, D.A., Kelly, D.C., Thomas, E., Nicolo, M., Raffi, I., Lourens, L.J., McCarren, H., Kroon, D., 2005. Rapid acidification of the ocean during the Paleocene–Eocene Thermal Maximum. Science 308, 1611–1615.

Zachos, J.C., Dickens, G.R., Zeebe, R.E., 2008. An early Cenozoic perspective on greenhouse warming and carbon-cycle dynamics. Nature 451, 279–283. http://dx.doi.org/10.1038/nature06588.

Zachos, J.C., McCarren, H.K., Murphy, B., Röhl, U., Westerhold, T., 2010. Tempo and scale of late Paleocene and early Eocene carbon isotope cycles: implications for the origin of hyperthermals. Earth and Planetary Science Letters 299 (1–2), 242–249.

CHAPTER III

The Middle Eocene Climatic Optimum (MECO): a multi-proxy record of paleoceanographic changes in the South-East Atlantic

(ODP Site 1263, Walvis Ridge)

F. Boscolo Galazzo[a], E. Thomas[b,d], M. Pagani[b], C. Warren[b], V. Luciani[c], L. Giusberti[a]

To be submitted

a Department of Geosciences, University of Padova, Via G. Gradenigo 6, Italy

b Department of Geology and Geophysics, Yale University, New Haven, CT, USA

c Department of Physics and Earth Sciences, University of Ferrara, Via G. Saragat 1, Italy

d Department of Earth and Environmental Sciences, Wesleyan University, Middletown, CT, USA

Abstract

The Middle Eocene Climatic Optimum (MECO, ~40 Ma) is one of the major and less understood short-term Cenozoic climatic perturbations and interrupted the overall cooling trend of the middle Eocene with a global and transient (~500 Kyr) temperature increase in upper (below thermocline), intermediate and deep ocean waters. In order to investigate the paleoceanographic and paleoenvironmental repercussions of the MECO in an open ocean setting, we performed a multi-proxy study at Ocean Drilling Program Site 1263 (South-Eastern Atlantic). This study represents one of the first multi-proxy investigations of the MECO in a pelagic setting, and provides new insights in this large climatic perturbation. TEX_{86} and $\delta^{18}O$ records indicate a ~4°C total warming throughout the water column. There was no marked Carbon Isotope Excursion (CIE) associated with early warming during MECO, which has been explained by invoking warming due to emission of isotopically non-depleted carbon compounds. At some locations, mainly in the Southern Ocean, there is a short-term CIE during peak MECO warming only. The $\delta^{13}C$ records for Site 1263 do not show this shrt-term (~50 kyr) CIE. This lack of CIE during peak warming could have several explanations, including a lack of recovery of the short CIE interval, or geographic heterogeneity in the $\delta^{13}C$ records.

Foraminiferal mass accumulation rates declined markedly during the MECO, indicating a reduction of both planktic foraminiferal and export productivity. The surface to bottom $\delta^{13}C$ gradients do not indicate major changes in water column stratification, thus the more likely explanation for such a decrease in foraminiferal productivity is that it is was caused by the MECO warming . Such warming might have directly altered pelagic food webs affecting consumers' metabolic rates, remineralization of organic matter in the water column, and eventually the effective flux of organic matter to the sea-floor.

1. Introduction

The Middle Eocene Climatic Optimum (MECO) is a global warming event which, ~40 Ma ago, temporarily interrupted the long-term cooling trend which started at the end of the early Eocene Climate Optimum (EECO, ~49 Ma), and led to the formation of the Antarctic continental ice-sheet by the earliest Oligocene (~34 Ma; Zachos et al., 2001; Zachos et al., 2008; Cramer et al., 2009). The MECO was first recognized as a negative oxygen isotope excursion of ~1‰ in bulk carbonate and benthic foraminiferal tests in Southern Ocean cores (Bohaty and Zachos, 2003), then identified in the Atlantic Ocean, equatorial Pacific and central western Tethys (Jovane et al., 2007;

Bohaty et al., 2009; Edgar et al., 2010; Spofforth et al., 2010), confirming its global extent. The $\delta^{18}O$ records indicate warming of about 4-6°C of deep and intermediate waters, with a gradual onset followed by brief peak temperatures, then a rapid return to pre-event temperatures. High-resolution stratigraphic analysis and development of an orbitally tuned age model for cores from Site 1260 (tropical west Atlantic) resulted in an age estimate for the gradual warming of ~40.45-40.05 Ma, i.e., a duration of ~415 kyr, with peak warming at 40.05 $\pm$ 0.02 Ma (Westerhold and Röhl, 2013). The MECO occurred during a very long eccentricity cycle minimum, i.e., a time of relatively low seasonality and possibly low monsoonal precipitation. Aridification in central Asia initiated during the MECO acme and continued afterwards (Bosboom et al., 2014).

The duration of the MECO and its pattern of slow and gradual warming, punctuated by a rapid peak warming followed by abrupt cooling, differentiate it from the upper Paleocene-lower Eocene hyperthermal events, which are characterized by a more symmetrical pattern of warming and cooling with a duration of a few tens of thousands years, and generally occur during eccentricity maxima (Thomas and Zachos, 2000; Cramer, 2003; Bohaty et al., 2009; Bowen and Zachos, 2010; Galeotti et al., 2010; Stap et al., 2010; Zachos et al., 2010). Warming during these earlier hyperthermals was coeval with a negative carbon isotope excursion (CIE) and carbonate dissolution resulting from deep-sea ocean acidification (Zachos et al., 2005; Lunt et al., 2011; McInerney and Wing, 2011; Hoenisch et al., 2012). The combination of warming, acidification, and a negative carbon excursion indicates that these hyperthermals were caused by geologically rapid release of isotopically light carbon compounds into the ocean-atmosphere system (Zachos et al., 2005; 2008; McInerney and Wing, 2011; Hoenisch et al., 2012), but the rate, amount, source and release mechanism are still debated (Dickens, 2011; Zeebe and Zachos, 2013).

The MECO does not have such an unequivocal signature of isotopically light carbon release into the ocean-atmosphere system. The bulk and benthic $\delta^{13}C$ records in marine carbonates show considerable geographic and bathymetric variability, but usually are characterized by rising rather than declining $\delta^{13}C$ values during the gradual warming, with a transient, ~0.5‰ negative CIE with a duration of about 50 kyr during peak warming at some sites, but not pronouncedly present at others (Bohaty et al., 2009; Edgar et al., 2010; Westerhold and Röhl, 2013). As to ocean acidification, the MECO coincided with a widespread, ~1 myr long decrease in carbonate mass accumulation rate (MAR) at sites at depths greater than 3000 m in the Indian Ocean and SE Atlantic Oceans (Peterson and Backman, 1990; Bohaty et al., 2009). In the Pacific, the carbonate mass accumulation rates declined during MECO at sites below 2000 m depth (Hancock and Dickens, 2005; Bohaty et al., 2009).

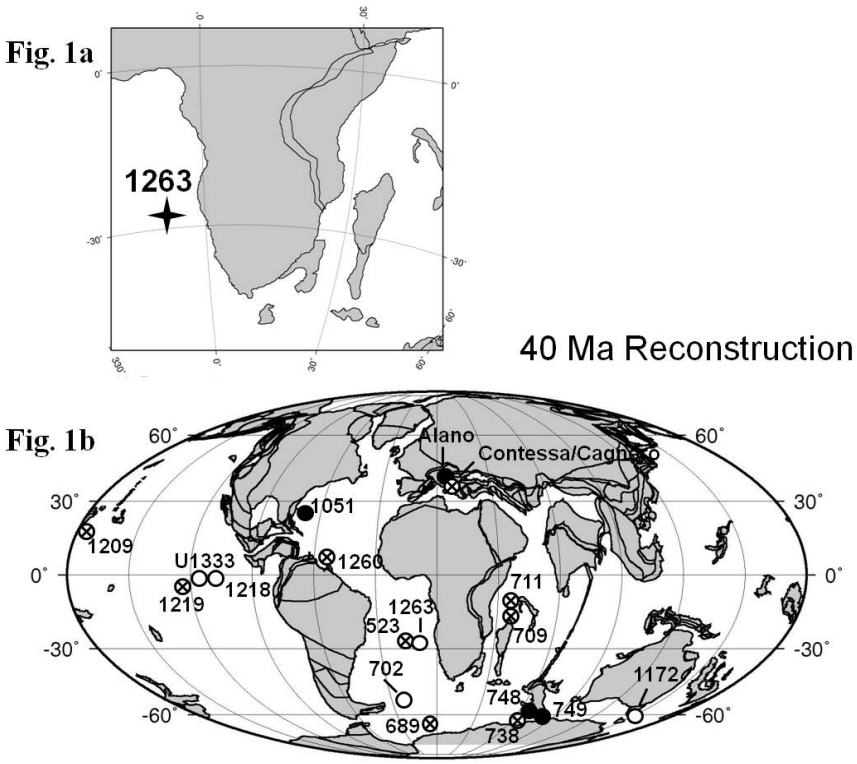

Figure 1. (a) Paleogeographic reconstruction showing the location of ODP Site 1263. (b) Paleogeographic reconstruction showing oceanic (ODP - DSDP) sites and onland sections where the MECO has been described. Sites with inferred increased productivity during the MECO are labeled with solid circles, sites with inferred decreased or unchanged productivity are labeled with open circles, sites where no data are available are labeled with open circles with a cross. Approximate positions at 40 Ma are plotted on a paleogeographic reconstruction from the Ocean Drilling Stratigraphic Network (GEOMAR, Kiel, Germany).

The Calcium carbonate Compensation Depth (CCD) shallowed from ~4100 to ~3200 m depth (Pälike et al., 2012), preservation of nannofossils worsened (Toffanin et al., 2013), and carbonate-shelled benthic foraminifera markedly decreased in abundance (Takata et al., 2013). This rise of the CCD occurred in the 2 myr interval between Carbonate Accumulation Events CAE-3 and CAE-4 (Lyle et al., 2005, 2008; Pälike et al., 2012), but the warming has not been unequivocally recognized at all Pacific sites, possibly due to low sediment accumulation rates (e.g., Dawber and Tripati, 2011). The MECO thus coincided with one of several episodes of shallowing of the CCD superimposed on a longer-term trend of falling CCD in the Pacific Ocean (Pälike et al., 2012).

The duration of MECO (~415 kyr) is too long for an episode of ocean acidification, since at these time scales ocean acidification would have been buffered, according to carbon cycle models (e.g., Ridgwell and Schmidt, 2010; Hoenisch et al., 2012; Sluijs et al., 2013). In conclusion, the MECO has been argued to be a global carbon cycle perturbation with warming caused by rising CO_2 levels (Bijl et al., 2010), but the lack of a CIE contemporaneous with the warming combined with its duration causes MECO to remain poorly understood (Sluijs et al., 2013). The ~40-50 kyr

(Westerhold and Röhl, 2013) peak event of MECO could have been equivalent to a hyperthermal event, with combined peak warmth, CIE and carbonate dissolution due to emission of isotopically light carbon compounds into the exospheric carbon cycle, but this would have been superimposed on a longer period of warming, e.g., at the crossing of a threshold level of warming, with the full MECO a more complex event.

Only few studies have focused on MECO's paleoenvironmental and paleobiotic consequences, including studies on an Italian section in western Tethys deposited at middle-bathyal paleodepth, (Spofforth et al., 2010; Luciani et al., 2010; Toffanin et al., 2011; Boscolo Galazzo et al., 2013, see Chapter 2). Data from this Tethyan site record higher export productivity during peak and after the MECO (Boscolo Galazzo et al., 2013). Preliminary benthic foraminiferal data indicate increased productivity at peak MECO at Site 1051 as well (NW Atlantic; Moebius et al., 2013), and siliceous phytoplankton responded to MECO by increased productivity at Southern Ocean Site 748 and 749 (Indian Ocean sector; Witkowski et al., 2012). At Site 748, preliminary data on benthic foraminiferal assemblages and a sedimentary Cerium-anomaly suggest decreased bottom water oxygenation coinciding with peak-MECO, increased productivity and export productivity during the full MECO (Moebius et al., 2013). The MECO event led to a significant crisis of muricate planktic foraminifera (acarininids and morozovelloids; Luciani et al., 2010; Edgar et al., 2012), and temporary loss of photosymbionts (bleaching) in *Acarinina* (Edgar et al., 2012).

In contrast, dinocyst data for ODP Site 1172, in a marginal marine shelf area at southern high latitudes, indicate lowered productivity (Bijl et al., 2010). Calcareous nannofossil assemblages suggest increased oligotrophy as well at Site 702 (Subpolar South Atlantic) at peak-MECO (Pea, 2011). The Pacific CAEs have been argued to be high productivity events (as confirmed by tentative benthic foraminiferal data; Takata et al., 2013), with MECO in between two such events being a relatively low productivity event at equatorial Pacific sites (Lyle et al., 2005; 2008). The record of oceanic productivity during the MECO thus indicates geographic variability (Fig. 1).

Further studies in multiple ocean basins and across depth transects are necessary to gain a global picture of MECO, the magnitude, bathymetric and geographic extent of warming, carbonate dissolution and the transient CIE during peak MECO, and its potential causes and ecological consequences, especially oceanic productivity. We present multiproxy data across the MECO at ODP Site 1263, in the mid-latitude southeastern Atlantic Ocean (Walvis Ridge, Zachos et al., 2004; Bohaty et al., 2009). We generated stable oxygen and carbon isotopic records for benthic and planktic foraminifera, in order to investigate the expression of the event throughout the water column. To evaluate relative sea surface temperature (SST) changes during the MECO, we generated TEX_{86} data, because planktic foraminifera in carbonate oozes generally are recrystallized

on the sea floor at low temperatures, and give temperatures lower than those in upper ocean waters (Schrag et al., 1995; Schrag, 1999; Pearson et al., 2001; 2007). Carbon isotope records were used to infer changes in ocean stratification, and compared with benthic foraminiferal accumulation rates (BFAR). This study is the first multi-proxy investigation of the MECO in a SE Atlantic, open ocean setting, and aims to improve our understanding of this climatic perturbation and its paleoceanographic and paleoecological repercussions.

2. Location and setting

ODP Site 1263 (28°53' S; 2°78' E, modern water depth 2717 m; ~800 km off the coast of Africa) was drilled during ODP Leg 208 on the north-facing flank of Walvis Ridge (SE Atlantic Ocean; Zachos et al., 2004), in between the Cape Basin to the south and the Angola basin to the north (Figs. 1, 2).

Presently, Site 1263 lies beneath the eastern part of the central subtropical gyre outside the eastern boundary current with its associated regions of high productivity. The seafloor at Site 1263 is bathed by Antarctic Intermediate Water (AAIW), whereas North Atlantic Deep Water (NADW) is present at slightly greater depths (Klevenz et al., 2008). The Site 1263 location is characterized by a mean annual sea surface temperature of 20.8°C, with the highest temperature of ~24°C during the Austral summer and the lowest winter temperature about 18°C. At 2500 meters depth, the temperature is about 2.5°C (Levitus, 1994). Mixed layer depth varies between 5.5 and 133.5 meters, with minimum values during the Austral summer and maximum values during the Austral winter (Levitus, 1994).

In the middle Eocene, Site 1263 was at a paleodepth of about 2000 m (Zachos et al., 2004), and likely bathed by a southern-sourced intermediate to deep water mass (Via and Thomas, 2006; Thomas and Via; 2007; Stap et al., 2010). Eocene sediments at Site 1263 are nannofossil ooze, foraminifer-bearing nannofossil ooze, clay-bearing nannofossil ooze, and chalky nannofossil ooze, with a low concentration of total organic carbon (TOC 0.86–0.00 wt%; mean = 0.09 wt%; Zachos et al., 2004). Sediments vary in color between light gray and gray at decimeter scale, with white, 1-4 cm 'blebs' surrounded by dark haloes containing fine-grained black to brown oxides, which may be burrows (Zachos et al., 2004).

We selected Site 1263 for our study of the MECO because it has a complete and relatively expanded record across MECO (average linear sedimentation rate for the studied interval: 0.76 cm/k.y.; Bohaty et al., 2009), and well-constrained nannofossil biostratigraphy (Fornaciari et al., 2010). The bulk oxygen isotope record shows that the MECO occurs between 142.5 and 137.9 mcd,

with the peak event at 138.7 - 137.9 mcd, and a brief recovery phase ending at 137.4 mcd (Bohaty et al., 2009). The bulk $\delta^{13}C$ record shows a slight increase at the start of MECO followed by fluctuations, with one, slight, negative excursion coinciding with the peak $\delta^{18}O$ values. The $CaCO_3$% values fluctuate around 90% throughout the studied interval, without significant decrease during MECO (Bohaty et al., 2009).

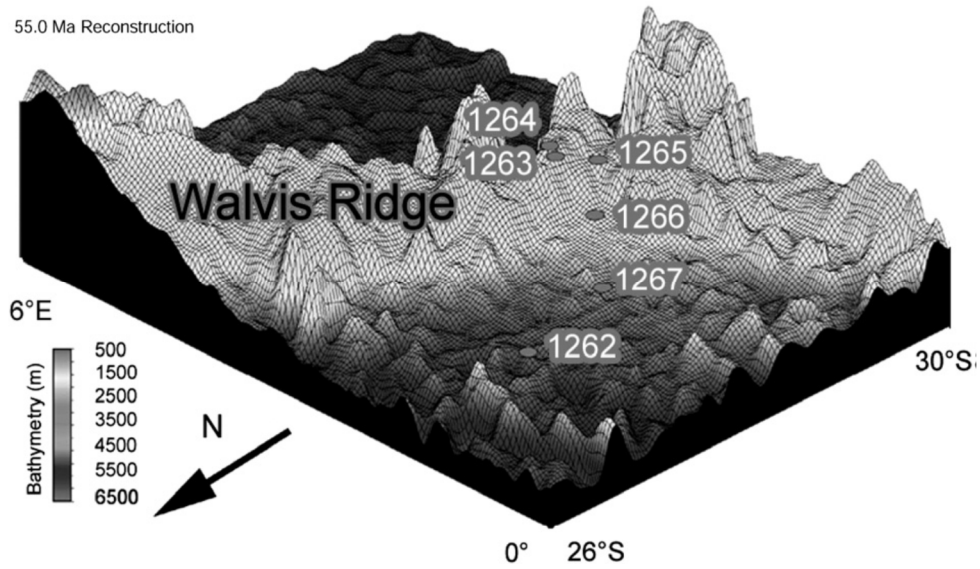

Figure 2. Three-dimensional diagram of the Leg 208 drill site locations (modified after Zachos et al., 2004).

3. Methods

We generated bulk $CaCO_3$ and TEX_{86} data on 46 samples (Appendix 3). The bulk isotope record has a 20 cm resolution within the MECO, 40 cm above and below. An additional set of 34 samples spaced at 40 cm was used for foraminiferal stable isotope analysis and accumulation rate calculations (Appendix 3).

3.1. Stable isotope measurements

Samples were air-dried and weighed, disaggregated in de-ionized water, and washed through sieves with mesh size ≥38, ≥63 and ≥500 μm. The size fraction larger than 63 μm was weighed and split in two equal parts with a precision micro-splitter. One half was used for hand-picking and isotopical analyses of foraminifera, the other for quantitative faunal analysis (Chapter 4), of which only benthic foraminiferal accumulation rates will be used in this chapter. Benthic foraminiferal stable isotope records ($\delta^{13}C$ and $\delta^{18}O$) were generated for the species *Nuttallides truempyi*, following taxonomy as outlined by van Morkhoven et al. (1986). This Late Cretaceous-Paleogene species underwent diachronous extinction by the late Eocene–earliest Oligocene (Berggren and Aubert, 1976; Tjalsma and Lohmann, 1983; Thomas, 1985). It is considered to have been epifaunal because of its morphology, the epifaunal microhabitat of its modern descendant *Nuttallides umbonifera* (Thomas, 1998; 2007), and its carbon isotope values (Thomas and Shackleton, 1996; Katz et al., 2003). Planktic foraminiferal stable isotope records ($\delta^{13}C$ and $\delta^{18}O$) were generated on mixed species of the surface-dwelling, photosymbiont-bearing genus *Acarinina* (Pearson et al., 2006; Ezard et al., 2011). We tried to consistently select the species *Acarinina topilensis*, *A. praetopilensis* and *A. pseudotopilensis* to limit inter-specific variability, but this was not always possible due to the drastic decrease in abundance of muricate planktic foraminifera in the peak-MECO interval and somewhat higher in the core.

Benthic and *Acarinina* stable isotope analyses were carried out on *N. truempyi* and *Acarinina* specimens handpicked from the size fraction between 250 and 180 μm, from samples between 145 to 132 meter composite depth (mcd). We also generated a stable isotope record at 40 cm resolution for the mixed layer genus *Globigerinatheka* (e.g., Pearson et al., 2006) for the 145-136 mcd interval, picked from the ≥500 μm size fraction.

Bulk $CaCO_3$ stable isotopes were generated for the interval between 147-132 mcd. Bulk and foraminiferal samples were analyzed for $\delta^{18}O$ and $\delta^{13}C$ isotopes by acid digestion using an individual vial acid drop ThemoScientific Kiel IV carbonate device interfaced to Thermo Scientific MAT-253 dual-inlet isotope ratio mass spectrometer (IRMS) at University of California, Santa Cruz. Samples were reacted at 75°C in orthophosphoric acid (specific gravity = 1.92 g/cm3) to generate carbon dioxide and water. During this procedure, water is cryogenically removed from CO_2 and non-condensable gases are pumped away, prior to introduction of the purified CO_2 into the IRMS.

During a run sequence, calibrated in-house standard Carrera Marble is used to correct the data including a drift correction. Four NBS-18 limestone standards are used in conjunction with Carrera

Marble to correct for instrument specific source ionization effects. Two NBS-19 limestone samples are run "as-a-sample" to monitor quality control and long-term performance. Carrera Marble has been extensively calibrated against NIST Standard Reference Materials (NBS-19, NBS-18, and LSVEC) and as part of intercomparison studies with other stable isotope laboratories. Corrected delta values are expressed relative to international standards PDB (PeeDee Belemnite) for $\delta^{13}C$ and $\delta^{18}O$.

To compare our records with those in Bohaty et al. (2009), oxygen isotope values were converted to paleotemperature using the equation of Shackleton (1974), assuming a global mean $\delta^{18}O$ for seawater ($\delta^{18}O_{sw}$) of -1.0‰, representing an ice free world (Zachos et al., 1994; Huber et al., 2003; Burgess et al., 2008; Bohaty et al., 2009). An ice-free world is a working-hypothesis; the presence of small to moderate continental ice-sheet over Antarctica cannot be ruled out for this time period (Tripati et al., 2005; Edgar et al., 2007; Dawber and Tripati, 2011; Bohaty et al., 2009).

3.2. Tetraether Lipid Analysis

Samples were processed and analyzed for tetraethers in the Organic Biogeochemistry and Paleoclimatology Laboratory at Yale University following Schouten et al. (2002; in press). Compounds were extracted from freeze-dried sediment samples with a soxhlet extractor using a 2:1 dichloromethane:methanol solvent mixture. The lipid extracts were then separated into apolar, ketone, and polar fractions via silica gel pipette column chromatography. Glycerol dialkyl glycerol tetraether (GDGT) lipids were further purified via alumina pipette chromatography and filtered through 0.45 µm glass fiber filters. GDGTS were analyzed by high-performance liquid chromatography mass spectrometry (HPLC/MS) on an Agilent 1100 series LC/MSD. A Prevail Cyano column was used with 99:1 hexane:isopropanol as eluent. TEX_{86} values were calculated using the equation (Schouten et al. (2002):

$$TEX_{86} = [GDGT2 + GDGT3 + crenarchaeolregioisomer]/$$
$$[GDGT1 + GDGT2 + GDGT3 + crenarchaeolregioisomer]$$

Different calibrations are used to derive temperature estimates from GDGTs analysis (e.g., Pearson & Ingalls 2013). Kim et al. (2010) recommend the use of the TEX^{H}_{86} for SSTs range above 15°C, implying it would be appropriate for the middle Eocene subtropics, but Hollis et al. (2012) show the best fit among Eocene low-latitudes SSTs derived from carbonate proxies and >0.85

TEX_{86} values occurs with the Liu et al. (2009) calibration. We thus used both the high-temperature logarithmic calibration of Kim et al. (2010):

$$SST = 68.4[\log(TEX_{86})] + 38.6,$$

and the non-linear calibration of Liu et al. (2009):

$$SST = 50.475 - 16.332(1/TEX_{86})$$

The Branched and Isoprenoid Tetraethers Index, a proxy for terrestrial organic matter input was calculated following Hopmans et al. (2004), in order to evaluate the potential for terrestrial organic matter input biasing the TEX_{86} – derived temperatures:

$$BIT = [I + II + III]/[I + II + III] + IV,$$

where compounds I, II, and III are branched GDGTs primarily derived from soil-dwelling bacteria, and compound IV is crenarchaeol, an isoprenoidal GDGT primarily derived from marine Archaea, a compound distinct from the crenarchaeol regioisomer used in the calculation of TEX_{86}.

3.3. Foraminiferal Accumulation Rates Calculation

The benthic foraminiferal accumulation rate (BFAR) was calculated from the numbers present in representative splits of the size fraction ≥63 μm containing a total number of benthic foraminiferal specimens ≥400, then corrected to the weight of bulk sediment. We calculated the coarse fraction as the weight ratio of the dry ≥63 μm size fraction to the bulk dry sediment weight. The fine fraction was calculated as the weight ratio of the bulk dry sediment minus the coarse fraction weight, to the bulk dry sediment. Coarse and fine fractions accumulation rates (CFAR and FFAR) were calculated using linear sedimentation rates (LSR) and dry bulk density (DBD). Linear sedimentation rates (LSR; cm/kyr) were derived from the age model in Bohaty et al. (2009). Dry bulk density (DBD; g/cm^3) was estimated by extrapolating the density values for the studied interval (Zachos et al., 2004), which show little variability. The benthic foraminiferal accumulation rate (BFAR) was calculated following Herguera and Berger (1991):

$$BFAR\ (number\ of\ specimens\ cm^{-2}\ kyr^{-1}) = N/g * LSR*DBD,$$

where N/g is the number of benthic foraminifera per gram dry bulk sediment, LSR is the linear sedimentation rate (cm/kyr) and DBD is the dry bulk density (g/cm^3).

The BFAR is a proxy for total organic matter flux reaching the seafloor (e.g., Gooday et al., 2003; Jorissen et al., 2007), because benthic foraminifera rely on the organic matter produced in the surface and exported down in the water column. The organic flux reaching the sea floor is a function of primary productivity and remineralization of organic matter in the water column (e.g., Henson et al., 2012; Arndt et al., 2013). We used CFAR as an approximation of the planktic foraminiferal accumulation rates, because in pelagic sediments not significantly affected by dissolution this fraction dominantly consists of planktic foraminifera (Diester-Haass, 1995). In typical oceanic calcareous oozes dominantly constituted by calcareous nannofossils, FFAR can, with some caution, be considered indicative of the calcareous nannofossils accumulation rate.

3.4. Chronology

We used the age model adopted by Bohaty et al. (2009). A reliable magnetostratigraphy is not available for Site 1263, and this age model was derived through correlation with sites with a well-constrained magnetostratigraphy. We report data as a function of depth (meter composite depth, mcd) and age (Berggren et al., 1995; Cande and Kent 1995). Time resolution across the MECO is of 25 kyr for the bulk record and 50 kyr for the foraminiferal records.

4. Results

4.1. Oxygen Isotope Records

The MECO negative $\delta^{18}O$ excursion is markedly present in the benthic, bulk and *Globigerinatheka* records. In contrast, the *Acarinina* record does not show an excursion, but only fluctuations of about -0.4‰ from the base of the studied interval up to 136.8 mcd (Fig. 3). Above that level, values fluctuate, but generally increase slightly to the top of the studied section. The *Globigerinatheka* $\delta^{18}O$ values decrease upward from the beginning of the record (145 mcd), with a series of fluctuations towards progressively lower values. The increase becomes more pronounced at ~140.4 mcd, with the lowest values at 139.6 - 138.4 mcd, for a total excursion of -0.9‰ (~4°C), from 0.4 to -0.5‰. The record shows a rapid recovery to pre-excursion values within 40 cm (138.4 - 138 mcd), corresponding to ~60 kyr (Fig. 3).

Our bulk $\delta^{18}O$ data closely match those in Bohaty et al. (2009), with stable values around 0.5‰ from the base (147 mcd; 41.2 Ma) up to ~142.60 mcd. From there on, values gradually decrease upwards to ~139 mcd, where a sharp negative shift of ~0.4‰ is recorded. The minimum value occurs at 138.7-138.1 mcd, and the overall excursion is -1‰ (corresponding to 4°C; Fig. 3). Values recover rapidly above that level, to reach pre-event values at 137.4 mcd, 70 cm (100 kyr) above the minimum value. Between 137.3 and 136 mcd, $\delta^{18}O$ values start to increase gradually to the top of the studied interval (Fig. 3). The benthic foraminiferal $\delta^{18}O$ record on *Nuttallides truempyi* is stable, fluctuating around about 0.6‰, from the base up to ~140.8 mcd, and then values markedly decrease upward, with minima at 138.4 - 138 mcd, reaching a total excursion of -0.9‰ (Fig. 3). The maximum temperature excursion is 4°C, from 9.5 to 13.5°C. The recovery starting at 138 mcd reaches pre-excursion values at 136 mcd, 200 cm (270 kyr) above the peak minimum values (Fig. 3).

The main phases of the MECO, i.e., its onset, peak-warming and termination appear to be recorded at slightly different times in the different records, with the *Globigerinatheka* record showing the changes first, followed by the bulk and then the *N. truempyi* record (Fig. 3). In addition, the MECO and peak warming apparently have a shorter duration in the benthic and bulk data than in the *Globigerinatheka* record. The recovery to pre-excursion values is very sharp in the *Globigerinatheka*, record, progressively slower and more gradual in the bulk and *N. truempyi* record (Fig. 3).

The magnitude of the change in $\delta^{18}O$ values during MECO warming is the same (~4°C) in the benthic, bulk and *Globigerinatheka* records, but the shape of the excursion differs. The benthic record shows a more rapid decrease, and a more gradual recovery than the *Globigerinatheka* and bulk records, and the benthic excursion has thus a more symmetrical shape than those in bulk carbonate and planktic foraminifera (Fig. 3). $\delta^{18}O$ values of bulk and benthic foraminifera are similar (Fig. 3-4), with values after the MECO excursion heavier in bulk than in *N. truempyi*. *Globigerinatheka*, a surface dweller genus that formed a late ontogenetic (possibly gametogenic) calcite crust deeper in the water column (Sexton et al., 2006; Premoli Silva et al., 2006; Burgess et al., 2008), yields generally slightly lower values than *N. truempyi* and bulk (Fig 3-4). *Acarinina*, a photosymbiont-bearing genus calcifying within the mixed layer, has somewhat lighter $\delta^{18}O$ values above and below the MECO interval, but because of the lack of an excursion in its record the values overlap with the *Globigerinatheka*, bulk and *N. truempyi* records in this interval (Fig. 4).

4.2. TEX_{86} record and BIT index

Isoprenoid GDGTs containing cyclopentane rings have very low abundances over the studied interval. Despite analysis of large (50 cm^3) samples, only 29 of the 46 samples analyzed for isoprenoid GDGTs were above the detection limit, with samples between 147 to 143 mcd and from 138 mcd up to the top of the studied interval generally below this limit. The abundance of marine GDGTs was somewhat higher between 142 – 138 mcd, coincident with the MECO.

Using the high temperature calibration of Kim et al. (2010), TEX_{86} values around 0.76 between 147 and 145.22 mcd imply a mean surface temperature of ~30.5°C (Fig. 3). A gradual increase upsection of 0.4 in TEX_{86} values occurs between ~144.8 mcd and 142 mcd, implying warming from 30.5 to 33°C (Fig. 3). From 141.5 mcd upward, TEX_{86} derived SST shows an abrupt further increase of 1°C. Higher in the section there are strong fluctuations, with a large decrease (from 0.9 to 0.7) between ~140 and 138.7 mcd, followed upwards by rapid recovery to the highest temperature recorded of ~34.5°C between 138.7 and 138.3 mcd, followed by a rapid decrease to 29°C (Fig. 3).

The total maximum SST excursion applying the high temperature calibration of Kim et al. (2010) is 4.5°C (Fig. 3). The use of the calibration of Liu et al. (2009) results in the same trend, but lower overall temperatures and less warming (3°C, from background 29 to 32°C at peak-warmth). The temperature difference between the two methods is within the calibration errors in our data (Liu et al., 2009; Kim et al., 2010). Both temperatures are much higher than those estimated from $\delta^{18}O$ values, although the size of the excursion is similar. The surface temperatures are considerably warmer than those reported for Eocene Thermal Maximum 2 from a single TEX_{86} data point integrated over 35 cm of sediment at Site 1263 (~25°C; Stap et al., 2010, using both the Kim et al., 2010 and Liu et al., 2009 calibrations).

The BIT index has very high values in all samples, reaching 0.8 in some (mean 0.55). Such high values are usually found in coastal environments in close proximity to a large fresh water influx carrying terrestrially derived organic matter (Hopmans et al., 2004; Smith et al., 2012). A BIT index >0.3 has been described as implying that TEX_{86} temperature estimates are compromised due to the presence of soil-derived isoprenoid GDGTs (Weijers et al., 2006). We argue, however, that for our Site 1263 data it is unrealistic to assume that a large amount of land derived organic matter caused the BIT index to be above 0.5, as it is an open ocean setting ~800 km away from land (Moore et al., 1984), characterized by low TOC (~0.09 wt%; Zachos et al., 2004). None of the samples had above detection limit long chain *n*-alkanes with odd-over-even carbon predominance, indicative of a terrestrial higher plants origin, indicating that it is improbable that a large amount of organic matter was laterally advected and reached Site 1263. In addition, the correlation coefficient between the BIT index and TEX_{86} is statistically not significant (R^2=0.1763) (Huguet et al., 2009).

We therefore interpret the high BIT index values as caused by the very low abundance of isoprenoid GDGTs, and do not think our SSTs are biased by soil derived isoprenoid GDTGs.

4.3. Carbon Isotope Records

Due to photosynthetic activity preferentially taking up isotopically light carbon in the photic zone, and the action of the biological pump moving organic matter to the sea floor, the $\delta^{13}C$ values of bulk carbonate (dominantly calcareous nannofossils) and planktic foraminifera are expected to be heavier than those of benthic foraminifera. In most samples, the mixed layer dweller *Acarinina* indeed has heavier values than the deeper calcifying *Globigerinatheka*, and bulk values reflect thermocline depths, with the benthic values ~1.5‰ heavier (Fig. 4).

The *Acarinina* $\delta^{13}C$ record, as its $\delta^{18}O$ record, shows no trend with depth in core, only fluctuations (Fig. 4). The *Globigerinatheka* $\delta^{13}C$ record from the base to ~142 mcd shows slight fluctuations (-0.2‰) around an average value of 2.5‰, then an increase from ~141.4 mcd culminating at ~139.5 mcd, with peak values of 3‰, coinciding with the lowest $\delta^{18}O$ values. Higher in the record, the $\delta^{13}C$ values decrease, but remain higher than pre-event throughout the studied interval (Fig. 4). The bulk $\delta^{13}C$ record shows minor (0.2‰) fluctuations around a mean value of 2.2‰ from the base up to 137.8 mcd, with minimum $\delta^{18}O$ values coinciding with a negative fluctuations (Fig. 4). At 137.8 mcd, the bulk $\delta^{13}C$ values increase up-section by about a 0.5‰, and then remain stable throughout the studied interval (Fig. 4). The benthic $\delta^{13}C$ record shows an increase starting from ~144 to ~141 mcd, and then remains stable with a small decline at ~138 mcd, the top of the MECO interval, where the maximum negative $\delta^{18}O$ excursion occurs. Above this short excursion the values increase, then remains stable, fluctuating around 1.2 ‰ (Fig. 4).

Overall, the $\delta^{13}C$ records of *Globigerinatheka*, benthic and bulk gradually become isotopically heavier upwards in the section. The $\delta^{13}C$ increase coincides with the MECO oxygen isotope excursion to lighter values in the benthic and *Globigerinatheka* records, whereas the increase starts above the MECO interval in the bulk record. In contrast to records for other sites (e.g., Southern Ocean Sites 738 and 738; Bohaty et al., 2009; Sluijs et al., 2013; Fig. 5), there is no short negative CIE in any of the records corresponding to peak warming (minimum in the $\delta^{18}O$ records) at Site 1263, although the bulk and benthic records shows a minor decrease at the top of the MECO interval (~138 mcd; Fig. 4).

4.4. Foraminiferal and Fine Fraction accumulation rates

Benthic foraminiferal and coarse fraction accumulation rates covary throughout the studied interval. From the base of the studied interval, both CFAR and BFAR increase, reaching peak values at about 142-141 mcd. Values then decrease upsection, reaching a minimum at about 139 mcd, the interval of peak MECO warming. Above this interval values fluctuate around stable values (Fig. 6).

FFAR stably fluctuates throughout the studied interval (Fig. 6).

5. Discussion

5.1. Temperature anomaly

The planktic foraminiferal assemblage at Site 1263 is moderately well-preserved, with tests exhibiting a "frosty" state of preservation (Sexton et al., 2006). Planktic foraminifera in carbonate ooze, as at Site 1263, and as contrasted with clay-rich sediment, generally are diagenetically altered, giving apparent sea surface temperatures which have been lowered due to diagenesis and recrystallization at the much lower temperatures on the sea floor (e.g., Schrag et al., 1995; Schrag 1999; Pearson et al., 2001; Stap et al., 2010; Kozdon et al., 2011). The observation that $\delta^{18}O$ values in the mixed layer dwelling *Acarinina*, in the subsurface dweller *Globigerinatheka*, in bulk carbonate, and in benthic foraminifera, differ by less than the $\delta^{18}O$ equivalent of ~2-3°C maximum indicates that recrystallization has indeed been severe, in agreement with observations on nearby Site 525 (Schrag et al., 1995). These differences are observed at levels below and above the MECO interval only, disappearing during the event, due to the lack in excursion in the $\delta^{18}O$ record of *Acarinina* (Fig. 4).

The *Acarinina*-derived temperatures (mixed layer) appear to be the most compromised, because there is no excursion during the MECO-interval, despite observations that excursions may remain in the record even during major recrystallization (Sexton et al., 2006). Possibly, their tests are more porous and thus more easily recrystallized than those of *Globigerinatheka* (Sexton et al., 2006). *Acarinina* were less abundant during MECO (Degasperi, master thesis in progress), so it is possible that the lack of excursion is in part caused by bioturbational mixing of pre- and post-event specimens from the layers with more abundant *Acarinina*.

Globigerinatheka is considered a mixed-layer dweller symbiont-bearing genus (Pearson et al. 1993; Pearson et al. 2001; Wade and Kroon, 2002). However, carbon and oxygen isotopes derived from its tests often display values indicative of deeper waters (Wade, 2004; Sexton et al., 2006; Burgess et al., 2008; present study, Fig. 4), and a late-stage calcification has been inferred for this genus, with $CaCO_3$ crusts formed deeper in the water column (Pearson et al., 2001; Premoli-Silva et al., 2006). Due to the important component of deeper water calcite in its test, *Globigerinatheka* can be considered largely a subsurface waters indicator yielding information about depths between the mixed-layer and the thermocline (Boersma et al., 1987; Wade, 2004; Sexton et al., 2006).

A subsurface depth habitat for *Globigerinatheka* has been also inferred from boron isotopes analysis (Pearson and Palmer, 1999).

Accordingly, we consider *Globigerinatheka* as an indicator of subsurface waters. However, the heavy $\delta^{18}O$ values displayed by our record are not completely explained by a subsurface depth habitat (Hollis et al., 2012), and likely reflect a combination of diagenetic alteration and subsurface isotopic signature. The major constituents of the pelagic sediments at Walvis Ridge are calcareous nannofossils, as shown by the very high FFAR as compared to CFAR (Fig. 6). The bulk oxygen and carbon isotopic record should therefore reflect primarily the isotopic composition of the lower photic zone where these organisms dominantly calcify (Stoll, 2005; Stap et al., 2009).Even at the maximum observed distance between the surface $\delta^{18}O$ values and the benthic values, before the MECO, the bottom water temperature was about 12°C, whereas surface temperature would have been ~14°C, without considering the effects of recrystallization (Fig. 4). This difference is even smaller than that recognized for ETM2 at Site 1263, about 4°C (Stap et al., 2010). Such an apparent small difference in temperature between the upper layers of the water column and waters at about 2000 m deep at a paleolatitude of about 28°S seems highly improbable. The deep-water temperature values are as expected, i.e., similar to bulk values at high latitude Site 689 (Bohaty et al., 2009), which reflects the temperature of the deep-waters which are derived from high southern latitudes. At about 41 Ma, just before the MECO, the high latitudes had already cooled from the Early Eocene Climate Optimum (Tripati et al., 2005; Dawber and Tripati, 2011), whereas the low latitudes probably remained warm, with surface water temperatures around 30-35°C (Pearson et al., 2007). We are thus convinced that the generated planktic foraminiferal $\delta^{18}O$ data cannot be used to approximate mixed layer temperatures, as generally recognized (Pearson et al., 2001).

TEX_{86} yields background SSTs around 30°C, significantly higher (9-6°C) than present-day mean annual and summer temperature at the same latitude (Levitus, 1994), but consistent with middle to late Eocene SST records for mid to low latitudes (Pearson et al., 2007; Liu et al., 2009; Zhang et al., 2013).

The TEX_{86} record indicates a phase of surface water warming in the interval between 143 and 138 mcd, corresponding to the MECO interval as identified by Bohaty et al. (2009) at Site 1263 (Fig. 3). Our TEX_{86} record however, shows an earlier onset of warming at 145 mcd (Fig. 3), not reflected in the bulk and benthic $\delta^{18}O$ records (Bohaty et al., 2009; present study). As addressed in more detail below, the time lags in our temperature records are difficult to explain, and we are not confident about their meaning or primary origin.

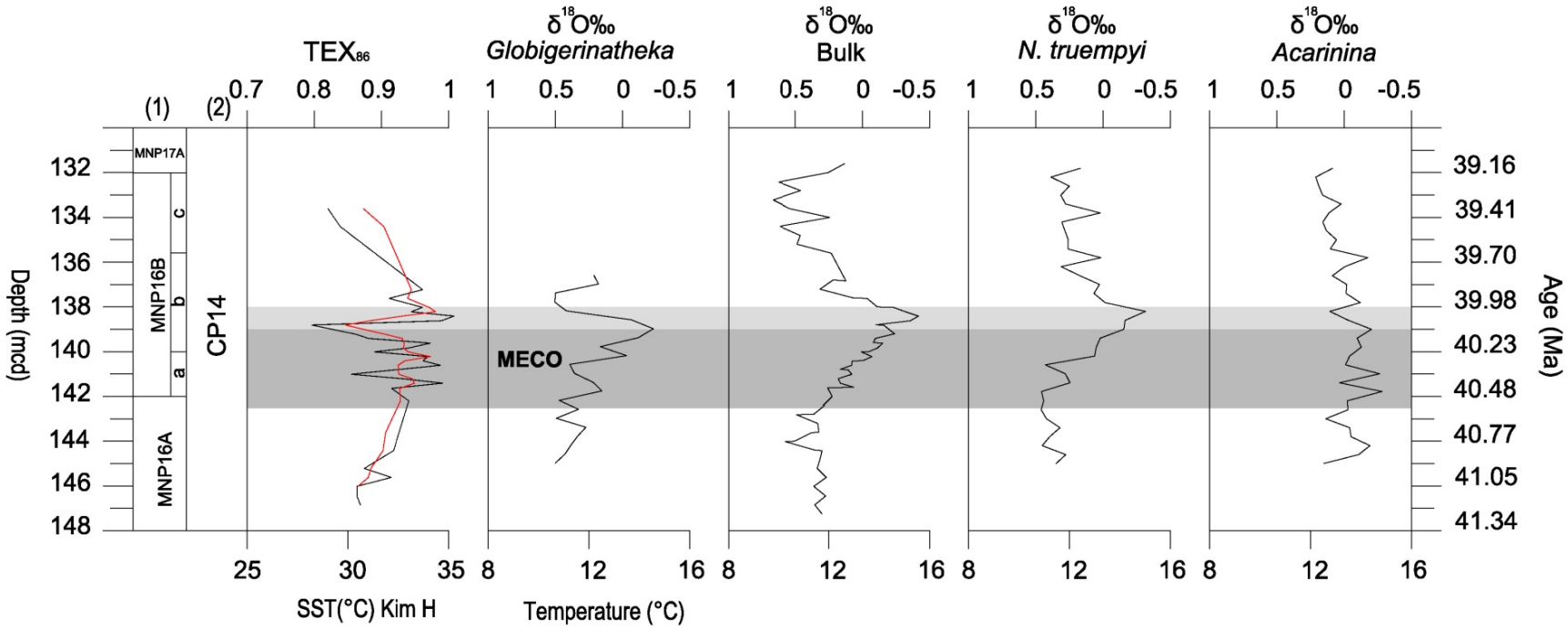

Figure 3. ODP Site 1263 TEX_{86} and $\delta^{18}O$ data plotted versus meters composite depth. The red line in the TEX_{86} plot is a 3-point running mean. The $\delta^{18}O$ axis is inverted to give a positive temperature increase in the upward direction, and the absolute temperature scale is calculated using the temperature equation of Shackleton (1974) and assumes a $\delta^{18}O_{sw}$ value of -1.0‰ for the duration of the record. The area shaded in gray highlights the entire MECO interval. The light gray area denotes the peak of the MECO event. Biostratigraphy after Fornaciari et al. (2010) following: (1) calcareous nannofossils zonation of Fornaciari et al. (2010) and (2) nannofossils standard zonation of Okada and Bukry (1980). Age model after Bohaty et al. (2009).

The TEX_{86} record in the MECO interval reaches the higher temperatures, but also shows strong fluctuations (Fig. 3). Such fluctuations may be at least partially explained by bioturbation. GDGT molecules, likely associated with the fine-grained sediment fraction (Shah et al., 2008), may have been more easily bioturbated downward than larger particles (Thompson et al., 1995), producing random temperature fluctuations in the record. The sediments at Site 1263 may not just have suffered homogeneization through bioturbation, but may have been disturbed by large burrowers, with some samples possible representing vertical burrows (halos). However, these fluctuations may also have an explanation in the ecology of marine Thaumarchaeota (see discussion in paragraph 5.3), the predominant GDGTs producers in the ocean (Pearson and Ingall, 2013).

Our various temperature proxies show warming by about 4°C during the MECO in surface as well as deeper waters (Fig. 3), similar to that described at other sites (Bohaty and Zachos, 2003; Bohaty et al., 2009; Bijl et al., 2010), and indicating warming throughout the water column in the south-eastern Atlantic. This uniform warming of the water column suggests that SSTs of the Southern Ocean, the source of Atlantic intermediate and deep waters (Via and Thomas, 2006; Thomas and Via, 2007), were experiencing a degree of warming very similar to that of the mid-latitudes.

Hence, southern high latitudes were not experiencing polar amplification of temperature rise during the MECO, suggesting that the forcing causing such amplification was small in the middle Eocene or, as observed for current global warming, did not affect high southern latitudes (IPCC 2001; Holland and Bitz, 2003). This is according to expectation if the presence of sea ice is a major factor in the present Arctic polar amplification (e.g., Kumar et al., 2010).

Site 1263 surface to bottom waters temperature records (both TEX_{86} and $\delta^{18}O$) may show timing differences in recording the main phases of the MECO (onset, peak-warming, termination), with a progressively greater delay moving from surface to deeper water (Fig. 3). The observed time lags among our temperature records are difficult to understand. Similar differences are evident at other sites. The earlier beginning and longer duration of the peak-warming phase in the bulk as compared to the benthic record (Fig. 3) was observed also by Bohaty et al. (2009) at high latitude Sites 738 and 748; the slower recovery toward pre-event temperature after MECO peak displayed by the benthic record (Fig. 3) is evident at Site 1218 in the equatorial Pacific (Lear et al., 2004; Tripati et al., 2005) in addition to the records of Bohaty et al. (2009).

We are not certain whether the apparent differences in timing in our various proxy records reflect true primary differences in timing of the temperature changes. The apparent differences in the timing of records obtained on different size fractions may have been caused at least in part by differential bioturbation, because different size fractions in Holocene carbonate sediment generally

have significantly different ages, as determined by ^{14}C analyses (Thompson et al., 1995). This may account for the earlier onset of warming displayed by the TEX_{86} record, as finer sediment particles may be

more prone to be moved downward by bioturbational processes (Thompson et al., 1995). Detailed records across the Paleocene-Eocene hyperthermal events also show differences in timing of events in bulk and foraminiferal carbonate, which can only in part be explained by actual difference in timing of the signal (Thomas, 2003; Sluijs et al., 2007).

The incoherencies among the $\delta^{18}O$ records may also represent artifacts due to a severe diagenesis differentially affecting different horizons (thus different sediment characteristics and differential diagenesis) or tests utilized.

However, the upper water column indicators (*Globigerinatheka* and TEX_{86}) consistently record each phase of the MECO earlier than deeper water indicators (bulk and benthic records; Fig. 3), raising the possibility that these differences may be at least in part a real primary signal, with effects of warming earliest observed closer to the surface, similar to what has been proposed (Thomas et al., 2002), though not generally accepted (Sluijs et al., 2007) for the PETM. This is the first MECO study showing coupled surface and deep water records, so no comparison with other sites are possible. Further multi-sites surface to bottom records across the MECO will help to clarify the nature and the meaning of the apparent lags at Site 1263.

5.2. The MECO CIE conundrum

Unlike the PETM and other transient warming events, a large negative $\delta^{13}C$ excursion (CIE) is not associated with the onset of the MECO (Bohaty and Zachos, 2003; Bohaty et al., 2009; Sluijs et al., 2013). The main features of the carbon isotope record during MECO are (Bohaty et al. (2009): (1) a progressive, long-term increase in benthic and bulk $\delta^{13}C$ paralleling the gradual warming at Southern Ocean sites and some bulk and fine fraction records from the Atlantic ocean; (2) a brief negative carbon isotope excursion coincident with the MECO peak; (3) an interval of peak $\delta^{13}C$ values in both benthic and bulk records between 39.9 and 39.2 Ma, closely following the warmer phase.

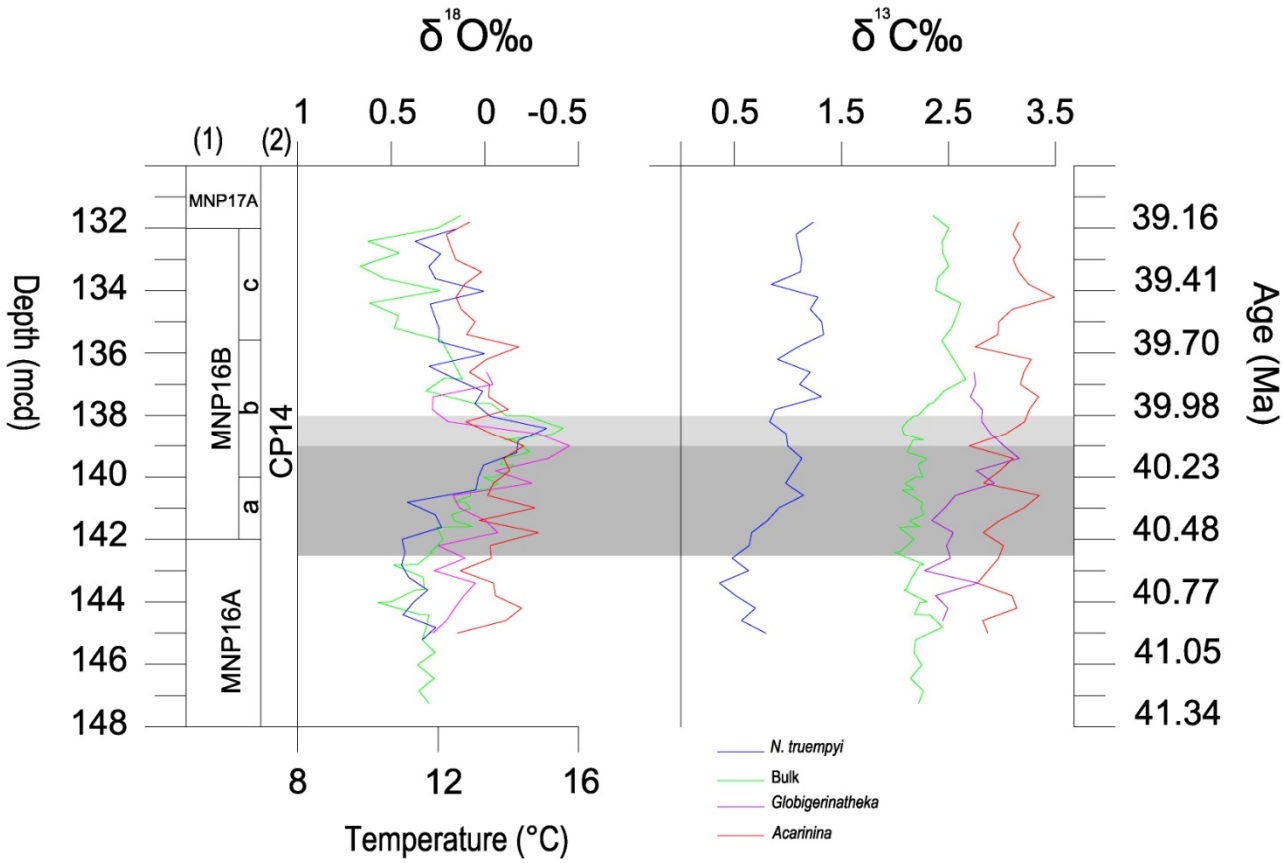

Figure 4. ODP Site 1263 oxygen and carbon isotope records across the studied interval. The $\delta^{18}O$ axis is inverted to give a positive temperature increase in the upward direction, and the absolute temperature scale is calculated using the temperature equation of Shackleton (1974) and assumes a $\delta^{18}O_{sw}$ value of -1.0‰ for the duration of the record. The area shaded in gray highlights the entire MECO interval. The light gray area denotes the peak of the MECO event. Biostratigraphy after Fornaciari et al. (2010) following: (1) calcareous nannofossils zonation of Fornaciari et al. (2010) and (2) nannofossils standard zonation of Okada and Bukry (1980). Age model after Bohaty et al. (2009).

At Site 1263, the benthic $\delta^{13}C$ record shows an increasing trend starting at ~40.8 Ma and peaking within 39.9 – 39.2 Ma (Fig. 4), consistent with the Southern Ocean benthic records (Bohaty et al. (2009). The benthic record at Site 1263, however, shows only a slight negative fluctuation coinciding with the MECO peak (-0.2‰), no significant negative carbon isotope excursion (Fig. 4). The bulk record at Site 1263 also lacks a pronounced negative CIE (<-0.2‰) and positive peaks after the maximum warming (Fig. 4), consistent with the bulk record of Bohaty et al. (2009). Our planktic records lack the negative CIE as well, rather showing a phase of quite high $\delta^{13}C$ values across the MECO peak (Fig. 4). It is generally assumed that the carbon isotope signal is not much affected by diagenesis (e.g., Sexton et al., 2006; Stap et al., 2009) or burial depth (Schrag et al., 1995), and severe diagenetic alteration has been shown to deplete rather than increase calcite carbon isotopic values (Jiang et al., 2007). Hence, the coherent lack of a significant negative CIE in our $\delta^{13}C$ records should not reflect an artifact due to diagenetic alteration. We also exclude the presence

of an unconformity since the MECO peak warming interval is well recorded at Site 1263 (Bohaty et al., 2009). Possibly, the foraminiferal $\delta^{13}C$ records have a resolution too low to resolve the CIE (50 kyr), but the bulk record has a ~25 kyr resolution and should have shown this event.

To evaluate the geographic and bathymetric extent of the negative CIE at peak MECO is essential for constraining forcing mechanisms of peak MECO, as well as the mechanism and degree of disturbance of the carbon cycle during the event. In the available records, a CIE is not everywhere clearly expressed (Fig. 5), and it varies in magnitude (see fig. 4 in Spofforth et al., 2010). Well-expressed negative CIEs (of 0.5‰) at peak MECO warming are present at Sites 738, 748 (Southern Ocean, Kerguelen Plateau), and the Tethyan Alano section (Bohaty et al., 2009; Edgar et al., 2010; Spofforth et al., 2010). Site 1051 (Black Nose) might have a CIE, but it is small and the timing may not be the same as at other sites (Spofforth et al., 2010). The record for Site 702 (Southern Ocean) has a negative, but small CIE. The bulk $\delta^{13}C$ record at Site 689 (Weddell Sea, Southern Ocean) shows no more than a slight negative fluctuation (Bohaty et al., 2009), comparable with those observed at Site 1263 (Bohaty et al., 2009; present study). Although the record of the basal-middle MECO is not continuous at Site 689, the MECO peak warming is recorded and apparently complete. At Site 523 (South Atlantic, Walvis Ridge) a CIE seems to be present, but an unconformity interrupts the critical peak-MECO interval (Bohaty et al., 2009), complicating the evaluation. At the Contessa Highway and Monte Cagnero sections (central-western Tethys) the very noisy $\delta^{13}C$ signals (Jovane et al., 2007; Savian et al., 2013) make the evaluation difficult, but at least for the Monte Cagnero record a CIE seems excluded.

To infer the degree and the nature of a disturbance of the global carbon cycle during the MECO from the available $\delta^{13}C$ records thus is complex. The heterogeneity of the negative CIEs at MECO peak-warming may be an effect of its short duration (~50 kyr), so that the less expanded records are not complete. However, even in the sections where it is well recorded, the CIE is considerably less marked (~0.5‰) than negative CIEs of early Eocene hyperthermals (e.g., Lourens et al., 2005; Stap et al., 2010; McInerney and Wing, 2011). To explain the timing and pattern of warming, $\delta^{13}C$ changes, and the lack of a negative $\delta^{13}C$ excursion at the onset of the event, Bohaty et al. (2009) hypothesized enhanced degassing of CO_2 from either magmatic sources (i.e., arc or intraplate hot spot volcanism) or metamorphic decarbonation in orogenic belts. Increased emissions of carbon from these sources indeed

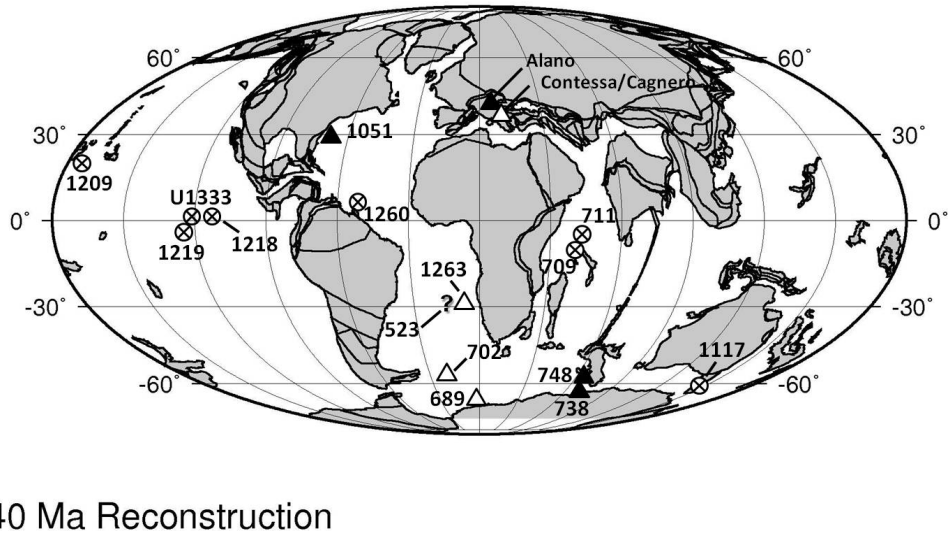

Figure 5. Oceanic (ODP - DSDP) sites and onland sections where the MECO has been described. Approximate positions at 40 Ma are plotted on a paleogeographic reconstruction from the Ocean Drilling Stratigraphic Network (GEOMAR, Kiel, Germany). Sites were the CIE is well expressed are labeled with solid triangles, sites with a doubtful CIE are labeled with an open triangles, sites where no data are available are labeled with open circles with a cross.

may not induce significant changes in marine carbonate $\delta^{13}C$ values (Thomas and Shackleton, 1996; Kump and Arthur, 1999; Bohaty et al., 2009) and explain the decoupling of warming ($\delta^{18}O$) and $\delta^{13}C$ signals across the MECO onset and gradual warming. Bohaty et al. (2009) and Sluijs et al., (2013) hypothesized that the brief carbon isotope excursion at peak MECO warming may have resulted from

the destabilization of methane clathrates following the initial gradual warming, and after reaching a threshold level of warming.

The present records clearly show that early MECO warming was not coeval with a negative CIE, so if this warming resulted from increasing CO_2 levels the carbon source must have been not highly isotopically depleted, thus be volcanic or metamorphic. The nature and timing of the small CIE lasting about 50 kyr, i.e., a duration similar to that of some early Eocene hyperthermals but at smaller magnitude, is not presently well defined, with timing, duration and size variable between records. The most clearly defined CIE (Fig 5) occur in high latitude sections close to continental margins, and in more marginal Tethyan basins.

The carbon isotope record of MECO may have been complicated, with local and regional factors superimposed on a global signal. An acceleration of the hydrological cycle and weathering has been inferred for high to mid latitude areas for warm periods, including the PETM and EECO (e.g., Pagani et al., 2006; Giusberti et al., 2007; Slotnick et al., 2012). The increased precipitation may have led to increased nutrient influx, resulting in eutrophication. In the more marginal and

continental basins, eutrophication was commonly associated with peak MECO warming and the period directly afterwards. In the mid-latitude Alano section an eight meters thick sapropelic interval starts just above the peak of the MECO, indicating also a phase of intense organic carbon production and burial (Luciani et al., 2010; Spofforth et al., 2010). Extensive deposition of organic-rich layers occurred also in other marginal basins (Beniamovski et al., 2003). The carbon isotope records in coastal areas or marginal basins thus may have been strongly influenced by local to regional high organic carbon burial rates, inducing an abrupt increase in $\delta^{13}C$ values in carbonates (Jovane et al, 2007; Bohaty et al., 2009; Spofforth et al., 2010; Edgar et al., 2010; Savian et al., 2013). As suggested by Bohaty et al. (2009) and Spofforth et al. (2010), a widespread increase in organic carbon burial after the MECO might have been an efficient negative feedback mechanism to draw down pCO_2 levels, deepening the CCD and drive the abrupt cooling which followed the warmest interval of the MECO.

In conclusion the interpretation of the MECO $\delta^{13}C$ records in terms of changes in the global carbon cycle, and inorganic and organic carbon flux changes is difficult, with presently not sufficient information on sufficient locations and good time control available (Kump and Arthur, 1999; Bohaty et al., 2009; Spofforth et al., 2010). More globally distributed information at high time resolution and with excellent age control is necessary to fully document this event.

5.3. Repercussions of MECO warming on marine food webs and transfer of organic matter to the sea-floor

Toward the MECO peak-warming, the *Globigerinatheka* $\delta^{13}C$ values show a progressive increase not paralleled in the bulk record (Fig. 4). Assuming that no changes occurred in the mean living depth of the population, and in the *Globigerinatheka* isotopic fractionation, this may be interpreted as an upward expansion of the thermocline and increased thermal stratification. Overall, however, the stable carbon isotope records at Site 1263 indicate a well-developed stratification and no large changes in stratification (e.g. caused by intermediate water circulation changes) during the MECO (Fig. 4).

Benthic foraminifera and coarse fraction accumulation rates increase from the beginning of the record up to the basal part of the bulk $\delta^{18}O$ negative excursion. After the highest values are reached, values rapidly decrease across the MECO with the lowest rates reached during the MECO peak-warming (Fig. 6). Our records do not extend sufficiently far below the MECO to evaluate whether the apparent increasing trend just above the beginning of our records is linked to the event, but the onset appears to occur before the MECO.

The observed BFAR decrease during the MECO indicates that at Site 1263, the amount of organic matter arriving at the sea floor declined, hence the decline in BFAR. The parallel decrease in the CFAR (Fig. 6) indicates a concomitant decrease in planktic foraminiferal productivity, since there is no evidence of carbonate dissolution (e.g., decrease in calcium carbonate mass accumulation rate; Bohaty et al., 2009) and foraminiferal preservation remains constant. The decrease in foraminiferal accumulation rates may indicate that surface water warming significantly affected food webs in the upper water column, thus productivity by the heterotroph planktic foraminifera, eventually leading to a decrease in the organic matter flux to the sea-floor

Temperature is known to influence food web structure through resource limitation or specific effects of temperature on consumers or producers (e.g., Richardson and Schoeman, 2004; Muren et al., 2005; O'Connor et al., 2009). Microcosms food-webs experiments indicate that an increase in SST in nutrient-limited conditions, such as oceanic stably stratified areas, slightly affects photosynthetic and primary production rates, while it can significantly reduce heterotrophs productivity and biomass (O'Connor et al., 2009). This effect has been attributed to a warming-induced increase in heterotrophs' metabolic activities and costs that exceed available primary production (Lopez-Urrutia et al., 2006; O'Connor et al., 2009).

The decrease in planktic foraminiferal productivity across the MECO at Site 1263, suggests warming may have acted in a similar fashion increasing planktic heterotrophs metabolic rates in a context of unvaried conditions of primary productivity. The well-developed water column stratification at Site 1263 (Fig. 4), possibly increased in the upper MECO, likely efficiently separated surface waters from nutrients richer deeper waters, as occurring in modern central gyres. In such nutrient-limited surface waters, a temperature-induced increase in phytoplankton productivity was probably constrained (Sarmiento et al., 2004) so that primary productivity could not supply the increased food needs of heterotrophs such as planktonic foraminifera. This hypothesis is supported by the FFAR which does not suggest significant changes in nannofossil accumulation rate across the MECO (Fig. 6), and may indicate primary producers productivity was not substantially changed.

At Site 1263, the symbiont-bearing acarininids decreased in relative abundance across the MECO (Degasperi, master thesis in progress). Since this group belongs to the warm indices, they would be expected to increase in abundance during the MECO warming. A crisis in the symbiotic relationship with photosynthetic algae (bleaching) (Edgar et al., 2012), could be a possible explanation for such

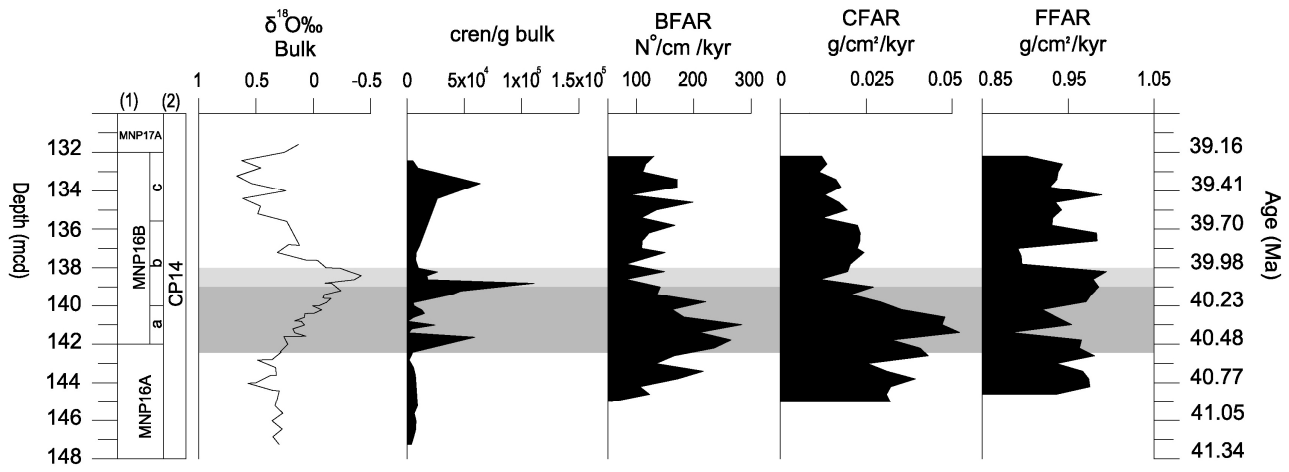

Figure 6. ODP Site 1263 benthic foraminiferal, coarse fraction and fine fraction accumulation rates (BFAR, CFAR, FFAR) and Cren/g bulk plotted versus depth. Cren/g bulk is the abundance of the biomarker crenarchaeol to the weight of bulk sediment. The area shaded in gray highlights the entire MECO interval. The light gray area denotes the peak of the MECO event. Biostratigraphy after Fornaciari et al. (2010) following: (1) calcareous nannofossils zonation of Fornaciari et al. (2010) and (2) nannofossils standard zonation of Okada and Bukry (1980). Age model after Bohaty et al. (2009).

decrease. Causes of bleaching may be a change in nutrient availability or pH of surface waters, in addition to the warming itself (Edgar et al., 2012). However, causes of bleaching are still poor known, and several stress factors such as high sea-surface temperatures, increased ultraviolet radiation, hypersalinity, starvation, and acidification have been invoked (e.g., Douglas, 2003 and references therein).

The decrease in BFAR suggests that the increased remineralization of organic matter in the upper water column drove a marked reduction of the flux of food to the seafloor. Possibly, deep water warming during the MECO acted in enhancing benthic foraminiferal metabolic rates as well, exacerbating their starvation (e.g., Olivarez Lyle and Lyle, 2006; Thomas, 2007). In addition, the decline of planktic foraminiferal productivity might also have contributed to decreased transport of organic matter to the seafloor, by decreasing ballasting of organic matter by carbonate (Klaas and Archer, 2002; Passow and Carlson, 2012).

The decreasing foraminiferal accumulation rates across the MECO at Site 1263 coincide with higher abundance of the GDGT crenarchaeol (Fig. 6), a marker for Thaumarchaeota abundance (e.g., Fietz et al., 2011; Pearson and Ingall, 2013). Thaumarchaeota are mesophilic Archaea ubiquitous in marine environments throughout the water column. They are chemoautotrophic and ammonia-oxidizing (Pearson and Ingall, 2013), and their increase may further indicate increased remineralization of organic matter in the water column.

Factors that influence where Thaumarchaeota grow relative to the thermocline and the chemocline may affect paleoproxies based on GDGTs (Pearson and Ingall, 2013). Since the majority of archaeal ammonia oxidation occurs at deep-photic zone to mesopelagic depths (Pearson and Ingall, 2013) increasing GDGTs depth-production (and export) relative to GDGTs surface-production, may explain the large variability and the negative shifts in the TEX_{86} record during the MECO (Fig. 3; Turich et al., 2007).

Foraminiferal productivity shows just a slight recovery after the MECO (Fig. 6) and did not reach pre-event levels in the studied interval, which may indicate that communities needed a long time (>800 kyr) before complete recovery after the perturbation. However, post-MECO conditions at Site 1263 may also have been somewhat different than in pre-MECO times, causing an overall lower productivity (Chapter 4).

Summarizing, our data point to a significant change in marine food-webs at pelagic to mesopelagic depths during the MECO at the open ocean Site 1263. The most likely explanation for the decline in foraminiferal accumulation rates is a temperature-induced change in metabolic rates, in which metabolic rates in primary producers increased less than in heterotrophs as nutrient-limitation prevented a higher primary productivity. Reduced carbonate ballasting of organic matter and increased water column remineralization caused a decrease in the flux of organic matter to the sea floor and hence of the BFAR.

6. Summary and Conclusion

(1) This study represents one of the first multi-proxy investigation of the MECO in an open ocean setting, providing new insight in this large climatic perturbation. The surface to bottom waters temperature records at Site 1263 (Walvis Ridge) indicate a uniform warming of ~4°C throughout the water column, indicating equal warming of mid and high southern latitudes during the MECO. Additional surface to bottom records across the MECO are needed in order to decipher the nature and the meaning of the apparent lags in our temperature records.

(2) The $\delta^{13}C$ records for Site 1263 show a pattern of changes across the MECO coherent with those of previously published records (Bohaty et al., 2009), but the brief negative carbon isotope excursion (CIE) at MECO peak-warming is poorly expressed, with just slight negative fluctuations recorded only in the benthic and bulk records. In general, the CIE at MECO peak warming is much less pronounced and less clearly globally expressed than those of early Eocene hyperthermals (Bohaty et al., 2009, Spofforth et al., 2010). This may be due to the short duration of the CIE and a

lack of complete and expanded sections, or, in this study, inadequate time resolution in the critical interval. Alternately, the small size of the CIE and its regional variability may be due to complex local and regional changes in carbon cycling superimposed on a global signal, e.g. release of a small amount of isotopically negative carbon compounds such as clathrates.

Enhanced weathering may have led to a phase of local to regional enhanced burial of organic carbon in the Central-Western Tethys (Beniamovski et al., 2003; Spofforth et al., 2010) through eutrophication and increasing stratification in marginal basins and coastal areas (e.g., Luciani et al., 2010; Boscolo Galazzo et al., 2013), accounting also for the global abrupt $\delta^{13}C$ increase after the MECO peak (Kump and Arthur, 1999). Enhanced organic carbon burial may also explain the rapid drawdown of pCO_2 levels and the abrupt cooling following the MECO highest temperatures (Bohaty et al., 2009).

(3) During MECO warming, nutrient-limited surface waters at Site 1263 probably limited a temperature-induced increase in primary producers, leading to a progressive heterotroph starvation, as seen in the significant decrease in planktonic foraminiferal productivity and biomass at Site 1263. This would lead to increased water column remineralization of the organic matter as indicated by a significant increase in the abundance of the chemoautotrophic ammonia-oxidizing Thaumarchaeota Archaea (Pearson and Ingall, 2013), and reduced transport of organic matter to the seafloor, potentially exacerbated by decreased carbonate ballasting of organic matter.

References

Arndt, S., Jørgensen, B.B., LaRowe, D.E., Middelburg, J.J., Pancost, R.D, Regnier, P., 2013. Quantifying the degradation of organic matter in marine sediments: A review and synthesis. Earth-Science Reviews, 123, 53–86.

Beniamovski, V.N., Alekseev, A.S., Ovechkina, M.N., Oberhänsli, H., 2003. Middle to Upper Eocene disoxic–anoxic Kuma Formation (northeast Peri-Tethys): biostratigraphy and paleoenviroments. In: Wing, S.L., Gingerich, P.D., Schmitz, B., Thomas, E., (Eds.). Causes and Consequences of Globally Warm Climates in the Early Paleogene. Boulder, Colorado, Geological Society of America Special Paper, 369, 95–112.

Berggren, W.A., Aubert, J., 1976. Eocene benthonic foraminiferal biostratigraphy and paleobathymetry of Orphan Knoll (Labrador Sea). Micropaleontology, 22, 327–346.

Berggren, W.A., Kent, D.V., Swisher III, C.C., Aubry, M.P., 1995. A revised Cenozoic geochronology and chronostratigraphy. Special Publication SEPM Society of Sedimentary Geology 54, 129–212.

Bijl, P.K., Houben, A.J.P., Schouten, S., Bohaty, S.M., Sluijs, A., Reichart, G.J., Sinninghe Damsté, J.S., Brinkhuis, H., 2010. Transient middle Eocene atmospheric CO_2 and temperature variations. Science, 330, 819–821.

Boersma, A., Premoli Silva, I., Shackleton, N.J., 1987. Atlantic Eocene planktonic foraminiferal paleohydrographic indicators and stable isotope paleoceanography. Paleoceanography, 2, 287-331.

Bohaty, S.M., Zachos, J.C., 2003. A significant Southern Ocean warming event in the late middle Eocene. Geology, 31, 1017–1020.

Bohaty, S.M., Zachos, J.C., Florindo, F., Delaney, M.L., 2009. Coupled greenhouse warming and deep-sea acidification in the Middle Eocene. Paleoceanography, 24, PA2207, http://dx.doi.org/10.1029/2008PA001676.

Bosboom, R.E., Abels, H.A., Hoorn, C., van den Berg, B.C.J., Guo, Z., Dupont-Nivet, G., 2014. Aridification in continental Asia after the Middle Eocene Climatic Optimum (MECO). Earth and Planetary Science Letters, 389, 34-42.

Boscolo Galazzo, F., Giusberti, L., Luciani, V., Thomas, E., 2013. Paleoenvironmental changes during the Middle Eocene Climatic Optimum (MECO) and its aftermath: The benthic foraminiferal record from the Alano section (NE Italy). Palaeogeography, Palaeoclimatology, Palaeoecology, 378, 22-35.

Burgess, C.E., Pearson, P.N., Lear, C.H., Morgans, H.E.G., Handley, L., Pancost, R.D., Schouten, S., 2008. Middle Eocene climate cyclicity in the southern Pacific: Implications for global ice volume. Geology, 36, 651–654.

Cande, S.C., Kent, D.V., 1995. Revised calibration of the geomagnetic polarity timescale for the Late Cretaceous and Cenozoic. Journal of Geophysical Research, 100, 6093–6095.

Cramer, B.S., Toggweiler, J.R., Wright, M.E., Katz, J.D., Miller, K.G., 2009. Ocean overturning since the Late Cretaceous: Inferences from a new benthic foraminiferal isotope compilation. Paleoceanography, 24, PA4216, doi:10.1029/2008PA001683.

Dawber, C.F., Tripati, A.K., 2011. Constraints on glaciation in the middle Eocene (46–37 Ma) from Ocean Drilling Program (ODP) Site 1209 in the tropical Pacific Ocean. Paleoceanography, 26, PA2208, doi:10.1029/2010PA002037.

Dickens, G.R., 2011. Down the Rabbit Hole: toward appropriate discussion of methane release from gas hydrate systems during the Paleocene-Eocene thermal maximum and other past hyperthermal events. Climate of the Past, 7, 831-846.

Diester-Haass, L., 1995. Middle Eocene to early Oligocene paleoceanography of the Antarctic Ocean (Maud Rise, ODP Leg 113, Site 689): change from a low to a high productivity ocean. Palaeogeography, Palaeoclimatology, Palaeoecology, 113, 311-334.

Douglas, A.E., 2003. Coral bleaching – how and why? Marine Pollution Bulletin, 46, 385–392.

Edgar, K.M., Wilson, P.A., Sexton, P.F., Gibbs, S.J., Roberts, A.P., Norris, R.D., 2010. New biostratigraphic, magnetostratigraphic and isotopic insights into the Middle Eocene Climatic Optimum in low latitudes. Palaeogeography, Palaeoclimatology, Palaeoecology, 297, 670–682.

Edgar, K.M., Bohaty, S.M., Gibbs, S.J., Sexton, P.F., Norris, R.D., Wilson, P.A., 2012. Symbiont 'bleaching' in planktic foraminifera during the Middle Eocene Climatic Optimum. Geology, 41, 15-18.

Ezard, T.H., Aze, T., Pearson, P.N., Purvis A., 2011. Interplay between changing climate and species' ecology drives macroevolutionary dynamics. Science, 332, 349-351.

Fietz, S., Martínez-Garcia, A., Huguet, C., Rueda, G., Rosell-Melé, A., 2011. Constraints in the application of the Branched and Isoprenoid Tetraether index as a terrestrial input proxy. Journal of Geophysical Research, 116, doi: 10.1029/2011JC007062.

Fornaciari, E., Agnini, C., Catanzariti, R., Rio, D., Bolla, E.M., Valvasoni, E., 2010. Mid-Latitude calcareous nannofossil biostratigraphy and biochronology across the middle to late Eocene transition. Stratigraphy, 7-4, 229-264.

Galeotti, S., Krishnan, S., Pagani, M., Lanci, L., Gaudio, A., Zachos, J.C., Monechi, S., Morelli, G., Lourens, L., 2010. Orbital chronology of Early Eocene hyperthermals from the Contessa Road section, central Italy. Earth and Planetary Science Letters, 290, 192–200.

Giusberti, L., Rio, D., Agnini, C., Backman, J., Fornaciari, E., Tateo, F., Oddone, M., 2007. Mode and tempo of the Paleocene-Eocene thermal maximum in an expanded section from the Venetian pre-Alps. Geological Society of America Bulletin, 119, 391–412.

Gooday, A.J., 2003. Benthic foraminifera (Protista) as tools in deep-water palaeoceanography: Environmental influences on faunal characteristics. Advances in Marine Biology, 46, 1–90.

Henson, S.A., Sanders, R., Madsen, E., Morris, P.J., Le Moigne, F., Quartly, G.D., 2011. A reduced estimate of the strength of the ocean's biological carbon pump. Geophysical Research Letters, 38, L04606.

Herguera, J.C., Berger, W., 1991. Paleoproductivity from benthonic foraminifera abundance: Glacial to postglacial change in the west-equatorial Pacific. Geology, 19, 1173–1176.

Hoenisch, B., Ridgwell, A., Schmidt, D.N., Thomas, E., Gibbs, S.J., Sluijs, A., Zeebe, R., Kump, L., Martindale, R.C., Greene, S.E., Kiessling, W., Ries, J., Zachos, J.C., Royer, D.L., Barker, S., Marchitto Jr., T.M., Moyer, R., Pelejero, C., Ziveri, P., Foster, G.L., Williams, B., 2012. The geological record of ocean acidification. Science, 335, 1058–1063.

Holland, M.M., Bitz, C.M., 2003. Polar amplification of climate change in coupled models. Climate Dynamics, 21, 221–232.

Hollis, C.J., Taylor, K.W.R., Handley, L., Pancost, R.D., Huber, M., Creech, J.B., Hines, B.R., Crouch, E.M., Morgans, H.E.G., Crampton, J.S., Gibbs, S., Pearson, P.N., Zachos, J.C., 2012. Early Paleogene temperature history of the Southwest Pacific Ocean: Reconciling proxies and models. Earth and Planetary Science and Letters, 349–350, 53–66.

Hopmans, E.C., Weijers, J.W.H., Schefuss, E., Herfort, L., Sinninghe Damsté, J.S., Schouten, S., 2004. A novel proxy for terrestrial organic matter in sediments based on branched and isoprenoidal tetraether lipids. Earth and Planetary Science Letters, 224, 107-116.

Huber, M., Sloan, L., Shellito, C., 2003. Early Paleogene oceans and climate: A fully coupled modeling approach using the NCAR CCSM. In: Wing, S.L., Gingerich, P.D., Schmitz, B., and Thomas, E., (Eds.). Causes and Consequences of Globally Warm Climates in the Early Paleogene. Boulder, Colorado, Geological Society of America Special Paper, 369, 25-47.

Huguet, C., Kim, J.H., de Lange, G.J., Sinninghe Damsté, J.S., Schouten, S., 2009. Effects of long term oxic degradation on the U-37(K'), TEX_{86} and BIT organic proxies. Organic Geochemistry, 40, 1188–1194.

IPCC, Climate Change (2001) The scientific basis. Contribution of Working Group 1 to the Third Assessment Report of the Intergovernmental Panel on Climate Change. In: Houghton, J.T., Ding, Y., Griggs, D.J., Noguer, M., van der Linden, P.J., Dai, X., Maskell, K., Johnson, C.A. (Eds.). Cambridge University Press, Cambridge, UK, pp. 881.

Jiang, S., Wise Jr., S.W., Wang, Y., 2007. Cause of the middle/late Miocene carbonate crash: dissolution or low productivity? In: Teagle, D.A.H., Wilson, D.S., Acton, G.D., and Vanko, D.A., (Eds.). Proceedings of the Ocean Drilling Program, Scientific Results, 206. Ocean Drilling Program, College Station, TX, 1–24.

Jorissen, F.J., Fontanier, C., Thomas, E., 2007. Paleoceanographical proxies based on deep-sea benthic foraminiferal assemblage characteristics. In: Hillaire-Marcel, C., de Vernal, A., (Eds.). Developments in Marine Geology: Proxies in Late Cenozoic Paleoceanography, vol. 1. Elsevier, Amsterdam, 264–325.

Jovane, L., Florindo, F., Coccioni, R., Dinare's-Turell, J., Marsili, A., Monechi, S., Roberts, A.P., Sprovieri, M., 2007. The middle Eocene climatic optimum event in the Contessa Highway section, Umbrian Apennines, Italy. Geological Society of American Bulletin, 119, 413–427.

Katz, M. E., Katz, D.R., Wright, J.D., Miller K.G., Pak, D.K., Shackleton, N.J., Thomas, E., 2003. Early Cenozoic benthic foraminiferal isotopes: Species reliability and interspecies correction factors. Paleoceanography, 18, doi:10.1029/2002PA00079.

Kim, J.H., Meer, J.v.d., Schouten, S., Helmke, P., Willmott, V., Sangiorgi, F., Koç, N., Hopmans, E.C., Sinninghe Damsté, S., 2010. New indices and calibrations derived from the distribution of crenarchaeal isoprenoid tetraether lipids: Implications for past sea surface temperature reconstructions: Geochimica et Cosmochimica Acta, 74, 4639-4654.

Klaas, C., Archer, D.E., 2002, Association of sinking organic matter with various types of mineral ballast in the deep sea; implications for the rain ratio. Global Biogeochemical Cycles, 16, 1116, doi: 10.1029/ 2001GB001765.

Klevenz, V., Vance, D., Schmidt, D.N., Mezger, K., 2008. Neodymium isotopes in benthic foraminifera: Core-top systematics and a down-core record from the Neogene south Atlantic. Earth and Planetary Science Letters, 265, 571-587.

Kozdon, R., Kelly, D.C., Kita, N.T., Fournelle, J.H., Valley, J.W., 2011. Planktonic foraminiferal oxygen isotope analysis by ion microprobe technique suggests warm tropical sea surface temperatures during the Early Paleogene. Paleoceanography, 26, PA3206, doi:10.1029/2010PA002056.

Kumar, A., Perlwirz, J., Eischeid, J., Quan, X., Xu, T., Zhang, T., Hoerling, M., Jha, B., Wang, W., 2010. Contribution of sea ice loss to Arctic amplification. Geophysical Research Letters, 37, L21701, doi:10.1029/2010GL045022.

Kump, L.R., Arthur, M.A., 1999. Interpreting carbon-isotope excursions: Carbonates and organic matter. Chemical Geology, 161, 181–198.

Lear, C.H., Rosenthal, Y., Coxall, H.K., Wilson, P.A., 2004. Late Eocene to early Miocene ice sheet dynamics and the global carbon cycle. Paleoceanography, 19, PA4015, doi:10.1029/2004PA001039.

Levitus, S., Antonov, J., Boyer, T.P., 1994. Interannual variability of temperature at a depth of 125 m in the North Atlantic Ocean. Science, 266, 96–99.

Liu, Z., Pagani, M., Zinniker, D., DeConto, R., Huber, M., Brinkhuis, H., Shah, S.R., Leckie, R.M., Pearson, A., 2009. Global cooling during the Eocene-Oligocene climate transition. Science, 323, 1187-1190.

Lopez-Urrutia, A., San Martin, E., Harris, R.P., Irigoien, X., 2006. Scaling the metabolic balance of the oceans. Proceedings of the National Academy of Science of the United States of America, 103, 8739–8744.

Lourens, L.J., Sluijs, A., Kroon, D., Zachos, J.C., Thomas, E., R□hl, U., Bowles, J., Raffi, I., 2005. Astronomical pacing of late Palaeocene to early eocene global warming events. Nature, 435, 1083–1087.

Luciani, V., Giusberti, L., Agnini, C., Fornaciari, E., Rio, D., Spofforth, D.J.A., Pälike, H., 2010. Ecological and evolutionary response of Tethyan planktonic foraminifera to the middle Eocene

climatic optimum (MECO) from the Alano section (NE Italy). Palaeogeography, Palaeoclimatology, Palaeoecology, 292, 82–95.

Lunt, D., Ridgwell, A., Sluijs, A., Zachos, J., Hunter, S., Haywood, A., 2011. A model for orbital pacing of methane hydrate destabilization during the Palaeogene. Nature Geoscience, 4, 775–778.

Lyle, M., Barron, J., Bralower, T.J., Huber, M., Olivarez Lyle, A., Ravelo, A.C., Rea, D.K, Wilson, P.A., 2008. Pacific Ocean and Cenozoic evolution of climate, Review of Geophysics, 46, RG2002.

Lyle, M., Lyle Olivarez, A., Backman, J., Tripati, A., 2005. Biogenic sedimentation in the Eocene equatorial Pacific — the stuttering greenhouse and Eocene carbonate compensation depth. In: Lyle, M., and Firth, (Eds.). Proceedings of the Ocean Drilling Program, Scientific results, 199, 1-35. Ocean Drilling Program, College Station, TX.

McInerney, F.A., Wing, S.L., 2011. The Paleocene-Eocene thermal maximum: a perturbation of carbon cycle, climate, and biosphere with implications for the future. Annual Review of Earth and Planetary Sciences, 39, 489–516.

Moebius, I., Friedrich, O., Edgar, K.M., Scher, H.D., Sexton, P., 2013. Bottom water changes in the subtropical North Atlantic and the Southern Ocean associated to the Middle Eocene Climatic Optimum. AGU 2013 Fall Meeting Abstract (Control ID: 1805987), San Francisico 9-13 December 2013.

Moore, T.C., Rabinowitz, P.D., Borella, P.E., Shackleton, N.J., Boersma A., 1984. History of the Walvis Ridge. In: Moore, Jr. T.C., and Rabinowitz, P.D., (Eds.). Initial Reports of the Deep Sea Drilling Project, Washington, (U.S. Government Printing Office), 74, pp. 873-894.

Muren, U., Berglund, J., Samuelsson, K., Andersson, A., 2005. Potential effects of elevated sea-water temperature on pelagic food webs. Hydrobiologia, 545, 153–166.

Olivarez Lyle, A., Lyle, M.W., 2006. Missing organic carbon in Eocene marine sediments: Is metabolism the biological feedback that maintains end-member climates? Paleoceanography, 21, PA2007, doi:10.1029/2005PA001230.

O'Connor, M., Piehler, M.F., Leech, D.M., Anton, A., Bruno, J.F., 2009. Warming and resource availability shift food web structure and metabolism. Plos Biology, 7-8, 1-6.

Pagani, M., Pedentchouk, N., Huber, M., Sluijs, A., Schouten, S., Brinkhuis, H., Sinninghe Damsté, J.S., Dickens, G.R., and the Expedition 302 Scientists, 2006. Arctic hydrology during global warming at the Palaeocene/Eocene thermal maximum. Nature, 442, 671-675.

Pälike, H., Lyle, M.W, Nishi, H., Raffi, I., et al., 2012. A Cenozoic record of the equatorial Pacific carbonate compensation depth. Nature, 488, 609-615.

Passow, U., Carlson, C.A., 2012. The biological pump in a high CO_2 world. Marine Ecology Progress Series, 470, 249-271.

Pea, L., 2011. Eocene-Oligocene paleoceanography of the subantarctic South Atlantic: Calcareous Nannofossil reconstructions of temperature, nutrient, and dissolution history. Ph.D. thesis, pp. 205, Dottorato di Ricerca in Scienze della Terra XXIII° Ciclo, Università degli Studi di Parma (Italy).

Pearson, A., Ingalls, A.E., 2013. Assessing the Use of Archaeal Lipids as Marine Environmental Proxies. Annual Review of Earth and Planetary Sciences, 41, 359–384.

Pearson, P.N., Palmer, M.R., 2000. Atmospheric carbon dioxide concentrations over the past 60 million years. Nature, 406, 695–699.

Pearson, P.N., Shackleton, N.J., Hall, M.A., 1993. Stable isotope paleoecology of Middle Eocene planktonic foraminifera and multi-species isotope stratigraphy, DSDP Site 523, South Atlantic. Journal of Foraminiferal Research, 23, 123-140.

Pearson, P.N., Ditchfield, P.W., Singano, J., Harcourt-Brown, K.G., Nicholas, C.J., Olsson, R.K., Shackleton, N.J., Hallk, M.A., 2001. Warm tropical sea surface temperatures in the Late Cretaceous and Eocene epochs. Nature, 413, 481-488.

Pearson, P.N., Olsson, R.K., Hemblen, C., Huber, B.T., Berggren, W.A., 2006. Atlas of Eocene Planktonic Foraminifera: Cushman Special Publication, 41, 513 pp.

Pearson, P.N., van Dongen, B.E., Nicholas, C.J., Pancost, R.D., Schouten, S., Singano, J.M., Wade, B.S., 2007. Stable warm tropical climate through the Eocene Epoch. Geology, 35, 211-214.

Premoli Silva, I., Wade ,B., Pearson, P.N., 2006. Taxonomy, biostratigraphy, and phylogeny of *Globigerinatheka* and *Orbulinoides*. In: Pearson, P.N., Olsson, R.K., Huber, B.T., Hemleben, C., and Berggren W.A., (Eds). Atlas of Eocene planktonic foramifera. Cushman Foundation Special Publication, 41, p. 169-212.

Richardson, A.J., Schoeman, D.S., 2004. Climate impacts on plankton ecosystems in the Northeast Atlantic. Science, 305, 1609–1613.

Ridgwell, A., Schmidt, D.N., 2010. Past constraints on the vulnerability of marine calcifiers to massive carbon dioxide release. Nature Geosciences, 3, 196-200.

Sarmiento, J.L., Slater, R., Barber, R., Bopp, L., Doney, S.C., Hirst, A.C., Kleypas, J., Matear, R., Mikolajewicz, U., Monfray, P., Soldatov, V., Spall, S.A., Stouffe, R., 2004. Response of ocean ecosystems to climate warming. Global Biogeochemical Cycles, 18, GB3003.

Savian, J.F., Jovane, L., Trindade, R.I.F., Frontalini, F., Coccioni, R., Bohaty, S.M., Wilson, P.A., Florindo, F., Roberts, A., 2013. Middle Eocene Climatic Optimum (MECO) in the Monte Cagnero Section, Central Italy. Latinmag Letters, 3, Special Issue, PC02, 1-8. Proceedings Montevideo, Uruguay.

Schouten, S., Hopmans, E.C., Schefuss, E., Sinninghe Damsté, J.S., 2002. Distributional variations in marine crenarchaeotal membrane lipids: a new tool for reconstructing ancient sea water temperatures? Earth and Planetary Science Letters, 204, 265-274.

Schouten, S., Hopmans, E.C., Rosell-Melé, A., Pearson, A., Adam, P., Bauersachs, T., Bard, E., Bernasconi, S.M., Bianchi, T.S., Brocks, J.J., et al., in press. An interlaboratory study of TEX_{86} and BIT analysis of sediments, extracts, and standard mixtures. Geochemistry, Geophysics, Geosystems, doi: 10.1002/2013GC004904.

Schrag, D.P., Depaolo, D.J., Richter, F.M., 1995. Reconstructing past sea surface temperatures: Correcting for diagenesis of bulk marine carbonate. Geochimica and Cosmochimica Acta, 59, 2265–2278.

Sexton, P.F., Wilson, P.A., Pearson, P.N., 2006. Microstructural and geochemical perspectives on planktic foraminiferal preservation: ‘‘Glassy’’ versus ‘‘Frosty’’. Geochemistry, Geophysics, Geosystems, 7, Q12P19, doi:10.1029/2006GC001291.

Shackleton, N.J., 1974. Attainment of isotopic equilibrium between ocean water and the benthonic foraminifera genus *Uvigerina*: Isotopic changes in the ocean during the last glacial, in Les Méthodes Quantitatives D’étude des Variations du Climat au Cours du Pléistocéne, Colloques internationaux Centre national de la recherche scientifique, 219, 203–209.

Slotnick, B.S., Dickens, G.R., Nicolo, M.J., Hollis, C.J., Crampton, J.S., Zachos, J.C., Sluijs, A., 2012. Large-Amplitude Variations in Carbon Cycling and Terrestrial Weathering during the Latest Paleocene and Earliest Eocene: The Record at Mead Stream, New Zealand. The Journal of Geology, 120, 487–505.

Sluijs, A., Bowen, G.J., Brinkhuis, H., Lourens, L.J., Thomas, E., 2007. The Palaeocene-Eocene Thermal maximum super greenhouse: biotic and geochemical signatures, age models and mechanisms of climate change. In: Williams, M., Haywood, A.M., Gregory, F.J. and Schmidt, D.N., (Eds). Deep-Time Perspectives on Climate Change: Marrying the Signal from Computer Models and Biological Proxies. The Micropaleontological Society, Special Publication, 323-349.

Sluijs, A., Zeebe, R.E., Bijl, P.K., Bohaty, S.M., 2013. A middle Eocene carbon cycle conundrum. Nature Geosciences, doi: 10.1038/NGEO1807.

Smith R.W., Bianchi T.S., Li X., 2012. A re-evaluation of the use of branched GDGTs as terrestrial biomarkers: Implications for the BIT Index. Geochimica et Cosmochimica Acta, 80, 14–29.

Spofforth, D.J.A., Agnini, C., Pälike, H., Rio, D., Fornaciari, E., Giusberti, L., Luciani, V., Lanci, L., Muttoni, G., 2010. Organic carbon burial following the Middle Eocene Climatic Optimum (MECO) in the central-western Tethys. Paleoceanography, 25, PA3210.

Stap, L., Lourens, L.J., Thomas, E., Sluijs, A., Bohaty, S., Zachos, J.C., 2009. High-resolution deep-sea carbon and oxygen isotope records of Eocene Thermal Maximum 2 and H2. Geology, 38, 208–210.

Stoll, H.M., 2005. Limited range of interspecific vital effects in coccolith stable isotopic records during the Paleocene-Eocene thermal maximum. Paleoceanography, 20, PA1007, doi:10.1029/2004PA001046.

Takata, H., Nomura, R., Tsujimoto, A., Khim, B., Chung, I., 2013. Abyssal benthic foraminifera in the eastern equatorial Pacific (IODP exp 320) during the Middle Eocene. Journal of Paleontology, 87-6, 1160–1185.

Thomas, D.J., Via, R.K., 2007. Neogene evolution of Atlantic thermohaline circulation: Perspective from Walvis Ridge, southeastern Atlantic Ocean. Paleoceanography, 22, PA2212, doi:10.1029/2006PA001297.

Thomas, E., 1985. Late Eocene to Recent deep-sea benthic foraminifers from the central equatorial Pacific Ocean. In: Mayer, L., Theyer, F., et al., (Eds.). Initial Reports of the Deep Sea Drilling Project , Washington (U.S. Government Printing Office), 85, pp. 655 – 694.

Thomas, E., 1998. The biogeography of the late Paleocene benthic foraminiferal extinction, in Aubry, M.P., Lucas, S.G., and Berggren, W.A., (Eds.). Late Paleocene-early Eocene biotic and climatic events in the marine and terrestrial records. New York, Columbia University Press, pp. 214–243.

Thomas, E., 2003. Extinction and food at the seafloor: A high-resolution benthic foraminiferal record across the Initial Eocene Thermal Maximum, Southern Ocean Site 690. In: Wing, S.L., Gingerich, P.D., Schmitz, B., and Thomas, E., (Eds.). Causes and Consequences of Globally Warm Climates in the Early Paleogene. Boulder, Colorado, Geological Society of America Special Paper, 369, 319–332.

Thomas, E., 2007. Cenozoic mass extinctions in the deep sea: What perturbs the largest habitat on Earth? In: Monechi, S., Coccioni, R., and Rampino, M.R., (Eds.). Large Ecosystem Perturbations: Causes and Consequences. Geological Society of America Special Paper, 424, 1–23.

Thomas, E., Zachos, J.C., 2000. Was the late Paleocene thermal maximum a unique event? GFF, 122, 169-170.

Thompson, J., Cook, G.T., Anderson, R., MacKenzie, A.B., Harkness, D.D., McCave, I.N., 1995. Radiocarbon age offsets in different-sized carbonate components of deep-sea sediments. Radiocarbon, 37, 91–101.

Tjalsma, R.C., Lohmann, G.P., 1983. Paleocene–Eocene bathyal and abyssal benthic foraminifera from the Atlantic Ocean. Micropaleontology, Special Publication, 4, 1–90.

Toffanin, F., Agnini, C., Fornaciari, E., Rio, D., Giusberti, L., Luciani, V., Spofforth, D.J.A., Pälike, H., 2011. Changes in calcareous nannofossil assemblages during the Middle Eocene Climatic Optimum: clues from the central-western Tethys (Alano section, NE Italy). Marine Micropaleontology, 81, 22–31.

Toffanin, F., Agnini, C., Rio, D., Acton, G., Westerhold, T., 2013. Middle Eocene to early Oligocene calcareous nannofossil biostratigraphy at IODP Site U1333 (equatorial Pacific). Micropaleontology, 59-1, 69-82.

Tripati, A., Backman, J., Elderfield, H., Ferretti, P., 2005. Eocene bipolar glaciations associated with global carbon cycle changes. Nature, 436, 341–346.

Turich, C., Freeman, K.H., Bruns, M.A., Conte, M., Jones, A.D., Wakeham, S.G., 2007. Lipids of marine Archaea: Patterns and provenance in the water-column and sediments. Geochimica et Cosmochimica Acta, 71, 3272–3291.

Van Morkhoven, F.P.C.M., Berggren, W.A., Edwards, A.S., 1986. Cenozoic Cosmopolitan deep-sea benthic foraminifera. Bullettin des Centres de Recherches Exploration-Production Elf-Aquitane, Mèmoire, 11, 11–421.

Via, R.K., Thomas, D.J., 2006. Evolution of Atlantic thermohaline circulation–Early Oligocene onset of deep-water production in the North Atlantic. Geology, 34, 441–444.

Wade, B.S., Kroon, D., 2002. Middle Eocene regional climate instability: Evidence from the western North Atlantic. Geology, 30, 1011–1014.

Wade B.S., 2004. Planktonic foraminiferal biostratigraphy and mechanisms in the extinction of *Morozovella* in the late middle Eocene. Marine Micropaleontology, 51, 23–38.

Weijers, J.W.H., Schouten S., Spaargaren, O.C., Sinninghe Damsté, J.S., 2006. Occurrence and distribution of tetraether membrane lipids in soils: implications for the use of the TEX_{86} proxy and the BIT index. Organic Geochemistry, 37, 1680–1693.

Westerhold, T., R□hl, U., 2013. Orbital pacing of Eocene climate during the Middle Eocene Climate Optimum and the chron C19r event–missing link found in the tropical western Atlantic. Geochemistry, Geophysics, Geosystems, 14, 4811-4825.

Winguth, A.M.E., Thomas, E., Winguth, C., 2012. Global decline in ocean ventilation, oxygenation, and productivity during the Paleocene-Eocene Thermal Maximum: Implications for the benthic extinction. Geology, 40, 263–266.

Witkowski, J., Bohaty, S.M., McCartney, K., Harwood, D.M., 2012. Enhanced siliceous plankton productivity in response to middle Eocene warming at Southern Ocean ODP Sites 748 and 749. Palaeogeography, Palaeoclimatology, Palaeoecology, 326–328, 78–94.

Zachos, J.C., Stott, L.D., Lohmann, K.C., 1994. Evolution of early Cenozoic marine temperatures. Paleoceanography, 9, 353-387.

Zachos, J.C., Pagani, M., Sloan, L.C., Thomas, E., Billups, K., 2001. Trends, rhythms, and aberrations in global climate 65 Ma to present. Science, 292, 686–693.

Zachos, J.C., Kroon, D., Blum, P., et al., 2004. Proceedings of the Ocean Drilling Program, Initial Reports, 208. Ocean Drilling Program, College Station, TX, pp. 1–112.

Zachos, J.C., Röhl, U., Schellenberg, S.A., Sluijs, A., Hodell, D.A., Kelly, D.C., Thomas, E., Nicolo, M., Raffi, I., Lourens, L.J., McCarren, H., Kroon, D., 2005. Rapid acidification of the ocean during the Paleocene–Eocene Thermal Maximum. Science, 308, 1611–1615.

Zachos, J.C., Dickens, G.R., Zeebe, R.E., 2008. An early Cenozoic perspective on greenhouse warming and carbon-cycle dynamics. Nature, 451, 279–283.

Zachos, J.C., McCarren, H.K., Murphy, B., Röhl, U., Westerhold, T., 2010. Tempo and scale of late Paleocene and early Eocene carbon isotope cycles: implications for the origin of hyperthermals. Earth and Planetary Science Letters, 299, 242–249.

Zhang, Y., Pagani, M., Liu, Z., Bohaty, S.M., DeConto, R., 2013. A 40-million-year history of atmospheric CO_2. Philosophic Transactions of the Royal Society of London A, 0.1098/rsta.2013.0096.

Zeebe, R.E., Zachos, J.C., 2013. Long-term legacy of massive carbon input to the Earth system: Anthropocene vs. Eocene. Philosophic Transactions of the Royal Society of London A, 10.1098/rsta.2012.0006.

CHAPTER IV

Benthic foraminiferal response to the Middle Eocene Climatic Optimum (MECO) in the South-Eastern Atlantic (ODP Site 1263)

F. Boscolo Galazzo[a], E. Thomas[b,c], L. Giusberti[a]

To be submitted

a Department of Geosciences, University of Padova, Via G. Gradenigo 6, Italy

b Department of Geology and Geophysics, Yale University, New Haven, CT, USA

d Department of Earth and Environmental Sciences, Wesleyan University, Middletown, CT, USA

Abstract

The response of marine biota to the Middle Eocene Climatic Optimum (MECO) is still poorly constrained, and specifically changes in deep-sea benthic foraminiferal faunas during this period of global warming have been little documented. We carried out a quantitative study on benthic foraminiferal assemblages at lower-bathyal ODP Site 1263 (Walvis Ridge, SE Atlantic), providing one of the first documentations of benthic foraminiferal assemblage changes during MECO in an open ocean setting. Our results indicate that there was no major temporary or persistent turnover in benthic foraminiferal faunas in the SE Atlantic Ocean. Benthic foraminiferal assemblage composition and accumulation rates indicate that the delivery of food to the sea-floor increased during the early stages of surface and deep-sea warming of MECO, with the largest increase in the absolute and relative abundance of phytodetritus exploiters indicating that the increased food delivery was for a large part seasonal or otherwise interrupted. During the later stage and maximum warming, delivery of food to the seafloor declined markedly. The marked decrease in both infaunal and epifaunal accumulation rates indicates that the low flux of organic matter during the more extreme parts of MECO did not give an advantage to a specific ecological niche, but made the sea-floor relatively hostile to all taxa. Paleoceanographic reconstructions combined with our benthic foraminiferal data suggest that it was mainly the warming in itself that caused the reduction in the flux of organic matter to the sea floor during the MECO at Site 1263, increasing the metabolic rates of pelagic consumers and remineralization of organic matter in the water column.

1. Introduction

After the Early Eocene greenhouse (55-50 Ma), Earth's climate shifted to a long term cooling trend leading to significant glaciation of Antarctica by the early Oligocene (~34 Ma; Zachos et al., 2001; Zachos et al., 2008; Cramer et al., 2009). Superimposed on this cooling trend, there were several episodes of warming (Bohaty and Zachos, 2003; Sexton et al., 2006; Edgar et al., 2007b; Ivany et al., 2008; Bohaty et al., 2009). The Middle Eocene Climatic Optimum (MECO) at about 40 Ma ago was the largest reversal in the Eocene long-term cooling, with a 4-6°C global temperature increase lasting ~400 kyr. The response of the marine biota to the Middle Eocene Climatic Optimum (MECO) is still poorly constrained.

Published micropaleontological records have highlighted significant biotic changes during the MECO, but the data have a patchy geographical and bathymetric distribution, with different publications focusing on different organisms, so that a fairly complete reconstruction of changes in ecosystems and even broad factors such as oceanic productivity is not yet possible (Bijl et al., 2010;

Luciani et al., 2010; Edgar et al., 2012; Witkowski et al., 2012; Toffanin et al., 2011, 2013; Boscolo Galazzo et al., 2013; Moebius et al., 2013; Witkowski et al., 2014).

Specifically, there is as yet little information on the effects of MECO on deep-sea benthic foraminiferal faunas, which had shown major extinction during the extreme warming of the Paleocene-Eocene Thermal Maximum, with lesser assemblage changes and lowered diversity during lesser hyperthermal events (Thomas, 2007; Stap et al., 2010). Benthic foraminifera have been studied across the stratigraphic interval encompassing CAE3 and CAE4 at abyssal IODP Site U1333 (equatorial Pacific), with MECO occurring between these two events, but the record is severely biased by carbonate dissolution (Takata et al., 2013). Preliminary benthic foraminiferal data are available for ODP Sites 1051 (NW Atlantic) and 748 (Southern Ocean; Moebius et al., 2013). At Site 1051, benthic foraminiferal accumulation rate indicates increased benthic productivity coincident with peak-MECO warming, and at Site 748 there are indications of decreasing oxygen levels during peak-MECO (Moebius et al., 2013).

A complete reconstruction of benthic foraminiferal changes across the MECO is so far available only for the Alano section (central-western Tethys; Boscolo Galazzo et al., 2013, Chapter 2), which was located on a continental margin.

In order to gain new insights into the effects of MECO repercussions on deep-sea floor biota in an open ocean setting, we performed a quantitative study on benthic foraminiferal assemblages at Ocean Drilling Program Site 1263 (South-Eastern Atlantic). ODP Site 1263 contains one of the few continuous records of the MECO, and is not significantly affected by carbonate dissolution (Bohaty et al., 2009), thus suitable to investigate faunal and paleoenvironmental changes related to this climatic perturbation in the southeastern Atlantic.

2. Location and Setting

ODP Site 1263 (28°53' S; 2°78' E, Fig. 1; present water depth 2717 m; ~800 km off the coast of Africa) represents the shallow end-member of a depth-transect drilled on the north-facing flank of Walvis Ridge during ODP Leg 208 (SE Atlantic Ocean; Zachos et al., 2004). Site 1263 lies beneath the eastern part of the central subtropical gyre, outside the eastern boundary current with its associated high productivity. The seafloor at Site 1263 is presently bathed by Antarctic Intermediate Water (AAIW), with North Atlantic Deep Water (NADW) at slightly greater depths (Klevenz et al., 2008).

In the middle Eocene, Site 1263 was at a paleodepth of about ~2000 m (upper abyssal; Zachos et al., 2004), and likely bathed by a southern-sourced, intermediate to deep water mass (Via and Thomas, 2006; Thomas and Via; 2007; Stap et al., 2010). Eocene sediments at Site 1263 consist of nannofossil ooze, foraminifer-bearing nannofossil ooze, clay-bearing nannofossil ooze, and chalky nannofossil ooze, with a low concentration of total organic carbon (TOC 0.86–0.00 wt%; mean = 0.09 wt%; Zachos et al., 2004). Sediments vary in color between light gray and gray at decimeter scale, with white, 1-4 cm 'blebs' surrounded by dark haloes containing fine-grained black to brown oxides. These may represent fairly large, single burrows (Zachos et al., 2004).

Site 1263 has a complete and relatively expanded record across MECO (average linear sedimentation rate for the studied interval: 0.76 cm/k.y.; Bohaty et al., 2009), and well constrained nannofossil biostratigraphy (Fornaciari et al., 2010). The MECO occurs between 142.5 and 137.9 meters composite depth (mcd), with the peak event at 138.7-137.9 mcd, and a brief recovery phase ending at 137.4 mcd. The $CaCO_3$% values fluctuate around 90% throughout the studied interval (Bohaty et al., 2009).

3. Methods

Samples were air-dried and weighed, disaggregated in distilled water, and sieved at mesh sizes ≥38, ≥63 and ≥500 μm. The size fraction larger than 63 μm was weighed and split in two equal parts with a precision micro-splitter. One half was used for isotope analysis (Chapter 2), the other for quantitative faunal analysis.

We used the smaller size fraction for the quantitative faunal analysis in order to do not miss the signal of small taxa which may carry important paleoenvironmental indications in deep sea records (e.g., Thomas et al., 1985; Boltovskoy et al., 1992; Gooday, 1993; Thomas and Gooday, 1996).

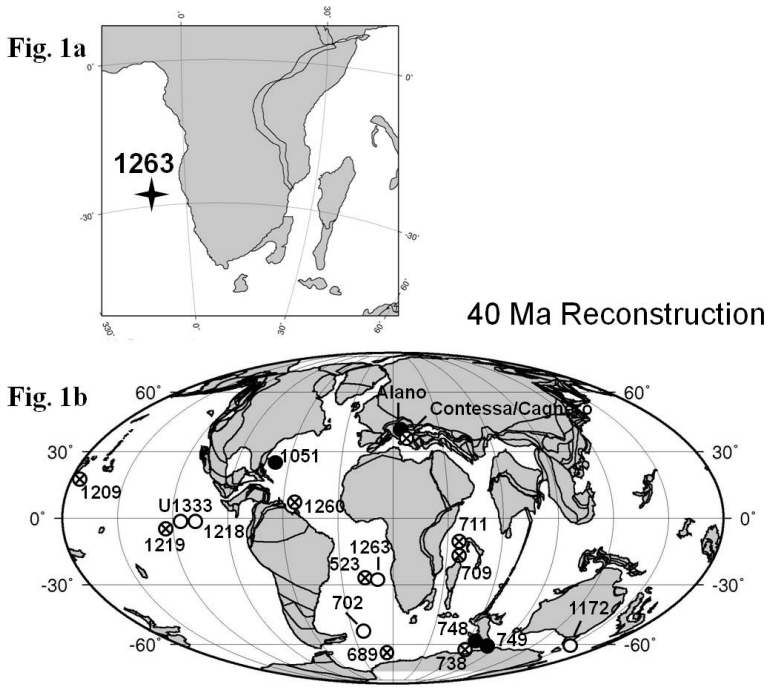

Figure 1. (a) Paleogeographic reconstruction showing the location of ODP Site 1263. (b) Paleogeographic reconstruction showing oceanic (ODP - DSDP) sites and onland sections where the MECO has been described. Sites with inferred increased productivity during the MECO are labeled with solid circles, sites with inferred decreased or unchanged productivity are labeled with open circles, sites where no data are available are labeled with open circles with a cross. Approximate positions at 40 Ma are plotted on a paleogeographic reconstruction from the Ocean Drilling Stratigraphic Network (GEOMAR, Kiel, Germany).

The studied interval spans 13 m, from 145 up to 132 mcd, and encompasses 3 m below the MECO and up to 6 m above the end of the event. We analyzed 33 samples with a regular spacing of 40 cm throughout the studied interval, corresponding on average to ~50 ky.

The quantitative analysis was based on representative splits of residues containing ≥400 specimens of benthic foraminifera.

About 150 taxa were recognized at specific or higher taxonomic levels (Appendix A). The classification at the generic level follows Loeblich and Tappan (1987); for the classification at specific level we followed mainly: Proto Decima and Bolli (1978), Tjalsma and Lohmann (1983), Miller and Katz (1983), van Morkhoven et al. (1986), Boltvskoy and Boltvskoy (1989), Watanabe (1989), Ortiz and Thomas (2006), Holbourne et al. (2013), with taxonomy for uniserial taxa with complex apertures following Hayward et al. (2013).

Specimens of the most representative taxa were photographed using SEM at the C.U.G.A.S. (Centro Universitario Grandi Apparecchiature Scientifiche) of the Padova University, Italy, and illustrated on Plates I and II.

Relative abundance of common taxa (>5%) was calculated together with faunal indices commonly used in paleoenvironmental reconstruction, including the Fisher α diversity index (using the PAST

package; Hammer et al., 2001), the absolute abundance (N/g: number of benthic foraminifera per bulk gram of sediment), and the infaunal–epifaunal ratio. The total absolute abundance was then used to calculate the benthic foraminiferal accumulation rate (BFAR) as described in Chapter 3. Accumulation Rates (AR) for the more common taxa were calculated by multiplying BFAR with the fractional abundance of the taxon in the population.

The comparison of fossil and recent communities of benthic foraminifera, in addition to test morphological analysis, is commonly used to infer microhabitat preferences and environmental parameters such as the nutrient supply to the sea floor, and/or sea water oxygenation (e.g., Bernhard, 1986; Jorissen et al., 1995; Fontanier et al., 2002; Jorissen et al., 2007). We inferred a similar ecological niche for the species *Epistominella exigua*, *Alabamina weddellensis, Epistominella vitrea* as they have in the present day oceans, lumping together their relative abundance in the phytodetritus-exploiter group (e.g., Gooday, 1993; 2003; Ohkushi et al., 2000; Thomas et al., 1995; Thomas and Gooday, 1996). Presently, *Epistominella exigua* is one of the 25 globally most widely distributed benthic foraminifera, occurring in all oceans except the Mediterranean, over a depth range of 500-7500 m (Pawlowski and Holzmann, 2008). Both *Epistominella exigua* and *Alabamina weddellensis* are very common species, with wide geographic and bathymetric ranges (e.g., Gooday 2003). In open ocean settings, where the overall annually averaged organic matter flux is not too high, they are the common species associated with seasonally fluctuating food supply (e.g., Sun et al., 2006), and in the temperate North-East Atlantic Ocean they are commonly found living within phytodetrital aggregates (e.g., Gooday, 1993, 2003). *Epistominella exigua* and *Alabamina weddellensis* bloom opportunistically when spring phytoplankton blooms cause seasonal deposition of phytodetritus to the sea-floor, leading to the build-up of large populations (Thomas et al., 1995; Gooday et al., 1996; Sun et al., 2006). In the paleontological record these species may be used to identify periods when seasonal phytodetritus deposition influenced benthic communities (Smart et al., 1994; Thomas et al., 1995). We do not know exactly what the ecological differences are between *E. exigua* and *A. weddellensis*, and their fluctuations in relative abundance are not always similar (e.g., Thomas et al., 1995S Ohkushi et al., 2000; Sun et al., 2006). The occurrences of *Epistominella vitrea* are less documented than those of the other two, species, but it also has a broad bathymetric (neritic to lower bathyal) and geographical distribution (Gooday and Hughes, 2002; Pawlowsky et al., 2007). This taxon is one of the most abundant species at a lower bathyal site at Rockall Trough (NE Atlantic) with widespread deposition of phytodetritus (Gooday and Hughes, 2002). *E. vitrea* like *E. exigua* and *A. weddellensis*, has a small, smooth-walled and thin test with few chambers (Plate I). Species with small, thin tests with few chambers and broad bathymetric and geographical distributions may

generally be phytodetritus exploiters, with their morphology reflecting opportunistic behavior and the ability to respond to food pulses with rapid growth and reproduction (Gooday, 1993). Possibly, we lack sufficient documentation on *E. vitrea* in present day oceans because many studies focus on size fractions above 100 µm, thus missing its small tests (e.g., Gooday 1993).

Abundant occurrences of the cosmopolitan *Globocassidulina subglobosa* have been related to a number of variables, including water masses (e.g., Mackensen et al., 1995), and pulsed food inputs (Gooday 1994; Gupta and Thomas, 2003). The species is common close to Antarctica, where growing conditions are highly seasonal and it feeds on diatoms (Suhr et al., 2003). In the modern eastern South Atlantic it has been associated with vigorous bottom currents and sandy sediments (Schmiedl et al., 1997). The species sometimes co-varies with *N. umbonifera* (Sun et al., 2006; Smart et al., 2007), and has been suggested to be opportunistic because it peaks after the extinction at the Paleocene Eocene Thermal Maximum (Alegret et al., 2009; 2010; d'Haenens et al., 2012).
The epifaunal species *N. truempyi* and its descendant *N. umbonifera* are generally common at great depths. *N. truempyi* became extinct at the end of the Eocene (e.g. Thomas 1985). Its living descendant *N. umbonifera* is considered typical for regions with low, non-seasonal food supply (e.g., Gooday, 2003; Loubere 1991, 1997; Schmiedl et al., 1997; Jorissen et al., 2007; Sun et al., 2006), possibly combined with carbonate corrosive waters (Bremer and Lohmann, 1982). Similar environmental conditions have been supposed for the ancestral species (Thomas, 1998).

We assigned species to epifaunal and infaunal groups by comparing their test morphology with the morphology of morphogroups as described in Corliss (1985), Jones and Charnock (1985), Corliss and Chen (1988), and Mancin et al. (2013). Infaunal calcareous taxa were further arranged in the following categories: bi-triserial taxa (including all the bolivinoids and buliminids), uniserial hyaline (including *Laevidentalina*, *Nodosarella*, *Nodosaria*, *Glandulonodosaria*, *Siphonodosaria*, *Strictocostella*), planispiral infaunal (including *Nonion*, *Nonionella*, *Pullenia*).
We realize that caution is needed in applying taxonomic uniformitarianism, due to our limited knowledge of the biology and ecology of living species. Even for many living species, the relation between test morphology and microhabitat has not been directly observed, but is extrapolated from data on other taxa (e.g., Jorissen, 1999). The assignment of modern foraminifera to microhabitats based on their morphology may be accurate only about 75% (Buzas et al., 1993): comparisons between past and recent environments thus need careful evaluation

4. Results

At Site 1263, the benthic foraminiferal assemblage is dominated by calcareous hyaline forms, with agglutinated taxa representing less than 1% of the assemblage throughout the studied interval (Appendix 4). The preservation of benthic foraminifera is generally good, but SEM-images of tests reveal the extensive presence of secondary calcite, particularly affecting small specimens.

4.1. Paleobathymetry

Site 1263 was located at about 2.0 km water depth in the middle Eocene as derived by backtracking (Zachos et al., 2004), similar to that of DSDP sites drilled on Leg 74. The abundant to common occurrence of *Nuttallides umbonifera*, *Nuttallides truempyi*, *Bolivinoides huneri* and *Epistominella exigua*, whose bathymetric distribution was lower bathyal to abyssal in the Paleogene (e.g., van Morkhoven et al., 1986, Alegret and Thomas, 2001; Holbourn et al., 2013), indicate a paleodepth of 1.5-2.0 km, confirming the previous estimate.

4.2. Faunal composition at Site 1263 and changes across the Middle Eocene Climatic Optimum

Benthic foraminiferal assemblages show a moderate, fluctuating faunal diversity (Fisher α ~15; Fig. 2), which tend to gradually decrease upward in the section, but diversity was high during peak MECO. The relative abundance of epifaunal species fluctuates around 60% of the assemblage (Fig. 2) throughout the section, i.e. somewhat more than half of the total abundance. As is common for deep-sea assemblages, the benthic foraminiferal faunas at Site 1263 are characterized by relatively few abundant and common rare species (e.g., Thomas, 1985; Boltovskoy, 1992). Among epifaunal taxa, the most abundant species are *Nuttallides truempyi* (~15%, peaks to ~28%) and *N. umbonifera* (13%, peaks to ~18%). Species of the phytodetritus-exploiter group are also common (ca. 15%, peaks up to ~30%), with *Epistominella vitrea* representing the most abundant taxon (ca. 8%, peaks up to 20%; Figs. 3, 4).

The epifaunal, oligotrophic *Nuttallides truempyi*, *N. umbonifera* and the relatively oligotrophic, seasonally supplied phytodetritus-exploiter group together make up ~40% of the entire fauna (Fig. 3; Plate I). *N. umbonifera* and the phytodetritus-exploiter group have very similar patterns in the whole studied interval, with closely covarying records within 145 and 136 mcd (Fig. 3).

Plate I

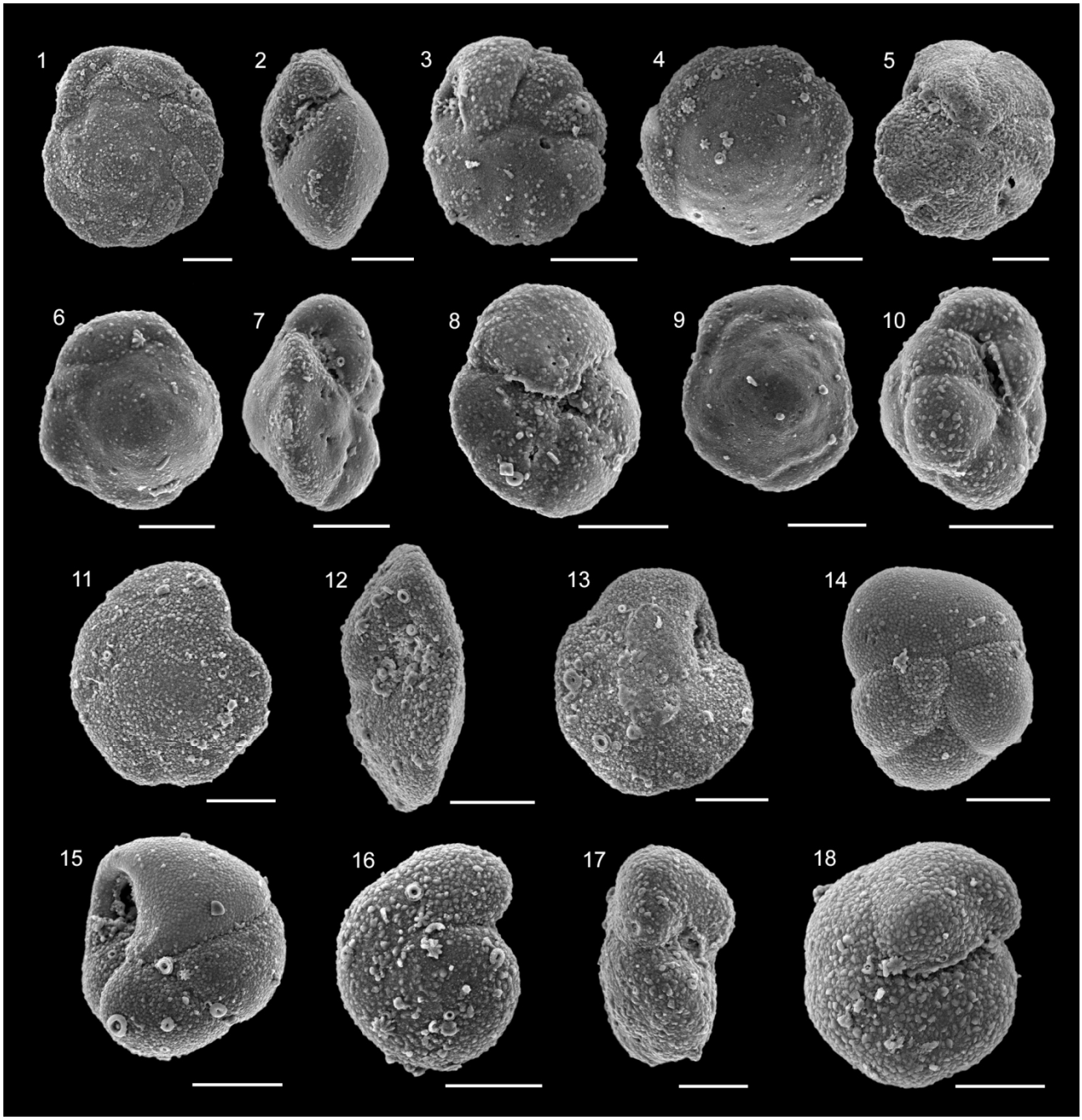

Plate I. Scale bar = 50 μm Fig. 1 *Nuttallides umbonifera* (Cushman, 1933) spiral view, sample 8793; Fig. 2 *Nuttallides umbonifera* (Cushman, 1933) lateral view, sample 8785; Fig. 3 *Nuttallides umbonifera* (Cushman, 1933) umbilical view, sample 8793; Fig. 4 *Nuttallides umbonifera* (Cushman, 1933) spiral view, sample 8793; Fig. 5 *Nuttallides umbonifera* (Cushman, 1933) umbilical view, sample 8785; Fig. 6 *Alabamina weddellensis* (Earland, 1936) spiral view, sample 8785; Fig. 7 *Alabamina weddellensis* (Earland, 1936) lateral view, sample 8785; Fig. 8 *Alabamina weddellensis* (Earland, 1936) umbilical view, sample 8793; Fig. 9 *Alabamina weddellensis* (Earland, 1936) spiral view, sample 8785; Fig. 10 *Alabamina weddellensis* (Earland, 1936) lateral view, sample 8793; Fig. 11 *Epistominella exigua* (Brady, 1884) spiral view, sample 8785; Fig. 12 *Epistominella exigua* (Brady, 1884) lateral view, sample 8785; Fig. 13 *Epistominella exigua* (Brady, 1884) umbilical view, sample 8795; Fig. 14 *Epistominella vitrea* Parker, 1953 spiral view, sample 8785; Fig. 15 *Epistominella vitrea* Parker, 1953 umbilical view, sample 8785; Fig. 16 *Gyroidinoides mediceus* (Emiliani, 1954) spiral view, sample 8793; Fig. 17 *Gyroidinoides mediceus* (Emiliani, 1954) lateral view, sample 8785; Fig. 18 *Gyroidinoides mediceus* (Emiliani, 1954) umbilical view, sample 8793.

Other well represented taxa are *Bolivinoides huneri* (mean relative abundance ~10%; Plate II) which periodically shows peaks above 20%, and *Globocassidulina subglobosa* (10%; Fig. 4). The percentage of hyaline, uniserial taxa is about 7% in the lower part of the studied interval, and decreases upward, but with a peak of ~10% close to the peak of MECO. Planispiral infaunals are close to 5% in the lower part of the studied interval, then decrease markedly upward (Fig. 4; Plate II). The decrease in these two groups of species upward may cause the upward decrease in diversity (Fig. 2).

Relatively common taxa are small epifaunal species, including *Clinapertina* spp., *Gyroidinoides mediceus, Gyroidinoides* spp. and *Cibicidoides lamontdohertyi,* all reaching relative abundances close to ~5% (Plate I, II). The cumulative percentage of *Clinapertina* species shows an upward increase, with abundances close to 10% at the top of the studied interval (Fig. 4).

Bi-triserial species other than *B. huneri* are not abundant (cumulative abundance 10%), and mainly represented by *Caucasina* sp., *Bulimina* cf. *elongata, Bulimina tuxpamensis* and *Buliminella grata-B. beaumonti* (Fig. 4; Plate II).

From the base of our record (145 mcd), the benthic foraminiferal accumulation rate (BFAR), and coarse fraction accumulation rate (CFAR) increase upward, reaching a peak in the middle of the early MECO warming (141-141.5 mcd). Over the same interval, the relative abundances of *N. umbonifera* and the phytodetritus-exploiter group increase, whereas infaunal percentage decrease (Figs. 2, 3). At their peak, *N. umbonifera* and the phytodetritus-exploiter group make up to 35% of the assemblage, and BFAR and CFAR reach values around 300 and 0.0050 respectively (Figs. 2, 3). Noticeably, during the highest BFAR, the AR of infaunal species, *N. truempyi*, *N. truempyi* and the phytodetritus exploiters all increase, but the AR of the phytodetritus species increases more than these of the other groups, so that the % infaunal species decreases.

BFAR and CFAR values start to decrease up-section at 141 mcd, both reaching a minimum at about 139 mcd, the peak MECO warming. The relative abundance of *N. umbonifera* and the phytodetritus-exploiter group decrease as well, reaching values close to 5% at peak-MECO warming (Figs. 2, 3). A marked decrease is shown also by *C. lamontdohertyi,* which almost disappears at peak MECO warming (Fig. 4). The decrease of these taxa is paralleled by 8% increase of the species *N. truempyi,* which remains high throughout the MECO. Except for a single sample in the post-MECO interval in which *N. truempyi* peaks up to 28%, the MECO is the interval with the higher percentages of this species (~23%; Fig. 3). During peak MECO, the infaunal % is fairly high, and there are peaks in relative abundance of *G. subglobosa*, *Clinapertina* spp., and planispiral infaunal species. The total infaunal relative abundance shows a slight increase at about 139.5 mcd, lasting up to the end of the MECO peak-warming (Figs. 3, 4).

After peak MECO, BFAR and CFAR fluctuate and increase slightly, but never reach the peak values of early MECO. We studied only a few samples before the beginning of the initial phase of MECO warming, so can not be certain whether the assemblages returned to conditions before MECO. *N. umbonifera, C. lamontdohertyi*, and the phytodetritus-exploiter group rebound to their pre-event abundance, whereas *N. truempyi* decreases in relative abundance. There are no major changes between pre- and post MECO assemblages, with the possible exception of a decline in relative abundance of planispiral infaunal species and possible hyaline uniserial species. In addition, some sharp peaks in relative abundance of *N. truempyi*, phytodetritus-exploiter group and *Bolivinoides huneri* characterize the post-MECO interval, and correspond to higher accumulation rates, except for the peak in abundance of *B. huneri* at 136 mcd (Figs. 2, 4).

Some taxa, such as the bi-triserial species and *G. subglobosa* do not show apparent changes related with the MECO, but fluctuate in relative abundance throughout the entire studied interval. Peaks in relative abundance of *B. huneri* occur before, after and during MECO.

5. Discussion

5.1. Benthic foraminiferal fauna at Site 1263: Interpreting paleoenvironmental changes across the MECO.

The relative abundance and AR of the Phytodetritus-exploiters at Site 1263 do not suggest there were large and intensive episodes of phytodetritus deposition comparable with those nowadays occurring in the North-Eastern Atlantic and at high latitudes (e.g. Thomas et al., 1995; Sun et al., 2006). Presently, the systematic occurrence of large spring phytoplankton blooms is linked to the formation of a deep (>200 m) winter mixing layer, allowing for the up-ward redistribution of nutrients from deeper nutrient-rich waters during the winter (e.g., Miller and Wheeler, 2012). This results in large phytoplankton blooms in the spring, and a benthic foraminiferal assemblage strongly dominated by phytodetritus exploiting species (Gooday, 1993; Thomas et al., 1995; Nees et al., 1997; Ohkushi et al., 2000; Sun et al., 2006). We do not see such deep winter mixing in the subtropical South-East Atlantic even today (Levitus, 1994), with only weak spring blooms reported in this area (Lohmann, 1992). Only if phytodetritus accumulates persistently in a particular area will the abundance of phytodetritus-exploiters taxa be expressed in the fossil record (Thomas and Gooday, 1996).

Plate II

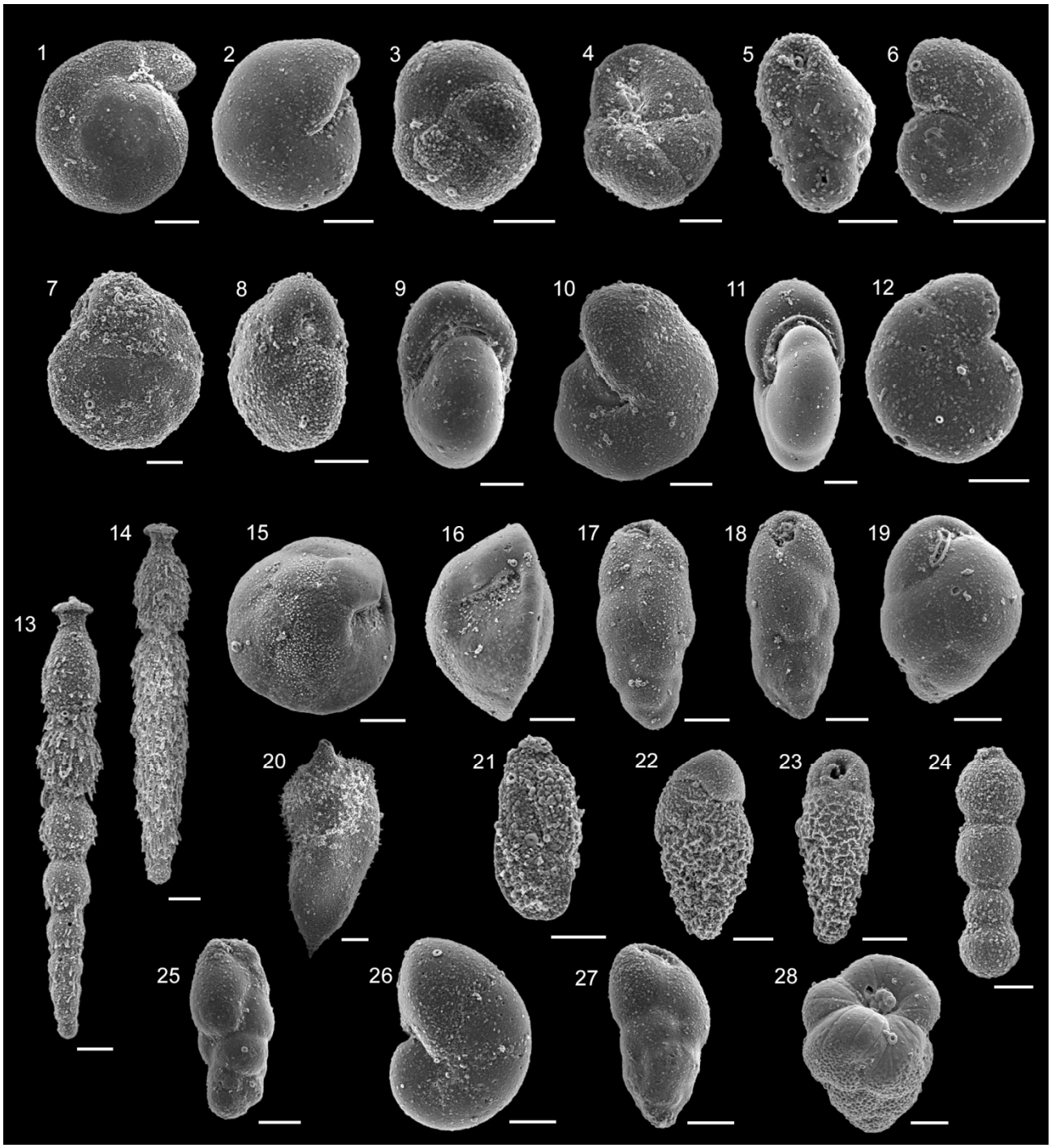

Plate II. Scale bar = 50 µm Fig. 1 *Clinapertina complanata* Tjalsma & Lohmann, 1983 spiral view, sample 8793; Fig. 2 *Clinapertina complanata* Tjalsma & Lohmann, 1983 umbilical view, sample 8793; Fig. 3-4 *Caucasina* sp., sample 8785; Fig. 5 *Caucasina schischkinskye* (Saimolova, 1947), sample 8785; Fig. 6 *Gyroidinoides depresuss* (Alth, 1850) spiral view, sample 8785; Fig. 7 *Cassidulina islandica* Nörvang, 1945, sample 8785; Fig. 8 *Stetsonia minuta* Parker, 1954 lateral view, sample 8793; Fig. 9 *Clinapertina subplanispira* Tjalsma & Lohmann, 1983 lateral view, 8785; Fig. 10 *Clinapertina subplanispira* Tjalsma & Lohmann, 1983 umbilical view, sample 8785; Fig. 11 *Clinapertina subplanispira* Tjalsma & Lohmann, 1983 lateral view, 8793; Fig. 12 *Gyroidinoides planulatus* (Cushman & Renz, 1941) spiral view, sample 8785; Fig. 13-14 *Srictocostella hispidula* (Cushman, 1939) sample 8793; Fig. 15 *Nuttallides truempyi* (Nuttall, 1930) spiral view, 8793; Fig. 16 *Nuttallides truempyi* (Nuttall, 1930) lateral view, 8793; Fig. 17-18 *Bulimina* cf. *elongata* d'Orbigny 1846, sample 8793; Fig. 19 *Turrilina robertsi* (Howe and Ellis, 1939) sample 8785; Fig. 20 *Pyrulina extensa* (Cushman, 1923), sample, 8785; Fig. 21 *Seabrookia rugosa* Watanabe, 1989, sample 8785; Fig. 22 *Bolivinoides huneri* (Howe, 1939), sample 8793; Fig. 23 *Bolivinoides huneri* (Howe, 1939) lateral view, sample 8793; Fig. 24 *Glandulonodosaria ambigua* (Neugeboren, 1856), sample 8793; Fig. 25 *Bulimina simplex* Terquem, 1882, sample 8785; Fig. 26 *Nonionella robusta* Plummer, 1931, sample 8793; Fig. 27 *Bulimina* cf. *elongata* d'Orbigny 1846, sample 8785; Fig. 28 *Buliminella beaumonti* Cushman and Renz, 1946, sample 8785.

These phytoplankton offsprings may have been induced by irregular and patchy transit of mesoscale eddies, which can induce short phytoplankton blooms in otherwise un-productive subtropical open-ocean areas characterized by a weak seasonality and a stable water column (e.g., Bidigare et al., 2003; McGillycuddy et al., 2007; Dore et al., 2008.)

The low BFAR and the abundance of the generally oligotrophic indicator species *Nuttallides umbonifera* and *N. truempyi* at Site 1263 suggest that the seafloor at the site was largely oligotrophic (Figs. 2, 3). In the studied site, well above the CCD, the common presence of *N. umbonifera* likely indicates an overall low organic matter flux rather than low $CaCO_3$ saturation. The ~40% of infaunal species (Figs. 2, 3) may seem to contrast with the interpretation of an oligotrophic sea-floor, and could be seen to indicate more mesotrophic conditions (Jorissen et al., 1995; Fontanier et al., 2002). However, a substantial part of the infaunal population is made up of *Globocassidulina subglobosa* and *Bolivinoides huneri* (Fig. 4). The living *G. subglobosa* sometimes co-varies with *N. umbonifera* (Sun et al., 2006), and may be common in oligotrophic areas characterized by pulsed food supply and phytodetritus deposition (Gooday, 1993; Gupta and Thomas, 2003; Suhr et al., 2003), in agreement with what we observed at Site 1263. The extinct *Bolivinoides huneri* (Plate II), was common in middle Eocene - Oligocene at lower bathyal to abyssal depths (Holbourn et al., 2013), suggesting a preference for low organic carbon flux relative to other buliminids which were much more abundant along continental margins. In lower Eocene sediments in the Bay of Biscay (NE Atlantic), *B. huneri* clusters together with *N. umbonifera* and other epifaunal taxa, rather than with other bi-triserials (d'Haenens et al., 2012). It morphologically resembles *Bolivinoides crenulata*, which has been inferred to prefer oligo-mesotrophic conditions (Boscolo Galazzo et al., 2013).

Other bi-triserial and uniserial hyaline taxa may indicate a higher and specifically more continuous food supply (e.g., Lutze and Coulbourn, 1984; Loubere, 1991; 1997; Jorissen et al., 1995; Thomas, 2007), and these are rare in our samples (Figs. 2, 4). On the whole, the character of the infaunal population at Site 1263 is in agreement we the interpretation of a largely oligotrophic environment, with occasionally higher surface productivity and pulsed delivery of food at the sea-floor.

BFAR and the relative abundance of the phytodetritus-exploiters and *N. umbonifera* show an apparent increasing trend just above the beginning of our records (145 mcd; Figs. 2, 3), but the record is too short to document this clearly.

The MECO did not lead to a major turnover of benthic foraminiferal assemblages, neither temporary nor persistent, at Site 1263, and in contrast to observations at the Tethyan Alano section (Boscolo Galazzo et al., 2013; Chapter 1), large compositional changes did not occur in the post-

Figure 2. $\delta^{18}O$ records and faunal variations across the MECO at ODP Site 1263 plotted against biostratigraphy and depth (mcd). Blue line = *Nuttallides truempyi* $\delta^{18}O$ record, red line = bulk carbonate $\delta^{18}O$; BFAR = benthic foraminiferal accumulation rate; CFAR = coarse fraction accumulation rate; Fisher α diversity index; Bi-triserial = cumulative relative abundance of the buliminids; Infaunal = infaunal to infaunal and epifaunal ratio; InfAR = infaunal taxa accumulation rate; Bi-triAR = bi-triserial taxa accumulation rate; *N.true*AR = *Nuttallides truempyi* accumulation rate; *N.umb*AR = *Nuttallides umbonifera* accumulation rate; Phyto-group accumulation rate = phytodetritus-exploiters group accumulation rate; Oxygen stable isotopes, BFAR and CFAR from Chapter 2. The area shaded in gray highlights the entire MECO interval. The light gray area denotes the peak of the MECO event. Biostratigraphy after Fornaciari et al. (2010) following: (1) calcareous nannofossils zonation of Fornaciari et al. (2010) and (2) nannofossils standard zonation of Okada and Bukry (1980).

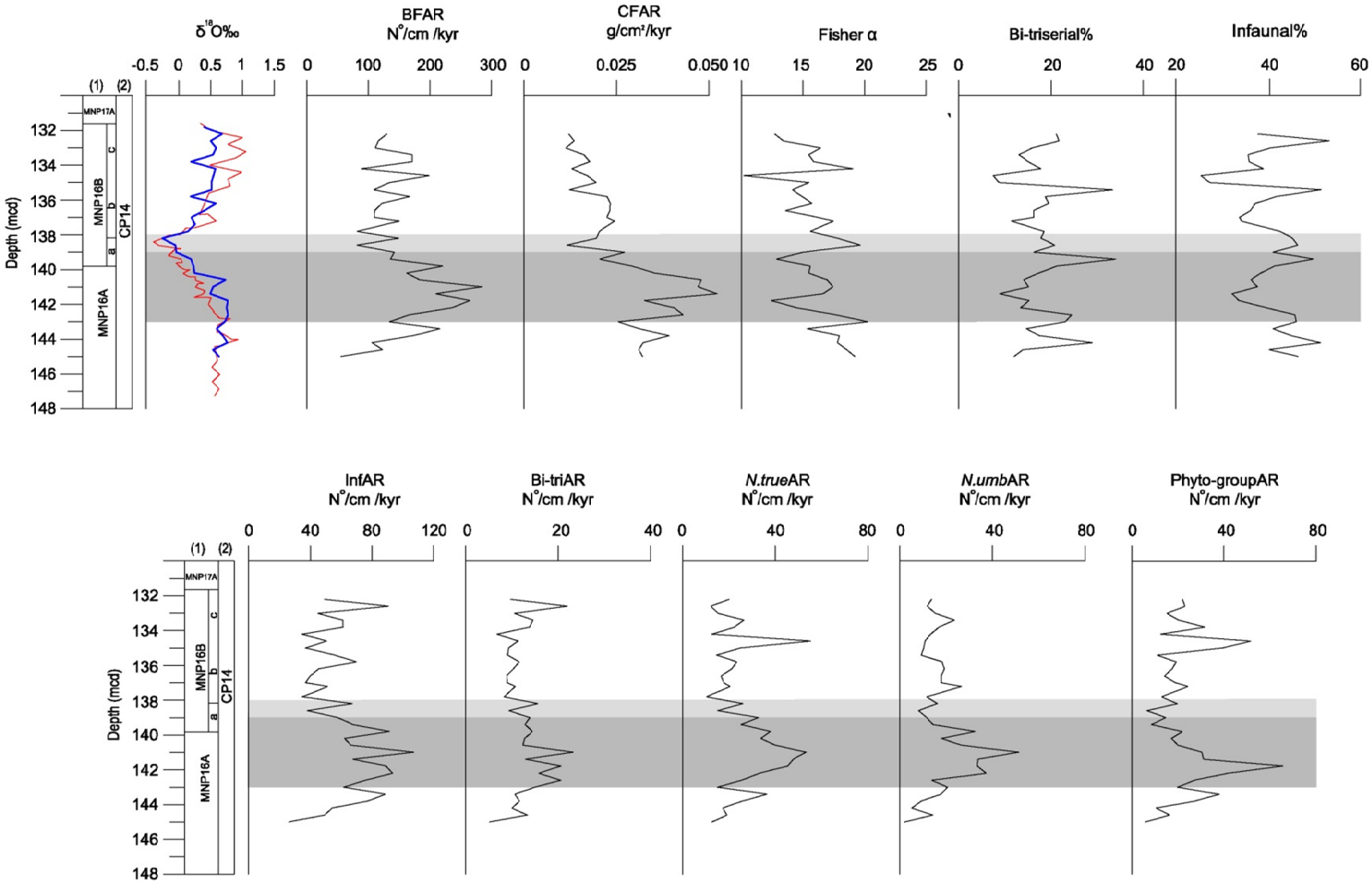

MECO interval either. The most striking changes across the MECO are the initial increase in BFAR at the same time as an increase in CFAR during the early part of the gradual warming, followed by the large decrease in BFAR along with a relative abundance decrease of phytodetritus-exploiters group and *N. umbonifera* (Figs. 2, 3). The $\delta^{13}C$ records for Site 1263 do not support a marked increase in stratification during the MECO (Chapter 3), so that the decrease in BFAR during peak MECO has been interpreted as indicating a decrease in food reaching the seafloor (Chapter 3). Such a decrease was probably linked to a warming-induced, increased heterotrophic metabolic rates, and organic matter remineralization in the water column (e.g, Lopez-Urrutia et al., 2006). CFAR decreases together with BFAR (Fig. 1), indicating a parallel decline in planktic foraminiferal productivity. The fact that surface surface waters at Site 1263 were probably nutrient limited, meant that the warming could not result in significant increase in primary productivity, leading to the progressive starvation of heterotrophs. The decreasing CFAR indicates that MECO-warming may have increased the metabolism of planktic consumers, enhancing the recycling of the organic matter in the water column, reducing export fluxes.

The significant decrease in the accumulation rates of each of the major taxon-groups in the assemblages (Fig. 1) indicate that the diminished flux of organic matter exacerbated the oligotrophy at the sea-floor, making it less hospitable to all taxa. Note that the increase in BFAR during the early part of MECO was much more pronounced among the phytodetritus-exploiters than among the other groups, suggesting that the early warming resulted in more interrupted food delivery to the sea floor, with lower infaunal %.

Possibly lower fluxes during peak MECO, when temperature rose even higher, were combined with enhanced metabolic rates of benthic foraminifera induced by warming of deep waters, leading to a greater starvation of the population when there was no increased delivery of food to the seafloor (Olivarez Lyle and Lyle, 2006; Winguth et al., 2012). The strong decrease in BFAR, phytodetritus-exploiter group and *N. umbonifera* percentages, occur above the onset of the bulk $\delta^{18}O$ negative excursion (~143 mcd), and coincides with the onset of decreasing benthic $\delta^{18}O$ values (at ~141.5 mcd; Fig. 1). As explained in Chapter 2, we are not confident about the nature of the time lags observed among the developed temperature records. The lowest BFAR and relative abundance values are reached at peak-MECO warming, suggesting that a worsening of the conditions paralleled the increase in surface and deep water temperatures (Figs. 2, 3).

Epifaunal taxa were greatly affected, with *N. umbonifera* and the phytodetritus exploiters showing a more pronounced decrease in accumulation rate, mirrored by their decreasing relative abundance across the MECO (Figs., 2, 3, 4). *Nuttallides umbonifera* is able to ingests fresh algal cells (similar

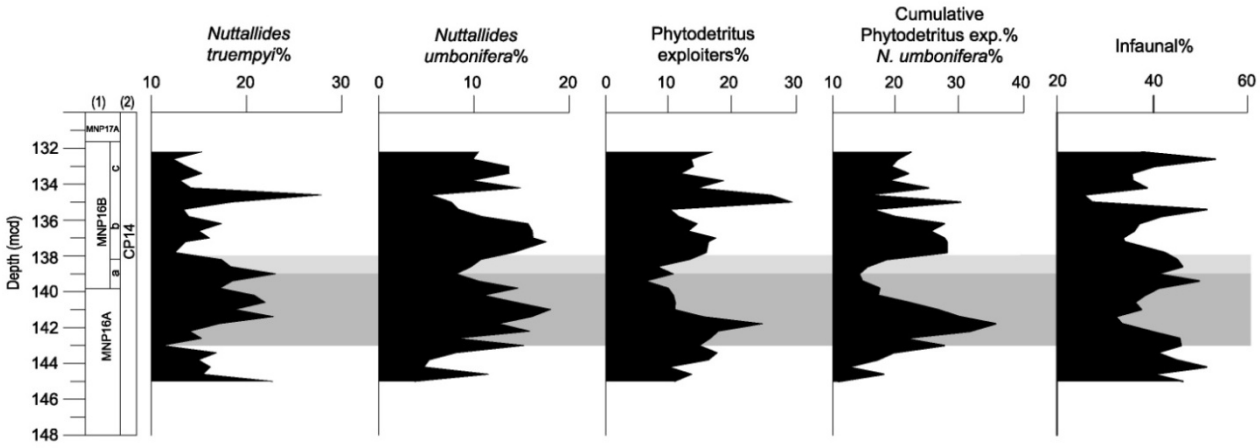

Figure 3. Relative abundance of the most abundant benthic foraminifera species and group of taxa across the MECO at ODP Site 1263 plotted against biostratigraphy and depth (mcd). Phytodetritus-exploiters group percentage (including *Epistominella exigua*, *E. vitrea*, *Alabamina weddellensis*); Cumulative phytodetritus-exp. – *N. umbonifera* = cumulative percentage of phytodetritus-exploiters group and *N. umbonifera*; Infaunal = infaunal to infaunal and epifaunal ratio. The area shaded in gray highlights the entire MECO interval. The light gray area denotes the peak of the MECO event. Biostratigraphy after Fornaciari et al. (2010) following: (1) calcareous nannofossils zonation of Fornaciari et al. (2010) and (2) nannofossils standard zonation of Okada and Bukry (1980).

to *Epistominella exigua*; Gooday, 1993), and these species may have a similar diet, with the first tolerant to a lower food supply. These taxa show similar patterns in relative abundance throughout most of the studied interval (Fig. 3), which may suggest a similar dependence for the supply of labile organic matter from the water column in oligotrophic environments. The parallel decrease in relative abundance of both may indicate that the oligotrophy at sea-floor may have overcome even the limits of food supply for *N umbonifera*.

The increase in relative abundance of *Nuttallides truempyi* across MECO does not correspond to an increase in AR of this taxon (Figs. 2, 3). The increase in relative abundance reflects that the species decreased less in AR than *N. umbonifera* and the phytodetritus exploiters (Fig. 2). At some sites, *N. truempyi* increased in relative abundance (including Site 1263 and other sites at Walvis Ridge; Thomas and Shackleton 1996; Foster et al., 2013) just after the extinction at the Paleocene/Eocene Thermal Maximum (PETM; Thomas, 1998; Thomas, 2007). The species, survived in the very warm and carbonate-corrosive waters (McCarren et al., 2008) at Site 1263, but became extinct at the end of the Eocene, and possibly was better suited to thrive in a warming environment than modern taxa now living in cold bottom waters.

The relative abundance of Infaunal species fluctuates throughout the studied interval, showing a slight increase across the MECO, while their cumulative accumulation rates parallel the decreasing trend of total BFAR (Fig. 2). The decrease in AR of infaunal taxa, specifically those of bi-triserial taxa, is generally more gradual than those of the most abundant epifaunals (Fig. 2), suggesting they

may have been less affected by the lowered of export productivity. Possibly, living within the sediment, they could at least in part survive using refractory organic matter (e.g., Fontanier et al., 2005; Jorissen et al., 2007).

At the end of peak-MECO warming, the relative abundances of the most common taxonomic groups rebounded to pre-event values, whereas the BFAR recovered more gradually (Figs. 2, 3, 4). We do not have sufficient sample coverage to evaluate pre-MECO conditions in detail, so we do not know whether post-MECO background conditions were somewhat different from pre-MECO conditions. The highest BFAR (and peak relative abundance of phytodetritus exploiters) occurred during the early part of gradual MECO-warming, and post-MECO conditions did not return to these conditions. The peaks of phytodetritus-exploiters in post-MECO, is associated with an upward decreasing diversity (Figs. 2, 3, 4). The decreasing diversity may have been caused by the decrease in relative abundance of the uniserial hyaline taxa and planispiral infaunals (Fig. 4), which are species rich groups, and their decline might suggest a lower/more pulsed organic matter flux (Thomas, 2007). Among the *Clinapertina* species, *C. subplanispira* (Plate II) is most abundant in the post-MECO interval; this taxon is possibly a low-food indicator and among the dominant taxa in the aftermath of the PETM at Walvis Ridge (Thomas and Shackleton, 1996; Thomas, 1998; Thomas, 2007).

5.2. Middle Eocene benthic foraminifera at Site 1263: towards modern faunas?

At Site 1263, we noted significantly high cumulative abundances of the phytodetritus-exploiting species *Epistominella exigua, E. vitrea* and *Alabamina weddellensis* (Plate I; Fig. 3). Together with *Epistominella vitrea*, these taxa reach percentages around 15-18%, with peaks greater than 20% (Fig. 3). The first two of these are long ranging taxa, reported in the literature since the late Paleocene-lowermost Eocene (e.g., Thomas et al., 1990; Boltovskoy et al., 1992). They were, however, not globally abundant in the Eocene, rapidly increased in abundance over the Eocene/Oligocene transition at high southern latitudes and by the middle Miocene became common in the equatorial Pacific (Thomas and Gooday, 1996; Thomas, 2007). *Epistominella vitrea* (Plate I) was not documented as significantly present at the same sites as the other two species. In the Southern Ocean, *E. vitrea* is documented at the Kerguelen Plateau since the late Miocene (Pawlowsky et al., 2007).

At Site 1263 and the deeper Site 1267, all 3 species are present at low levels, with rare peaks up to 15-18%, in samples just above the Ypresian/Lutetian boundary, and at much lower abundances before that time (Ortiz and Thomas, 2012). We document that these percentages

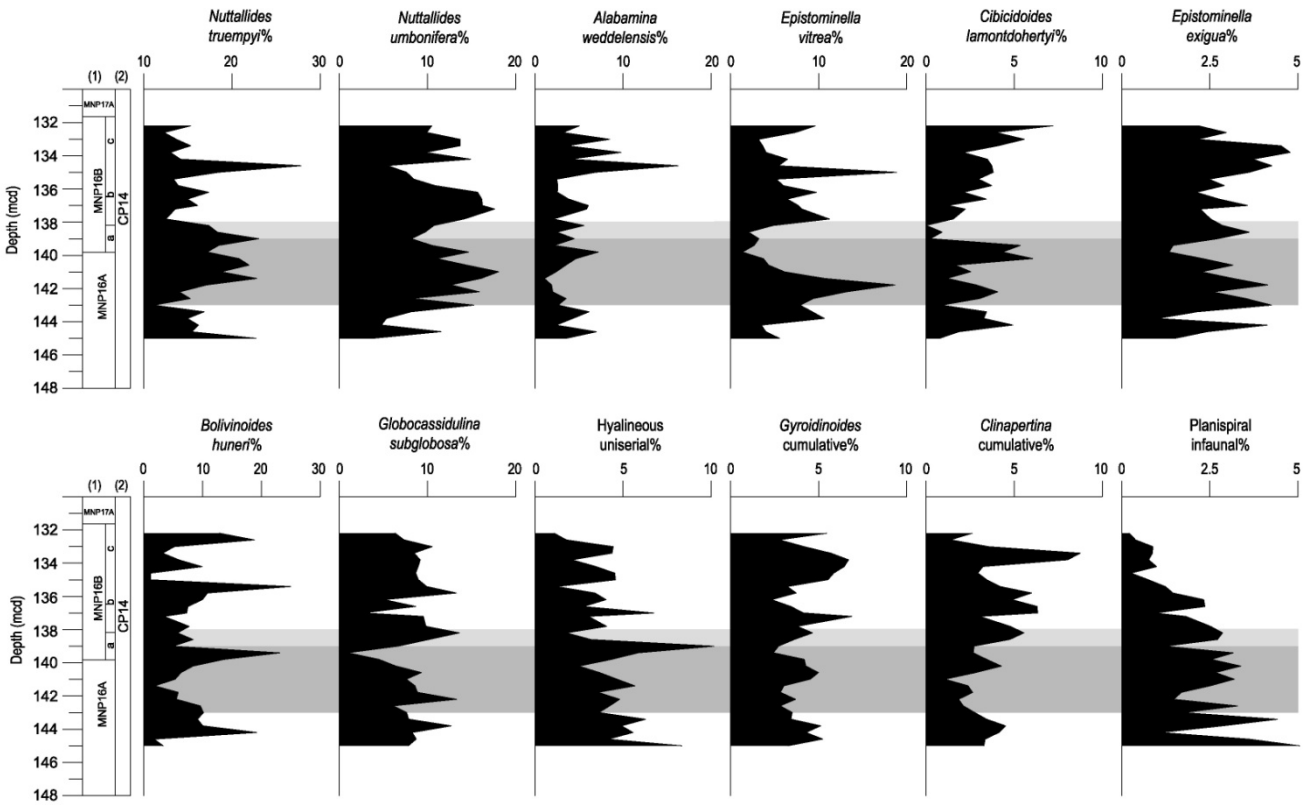

Figure 4. Relative abundance of selected benthic foraminifera species and group of taxa across the MECO at ODP Site 1263 plotted against biostratigraphy and depth (mcd). The area shaded in gray highlights the entire MECO interval. The light gray area denotes the peak of the MECO event. Biostratigraphy after Fornaciari et al. (2010) following: (1) calcareous nannofossils zonation of Fornaciari et al. (2010) and (2) nannofossils standard zonation of Okada and Bukry (1980).

persisted and increased in the mid-latitude SE Atlantic into the Bartonian. The three species remain common at Site 1263 in the ≥63 μm size fraction in the uppermost Priabonian, increasing significantly in abundance across and after the Eocene/Oligocene boundary (Fenero et al., 2010).

Comparable cumulative percentage of *A. weddellensis* and *E. exigua* (but not *E. vitrea*) have been reported at Southern Ocean Site 689 (Thomas and Gooday, 1996).

These three phytodetritus-exploiters are associated with *Nuttallides umbonifera* (Plate I), another common and worldwide distributed taxon in modern oceans. *N. umbonifera* is usually common in oligotrophic areas as subtropical abyssal plains (e.g., Sun et al., 2006), where the deposition of phytodetritus is not frequent, and at depths in between the lysocline and the calcium carbonate compensation depth (CCD; e.g., Holbourn et al., 2013).

A "modern"-type oceanic fauna significantly different from that one of the lower Paleogene, and characterized by the common occurrence of phytodetritus species and *N. umbonifera* at high latitudes, became established across the Eocene/Oligocene transition during a major faunal turnover, gradual over several millions of years (Thomas and Gooday, 1996; Thomas, 2007). With

the establishment of the Antarctic ice sheet in the earliest Oligocene and the strong increase in abundance of diatoms as primary produces (Falkowski et al., 2004; Norris et al., 2013), the seasonal supply of labile organic matter to the seafloor may have drastically increased. These conditions would have progressively advantaged species able to overcome prolonged oligotrophic periods, and/or rapidly profit from periodical and brief pulses of food to the sea-floor (Thomas and Gooday, 1996; Thomas, 2007).

Our data combined with these in Ortiz and Thomas (2012) show that *N. umbonifera* and the phytodetrius-exploiters already reached significant relative abundance in the middle Eocene at mid-latitude Site 1263, making up to ~25-30% of the assemblage by the time of MECO (Fig. 3). The abundance of these species, along with the low average faunal diversity and the low percentage of uniserial hyaline species (Figs. 2, 4) show resemblance to more recent open-ocean assemblages (Thomas and Gooday, 1996; Thomas, 2007). In contrast, at high southern latitude Sites 689 and 690 the uniserial species with complex apertures, also called the "extinction group" (Hayward et al., 2012) remained extremely abundant throughout the late Eocene.

This "modern" character of the middle Eocene assemblages at Site 1263, however, was only partial, since typical early Paleogene buliminids persisted (i.e., *Bulimina trinitatensis*, *B. tuxpamensis*, *B. semicostata*). Further, the long-ranging *Nuttallides truempyi* (Plate II), one of the most common species of the greenhouse oceans that became globally extinct at Eocene/Oligocene boundary, was present at relatively high relative abundances, co-occurring with its descendant *N. umbonifera* (Berggren and Aubert, 1976; Tjalsma and Lohmann, 1983; Thomas, 1985). In addition, the typical Paleogene *Clinapertina* group persisted. Other typical Paleogene taxa such as *Aragonia aragonensis* and *Abysammina* species, however, had become extinct at the end of the early Eocene (Ortiz and Thomas, 2012).

We therefore suggest that, at least in some oceanic areas, a "modern"-type assemblage was gradually emerging among the Paleogene fauna in the middle Eocene, as a prelude to the larger faunal turnover during the transition to the Cenozoic icehouse climate state (Thomas, 1990; Thomas, 2007). The nature of these earlier transitions during the climate change on the middle Eocene varied geographically (see e.g., the assemblage 3/assemblage 4 transition at Southern Ocean Site 689; Thomas 1990), possibly because there was large geographic variability in assemblages in the early Eocene (e.g., Tjalsma and Lohmann, 1984; Thomas, 1998; Takeda and Kaiho, 2007). Common *N. umbonifera* and *Pseudoparrella minuta* (= *Epistominella minuta*) have been reported in the lower Eocene in the North-Eastern Atlantic (d'Haenens et al. 2012), so that we could argue, in agreement with Ortiz and Thomas, 2012, that this faunal trend may have been in progress since the early Eocene, but undetected in investigations using larger size fractions.

It is plausible to suppose that the ocean environment was gradually but significantly changing in the middle Eocene, when the progressive cooling trend at high latitude had begun at the end of the Early Eocene Climatic Optimum (EECO). Even if high sea surface temperatures still persisted at low to mid-latitudes (Pearson et al., 2007; Liu et al., 2009), the high southern latitudes and therefore that deep waters that formed there, i.e., global deep and bottom waters, had already started to cool at the end of the early Eocene (Zachos et al., 2001; Huber and Thomas, 2008), and small to moderate glaciation may have occurred in Antarctica (Tripati et al., 2005; Thomas, 2008; Dawber and Tripati 2011). As a consequence, the equator-to-pole (horizontal) and surface-to-deep (vertical) temperature gradients in the ocean were increasing (Finkel et al., 2005; Bijl et al., 2013), and Earth was gradually moving toward its first clear step into icehouse conditions. The final step in this process occurred in the early Oligocene, with the rapid expansion of large Antarctic continental ice sheets, to reach sea level (Robert and Kennett, 1997; Zachos et al., 1999).

It is intriguing hypothesize that benthic foraminiferal faunal composition at Site 1263, similar to that observed across the Eocene/Oligocene climatic transition by Fenero et al. (2010) and with similarity to that across the early/middle Eocene transition (Ortiz and Thomas, 2012) may reflect these gradually changing oceanic conditions and the cooling of the deep oceans during this long-term transition of Earth's climate.

The abundance of phytodetritus taxa at Site 1263 suggests that pulsed deposition of labile organic matter as phytodetritus may have occurred at this location in the studied time interval, and before the strong increase in abundance of diatoms (Falkowski et al., 2004). Modern seasonal phytoplankton blooms are driven by diatoms and the haptophyte coccolithophores (Barlow, 1993; Miller and Wheeler, 2012). Interestingly, the late early Eocene saw the appearance of the successful *Noelaerhabdaceae* clade, the offsprings of which includes the most important bloom-forming coccolithophorids of the modern ocean. Therefore the early Eocene can be considered the time in which nannoplankton communities set course toward modern structure (Agnini et al., 2006). Possibly, in the middle Eocene, coccolithophorids were the principal bloom-generating phytoplankton group in open ocean, when diatoms where not yet a dominant component among eukaryotic phytoplankton (e.g., Falkowsky et al., 2004; Katz et al., 2004).

Our data on benthic foraminiferal assemblages in the size fraction <100 µm thus provide new insight in the evolution of the middle Eocene benthic foraminiferal faunas, suggesting that oceanic productivity and export fluxes may have been changing in response of changing climatic and oceanographic conditions and the appearance of new phytoplankton groups.

6. Conclusions

Analysis of benthic foraminiferal assemblages at the lower-bathyal to upper abyssal ODP Site 1263 on Walvis Ridge (South-East Atlantic), allowed us to evaluate the effect of MECO on deep-sea biota in an open ocean setting, away from the continental margins. The investigation of the >63 µm size fraction shows that phytodetritus-exploiting taxa were already an important component of benthic foraminiferal assemblages at this mid-latitude location in the middle Eocene. Oceanic productivity and fluxes of organic matter may thus have been changing in response of changing climatic and oceanographic conditions (i.e., high latitude and deep-water cooling) and the appearance of new phytoplankton groups. At Site 1263, the benthic foraminiferal assemblage is characterized by moderate to low faunal diversity, with general dominance of epifaunal over infaunal species. Common *N. umbonifera*, *N. truempyi* and phytodetritus exploiting taxa suggest a largely oligotrophic environment, with periodically but interrupted high surface productivity and pulsed deposition of labile, phytodetritus-like, organic matter to the sea-floor. The pulsed supply increased in the early part of gradual warming of MECO, then declined markedly toward peak MECO, indicating decreased delivery of food to the seafloor. The decreased relative abundances of phytodetritus-exploiters, *N. umbonifera* and other epifaunal species such as *C. lamontdohertyi* further suggests an overall reduction of the supply of primary produced labile organic matter to the sea-floor. There is no evidence of markedly increased water column stratification at the site in the $\delta^{13}C$ records (Chapter 3), and this reduction thus may have been an effect of accelerated metabolic activity of pelagic heterotrophs, and increased remineralization of organic matter in the water column, rather than decreased surface primary productivity.

The AR and relative abundance of infaunal taxa decreased less markedly across the MECO and their relative abundance slightly increased, possibly because they could survive on older refractory organic matter in the sediment. *N. truempyi* show peaks in the aftermath of the PETM at several oceanic sites (Thomas, 1998; Thomas, 2007), and its percentage increase across the MECO may indicate a greater adaption to warm deep-water temperatures than taxa presently living in cold bottom waters.

Foraminiferal accumulation rates and assemblage data indicate that at Site 1263 planktic and benthic communities were affected by the warming itself rather than by secondary effects of warming such as changing nutrient influx due to increased weathering. The warming at Site 1263 occurred under nutrient-limited conditions, so that the phytoplankton could not increase productivity when metabolic rates allowed it.

Marine biota appears to have been affected to a different extent in different areas during the MECO, responding to increased surface water productivity or nutrient availability (Alano Section, Site 1051, Sites 748-749; Villa et al., 2008; Luciani et al., 2010; Toffanin et al., 2011; Witkowski et al., 2012; Boscolo Galazzo et al., 2013; Moebius et al., 2013), oxygenation at the sea-floor (Alano section, Site 748; Boscolo Galazzo et al., 2013; Moebius et al., 2013), surface and deep water warming (Site 1263; present study), increased surface waters oligotrophy (Site 702 and 1172; Bijl et al., 2010; Pea, 2011). The data so far available hence indicate a complex global pattern of paleoenviromental and biotic changes across the MECO. Different oceanic and marine areas were significantly but diversely affected, based on how the MECO altered regional oceanographic conditions.

Appendix A. Taxonomic list of benthic foraminiferal taxa recognized in the Site 1263 (Walvis Ridge)

Agglutinant taxa

?*Ammodiscus* sp.
Arenobulimina sp.
Dorothia sp.
Eggerella bradyi=Verneuilina bradyi Cushman, 1911
Karreriella chapapotensis=Textularia chapapotensis Cole, 1928
Karreriella chilostoma
Karreriella subglabra
Karreriella cf. *cubensis* Cushman & Bermúdez
Karreriella sp. deformed specimens
Karreriella spp.
Plectina dalmatina = Gaudryina dalmatina Schubert, 1911 *sensu* Mathelin & Sztrakós (1993).
Spiroplectammina spectabilis = Spiroplecta spectabilis Grzybowski, 1898 *sensu* Kaminski and Gradstein, 2005
Subreophax sp.
Vulvulina haeringensis-eocaena group includes the following species:
- *Vulvulina haeringensis =Venilina haeringensis* Gümbel, 1868
- *Vulvulina eocaena* Montagne, 1941

Porcellaneous taxa

Quinqueloculina sp.
Spiroloculina sp.

Calcareous-hyaline taxa

Abyssammina incisa Schnitker & Tjalsma, 1980
Alabamina weddellensis = Eponides weddellensis Earland, 1936
Alabamina sp.
Angulogerina muralis = Uvigerina muralis Terquem, 1882
Anomalinoides capitatus = Rotalia capitata Gümbel, 1868.
Anomalinoides glabratus = Anomalina glabrata Cushman, 1924
Anomalinoides semicribratus = Anomalina pompilioides Galloway and Heminway var. *semicribrata* Beckmann, 1954
Anomalinoides spissiformis = Anomalina alazanensis Nuttall var. *spissiformis* Cushman & Stainforth, 1945.
Anomalinoides spp.
Aragonia aragonensis = Textularia aragonensis Nuttall, 1930.
Astacolus sp.
Bolivinoides crenulata = Bolivina crenulata Cushman, 1936
Bolivinoides huneri = Bolivina huneri Howe, 1939
Bolivina malovensis Heron-Allen and Earland, 1932
Bolivina spp.
Bulimina alazanensis Cushman, 1927
Bulimina cf. *alazanensis* Cushman, 1927. Small specimens with a distinctly triangular outline, chambers not visible, lateral sides slightly concave. Ornamentation consists of a single longitudinal

rib in the mid of each side, running from the basal end to the base of the last chamber and of a couple of ribs which profile each margin.
Bulimina glomarchallengeri Tjalsma and Lohmann, 1983
Bulimina impendens Parker & Bermúdez, 1937. Typical specimens.
Bulimina semicostata Nuttall, 1930
Bulimina simplex Terquem, 1882
Bulimina stalacta Cushman & Parker, 1936.
Bulimina trihedra Cushman, 1926
Bulimina tuxpamensis Cole, 1928
Bulimina cf. *elongata* d'Orbigny 1846. In this group we lumped together specimens similar to *B. elongata* d'Orbigny 1846 but characterized by a quite high morphological variability. Specimens belonging to this group often show differences in the position and shape of the aperture that we were not able to discern under stereoscopic microscope but which became evident only under SEM. For this reason we preferred to allocate all these specimens within this heterogeneous group. These forms are characterized by very small dimension, test elongate and slightly perforate, with numerous chambers often rather inflated in the last whorl. In some cases the tests are twisted on their major axis.
Bulimina spp.
Buliminella beaumonti Cushman and Renz, 1946
Buliminella grata Parker and Bermúdez, 1937
Undetermined buliminids
Caucasina schischkinskye = Bulimina schischkinskye Saimolova, 1947
Caucasina sp.
Cassidulina sp.
Cibicides spp.
Cibicidoides barnetti = Cibicides barnetti Bermúdez, 1949
Cibicidoides eocaenus = *Rotalia eocaena* Gümbel, 1868 *sensu* Van Morkhoven et al. (1986).
Cibicidoides grimsdalei = *Cibicides grimsdalei* Nuttall, 1930
Cibicidoides havanensis Cushman & Bermúdez, 1937
Cibicidoides lamontdohertyi Miller and Katz, 1987
Cibicidoides micrus = Cibicides micrus Bermúdez, 1949
Cibicidoides perlucidus = Cibicides perlucida Nuttall, 1932
Cibicidoides praemundulus Berggren & Miller, 1986
Cibicidoides praemundulus Berggren & Miller, 1986 juvenile specimens
Cibicidoides proprius = Cibicides (*Cibicidoides*) *proprius* Brotzen, 1948
Cibicidoides ungerianus = Rotalina ungeriana d'Orbigny, 1846.
Cibicidoides spp.
Clinapertina complanata Tjalsma & Lohmann, 1983
Clinapertina inflata Tjalsma & Lohmann, 1983
Clinapertina subplanispira Tjalsma & Lohmann, 1983
Clinapertina spp.
?*Clinapertina*
Discorbis sp.
Ellypsodimorphina
Ellypsoglandulina
Epistominella vitrea Parker, 1953
Epistominella exigua = Pulvinulina exigua Brady, 1884
Epistominella spp.
Eponides tumidulus = Truncatulina tumidula Brady, 1884
Eponides spp.
?*Eponides* sp.

Fursenkoina spp.
?*Fursenkoina* sp.
Glandulina sp.
Globimorphina spp.
Globobulimina spp.
Globocassidulina crassa = Cassidulina crassa d'Orbigny, 1839
Globocassidulina subglobosa = Cassidulina subglobosa Brady, 1881
Gyroidinoides danvillensis = Gyroidina danvillensis Howe and Wallace, 1932
Gyroidinoides depresuss = Rotalina depressa Alth, 1850
*Gyroidinoides gyrardanu*s = *Rotalina girardana* Reuss, 1851.
Gyroidinoides mediceus = Gyroidina medicea Emiliani, 1954
Gyroidinoides planulatus = Gyroidina planulata Cushman & Renz, 1941
Gyroidinoides subangulatus = Gyroidina soldanii d'Orbigny var. *subangulata* Plummer, 1927.
Gyroidinoides spp.
Hanzawaia ammophila = Rotalia ammophila Gümbel, 1868.
Hemirobulina sp.
Heronallenia pusilla Parr, 1938
Heronallenia sp.
Laevidentalina spp.
Lagena spp.
Lenticulina spp.
Low trochospiral hyalineous
*Neoconorbin*a sp.
Nodosarella spp.
Nodosaria spp.
Nonion havanense Cushman & Bermúdez, 1937.
Nonion spp.
Nonionella longicamerata Bandy, 1949
Nonionella robusta Plummer, 1931
Nonionella spp.
Nuttallides truempyi = Eponides truempyi Nuttall, 1930 *sensu* Van Morkhoven et al., 1986
Nuttallides umbonifera = Pulvinulinella umbonifera Cushman, 1933
Oridorsalis plummerae = Eponides plummerae Cushman, 1948
Oridorsalis umbonatus = Rotalina umbonata Reuss, 1851
Oridorsalis spp.
Ortomorphina spp.
Osangularia cf. *plummerae* Brotzen, 1940
Paleopolymorphina sp.
Pleurostomella spp.
Polymorphinids
Praeglobobulimina spp.
Pullenia eocaena Cushman & Siegfus, 1939
Pullenia quinqueloba Reuss, 1852
*Pullenia salisbury*i Stewart & Stewart, 1930
Pullenia sp.
Pseudopolymorphina sp.
Pseudouvigerina semilabiata Watanabe, 1989
?*Pseudouvigerina* sp.
Pyrulina extensa = Polymorphina extensa Cushman, 1923
Quadrimorphina profunda Schnitker & Tjalsma, 1980
Resigia westcotti Schnitker & Tjalsma, 1980

Reussella sp.
Saracenaria spp.
Seabrookia rugosa Watanabe, 1989
Siphonodosaria spp.
?*Sporobulimina eocaena* Bykova, 1959?
Stetsonia minuta Parker, 1954
Stilostomella hispidula = Ellipsonodosaria atlantisae Cushman var. *hispidula* Cushman, 1939
Stilostomella spp.
Turrilina robertsi = Bulimina robertsi Howe and Ellis, 1939
Turrilina sp.
Unilocular hyalineous
Uniserial hyalineous
Uvigerina chirana Cushman & Stone, 1947
?*Valvulineria* sp.

References

Agnini, C., Muttoni, G., Kent, D.V., Rio, D., 2006. Eocene biostratigraphy and magnetic stratigraphy from Possagno, Italy: The calcareous nannofossil response to climate variability. Earth and Planetary Science Letters, 241, 815– 830.

Alegret, L., Thomas, E., 2001. Upper Cretaceous and lower Paleogene benthic Foraminifera from northeastern Mexico. Micropaleontology, 47: 269-316.

Alegret, L., Thomas, E., 2008. Deep-Sea environments across the Cretaceous/Paleogene boundary in the eastern South Atlantic Ocean (ODP Leg 208, Walvis Ridge). Marine Micropaleontology, 64, 1–17.

Alegret, L., Ortiz, S., Molina, E., 2009. Extinction and recovery of benthic foraminifera across the Paleocene-Eocene Thermal Maximum at the Alamedilla section (Southern Spain), Palaeogeography, Palaeoclimatology, Palaeoecology 279, 186-200.

Alegret, L., Ortiz, S., Arenillas, I., Molina, E., 2010. What happens when the ocean is overheated? The foraminiferal response across the Paleocene-Eocene Thermal Maximum at the Alamedilla section (Spain). Geological Society of America Bulletin, 122, 1616-1624, doi:10.1130/B30055.1.

Barlow, R.G., Mantoura, R.F.C., Gough, M.A., Fileman, W.T., 1993. Pigment signature of the phytoplankton composition in the north-eastern Atlantic during the 1990 spring bloom. Deep-sea Research II, 40, 459-477.

Berggren, W.A., Aubert, J., 1976. Eocene benthonic foraminiferal biostratigraphy and paleobathymetry of Orphan Knoll (Labrador Sea). Micropaleontology, 22, 327–346.

Bidigare, R.R., Benitez-Nelson, C., Leonard, C.L., Quay, P.D., Parsons, M.L., Foley, D.G., Seki, M.P., 2003. Influence of a cyclonic eddy on microheterotroph biomass and carbon export in the lee of Hawaii. Geophysical Research Letters, 30-6, 1318, doi:10.1029/2002GL016393.

Bijl, P.K., Houben, A.J.P., Schouten, S., Bohaty, S.M., Sluijs, A., Reichart, G.J., Sinninghe Damsté, J.S., Brinkhuis, H., 2010. Transient middle Eocene atmospheric CO_2 and temperature variations. Science, 330, 819–821.

Bijl, P.K., Bendl, J.A.P., Bohaty, S.M., Pross, J., Schouten, S., Tauxe, L., Stickley, C.E., McKay, R.M., Röhl, U., Olneyk, M., Sluijs, A., Escutia, C., Brinkhuis, H., and Expedition 318 Scientists, 2013. Eocene cooling linked to early flow across the Tasmanian Gateway. Proceedings of the National Academy of Science, doi/10.1073/pnas.1220872110.

Bohaty, S.M., Zachos, J.C., 2003. A significant Southern Ocean warming event in the late middle Eocene. Geology, 31, 1017–1020.

Bohaty, S.M., Zachos, J.C., Florindo, F., Delaney, M.L., 2009. Coupled greenhouse warming and deep-sea acidification in the Middle Eocene. Paleoceanography, 24, PA2207, http://dx.doi.org/10.1029/2008PA001676.

Boltovskoy, E., Boltovskoy, D., 1989. Paleocene–Pleistocene benthic foraminiferal evidence of major paleoceanographic events in the eastern South Atlantic (DSDP Site 525, Walvis Ridge). Marine Micropaleontology, 14, 283–316.

Boltovskoy, E., Watanabe, S., Totah, V.I., Vera Ocampo, J., 1992. Cenozoic Benthic Bathyal Foraminifers of DSDP Site 548 (North Atlantic). Micropaleontology, 38-2, 183-207.

Boscolo Galazzo, F., Giusberti, L., Luciani, V., Thomas, E., 2013. Paleoenvironmental changes during the Middle Eocene Climatic Optimum (MECO) and its aftermath: The benthic foraminiferal record from the Alano section (NE Italy). Palaeogeography, Palaeoclimatology, Palaeoecology, 378, 22-35.

Bremer, M.L., Lohmann, G.P., 1982, Evidence for primary control of the distribution of certain Atlantic Ocean benthonic foraminifera by degree of carbonate saturation. Deep-Sea Research, v. 29, p. 987–998, doi:10.1016/0198-0149(82)90022-X.

Buzas, M.A., Culver, S.J., Jorissen, F.J., 1993. A statistical evaluation of the microhabitats of living (stained) infaunal benthic foraminifera. Marine Micropaleontology, 29, 73–76.

Corliss, B.H., 1985. Microhabitats of Benthic Foraminifera within deep-sea sediments. Nature 314, 435–438.

Corliss, B.H., Chen, C., 1988. Morphotype patterns of Norwegian Sea deep-sea benthic foraminifera and ecological implications. Geology, 16, 716–719.

Cramer, B.S., Toggweiler, J.R., Wright, M.E., Katz, J.D., Miller, K.G., 2009. Ocean overturning since the Late Cretaceous: Inferences from a new benthic foraminiferal isotope compilation. Paleoceanography, 24, PA4216, doi:10.1029/2008PA001683.

Dawber, C.F., Tripati, A.K., 2011. Constraints on glaciation in the middle Eocene (46–37 Ma) from Ocean Drilling Program (ODP) Site 1209 in the tropical Pacific Ocean. Paleoceanography, 26, PA2208, doi:10.1029/2010PA002037.

D'Haenens, S., Bornemann, A., Stassen, P., Spejer, R.P., 2012. Multiple early Eocene benthic foraminiferal assemblage and $\delta^{13}C$ fluctuations at DSDP Site 401 (Bay of Biscay–NE Atlantic). Marine Micropaleontology, 88–89, 15–35.

Dore, J.E., Letelier, R.M., Church, M.J., Lukas, R., Karl, D.M., 2008. Summer phytoplankton blooms in the oligotrophic North Pacific Subtropical gyre: historical perspective and recent observations. Progress in oceanography, 76, 2-38.

Edgar, K.M., Wilson, P.A., Sexton, P.F., Suganuma, Y., 2007b. No extreme bipolar glaciations during the main Eocene calcite compensation shift. Nature 448, 908–911

Edgar, K.M., Sexton, P., Norris, R., Wilson, P., Gibbs, S., 2007a. Evolutionary response of planktic foraminifera to a pronounced global warming event 40 Myr ago. Eos Transaction AGU, 88(52), Fall Meeting Suppl., Abstract OS14A-03.

Edgar, K.M., Wilson, P.A., Sexton, P.F., Gibbs, S.J., Roberts, A.P., Norris, R.D., 2010. New biostratigraphic, magnetostratigraphic and isotopic insights into the Middle Eocene Climatic Optimum in low latitudes. Palaeogeography, Palaeoclimatology, Palaeoecology, 297, 670–682.

Edgar, K.M., Bohaty, S.M., Gibbs, S.J., Sexton, P.F., Norris, R.D., Wilson, P.A., 2012. Symbiont 'bleaching' in planktic foraminifera during the Middle Eocene Climatic Optimum. Geology, 41, 15-18.

Falkowski, P.G., Katz, M.E., Knoll, A.H., Quigg, A., Raven, J.A., Schofield, O., Taylor, F.J.R., 2004. The Evolution of Modern Eukaryotic Phytoplankton. Science, 305, 354-360

Fenero, R., Thomas, E., Alegret, L., Molina, E., 2010. Evolución paleoambiental del tránsito Eoceno-Oligoceno en el Atlántico sur (Sondeo 1263) basada en foraminíferos bentónicos. Geogaceta, 49, 2010.

Finkel, Z.V., Katz, M.E., Wright, J.D., Schofield, O.M.E., Falkowski, P.G., 2005. Climatically driven macroevolutionary patterns in the size of marine diatoms over the Cenozoic. Proceedings of the National Academy of Sciences, 102-25, 8927-8932.

Fontanier, C., Jorissen, F.J., Licari, L., Alexandre, A., Anschutz, P., Carbonel, P., 2002. Live benthic foraminiferal faunas from the Bay of Biscay: faunal density, composition, and microhabitats. Deep-Sea Research I, 49, 751–785.

Fontanier, C., Jorissen, F.J., Chaillou, G., Anschutz, P., Grémare, A., Griveaud, C., 2005. Live foraminiferal faunas from a 2800 m deep lower canyon station from the Bay of Biscay: faunal response to focusing of refractory organic matter. Deep-Sea Research I, 52, 1189–1227.

Fornaciari, E., Agnini, C., Catanzariti, R., Rio, D., Bolla, E.M., Valvasoni, E., 2010. Mid-Latitude calcareous nannofossil biostratigraphy and biochronology across the middle to late Eocene transition. Stratigraphy, 7-4, 229-264.

Foster L.C., Schmidt D.N., Thomas E., Arndt S., Ridgwell A., 2013. Surviving rapid climate change in the deep sea during the Paleogene hyperthermals. Proceedings of the National Academy of Sciences, doi/10.1073/pnas.1300579110.

Gooday, A.J., 1993. Deep-sea benthic foraminiferal species which exploit phytodetritus: Characteristic features and controls on distribution: Marine Micropaleontology, 22, 187–205.

Gooday, A.J., 2003. Benthic foraminifera (Protista) as tools in deepwater palaeoceanography: environmental influences on faunal characteristics. Advances in Biology, 46, 1–90.

Gooday, A.J., Hughes, J.A., 2002. Foraminifera associated with phytodetritus deposits at a bathyal site in the northern Rockall Trough (NE Atlantic): seasonal contrasts and a comparison of stained and dead assemblages. Marine Micropaleontology, 46, 83-110.

Gupta, A.K., Thomas, E., 2003. Initiation of Northern Hemisphere glaciation and strengthening of the northeast Indian monsoon: Ocean Drilling Program Site 758, eastern equatorial Indian Ocean. Geology, 31, 47-50.

Hayward, B.W., Kawagata, S., Sabaa, A.T., Grenfell, H.R., van Kerckhoven, L., Johnson, K., Thomas, E., 2012, The Last Global Extinction (Mid-Pleistocene) of Deep-Sea Benthic Foraminifera (Chrysalogoniidae, Ellipsoidinidae, Glandulonodosariidae, Plectofrondicularиidae, Pleurostomellidae, Stilostomellidae), their Late Cretaceous-Cenozoic History and Taxonomy. Cushman Foundation for Foraminiferal Research, Spec. Vol., 43, 408 pp.

Holbourn, A., Henderson, A.S., MacLeod, N., 2013. Atlas of benthic foraminifera. Willey-Blackwell, 642 pp.

Huber, M., Thomas, E., 2008. Paleoceanography: Greenhouse Climates. In: Encyclopedia of Ocean Sciences, J.H. Steele, S.A. Thorpe and K.K. Turekian, (Eds.), 2nd edition, (Elsevier), p. 4229-4239, doi: 10.1016/B978-012374473-9.00701.3

Ivany, L.C., Lohmann, K.C., Hasiuk, F., Blake, D.B., Glass, A., Aronson, R.B., Moody R.M., 2008. Eocene climate record of a high southern latitude continental shelf: Seymour Island, Antarctica. Geological Society of America Bulletin, 120, 659–678.

Jones, R.W., Charnock, M.A., 1985. "Morphogroups" of agglutinated foraminifera. Their life positions and feeding habits and potential applicability in (paleo)ecological studies. Revue de Paléobiologie, 4, 311–320.

Jorissen, F.J., De Stigter, H.C., Widmark, J.G.V., 1995. A conceptual model explaining benthic foraminiferal microhabitats. Marine Micropaleontology, 26, 3–15.

Jorissen, F.J., 1999. Benthic foraminiferal successions across late Quaternary Mediterranean sapropels. In: Rohling, E.J. (Ed.), Fifth decade of Mediterranean paleoclimate and sapropel studies. Marine Geology, 153, 91–101.

Jorissen, F.J., Fontanier, C., Thomas, E., 2007. Paleoceanographical proxies based on deep-sea benthic foraminiferal assemblage characteristics. In: Hillaire-Marcel, C., de Vernal, A. (Eds.). Developments in Marine Geology: Proxies in Late Cenozoic Paleoceanography, vol. 1. Elsevier, Amsterdam, pp. 264–325.

Jovane, L., Florindo, F., Coccioni, R., Dinare's-Turell, J., Marsili, A., Monechi, S., Roberts, A.P., Sprovieri, M., 2007. The middle Eocene climatic optimum event in the Contessa Highway section, Umbrian Apennines, Italy. Geological Society of American Bulletin, 119, 413–427.

Katz E.M., Miller K.J., 1989. Oligocene to Miocene benthic foraminiferal and abyssal circulation changes in the North Atlantic. Micropaleontology, 33, 97-149.

Katz, M.E., Finkel, Z.V., Grzebyk, D., Knoll, A.H., Falkowski, P.G., 2004. Evolutionary trajectories and biogeochemical impacts of marine eukaryotic phytoplankton: Annual Reviews of Ecological and Evolutionary Systematics, 35, 523–526.

Klevenz, V., Vance, D., Schmidt, D.N., Mezger, K., 2008. Neodymium isotopes in benthic foraminifera: Core-top systematics and a down-core record from the Neogene south Atlantic. Earth and Planetary Science Letters, 265, 571-587.

Levitus, S., Antonov, J., Boyer, T.P., 1994. Interannual variability of temperature at a depth of 125 m in the North Atlantic Ocean. Science, 266, 96–99.

Liu, Z., Pagani, M., Zinniker, D., DeConto, R., Huber, M., Brinkhuis, H., Shah, S.R., Leckie, R.M., Pearson, A., 2009. Global cooling during the Eocene-Oligocene climate transition. Science, 323, 1187-1190.

Lohmann, G.P., 1992. Increasing seasonal upwelling in the subtropical South Atlantic over the past 700,000 yrs: Evidence from deep-living planktonic foraminifera. Marine Micropaleontology, 19, 1-12.

Lopez-Urrutia, A., San Martin, E., Harris, R., Irigolen, X., 2006. Scaling the metabolic balance of the oceans. Proceedings of the National Academy of Science, 103-23, 8739-8744.

Loeblich, A.R., Tappan, H., 1987. Foraminiferal genera and their classification, vol. 2. Van Nostrand Reinhold Company, New York, 1182 pp.

Loubere, P., 1991. Deep sea benthic foraminiferal assemblage response to a surface ocean productivity gradient: a test. Paleoceanography, 6, 193-204.

Loubere, P., 1997. Benthic foraminiferal assemblage formation, organic carbon flux and oxygen concentrations on the outer continental shelf and slope. Journal of Foraminiferal Research, 27, 93–100.

Luciani, V., Giusberti, L., Agnini, C., Fornaciari, E., Rio, D., Spofforth, D.J.A., Pälike, H., 2010. Ecological and evolutionary response of Tethyan planktonic foraminifera to the middle Eocene climatic optimum (MECO) from the Alano section (NE Italy). Palaeogeography, Palaeoclimatology, Palaeoecology, 292, 82–95.

Lutze, G.F., Coulbourn, W.T., 1984. Recent benthic foraminifera from the continental margin of Northwest Africa; community structure and distribution. Marine Micropaleontology, 8, 361– 40.

Lyle, M., Lyle Olivarez, A., Backman, J., Tripati, A., 2005. Biogenic sedimentation in the Eocene equatorial Pacific — the stuttering greenhouse and Eocene carbonate compensation depth. In: Lyle, M., and Firth, (Eds.). Proceedings of the Ocean Drilling Program, Scientific results, 199, 1-35. Ocean Drilling Program, College Station, TX.

Lyle, M., Barron, J., Bralower, T.J., Huber, M., Olivarez Lyle, A., Ravelo, A.C., Rea, D.K, Wilson, P.A., 2008. Pacific Ocean and Cenozoic evolution of climate, Review of Geophysics, 46, RG2002.

Lyle Olivarez, A., Lyle, M.W., 2006. Missing organic carbon in Eocene marine sediments: Is metabolism the biological feedback that maintains end-member climates? Paleoceanography, 21, PA2007, doi:10.1029/2005PA001230.

Mackensen, A., Schmiedl, G., Harloff, J., Giese, M., 1995. Deep-sea foraminifera in the South Atlantic Ocean: Ecology and assemblage generation. Micropaleontology, 41, 342-358.

Mancin, N., Hayward, B.W., Trattenero, I., Cobianchi, M., Lupi, C., 2013. Can the morphology of deep-sea benthic foraminifera reveal what caused their extinction during the mid-Pleistocene Climate Transition? Marine Micropaleontology, 104, 53-70.

McCarren, H., Thomas, E., Hasegawa, T., R□hl, U., Zachos, J.C., 2008. Depth-dependency of the Paleocene-Eocene Carbon Isotope Excursion: paired benthic and terrestrial biomarker records (ODP Leg 208, Walvis Ridge). Geochemistry, Geophysics, Geosystem, 9, Q10008, doi: 10.1029/2008GC002116.

McGillicuddy, Jr. D.J., Anderson, L.A., Bates, N.R., Bibby, T., Buesseler, K.O., et al., 2007. Eddy/Wind Interactions Stimulate Extraordinary Mid-Ocean Plankton Blooms. Science, 316, 10121-1025.

Miller, C.B., Wheeler, P.A., 2012. Biological Oceanography, second edition. Willey-Blackwell, 464 pp.

Moebius, I., Friedrich, O., Edgar, K.M., Scher, H.D., Sexton, P., 2013. Bottom water changes in the subtropical North Atlantic and the Southern Ocean associated to the Middle Eocene Climatic Optimum. AGU 2013 Fall Meeting Abstract (Control ID: 1805987), San Francisico 9-13 December 2013.

Nees, S., Altenbach, A.V., Kassens, H., Thiede, J., 1997. High resolution record of foraminiferal response to late Quaternary sea ice retreat in the Norwegian Greenland Sea. Geology 25, 659-662.

Ohkushi, K., Thomas, E., Kawahata, H., 2000. Abyssal benthic foraminifera from the northwestern Pacific (Shatsky Rise) during the last 298 kyr. Marine Micropaleontology, 38, 119–147.

Ortiz, S., Thomas, E., 2006. Lower-middle Eocene benthic foraminifera from the Fortuna Section (Betic Cordillera, south-eastern Spain). Micropaleontology, 52-2, 97–150.

Ortiz, S., and Thomas, E., 2012. Deep-sea turnover during the Ypresian-Lutetian transition, the inception of the Cenozoic global cooling trend. 34th IGC World Congress, Brisbane, Australia, 5-10 August 2012.

Pälike, H., Lyle, M.W, Nishi, H., Raffi, I., et al., 2012. A Cenozoic record of the equatorial Pacific carbonate compensation depth. Nature, 488, 609-615.

Pawlowski, J., Holzmann, M., 2008. Diversity and geographic distribution of benthic foraminifera: a molecular perspective. Biodiversity and Conservation, 17, 317-328.

Pawlowski, J., Bowser, S.S., Gooday, A.J., 2007. A note on the genetic similarity between shallow- and deep-water Epistominella vitrea in the Antarctic. Deep Sea Research Part II: Topical Studies in Oceanography, 54, 1720-1726.

Pea, L., 2011. Eocene-Oligocene paleoceanography of the subantarctic South Atlantic: Calcareous Nannofossil reconstructions of temperature, nutrient, and dissolution history. Ph.D. thesis, pp. 205, Dottorato di Ricerca in Scienze della Terra XXIII° Ciclo, Università degli Studi di Parma (Italy).

Pearson, P.N., van Dongen, B.E., Nicholas, C.J., Pancost, R.D., Schouten, S., Singano, J.M., Wade, B.S., 2007. Stable warm tropical climate through the Eocene Epoch. Geology, 35, 211-214.

Protodecima, F., Bolli, H.M., 1978. South East Atlantic DSDP Leg 40 Paleogene benthic foraminifers. In: Bolli, H.M., Ryan, W.B.F., et al., 1978. Initial Reports of the Deep Sea Drilling Project, vol. XL, Washington (U.S. Government Printing Office).

Peterson, L.C., Backman, J., 1990. Late Cenozoic carbonate accumulation and the history of the carbonate compensation depth in the western equatorial Indian Ocean. Proceedings of the Ocean Drilling Program Scientific Results, 115, 467– 507.

Robert, C., Kennett, J.P., 1997. Antarctic continental weathering changes during Eocene/Oligocene cryosphere expansion: clay mineral and oxygen isotope expansion. Geology, 25, 587.

Savian, J.F., Jovane, L., Trindade, R.I.F., Frontalini, F., Coccioni, R., Bohaty, S.M., Wilson, P.A., Florindo, F., Roberts, A., 2013. Middle Eocene Climatic Optimum (MECO) in the Monte Cagnero Section, Central Italy. Latinmag Letters, 3, Special Issue, PC02, 1-8. Proceedings Montevideo, Uruguay.

Schmiedl, G., Mackensen, A., Müller, P.J., 1997. Recent benthic foraminifera from the eastern South Atlantic Ocean. Dependence on food supply and water masses. Marine Micropaleontology, 32, 249-287

Sexton, P.F., Wilson, P.A., Norris, R.D., 2006. Testing the Cenozoic multisite composite $\delta^{18}C$ and $\delta^{13}C$ curves: New monospecific Eocene records from a single locality, Demerara Rise (Ocean Drilling Program Leg 207). Paleoceanography, 21, PA2019, doi:10.1029/2005PA001253.

Singh, R.K., Gupta, A.K., 2010. Deep-sea benthic foraminiferal changes in the eastern Indian Ocean (ODP Hole 757B): Their links to deep Indonesian (Pacific) flow and high latitude glaciation during the Neogene. Episodes, 33-2, 73-82.

Smart, C.W., King, S.C., Gooday, A., Murray, J.W., Thomas, E., 1994. A benthic foraminiferal proxy of pulsed organic matter paleofluxes. Marine Micropaleontology, 23, 89–99.

Smart, C.W., Thomas, E., Ramsay, A. T. S., 2007. Middle-late Miocene benthic foraminifera in a western equatorial Indian Ocean depth transect: Paleoceanographic implications. Palaeogeography, Palaoeclimatology, Palaeoecology 247, 402-420

Spofforth, D.J.A., Agnini, C., Pälike, H., Rio, D., Fornaciari, E., Giusberti, L., Luciani, V., Lanci, L., Muttoni, G., 2010. Organic carbon burial following the Middle Eocene Climatic Optimum (MECO) in the central-western Tethys. Paleoceanography, 25, PA3210.

Stap, L., Lourens, L., van Dijk, A., Schouten, S., Thomas, E., 2010. Coherent pattern and timing of the carbon isotope excursion and warming during Eocene Thermal Maximum 2 as recorded in planktic and benthic foraminifera. Geochemistry, Geophysics, Geosystems, 11, Q11011, doi:10.1029/2010GC003097.

Suhr, S.B., Pond, D.W., Gooday, A.J., Smith, C.R., 2003. Selective feeding by benthic foraminifera on phytodetritus on the western Antarctic peninsula: evidence from fatty biomarker analysis. Marine Ecology progress series 262, 153-162.

Sun, X., Corliss, B.H., Brown, C.W., Showers, W.J., 2006. The effect of primary productivity and seasonality on the distribution of deep-sea benthic foraminifera in the North Atlantic. Deep-Sea Research I, 53: 28-47

Takata, H., Nomura, R., Tsujimoto, A., Khim, B., Chung, I., 2013. Abyssal benthic foraminifera in the eastern equatorial Pacific (IODP exp 320) during the Middle Eocene. Journal of Paleontology, 87-6, 1160–1185.

Takeda, K., Kaiho, K., 2007. Faunal turnovers in central Pacific benthic foraminifera during the Paleocene–Eocene thermal maximum. Palaeogeography, Palaeoclimatology, Palaeoecology, 251, 175–197.

Tjalsma, R.C., Lohmann, G.P., 1983. Paleocene–Eocene bathyal and abyssal benthic foraminifera from the Atlantic Ocean. Micropaleontology Special Publication 4, 1–90.

Toffanin, F., Agnini, C., Fornaciari, E., Rio, D., Giusberti, L., Luciani, V., Spofforth, D.J.A., Pälike, H., 2011. Changes in calcareous nannofossil assemblages during the Middle Eocene Climatic Optimum: clues from the central-western Tethys (Alano section, NE Italy). Marine Micropaleontology, 81, 22–31.

Toffanin, F., Agnini, C., Rio, D., Acton, G., Westerhold, T., 2013. Middle Eocene to early Oligocene calcareous nannofossil biostratigraphy at IODP Site U1333 (equatorial Pacific). Micropaleontology, 59-1, 69-82.

Thomas, D.J., Via, R.K., 2007. Neogene evolution of Atlantic thermohaline circulation: Perspective from Walvis Ridge, southeastern Atlantic Ocean. Paleoceanography, 22, PA2212, doi:10.1029/2006PA001297.

Thomas, E., 1985. Late Eocene to Recent deep-sea benthic foraminifers from the central equatorial Pacific Ocean. In: Mayer, L., Theyer, F., et al., (Eds.). Initial Reports of the Deep Sea Drilling Project , Washington (U.S. Government Printing Office), 85, pp. 655 – 694.

Thomas, E., 1990. Late Cretaceous through Neogene deep-sea benthic foraminifers (Maud Rise, Weddell Sea, Antarctica): Proceedings of the Ocean Drilling Program, Scientific results, Volume 113: College Station, Texas, Ocean Drilling Program, 571–594.

Thomas, E., 1998, The biogeography of the late Paleocene benthic foraminiferal extinction. In: Aubry, M.P., Lucas, S.G., and Berggren, W.A., (Eds.). Late Paleocene-early Eocene biotic and climatic events in the marine and terrestrial records: New York, Columbia University Press, 214–243.

Thomas, E., 2007. Cenozoic mass extinctions in the deep sea: What perturbs the largest habitat on Earth? In: Monechi, S., Coccioni, R., and Rampino, M.R., (Eds.). Large Ecosystem Perturbations: Causes and Consequences. Geological Society of America Special Paper, 424, 1–23.

Thomas, E., 2008. Research Focus: Descent into the Icehouse, Geology, 36: 191-192.

Thomas, E., Gooday, A.J., 1996. Cenozoic deep-sea benthic foraminifers: Tracers for changes in oceanic productivity? Geology, 24, 355-358.

Thomas, E., and Shackleton, N. J., 1996. The Palaeocene-Eocene benthic foraminiferal extinction and stable isotope anomalies. Geological Society London Special Publication, 101: 401-441

Thomas, E., Booth, L., Maslin, M., Shackleton, N.J., 1995. Northeastern Atlantic benthic foraminifera during the last 45,000 years: changes in productivity seen from the bottom up. Paleoceanography, 10, 545–562, http://dx.doi.org/10.1029/94PA03056.

Tjalsma, R.C., Lohmann, G.P., 1983. Paleocene–Eocene bathyal and abyssal benthic foraminifera from the Atlantic Ocean. Micropaleontology, Special Publication, 4, 1–90.

Tripati, A., Backman, J., Elderfield, H., Ferretti, P., 2005. Eocene bipolar glaciations associated with global carbon cycle changes. Nature, 436, 341–346.

Van Morkhoven, F.P.C.M., Berggren, W.A., Edwards, A.S., 1986. Cenozoic Cosmopolitan deep-sea benthic foraminifera. Bullettin des Centres de Recherches Exploration- Production Elf-Aquitane, Mèmoire, 11, 11–421.

Via, R.K., Thomas, D.J., 2006. Evolution of Atlantic thermohaline circulation–Early Oligocene onset of deep-water production in the North Atlantic. Geology, 34, 441–444.

Watanabe, S., 1989. New genus and five new species in order foraminiferida. Revista Española de Micropaleontologìa, XXI-2, 265-272.

Villa, G., Fioroni, C., Pea, L., Bohaty, S.M., Persico, D., 2008. Middle Eocene–late Oligocene climate variability: Calcareous nannofossil response at Kerguelen Plateau, Site 748. Marine Micropaleontology, 69, 173 – 192.

Winguth, A.M.E., Thomas, E., Winguth, C., 2012. Global decline in ocean ventilation, oxygenation, and productivity during the Paleocene-Eocene Thermal Maximum: Implications for the benthic extinction. Geology, 40, 263–266.

Witkowski, J., Bohaty, S.M., McCartney, K., Harwood, D.M., 2012. Enhanced siliceous plankton productivity in response to middle Eocene warming at Southern Ocean ODP Sites 748 and 749. Palaeogeography, Palaeoclimatology, Palaeoecology, 326–328, 78–94.

Witkowski J., Bohaty S.M., Edgar K.M., Harwood D.M., 2014. Rapid fluctuations in mid-latitude siliceous plankton production during the Middle Eocene Climatic Optimum (ODP Site 1051, western North Atlantic). Marine Micropaleontolgy, in press.

Zachos, J.C., Dickens, G.R., Zeebe, R.E., 2008. An early Cenozoic perspective on greenhouse warming and carbon-cycle dynamics. Nature, 451, 279–283.

Zachos, J.C., Opdyke, B.N., Quinn, T.M., Jones, C.E., Halliday, A.N., 1999. Early cenozoic glaciation, antarctic weathering, and seawater $^{87}Sr/^{86}Sr$: is there a link? Chemical Geology, 161, 165–180

Zachos, J.C., Pagani, M., Sloan, L.C., Thomas, E., Billups, K., 2001. Trends, rhythms, and aberrations in global climate 65 Ma to present. Science, 292, 686–693.

Zachos, J.C., Kroon, D., Blum, P., et al., 2004. Proceedings of the Ocean Drilling Program, Initial Reports, 208. Ocean Drilling Program, College Station, TX, pp. 1–112.

CHAPTER 5

A middle Eocene micropaleontological trick: the case of Tethyan *Planorotalites*

F. Boscolo Galazzo[a], E. Thomas[b,c], V. Luciani[d], L. Giusberti[a]

a Department of Geosciences, University of Padova, Via G. Gradenigo 6, Italy

b Department of Geology and Geophysics, Yale University, New Haven, CT, USA

c Department of Earth and Environmental Sciences, Wesleyan University, Middletown, CT, USA

d Department of Physics and Earth Sciences, University of Ferrara, Via G. Saragat 1, Italy

Abstract

Morphologically uniform low-trochospiral foraminifera of problematic taxonomic assignment are an abundant component of foraminiferal fauna across the interval encompassing the Middle Eocene Climatic Optimum at the Alano and Monte Cagnero Tethyan sections (Northeastern and Central Italy respectively). Oxygen and carbon-isotope composition of such problematic specimens were measured and compared against isotopic values of coeval benthic (*Nuttallides truempyi*) and planktic foraminifera (*Acarinina* and *Subbotina*), from both the sections. The isotopic analysis revealed these low-trochospiral forms were surface dwelling planktic foraminifera and we refer them to the species *Planorotalites capdevilensis.* Abundance distribution and carbon isotope ratios at Alano and Monte Cagnero sections suggest *P. capdevilensis* may have been a mixed layer dweller without photosymbionts, and thus adapted to slightly more eutrophic conditions than the symbiont-bearing large acarininds and morozovellids.

1. Introduction

Study of middle Eocene foraminifera from the Alano section (Southern Alps, North-Eastern Italy; Boscolo Galazzo et al., 2013) revealed the occurrence of abundant, small, low-trochospiral foraminifera of problematic taxonomic assignment. This morphologically uniform, though variable, group of low-trochospiral taxa was common to abundant throughout the stratigraphic interval analyzed, spanning planktic foraminiferal Zones E11-12 to E13, and constitutes a characteristic component of the foraminiferal assemblage in the size fraction between 63-250 µm.

Their test morphology shares similarities with some benthic foraminiferal species, but also with planktic foraminifera, which makes it difficult to assign generic and specific names, and this difficulty is enhanced by their small size and relatively poor preservation, so that e.g., the exact size and shape of the aperture can not be seen in many specimens.

The specimens morphologically resemble species that have been assigned to the benthic genera *Nuttallides*, *Nuttalinella* and *Parrella*, and to the planktic genus *Planorotalites*. Detailed morphological investigation through scanning electron microscopy (SEM) was not sufficient to solve the correct taxonomic attribution of these specimens, and we could not identify the problematic forms observed in the Alano samples with confidence.

The same group of low-trochospiral forms is even more abundant in coeval samples from the Tethyan Monte Cagnero (M. Cagnero) section (North-Eastern Apennines, Central Italy). The specimens from the M. Cagnero section present the same morphological problems in their test

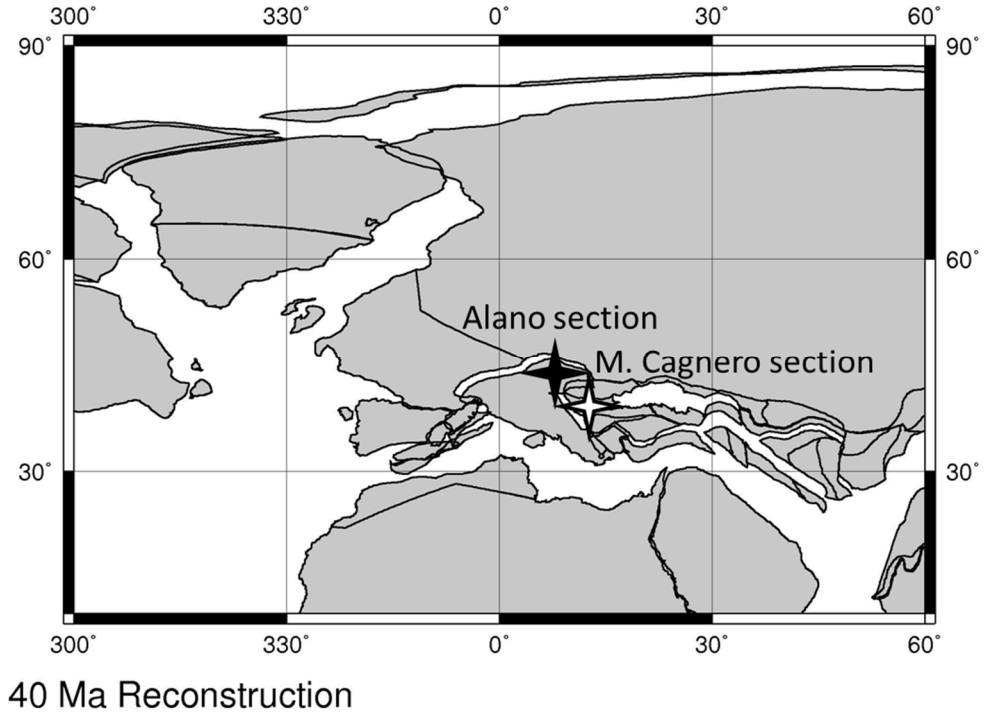

Figure 1. Paleogeographic reconstruction showing the location of the Alano and Monte Cagnero sections. Approximate positions at 40 Ma are plotted on a paleogeographic reconstruction from the Ocean Drilling Stratigraphic Network (GEOMAR, Kiel, Germany).

morphology, small size, and less than optimal preservation as those from Alano, and study of the additional specimens thus did not clarify their taxonomic assignment.

It is of primary importance to resolve whether these small forms are benthic or planktic foraminifera, because they represent an important component of the foraminiferal assemblages from the Alano and M. Cagnero Tethyan sections. The abundance of this group of small trochospirals in both Tethyan sections, characterized by different geological and paleogeographic settings, suggests they may represent a widespread and not yet well-documented component of middle Eocene Tethyan foraminiferal faunas. In the absence of significant carbonate dissolution, planktic foraminifera outnumber benthics by one to several orders of magnitude in deep water settings (e.g., van der Zwaan et al., 1990), so that even moderately abundant planktic foraminifera will be highly abundant as compared to benthics. The incorrect assignment of such abundant specimens to either the benthic or planktic category thus will cause severe bias in paleoceanographic reconstructions, lead to misinterpretation of faunal data, and miss potentially important paleoecological information.

In both the Monte Cagnero and Alano sections the interval considered here encompasses the Middle Eocene Climatic Optimum (MECO), a large global warming event which occurred about 40 Ma ago, interrupting the Eocene global cooling trend (Bohaty and Zachos, 2003; Bohaty et al., 2009). This time interval was of major important in the evolution of planktic foraminifera, with the

diachronous species-duration of the short-lived, warm-water species *Orbulinoides beckmanni*, the zonal marker for Zone E12 (or P13), overlapping with the event (Edgar et al., 2010; Luciani et al., 2010). The large morozovellids and acarininids, the dominant warm-water forms of the middle Eocene, became extinct a few million years later (Wade, 2004), after suffering loss of photosymbionts during the MECO (Edgar et al., 2012).

The distribution pattern of the abundant, small, trochospiral foraminifera across the MECO may hence provide important information about environmental and biotic effects of this major but still poorly understood climatic perturbation in central-western Tethys. We used isotopic data and information on the abundance of this group in samples from the Alano and Cagnero sections, to document that the middle Eocene low trochospiral forms were planktic foraminifera (*Planorotalites capdevilensis*), and speculate on possible explanations for their abundance pattern across the MECO.

2. Setting, lithology and biochronostratigraphy

The Alano section (45°54’50”N - 11°54’55”E) is characterized by a continuous and expanded middle to upper Eocene succession of grey marls in an outcrop along the Calcino torrent riverbed, close to the village of Alano di Piave (Venetian Prealps, northeastern Italy). The section consists of 120–130 m monotonous grey marls, with intercalated silty–sandy tuff layers and biocalcarenitic–calciruditic beds (Agnini et al., 2011), and spans the upper part of Chron C18r (~41.5 Ma) to the base of Chron C16r (~36.5 Ma). The marls were deposited at middle-bathyal paleodepth (Agnini et al., 2011; Boscolo et al., 2013, Chapter 2) in the Belluno Basin. A detailed, integrated biomagnetostratigraphic study was carried out by Agnini et al. (2011), with other studies focusing on planktic foraminifera (Luciani et al., 2010), organic carbon burial (Spofforth et al., 2010), calcareous nannoplankton (Toffanin et al., 201), and benthic foraminifera (Boscolo Galazzo et al., 2013). This study focuses on the interval from 10 to 32 m above the base of the section, within planktonic foraminiferal Zones E10–11, E12 and lower E13 (Berggren and Pearson, 2005), corresponding to P12 to lower P14 (Berggren et al., 1995). The MECO spans the interval between 13 and 17 m in the section (Spofforth et al., 2010). At 17 m, directly above the upper boundary of the MECO interval, an 8 m thick sapropelic interval interrupts the predominant marly lithology. This interval is characterized by a high TOC content (3%), and has been subdivided in two subunits, ORG1 and ORG2, separated by a 2 m interval with a normal marly lithology (Spofforth et al., 2010).

The Monte Cagnero section (43°38'50"N - 12°28'05"E) outcrops as a continuous sedimentary sequence of sediments formed in a pelagic setting, on the South-Eastern flank of the Monte Cagnero, near the town of Urbania, northeastern Apennines (Italy). The Monte Cagnero section spans the middle Eocene through the lower Oligocene, and was deposited at a lower bathyal paleodepth in the Umbria-Marche Basin (Jovane et al., 2013; Savian et al., 2013). Magnetobiostratigraphy of the Monte Cagnero section were carried out by Jovane et al. (2013). The lithology of the entire Eocene and Oligocene section consists of alternating reddish/greenish grey calcareous marl and marly limestones from the Scaglia Variegata and Scaglia Cinerea Formations (Jovane et al., 2013). Here, we focused on the interval between 60 and 65 meters, within foraminiferal Zones E10–11, E12 and lower E13 (Berggren and Pearson, 2005) or P12 to lower P14 (Berggren et al., 1995; Jovane et al., 2013), approximately coinciding with the MECO interval.

3. Materials and Methods

Foraminifera were extracted from the Alano marlstones trough disaggregation with 10–30% H_2O_2, for 1–2 hours, followed by washing over ≥63 and ≥450 μm sieves. When necessary, samples were additionally soaked in a surface-tension-active solution. Foraminifera were extracted from the hard marly-limestone and limestone of the Monte Cagnero section through the cold acetolyse technique of Lirer (2000). Residues were sieved through a 63 μm mesh and dried at 50°C. The size fraction larger than 63 μm was weighed, then split in two equal parts with a precision micro-splitter. More than 300 foraminifera were counted in the ≥63 μm size fraction. Absolute abundance (number of specimens/gr bulk sediment; N/g) of the benthic foraminifera and the low trochospiral forms were calculated.

For stable isotope analyses, ~150 monospecific low-trochospiral specimens were picked from the ≥63 μm size fraction. In addition, 10–20 *Acarinina* belonging the *topilensis-pseudotopilensis* group, 4-5 *Subbotina* spp., and 20–25 *Nuttallides truempyi* were picked from the ≥100 μm size fraction. *Nuttallides truempyi* is an epifaunal benthic foraminiferal species (Bralower et al., 1995; Katz et al., 2003), and *Acarinina* species are symbiont-carrying, mixed layer dwelling planktic foraminifera (e.g., Bralower et al., 1995; Pearson et al., 2001; Sexton et al., 2006). *Subbotina* is a deeper dwelling species, calcifying in the lower part or below the thermocline, and does not carry photosymbionts (Pearson et al., 2001; Sexton et al., 2006).

Foraminiferal samples were analyzed for $\delta^{18}O$ and $\delta^{13}C$ isotopes by acid digestion using an individual vial acid drop Thermo Scientific Kiel IV carbonate device interfaced to Thermo Scientific MAT-253 dual-inlet isotope ratio mass spectrometer (IRMS) at University of California,

Santa Cruz. Samples were reacted at 75°C in orthophosphoric acid (specific gravity = 1.92 g/cm3) to generate carbon dioxide and water. During this procedure, water is cryogenically removed from CO_2 and non-condensable gases are pumped away, prior to introduction of the purified CO_2 into the IRMS.

During a run sequence, calibrated in-house standard Carrera Marble is used to correct the data including a drift correction. Four NBS-18 limestone standards are used in conjunction with Carrera Marble to correct for instrument specific source ionization effects. Two NBS-19 limestone samples are run "as-a-sample" to monitor quality control and long term performance. Carrera Marble has been extensively calibrated against NIST Standard Reference Materials (NBS-19, NBS-18, and LSVEC) and as part of intercomparison studies with other stable isotope laboratories. Corrected delta values are expressed relative to international standards PDB (Pee Dee Belemnite) for $\delta^{13}C$ and $\delta^{18}O$.

4. Results

4.1. Stable isotopes

Despite the fact that planktic foraminiferal tests are generally recrystallized on the sea floor, so that their stable oxygen isotopic values become close to these of benthic foraminifera by recrystallization at the sea-floor temperatures (Pearson et al., 2001), we see very clear differences between the small trochospiral foraminifera and the epifaunal benthic species *Nuttallides truempyi*. Stable isotope analyses from both the Alano and Cagnero sections unquestionably, and despite recrystallization, indicate a planktic habitat for the small trochospiral forms. The oxygen isotope values of the low-trochospiral forms from both sections cluster with those for the mixed-layer dwelling planktic foraminiferal genus *Acarinina*, whereas they are considerably lighter ($\Delta\delta^{18}O$ ~1‰) than values for the benthic species *Nuttallides truempyi* (Figs. 2, 3). Benthic foraminiferal oxygen isotope values at the two sites are similar, reflecting a range of temperature between 17 to 21°C (Chapter 3). Some benthic foraminifera are offset in oxygen isotope values from equilibrium with the seawater in which they formed (vital effects), but no benthic species has such a large offset in $\delta^{18}O$ values (Katz et al., 2003; Smart and Thomas, 2006).

Carbon isotope values of the low-trochospiral forms are heavier ($\Delta\delta^{13}C$ ~0.8‰ Alano specimens; $\Delta\delta^{13}C$ ~0.4‰ Cagnero specimens) than those for the deep-dwelling *Subbotina*, and for specimens from the Cagnero section they are much heavier than the values for *N. truempyi* ($\Delta\delta^{13}C$ ~1‰; Figs. 2, 3). Specimens from both the Alano and Cagnero sections, have slightly lighter values ($\Delta\delta^{13}C$

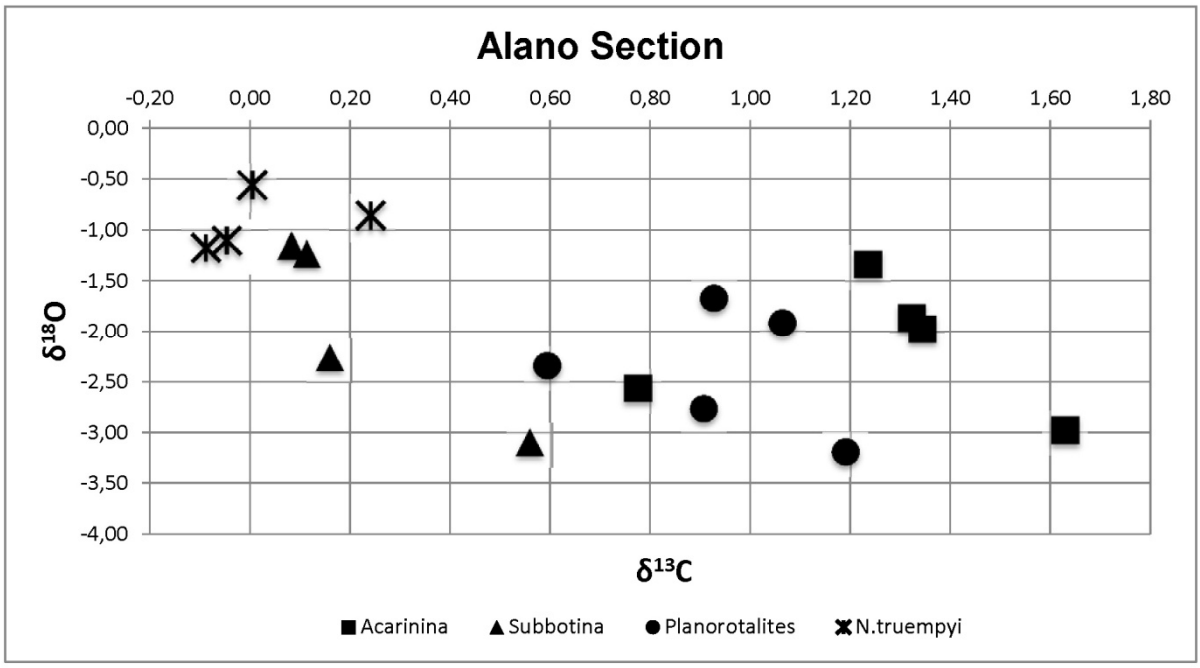

Figure 2. Carbon vs. oxygen plots for planktic and benthic specimens from Alano and M. Cagnero sections.

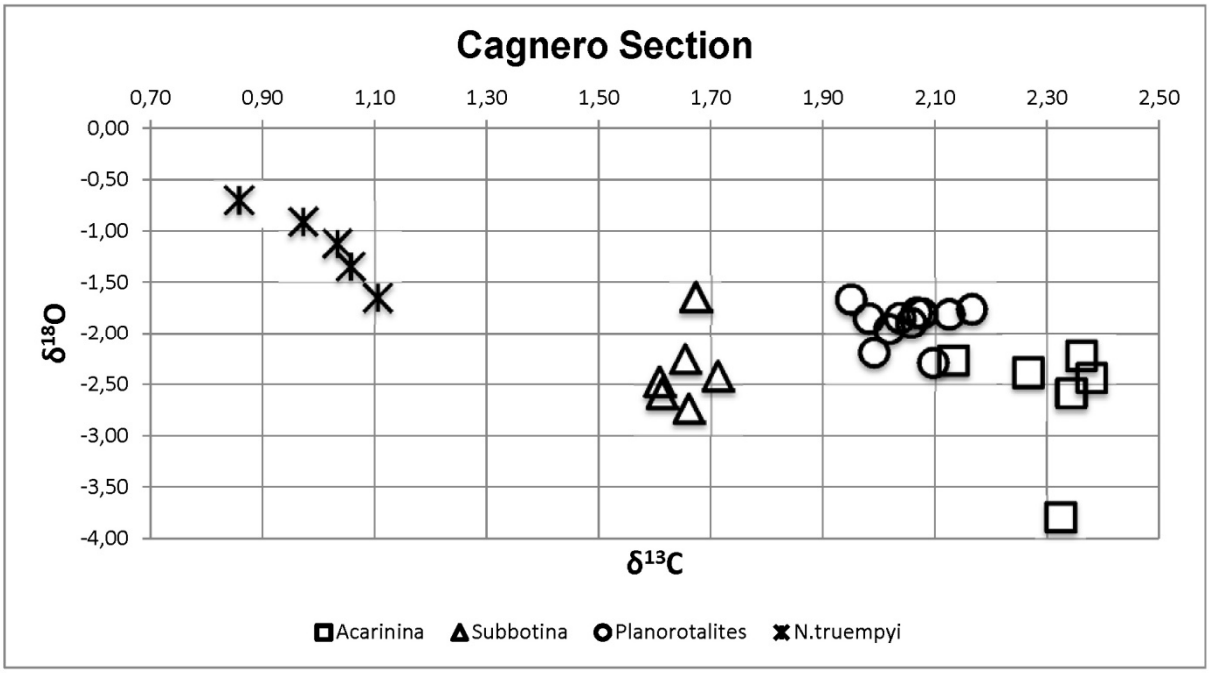

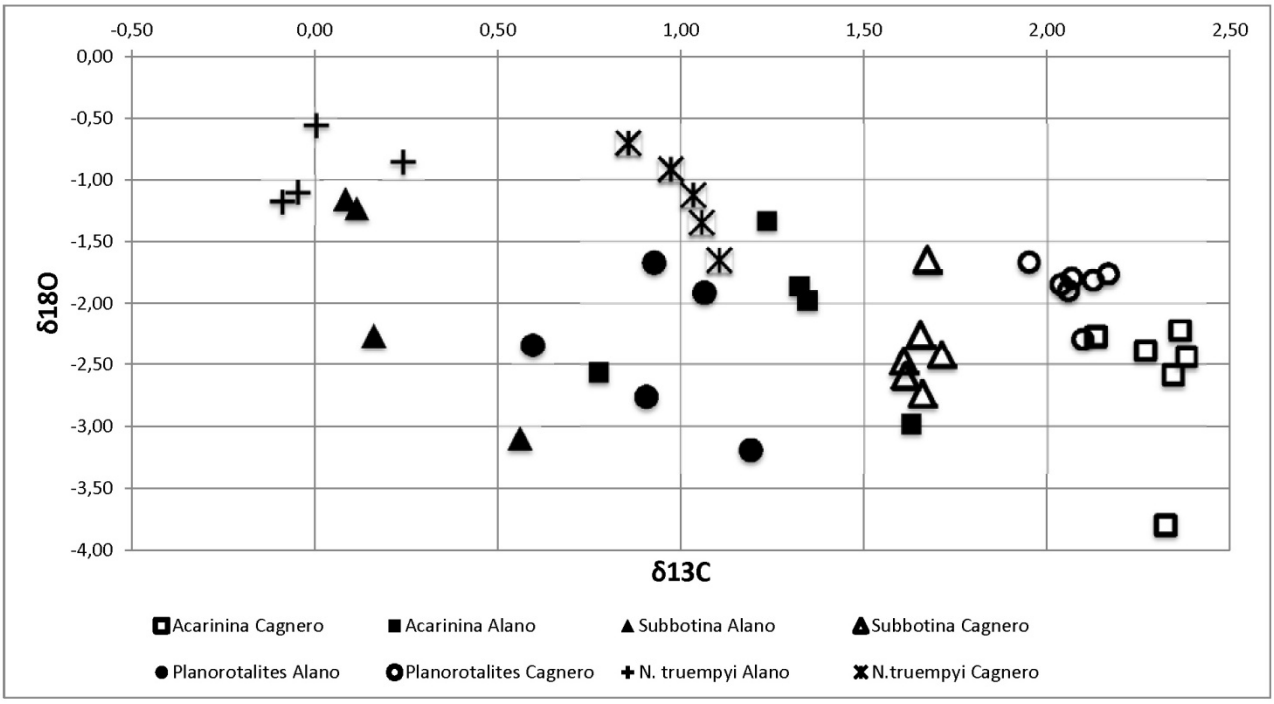

Figure 3. Carbon vs. oxygen plot for planktic and benthic specimens from Alano and M. Cagnero sections.

~0.3‰) than the mixed-layer symbiont-bearing genus *Acarinina* (Fig. 2, 3). In the Cagnero section the $\delta^{13}C$ values of planktic foraminifera cluster closer than in the Alano section (Fig. 2).

4.2. Genus and species attribution of the problematic low-trochospiral planktic foraminifera

The preservation of the small, trochospiral forms is problematic, and especially the apertures are not well visible, but their morphology allows us to refer them confidently to the genus *Planorotalites* (Pearson et al., 2006). The small, low-trochospiral, subcircular test, with the keeled outline, six to eight chambers in the last whorl, shallow and narrow umbilicus, and biconvex profile as well as the muricate walls, pustulate wall on the involute side, make the identification of the genus possible, despite the strong recrystallization and the lack of well-preserved apertures (Plate I).

We refer our morphotypes to the species *Planorotalites capdevilensis*, after considerable comparison to figured specimens (see taxonomy), although we cannot be certain due to the preservation. The presence of flush to slightly raised sutures on the spiral side, and the very flat almost equally biconvex text are typical for the species *P. capdevilensis*, and makes it is possible to distinguish it from e.g., *P. pseudoscitula*. We agree with Pearson et al. (2006) that *P. renzi* overlap in morphology, and thus may be a junior synonym of *P. capdevilensis*.

However, analysis of material with adequate state of preservation, and specifically well preserved apertures is necessary to attain a completely reliable species attribution.

4.3. Abundance pattern of Planorotalites capdevilensis at Alano and M. Cagnero sections

At Alano *P. capdevilensis*, shows moderately high abundances in the lowermost part of section, then progressively decreased in abundance across the MECO interval, and is virtually absent within the sapropel-like beds that characterize the post-MECO interval at Alano (Fig. 4; Spofforth et al., 2010; Boscolo-Galazzo et al., 2013). The highest absolute abundances are reached at the top of the studied interval, above the organic rich layer (Fig. 4). This pattern contrasts with that of benthic foraminiferal abundances, which increase across the MECO, and are relatively high in the sapropelic intervals. At the Monte Cagnero section, the absolute abundance of *P.* cf. *capdevilensis* fluctuates throughout the studied interval, slightly increasing across the MECO (Fig. 4). At ~63.5 m the *Planorotalites* species is very rare, whereas the benthic absolute abundance peaks to the highest value in the studied interval (Fig. 4). However, this short interval of marked decrease in abundance of *P. capdevilensis* coincides with a dissolution interval, causing a drastic drop in all planktic foraminifera and a decrease in preservation of benthic tests.

5. Discussion

Our carbon isotopic data show clear offsets among the analyzed genera, reflecting different depth habitat in the water column (Figs. 2, 3). The carbon isotope values for *Subbotina* specimens are the lowest among the analyzed planktic genera, compatible to the thermocline habitat generally attributed to this genus (Pearson et al., 2005; Ezard et al., 2011). *Acarinina* specimens display more positive values, consistent with a shallow depth habitat, and hosting of symbionts (Pearson et al., 2005).

The carbon stable isotope values of *P. capdevilensis* are heavier than those of *Subbotina,* and combined with the light oxygen isotope values suggest these forms were mixed layer dwellers, possibly living slightly deeper than acarininids (Figs. 3, 4). The lighter carbon isotope composition as compared to that of other muricates, e.g., *Acarinina* and *Morozovelloides* might be the result of their very small size (Pearson et al., 2001; present study). The species analyzed as *P. pseudoscitula* (Pearson et al., 2001) was later recognized as *P. capdevilensis* (Perason et al., 2006), and occupies a

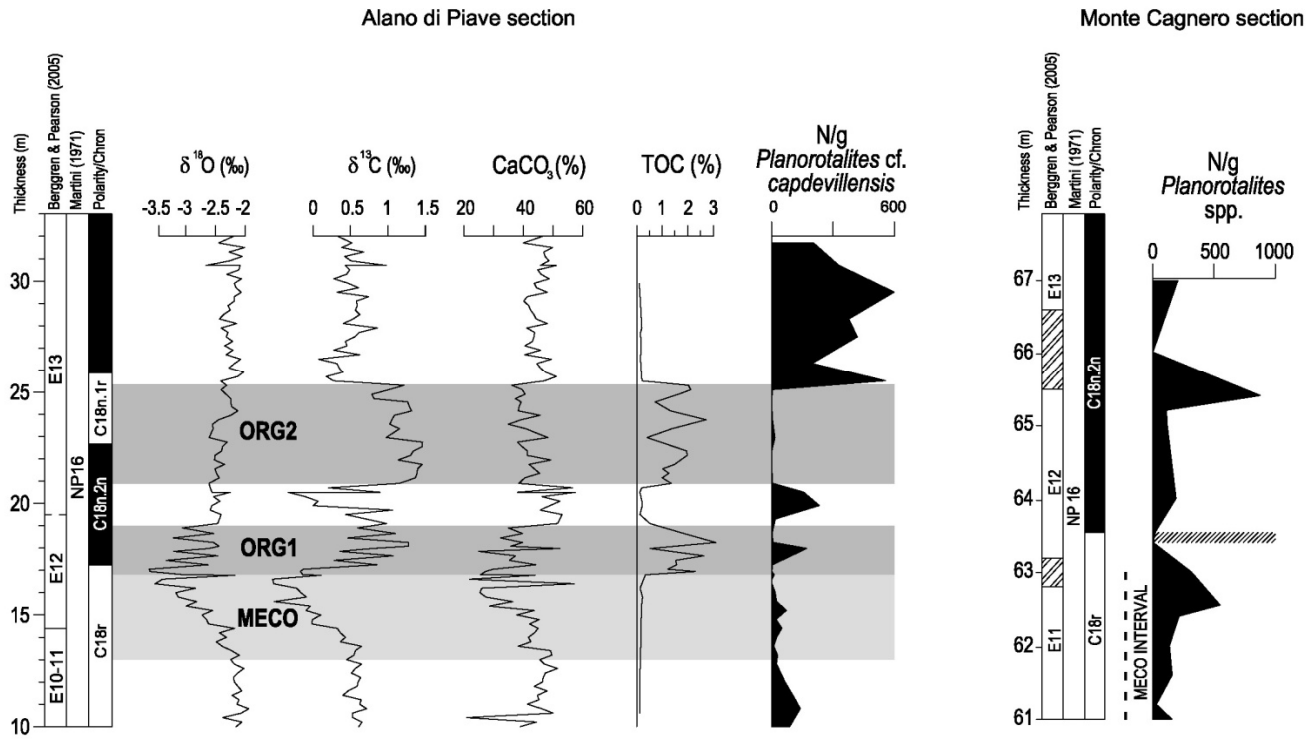

Figure 4. Abundance (N/g = number of specimens per gram) of *Planorotalites capdevilensis* across the MECO at Alano plotted against bio-magnetostratigraphy. Alano section stable isotopes ($\delta^{18}O$ and $\delta^{13}C$), total organic carbon (TOC%) and $CaCO_3$% records after Spofforth et al. (2010), bio-magnetostratigraphy after Agnini et al. (2011). Cagnero section magnetostratigraphy after Savian et al. (2013). MECO interval in the Cagnero section according to Savian et a. (2013), the hatched band indicates a level of carbonate dissolution.

very similar location in the $\delta^{18}O$-$\delta^{13}C$ plot as our specimens of *P. capdevilensis*. The carbon isotope values could indicate the absence of photosymbionts, but their small size alone could explain the values (Pearson et al., 2006; Birch et al., 2012). This species was indeed recognized as a mixed layer dweller (Pearson et al., 2006).

The species *Planorotalites capdevilensis*, has sometimes been referred to as *P. pseudoscitula* or *Globorotalia* (*Planorotalites*) *renzi* (see Taxonomy), and has in general been described as widely distributed in essentially (sub)tropical regions (Caribbean, Tethys) and austral (New Zealand) regions. There are few quantitative data on its geographical distribution (e.g., Toumarkine and Luterbacher, 1985; Wade, 2004; Pearson et al. 2006).

Planorotalites capdevilensis is rather abundant in sediments from ODP Site 1263 (South-East Atlantic; Degasperi, master thesis in progress) across the same stratigraphic interval as investigated here. At Site 1263, the reconstruction of the water column structure using stable isotopes (Chapter 3), suggest a stable stratification and likely relatively oligotrophic surface water conditions, as expected in an open ocean subtropical area, not influenced by an up-welling systems.

P. capdevilensis is thus common at a variety of sites, from pelagic Site 1263, to NW Atlantic Site 1252 (Wade, 2004) at a location close to a deeper site with high primary biosiliceous productivity across MECO (Site 1051; Witkowski et al., in press).

The planktic foraminiferal study across the MECO at the Alano section (Luciani et al., 2010) did consider the small size fraction, but *Planorotalites* was not recognized in the analysis, likely because these forms were attributed to benthic foraminifera or juveniles due their poor state of preservation. Comparison of our abundance data for the Alano section with those for other planktic foraminifera (Luciani et al., 2010) shows that the species is almost completely absent during the MECO and in the upper organic-rich layer directly postdating the MECO, i.e., during peak eutrophication of surface waters (Fig. 4; Luciani et al., 2010; Toffanin et al., 2011). However, dissolution of *Planorotalites* could have influenced our data, because its lowest abundance occur in the intervals with high values of the fragmentation index values. *P. capdevilensis* increased strongly in abundance after the deposition of the upper organic rich layer, when the larger muricates started to recover from MECO.

P. capdevilensis at the M. Cagnero section displays higher peak abundances than at Alano in a few samples. This site was in deeper water (~1-2 Km; Jovane et al., 2013, as compared to 0.6-0.8 Km for the Alano section; Boscolo Galazzo et al., 2013). Across the MECO interval at M. Cagnero, *Planorotalites capdevilensis* does not decrease in abundance, rather showing a slight increase (Fig. 4). Data on planktic foraminiferal assemblages (Luciani, unpublished data) do not show a strong increase in eutrophic indicators species, suggesting there was no marked eutrophication during the MECO, in contrast with Alano.

This observation agrees with our data on the carbon isotope values for benthic foraminifera, deep-dwelling planktic foraminifera, the low-trochospiral group and mixed-layer dwelling planktic foraminifera. All 4 groups have a lighter carbon isotope signature at Alano than their counterparts at M. Cagnero (Fig. 3). In addition, the four groups of foraminifera are more clearly separated in their isotope values at Cagnero than at Alano. The latter two observations may reflect the fact that Alano was in a rather small basin and not the open ocean, and primary productivity was high over the studied interval, with low oxygen conditions developing at some times. The lighter carbon isotope values at Alano reflect strong remineralization of organic matter in the water column (Chapter 2, 3), indicating *P. capdevilensis*, was able to thrive in waters where such remineralization was common.

According to the age models of Alano and M. Cagnero sections, the first section records a higher sedimentation rate following the post-MECO interval. The substantial increase in *P. capdevilensis* abundance above the post-MECO at Alano might be related both to a return to normal-productive

surface waters and/or to a better adaptation of this genus to the cooler conditions following the MECO. It is also possible that planorotaliids occupied to some extent the ecological niches permanently vacated by the large acarininids, which decreased in abundance during MECO and never fully recovered (e.g., Luciani et al., 2010; Edgar et al., 2012).

In conclusion, *P. capdevilensis* may have been a mixed layer dweller, without photosymbionts, and thus adapted to slightly more eutrophic conditions than the symbiont-bearing large acarininds and morozovellids, but less eutrophic than biserial and triserial planktonic species. They therefore could increase in abundance when the environment recovered from the eutrophication during and just after peak MECO at Alano, while the large acarininds never recovered from the symbiont bleaching during MECO (Wade, 2004).

6. Conclusions

Stable isotope data prove that the low trochospiral specimens abundant in middle Eocene samples from the Alano and M. Cagnero section are planktic foraminifera belonging to genus *Planorotalites*. The slightly raised sutures on the spiral side, and the flat, almost equally biconvex text as well as the pustulate ventral side allow a tentative assignment to the species *Planorotalites capdevilensis.*

The stable isotope data for *P. capdevilensis* indicate that the taxon was a mixed layer dwelling species, possibly slightly deeper than other muricates. Its relatively light carbon isotope signature may indicate a lack of photosymbionts, or be due to its small size.

Its widespread distribution in subtropical regions during the latter part of the middle Eocene, together with the differences in its abundance pattern across the MECO interval at the Alano and Cagnero section, suggest that the species was rather flexible, and may have become most abundant during conditions that were neither very oligotrophic (large acrininids and morozovellids dominant), nor very eutrophic (biserial and triserial taxa dominant).

Plate I

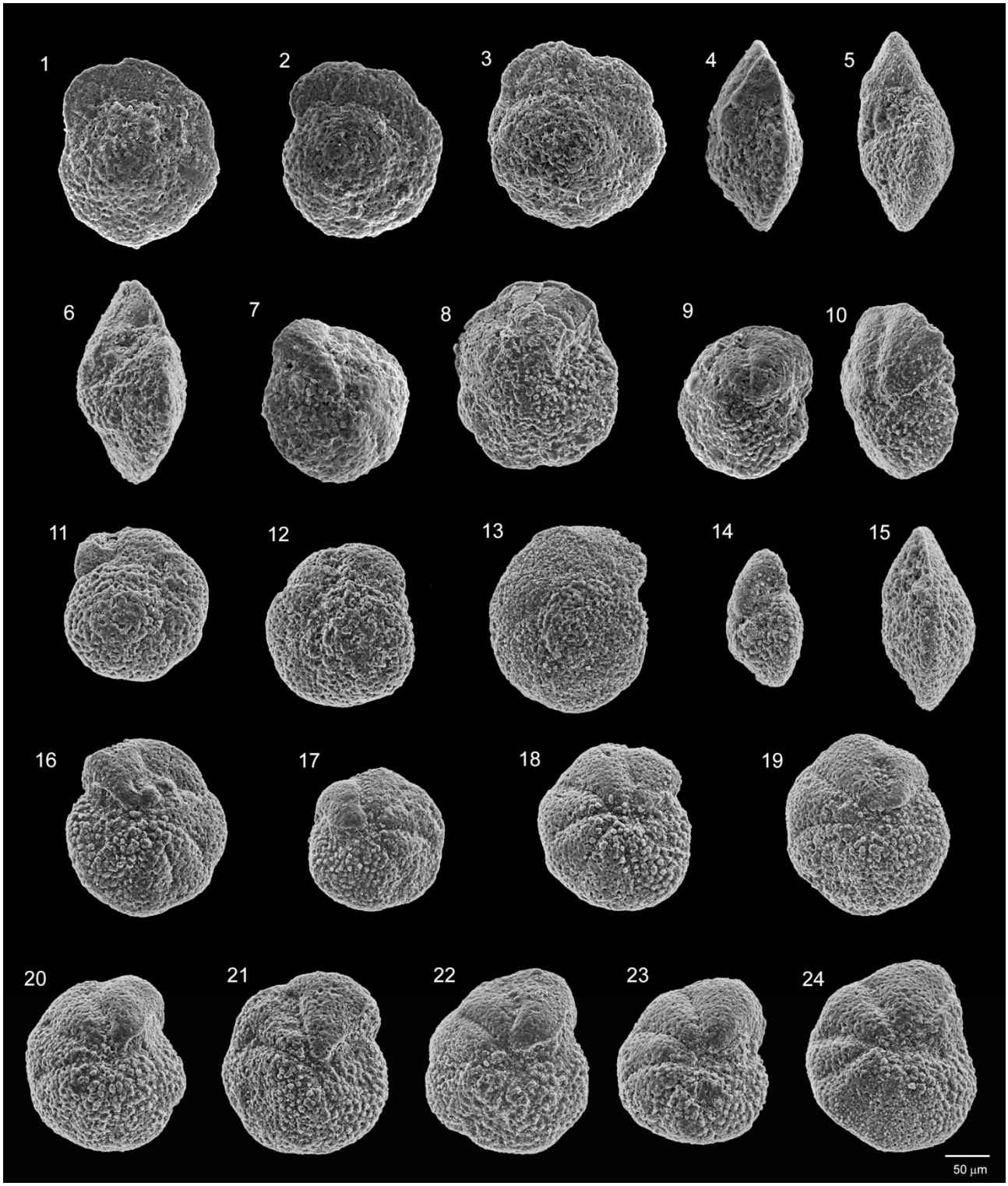

Plate I. *Planorotalites capdevilensis* (Cushman and Bermudez 1949), Fig. 1 spiral view, Alano section COL1065B-27.50 m; Fig. 2 spiral view, Alano section COL1265B-29.50 m; Fig. 3 spiral view, Alano section COL945B-26.30 m; Figs. 4-6 Alano section lateral view, COL945B-26.30 m; Fig. 7 umbilical view, Alano section COL1385-30.70 m; Fig. 8 umbilical view, Alano section COL1265B-29.50 m; Fig. 9 umbilical view, Alano section COL945B-26.30 m; Fig 10 lateral view, M. Cagnero section CAG 61.60-61.60 m; Fig. 11 spiral view, M. Cagnero section CAG 61.60-61.60 m; Figs. 12-13 spiral view, M. Cagnero section CAG 62-62.00 m; Fig. 14 lateral view, M. Cagnero CAG 62.55-62.55 m; Fig. 15 lateral view, M. Cagnero CAG 62-62.00 m; Figs. umbilical view, 16-20 M. Cagnero CAG 61.60-61.60 m; Figs. 21-24 umbilical view, M. Cagnero section CAG 62.55-62.55 m.

Appendix A. Taxonomy

Planorotalites capdevilensis (Cushman and Bermudez, 1949)

(Plate I, Fig. 1-24)

†*Globorotalia capdevilensis* Cushman and Bermudez, 1949, p. 32, pl. 6, figs. 10, 11

Globorotalia renzi Bollis 1957, p. 168, pl. 38, figs. 3a-c.

Globorotalia renzi Bolli, Postuma 1971, p. 208, fig. p. 209

Globorotalia renzi Bolli, Stainforth et al., 1975, p. 221, Fig. 81.

Planorotalites pseudoscitula Glaessner, Poore and Brabb, 1977, p. 264, pl. 7, figs. 12,13

Globorotalia (*Globorotalia*) *capdevilensis* Cushman and Bermudez, Cifelli and Belford, 1977, p.103 pl. 1; fig. 13-15

Planorotalites capdevilensis Cushman and Bermudez, Pearson et al., 2004, p. 36, pl. 1, figs. 22,23

Planorotalites capdevilensis Cushman and Bermudez, Wade 2004, pl. 1, figs. a, b.

Planorotalites capdevilensis Cushman and Bermudez, Pearson et al., 2006, p. 387, pl. 12.4, figs. 1-16

Test small, biconvex, close to circular, periphery smooth to slightly lobulate, especially in the last chambers. Imperforate keel, variable in strength. Wall is muricate, normal perforate, and non spinose. Early chambers on involute side covered with dense pustules, probably at least in part recrystallized. Chambers on involute side triangular in shape, 6-8 per whorl, gradually increasing in size. Sutures on involute side straight to slightly curved in earlier chambers visible, depressed. Sutures between earlier chambers not clearly visible because of pustules. Umbilicus narrow and depressed. On evolute side ~2.5-3 whorls visible, chambers trapezoidal, sutures between last chambers in some instances slightly depressed, otherwise limbate. Aperture has not been observed in our specimens.

References

Bolli, H.M., 1957. Planktonic Foraminifera from the Eocene Navet and San Fernando formations of Trinidad, B.W.I. Bulletin U.S. National Museum, 215, 155-172.

Bralower, T.J., Zachos, J.C., Thomas, E., Parrow, M.N., Paull, C.K., Kelly, D.C., Premoli-Silva, I., Sliter, W. V., 1995. Late Paleocene to Eocene Paleoceanography of the Equatorial Pacific Ocean: Stable Isotopes recorded at ODP Site 865, Allison Guyot. *Paleoceanography*, 10, 841-865

Cifelli, R., Belford, D.J., 1977. The types of several species of Tertiary planktonic foraminifera in the collections of the U.S. National Museum of Natural History. Journal of Foraminiferal Research, 7, 100-105

Cushman, J.A., Bermudez, P.J., 1949, Some Cuban species of *Globorotalia*. Cushman Laboratory for Foraminiferal Research Contributions, 25, pt. 2, 26-45.

Edgar, K.M., Wilson, P.A., Sexton, P.F., Gibbs, S.J., Roberts, A.P., Norris, R.D., 2010. New biostratigraphic, magnetostratographic and isotopic insights in the Middle Eocene Climatic Optimum in low latitudes. Palaeogeography, Palaeoclimatology, Palaeoecology, 297, 670–682

Edgar, K.M., Bohaty, S.M., Gibbs, S.J., Sexton, P.F., Norris, R.D., Wilson, P.A., 2013. Symbiont 'bleaching' in planktic foraminifera during the Middle Eocene Climatic Optimum. Geology, 41, 15-18.

Jovane, L., Savian, J.F.,Coccioni, R., Frontalini, F., Bancalà, G., Catanzariti, R., Luciani, V., Bonhaty, S.M., Wilson, P.A., Florindo, F., 2013. Integrated magnetobiostratigraphy of the middle Eocene-lower Oligocene interval from the Monte Cagnero section, central Italy. Geolgical Society of London Special Publication, 373, http://dx.doi.org/10.1144/SP373.13.

Katz, M.E., Wright, J.D., Katz, D.R., Miller, K.G., Pak, D.K., Shackleton, N.J., Thomas, E., 2003. Early Cenozoic benthic foraminiferal isotopes: species reliability and interspecies correction factors. *Paleoceanography*, 18, 1024, doi: 10.1029/2002PA000798.

Lirer, F., 2000. A new technique for retrieving calcareous microfossils from lithified lime deposits, Micropaleontology, 46, 365–369.

Luciani, V., Giusberti, L., Agnini, C., Fornaciari, E., Rio, D., Spofforth, D.J.A., Pälike, H., 2010. Ecological and evolutionary response of Tethyan planktonic foraminifera to the middle Eocene climatic optimum (MECO) from the Alano section (NE Italy). Palaeogeography, Palaeoclimatology, Palaeoecology, 292, 82–95

Pearson, P.N., Ditchfield, P.W., Singano, J., Harcourt-Brown, K.G., Nichols, C,J., Olsson, R.K., Shackleton, N.J., Hall, M.A., 2001, Warm tropical sea surface temperatures in the Late Cretcaeous and Eocene epochs. Nature ,413, 481-487.

Pearson, P.N., Nicholas, C.J., Singano, J.M., Bown, P.R., Coxal, H.K., van Dongen, B.E., Huber, B.T., Karega, A., Lees, J.A., Misaky, E., Pancost, R.D., Pearson, M., Roberts, A.P., 2004. Paleogene and Cretaceous sediment cores from the Kilwa and Lindi areas of coastal Tanzania. Tanzania Drilling Project Sites 1-5 . Journal of African Earth Sciences, 39, 25-62.

Pearson, P.N., Olsson, R.K., Hemleben, C., Huber, B.T., Berggren, W.A., 2006. Atlas of Eocene Planktonic Foraminifera, 513 pp.

Poore, R.Z., Brabb, E.E., 1977. Eocene and Oligocene planktonic foraminifera from the Upper

Butano Sandstone and type San Lorenzo Formation, Santa Cruz Mountains, California. Journal of Foraminiferal Research, 7, 249-272.

Postuma, J.A, 1971. Manual of Planktonic Foraminifera, 422 pp.

Savian, J.F., Jovane. L., Trindade, R.I. F., Frontalini. F., Coccioni, R., Bohaty, S.M., Wilson, P.A., Florindo, F., Roberts, A., 2013. Middle Eocene Climatic Optimum (MECO) in the Monte Cagnero Section, Central Italy. Latinmag Letters, 3, Spec. Issue PCO_2, 1-8.

Sexton, P.F., Wilson, P.A., Pearson, P.N., 2006. Palaeoecology of late middle Eocene planktic foraminifera and evolutionary implications. Marine Micropaleontology, 50, 1-16.

Stainforth, R.M., Lamb, J.L., Luterbacher, H.P., Beard, J.H, Jeffords, R.M. 1975. Cenozoic planktonic foraminiferal zonation and characteristics of index forms. Paleontological Contributions Article, 62, 425 pp.

Van der Zwaan, G.J., Jorissen, F.J., de Stigter, H.C., 1990. The depth dependency of planktonic/benthic foraminiferal ratios: constraints and applications. Marine Geology, 95, 1-16.

Wade, B.S., 2004. Planktonic foraminiferal biostratigraphy and mechanisms in the extinction of *Morozovella* in the late middle Eocene. Marine Micropaleontology, 51, 23-38.

Bibliography

Agnini, C., Muttoni, G., Kent, D.V., Rio, D., 2006. Eocene biostratigraphy and magnetic stratigraphy from Possagno, Italy: The calcareous nannofossil response to climate variability. Earth and Planetary Science Letters, 241, 815– 830.

Agnini, C., Fornaciari, E., Giusberti, L., Grandesso, P., Lanci, L., Luciani, V., Muttoni, G., Rio, D., Stefani, C., Pälike, H., Spofforth, D.J.A., 2011. Integrated bio-magnetostratigraphy of the Alano section (NE Italy): a proposal for defining the Middle–Late Eocene boundary. Geological Society of American Bullettin, 123 (5/6), 841–872, doi:10.1130/B30158.1.

Alegret, L., Thomas, E., 2001. Upper Cretaceous and lower Paleogene benthic Foraminifera from northeastern Mexico. Micropaleontology, 47: 269-316.

Alegret, L., Thomas, E., 2008. Deep-Sea environments across the Cretaceous/Paleogene boundary in the eastern South Atlantic Ocean (ODP Leg 208, Walvis Ridge). Marine Micropaleontology, 64, 1–17.

Alegret, L., Ortiz, S., Molina, E., 2009. Extinction and recovery of benthic foraminifera across the Paleocene-Eocene Thermal Maximum at the Alamedilla section (Southern Spain), Palaeogeography, Palaeoclimatology, Palaeoecology 279, 186-200.

Alegret, L., Ortiz, S., Arenillas, I., Molina, E., 2010. What happens when the ocean is overheated? The foraminiferal response across the Paleocene-Eocene Thermal Maximum at the Alamedilla section (Spain). Geological Society of America Bulletin, 122, 1616-1624, doi:10.1130/B30055.1.

Aller, R.C., Blair, N.E., 2006. Carbon remineralization in the Amazon-Guiana tropical mobile mudbelt: a sedimentary incubator. Continental Shelf Research 26, 2241-2259.

Alve, E., 1995. Benthic foraminiferal distribution and recolonization of formerly anoxic environments in Drammensfjord, southern Norway. Marine Micropaleontology 25, 169–186.

Alve, E., Bernhard, J.M., 1995. Vertical migratory response of benthic foraminifera to controlled oxygen concentrations in an experimental mesocosm. Marine Ecology Progress Series 116, 137–51.

Arndt, S., Jørgensen, B.B., LaRowe, D.E., Middelburg, J.J., Pancost, R.D, Regnier, P., 2013. Quantifying the degradation of organic matter in marine sediments: A review and synthesis. Earth-Science Reviews, 123, 53–86.

Barbieri, R., 1990. L'Eocene medio e superiore del Bacino di Tripolitania (Libia nord occidentale): biostratigrafia e paleoecologia. Bollettino della Società Paleontologica Italiana 29 (3), 253-271.

Barbieri, R., Benjamini, C., Monechi, S., Reale, V., 2003. Stratigraphy and benthic foraminiferal events across the middle–late Eocene transition in the western Negev, Israel. In: Prothero, D.R., Ivany, L.C., and Nesbitt, E.A., (Eds.), From Greenhouse to Icehouse: The Marine Eocene–Oligocene Transition: New York, Columbia University Press, pp. 453–470.

Barlow, R.G., Mantoura, R.F.C., Gough, M.A., Fileman, W.T., 1993. Pigment signature of the phytoplankton composition in the north-eastern Atlantic during the 1990 spring bloom. Deep-sea Research II, 40, 459-477.

Bralower, T.J., Zachos, J.C., Thomas, E., Parrow, M.N., Paull, C.K., Kelly, D.C., Premoli-Silva, I., Sliter, W. V., 1995. Late Paleocene to Eocene Paleoceanography of the Equatorial Pacific Ocean: Stable Isotopes recorded at ODP Site 865, Allison Guyot. *Paleoceanography*, 10, 841-865

Beniamovski, V.N., Alekseev, A.S., Ovechkina, M.N., Oberhänsli, H., 2003. Middle to Upper Eocene disoxic-anoxic Kuma Formation (northeast Peri-Tethys): Biostratigraphy and paleoenviroments. In: Wing, S.L., Gingerich, P.D., Schmitz, B., & Thomas, E., eds. Causes and Consequences of Globally Warm Climates in the Early Paleogene. Boulder, Colorado, Geological Society of America Special Paper 369, pp. 95–112.

Berger, W.H., Bonneau, M.-C., Parker, F.L., 1982. Foraminifera on the deep-sea floor: lysocline and dissolution rate. Oceanologica Acta, 5, 249–258.

Berggren, W.A., Aubert, J., 1976. Eocene benthonic foraminiferal biostratigraphy and paleobathymetry of Orphan Knoll (Labrador Sea). Micropaleontology, 22, 327–346.
Berggren, W.A., Pearson, P.N., 2005. A revised tropical to subtropical Paleogene planktonic foraminiferal zonation. Journal of Foraminiferal Research, 35, 279–298.

Berggren, W.A., Kent, D.V., Swisher III, C.C., Aubry, M.P., 1995. A revised Cenozoic geochronology and chronostratigraphy. Special Publication SEPM Society of Sedimentary Geology 54, 129–212.

Bernhard, J.M., Sen Gupta, B.K., 1999. Foraminifera of oxygen-depleted environments. In: Sen Gupta B.K. (Ed.), Modern Foraminifera. Kluwer Academic Press, 201-216.

Bernhard, J.M., Sen Gupta, B.K., Borne, P.F., 1997. Benthic foraminiferal proxy to estimate dysoxic bottom water oxygen concentrations, Santa Barbara Basin, US Pacific continental margin. Journal of Foraminiferal Research, 27, 301– 310.

Bernhard, J.M., Goldstein, S.T., Bowser, S.S., 2010. An ectobiont-bearing foraminifera, Bolivina pacifica, that inhabits microxic pore waters: cell-biological and paleoceanographic insight. Environmental Microbiology, 12(8), 2107–2119.

Bickert, T., Cordes, R., Wefer, G., 1997. Late Pliocene to mid-Pleistocene (2.6–1.0 Ma) carbonate dissolution in the western equatorial Atlantic: Results of ODP Leg 154, Ceara Rise. Proceedings of the ODP Scientific Results 154, 229-237.

Bidigare, R.R., Benitez-Nelson, C., Leonard, C.L., Quay, P.D., Parsons, M.L., Foley, D.G., Seki, M.P., 2003. Influence of a cyclonic eddy on microheterotroph biomass and carbon export in the lee of Hawaii. Geophysical Research Letters, 30-6, 1318, doi:10.1029/2002GL016393.

Bijl, P.K., Houben, A.J.P., Schouten, S., Bohaty, S.M., Sluijs, A., Reichart, G.J., Sinninghe Damsté, J.S., Brinkhuis, H., 2010. Transient middle Eocene atmospheric CO_2 and temperature variations. Science, 330, 819–821.

Bijl, P.K., Bendl, J.A.P., Bohaty, S.M., Pross, J., Schouten, S., Tauxe, L., Stickley, C.E., McKay, R.M., Röhl, U., Olneyk, M., Sluijs, A., Escutia, C., Brinkhuis, H., and Expedition 318 Scientists, 2013. Eocene cooling linked to early flow across the Tasmanian Gateway. Proceedings of the National Academy of Science, doi/10.1073/pnas.1220872110.

Boersma, A., Premoli Silva, I., Shackleton, N.J., 1987. Atlantic Eocene planktonic foraminiferal paleohydrographic indicators and stable isotope paleoceanography. Paleoceanography, 2, 287-331.

Bohaty, S.M., Zachos, J.C., 2003. A significant Southern Ocean warming event in the late middle Eocene. Geology, 31, 1017–1020.

Bohaty, S.M., Zachos, J.C., Florindo, F., Delaney, M.L., 2009. Coupled greenhouse warming and deep-sea acidification in the Middle Eocene. Paleoceanography, 24, PA2207. doi:10.1029/2008PA001676, 2009.

Bolli, H.M., 1957. Planktonic Foraminifera from the Eocene Navet and San Fernando formations of Trinidad, B.W.I. Bulletin U.S. National Museum, 215, 155-172.

Boltovskoy, E., Boltovskoy, D., 1989. Paleocene–Pleistocene benthic foraminiferal evidence of major paleoceanographic events in the eastern South Atlantic (DSDP Site 525, Walvis Ridge). Marine Micropaleontology, 14, 283–316.

Boltovskoy, E., Scott, D.B., Medioli, F.S., 1991. Morphological variations of benthic foraminiferal tests in response to changes in ecological parameters, a review. Journal of Paleontology, 65, 175–185.

Boltovskoy, E., Watanabe, S., Totah, V.I., Vera Ocampo, J., 1992. Cenozoic Benthic Bathyal Foraminifers of DSDP Site 548 (North Atlantic). Micropaleontology, 38-2, 183-207.

Bosboom, R.E., Abels, H.A., Hoorn, C., van den Berg, B.C.J., Guo, Z., Dupont-Nivet, G., 2014. Aridification in continental Asia after the Middle Eocene Climatic Optimum (MECO). Earth and Planetary Science Letters, 389, 34-42.

Boscolo Galazzo, F., Giusberti, L., Luciani, V., Thomas, E., 2013. Paleoenvironmental changes during the Middle Eocene Climatic Optimum (MECO) and its aftermath: The benthic foraminiferal record from the Alano section (NE Italy). Palaeogeography, Palaeoclimatology, Palaeoecology, 378, 22-35.

Bosellini, A., 1989. Dynamics of Tethyan carbonate platform. In: Crevello, P.D., James, L.W., Sarg, J.F., Read, J.F. (Eds.). Controls on Carbonate Platform and Basin Platform. Society for Sedimentary Geology (SEPM) Special Publication, 44, 3–13.

Bowen, G.J., Zachos, J.C., 2010. Rapid carbon sequestration at the termination of the Palaeocene-Eocene Thermal Maximum. Nature Geoscience, 3, 866-869.

Bradshaw, J.S., 1961. Laboratory experiments on the ecology of foraminifera. Contributions from the Cushman Foundation of Foraminiferal Research, 12, 87–106.

Bremer, M.L., Lohmann, G.P., 1982, Evidence for primary control of the distribution of certain Atlantic Ocean benthonic foraminifera by degree of carbonate saturation. Deep-Sea Research, v. 29, p. 987–998, doi:10.1016/0198-0149(82)90022-X.

Braga, G., De Biase, R., Grünig, A., Proto Decima, F., 1975. Foraminiferi bentonici del Paleocene ed Eocene della sezione di Possano. In: Bolli, H.M. (Ed.), Monografia Micropaleontologica sul Paleocene e l'Eocene di Possagno, Provincia di Treviso, Italia: Schweizerische Palaeontologische Abhandlungen, 97, 87-199.

Broecker, W.S., Clark, E., 1999. $CaCO_3$ size distribution: a paleocarbonate ion proxy? Paleoceanography, 14 (5), 596–604.

Burgess, C.E., Pearson, P.N., Lear, C.H., Morgans, H.E.G., Handley, L., Pancost, R.D., Schouten, S., 2008. Middle Eocene climate cyclicity in the southern Pacific: Implications for global ice volume. Geology, 36, 651–654.

Buzas, M.A., Culver, S.J., Jorissen, F.J., 1993. A statistical evaluation of the microhabitats of living (stained) infaunal benthic foraminifera. Marine Micropaleontology, 29, 73-76.

Cande, S.C., Kent, D.V., 1995. Revised calibration of the geomagnetic polarity timescale for the Late Cretaceous and Cenozoic. Journal of Geophysical Research, 100, 6093–6095.

Cetean, C.G., Setoyama, E., Kaminski, M.A., Neagu, T.R., Bubík, M., Filipescu, and Tyszka, S.J., 2011. Eobigenerina, a cosmopolitan deep-water agglutinated foraminifer, and remarks on late Paleozoic to Mesozoic species formerly assigned to Pseudobolivina and Bigenerina. In: Kaminski M.A., Flipescu S. (Eds.), Proceedings of the Eighth International Workshop on Agglutinated Foraminifera. Grzybowski Foundation Special Publication 16, 19-27.

Cifelli, R., Belford, D.J., 1977. The types of several species of Tertiary planktonic foraminifera in the collections of the U.S. National Museum of Natural History. Journal of Foraminiferal Research, 7, 100-105.

Cita, M.B., 1975. Stratigrafia della Sezione di Possagno. In: Bolli, H.M. (Ed.), Monografia Micropaleontologica sul Paleocene e l'Eocene di Possagno, Provincia di Treviso, Italia. Schweizerische Palaeontologische Abhandlungen, 97, 9–33.

Corliss, B.H., 1985. Microhabitats of Benthic Foraminifera within deep-sea sediments. Nature, 314, 435–438.

Corliss, B.H., Chen, C., 1988. Morphotype patterns of Norwegian Sea deep-sea benthic foraminifera and ecological implications. Geology, 16, 716–719.

Coxall, H.K., Wilson, P.A., Palike H., Lear, C.H., Backman J., 2005. Rapid stepwise onset of Antarctic glaciation and deeper calcite compensation in the Pacific Ocean. Nature, 433 (7021), 53–57.

Cushman, J.A., Bermudez, P.J., 1949, Some Cuban species of *Globorotalia*. Cushman Laboratory for Foraminiferal Research Contributions, 25, pt. 2, 26-45.

Cramer, B.S., Toggweiler, J.R., Wright, M.E., Katz, J.D., Miller, K.G., 2009. Ocean overturning since the Late Cretaceous: Inferences from a new benthic foraminiferal isotope compilation. Paleoceanography, 24, PA4216, doi:10.1029/2008PA001683.

Dawber, C.F., Tripati, A.K., 2011. Constraints on glaciation in the middle Eocene (46–37 Ma) from Ocean Drilling Program (ODP) Site 1209 in the tropical Pacific Ocean. Paleoceanography, 26, PA2208, doi:10.1029/2010PA002037.

Dickens, G.R., 2011. Down the Rabbit Hole: toward appropriate discussion of methane release from gas hydrate systems during the Paleocene-Eocene thermal maximum and other past hyperthermal events. Climate of the Past, 7, 831-846.

D'haenens, S., Bornemann, A., Stassen, P., Spejer, R.P., 2012. Multiple early Eocene benthic foraminiferal assemblage and $\delta^{13}C$ fluctuations at DSDP Site 401 (Bay of Biscay–NE Atlantic). Marine Micropaleontology, 88–89, 15–35.

Diester-Haass, L., 1995. Middle Eocene to early Oligocene paleoceanography of the Antarctic Ocean (Maud Rise, ODP Leg 113, Site 689): change from a low to a high productivity ocean. Palaeogeography, Palaeoclimatology, Palaeoecology, 113, 311-334.

Diester-Haass, L., Robert, C., Chamley, H., 1998. Paleoproductivity and climate variations during sapropel deposition in the eastern Mediterranean sea. In: Robertson, A.H.F., Emeis, K.-C., Richter, C., and Camerlenghi, A. (Eds.), Proceedings of the Ocean Drilling Program, Scientific Results 160, 227-248.

Dore, J.E., Letelier, R.M., Church, M.J., Lukas, R., Karl, D.M., 2008. Summer phytoplankton blooms in the oligotrophic North Pacific Subtropical gyre: historical perspective and recent observations. Progress in oceanography, 76, 2-38.

Douglas, A.E., 2003. Coral bleaching – how and why? Marine Pollution Bulletin, 46, 385–392.

Edgar, K.M., Sexton, P., Norris, R., Wilson, P., Gibbs, S., 2007a. Evolutionary response of planktic foraminifera to a pronounced global warming event 40 Myr ago. Eos Transaction AGU, 88(52), Fall Meeting Suppl., Abstract OS14A-03.

Edgar, K.M., Wilson, P.A., Sexton, P.F., Suganuma, Y., 2007b. No extreme bipolar glaciation during the main Eocene calcite compensation shift. Nature, 448, 908–911.

Edgar, K.M., Wilson, P.A., Sexton, P.F., Gibbs, S.J., Roberts, A.P., Norris, R.D., 2010. New biostratigraphic, magnetostratigraphic and isotopic insights into the Middle Eocene Climatic Optimum in low latitudes. Palaeogeography, Palaeoclimatology, Palaeoecology, 297, 670-682.

Edgar, K.M., Bohaty, S.M., Gibbs, S.J., Sexton, P.F., Norris, R.D., Wilson, P.A., 2012. Symbiont 'bleaching' in planktic foraminifera during the Middle Eocene Climatic Optimum. Geology, 41, 15-18.

Ezard, T.H., Aze, T., Pearson, P.N., Purvis A., 2011. Interplay between changing climate and species' ecology drives macroevolutionary dynamics. Science, 332, 349-351.

Falkowski, P.G., Katz, M.E., Knoll, A.H., Quigg, A., Raven, J.A., Schofield, O., Taylor, F.J.R., 2004. The Evolution of Modern Eukaryotic Phytoplankton. Science, 305, 354-360

Fenero, R., Thomas, E., Alegret, L., Molina, E., 2010. Evolución paleoambiental del tránsito Eoceno-Oligoceno en el Atlántico sur (Sondeo 1263) basada en foraminíferos bentónicos. Geogaceta, 49, 2010.

Fietz, S., Martínez-Garcia, A., Huguet, C., Rueda, G., Rosell-Melé, A., 2011. Constraints in the application of the Branched and Isoprenoid Tetraether index as a terrestrial input proxy. Journal of Geophysical Research, 116, doi: 10.1029/2011JC007062.

Finkel, Z.V., Katz, M.E., Wright, J.D., Schofield, O.M.E., Falkowski, P.G., 2005. Climatically driven macroevolutionary patterns in the size of marine diatoms over the Cenozoic. Proceedings of the National Academy of Sciences, 102-25, 8927-8932.

Fontanier, C., Jorissen, F.J., Licari, L., Alexandre, A., Anschutz, P., Carbonel, P., 2002. Live benthic foraminiferal faunas from the Bay of Biscay: faunal density, composition, and microhabitats. Deep-Sea Research I, 49, 751-785.

Fontanier, C., Jorissen, F.J., Chaillou, G., Anschutz, P., Grémare, A., Griveaud, C., 2005. Live foraminiferal faunas from a 2800 m deep lower canyon station from the Bay of Biscay: faunal response to focusing of refractory organic matter. Deep-Sea Research I, 52, 1189-1227.

Fornaciari, E., Agnini, C., Catanzariti, R., Rio, D., Bolla, E.M., Valvasoni, E., 2010. Mid-Latitude calcareous nannofossil biostratigraphy and biochronology across the middle to late Eocene transition. Stratigraphy, 7-4, 229-264.

Foster L.C., Schmidt D.N., Thomas E., Arndt S., Ridgwell A., 2013. Surviving rapid climate change in the deep sea during the Paleogene hyperthermals. Proceedings of the National Academy of Sciences, doi/10.1073/pnas.1300579110.

Friedrich O., 2009. Benthic foraminifera and their role to decipher paleoenvironment during mid-Cretaceous Oceanic Anoxic Events the “anoxic benthic foraminifera paradox”. Revue de Micropaléontologie, 177, 2-18.

Friedrich, O., Nishi, H., Pross J., Schmiedel G., Hemleben C., 2005. Millennial-to centennial scale interruptions of the Oceanic Anoxic Event 1b (early Albian, mid Cretaceous) inferred from benthic foraminiferal repopulation events. Palaios, 20, 64-77.

Galeotti, S., Krishnan, S., Pagani, M., Lanci, L., Gaudio, A., Zachos, J. C., Monechi S., Morelli, G., Lourens, L., 2010. Orbital chronology of Early Eocene hyperthermals from the Contessa Road section, central Italy. Earth Planetary Science and Letters, 290, 192-200.

Giusberti, L., Coccioni, R., Sprovieri, M., Tateo, F., 2009. Perturbation at the sea floor during the Paleocene-Eocene Thermal Maximum: Evidence from benthic foraminifera at Contessa Road, Italy. Marine Micropaleontology, 70, 102-119.

Gooday, A.J., 1993. Deep-sea benthic foraminiferal species which exploit phytodetritus: Characteristic features and controls on distribution: Marine Micropaleontology, 22, 187–205.

Gooday, A.J., 1996. Epifaunal and shallow infaunal foraminiferal communities at three abyssal NE Atlantic sites subject to differing phytodetritus input regimes. Deep-Sea Research I, 43, 1395-1421.

Gooday, A.J., 2003. Benthic foraminifera (Protista) as tools in deepwater palaeoceanography: environmental influences on faunal characteristics. Advances in Biology, 46, 1– 90.

Gooday, A.J., Rathburn, A.E., 1999. Temporal variability in living deep-sea benthic foraminifera. Earth-Science Reviews, 46, 187–212.

Gooday, A.J., Hughes, J.A., 2002. Foraminifera associated with phytodetritus deposits at a bathyal site in the northern Rockall Trough (NE Atlantic): seasonal contrasts and a comparison of stained and dead assemblages. Marine Micropaleontology, 46, 83-110.

Gooday, A.J., Levin, L.A., Linke, P., Heeger, T., 1992, The role of benthic foraminifera in deep-sea food webs and carbon cycling. In: Rowe, G.T., and Pariente, V., (Eds.). Deep-sea food chains and the global carbon cycle. Dordrecht, Kluwer Academic Publishers, 63–91.

Gooday, A.J., Bett, B.J., Shires, R., Lambshead, P.J.D., 1998, Deep-sea benthic foraminiferal diversity in the NE Atlantic and NW Arabian Sea: A synthesis. Deep-Sea Research Part II, Topical Studies in Oceanography, 45, 165–201.

Green, M.A., Aller, R.C., Aller, J.Y., 1993. Carbonate dissolution and temporal abundances of Foraminifera in Long Island Sound sediments. Limnology and Oceanography, 38(2), 33l-345.

Grünig, A., 1984. Phenotypic variation in Spiroplectammina, Uvigerina and Bolivina. Benthos 1983, Second Symposium on Benthic Foraminifera (Pau, April 1983), 249-255.

Grünig, A., 1985. Systematical description of Eocene foraminifera of Possagno (Northern Italy), Sansoain (Northern Spain) and Biarritz (Aquitaine, France). Memorie di Scienze Geologiche, 37, 251-302.

Grünig, A., Herb, R., 1980. Paleoecology of late Eocene benthonic foraminifera from Possagno (Treviso-Northern Italy). Cushman Foundation Special Publication, 18, 68-85.

Gupta, A.K., Thomas, E., 2003. Initiation of Northern Hemisphere glaciation and strengthening of the northeast Indian monsoon: Ocean Drilling Program Site 758, eastern equatorial Indian Ocean. Geology, 31, 47-50.

Hagn, H., 1956. Geologische und Paläontologische untersuchungen im Tertiär des Monte Brione und seiner umgebung (Gardasee, Ober-Italien). Palaentographica Abt. A, 107, 67-210.

Hayward, B.W., Kawagata, S., Sabaa, A.T., Grenfell, H.R., van Kerckhoven, L., Johnson, K., Thomas, E., 2012, The Last Global Extinction (Mid-Pleistocene) of Deep-Sea Benthic Foraminifera (Chrysalogoniidae, Ellipsoidinidae, Glandulonodosariidae, Plectofrondiculariidae, Pleurostomellidae, Stilostomellidae), their Late Cretaceous-Cenozoic History and Taxonomy. Cushman Foundation for Foraminiferal Research, Spec. Vol., 43, 408 pp.

Hammer, Ø., Harper, D.A.T., Ryan, P.D., 2001. PAST: Paleontological Statistics Software Package for Education and Data Analysis. Palaeontologia Electronica, 4(1), 9 pp., http://palaeoelectronica.org/2001_1/past/issue1_01.htm.

Hancock, H.J.L., Dickens, G.R., 2005. Carbonate dissolution episodes in Paleocene and Eocene sediment, Shatsky Rise, west-central Pacific. In: Bralower, T.J., Premoli Silva, I., Malone, M.J. (Eds.), Proc. ODP, Sci. Results, vol. 198. Available from World Wide Web: http://www-odp.tamu.edu/publications/198_SR/116/116.htm.

Henson, S.A., Sanders, R., Madsen, E., Morris, P.J., Le Moigne, F., Quartly, G.D., 2011. A reduced estimate of the strength of the ocean's biological carbon pump. Geophysical Research Letters, 38, L04606.

Herguera, J.C., Berger, W.H., 1991. Paleoproductivity from benthic foraminiferal abundance: Glacial to postglacial changes in the west equatorial Pacific. Geology, 19, 1173–1176.

Hoenisch, B., Ridgwell, A., Schmidt, D. N., Thomas, E., Gibbs, S. J., Sluijs, A., Zeebe, R., Kump, L., Martindale, R. C., Greene, S. E., Kiessling, W., Ries, J., Zachos, J. C., Royer, D. L., Barker, S., Marchitto T. M. Jr., Moyer, R., Pelejero, C., Ziveri, P., Foster, G. L., Williams, B., 2012. The Geological Record of Ocean Acidification. Science, 335, 1058-1063.

Holbourn, A., Henderson, A.S., MacLeod, N., 2013. Atlas of benthic foraminifera. Willey-Blackwell, 642 pp.

Holland, M.M., Bitz, C.M., 2003. Polar amplification of climate change in coupled models. Climate Dynamics, 21, 221–232.

Hollis, C.J., Taylor, K.W.R., Handley, L., Pancost, R.D., Huber, M., Creech, J.B., Hines, B.R., Crouch, E.M., Morgans, H.E.G., Crampton, J.S., Gibbs, S., Pearson, P.N., Zachos, J.C., 2012. Early Paleogene temperature history of the Southwest Pacific Ocean: Reconciling proxies and models. Earth and Planetary Science and Letters, 349–350, 53–66.

Hopmans, E.C., Weijers, J.W.H., Schefuss, E., Herfort, L., Sinninghe Damsté, J.S., Schouten, S., 2004. A novel proxy for terrestrial organic matter in sediments based on branched and isoprenoidal tetraether lipids. Earth and Planetary Science Letters, 224, 107-116.

Huber, M., Thomas, E., 2008. Paleoceanography: Greenhouse Climates. In: Encyclopedia of Ocean Sciences, J.H. Steele, S.A. Thorpe and K.K. Turekian, (Eds.), 2nd edition, (Elsevier), p. 4229-4239, doi: 10.1016/B978-012374473-9.00701.3

Huber, M., Sloan, L., Shellito, C., 2003. Early Paleogene oceans and climate: A fully coupled modeling approach using the NCAR CCSM. In: Wing, S.L., Gingerich, P.D., Schmitz, B., and Thomas, E., (Eds.). Causes and Consequences of Globally Warm Climates in the Early Paleogene. Boulder, Colorado, Geological Society of America Special Paper, 369, 25-47.

Huguet, C., Kim, J.H., de Lange, G.J., Sinninghe Damsté, J.S., Schouten, S., 2009. Effects of long term oxic degradation on the U-37(K'), TEX_{86} and BIT organic proxies. Organic Geochemistry, 40, 1188–1194.

IPCC, Climate Change (2001) The scientific basis. Contribution of Working Group 1 to the Third Assessment Report of the Intergovernmental Panel on Climate Change. In: Houghton, J.T., Ding, Y., Griggs, D.J., Noguer, M., van der Linden, P.J., Dai, X., Maskell, K., Johnson, C.A. (Eds.). Cambridge University Press, Cambridge, UK, pp. 881.

Ivany, L.C., Lohmann, K.C., Hasiuk, F., Blake, D.B., Glass, A., Aronson, R.B., Moody R.M., 2008. Eocene climate record of a high southern latitude continental shelf: Seymour Island, Antarctica. Geological Society of America Bulletin, 120, 659–678.

Jiang, S., Wise Jr., S.W., Wang, Y., 2007. Cause of the middle/late Miocene carbonate crash: dissolution or low productivity? In: Teagle, D.A.H., Wilson, D.S., Acton, G.D., and Vanko, D.A., (Eds.). Proceedings of the Ocean Drilling Program, Scientific Results, 206. Ocean Drilling Program, College Station, TX, 1–24.

Jones, R.W., Charnock, M.A., 1985. “Morphogroups” of agglutinated foraminifera. Their life positions and feeding habits and potential applicability in (paleo)ecological studies. Revue de Paléobiologie, 4, 311–320.

Jorissen, F.J., 1999. Benthic foraminiferal successions across late Quaternary Mediterranean sapropels. In: Rohling E.J. (Ed.), Fifth decade of Mediterranean paleoclimate and sapropel studies. Marine Geology, 153, 91-101.

Jorissen, F.J., De Stigter, H.C., Widmark, J.G.V., 1995. A conceptual model explaining benthic foraminiferal microhabitats. Marine Micropaleontology, 26, 3–15.

Jorissen, F.J., Fontanier, C., Thomas, E., 2007. Paleoceanographical proxies based on deep-sea benthic foraminiferal assemblage characteristics. In: Hillaire-Marcel, C., and de Vernal, A., (Eds.), Developments in Marine Geology. Proxies in Late Cenozoic paleoceanography, vol. 1 Elsevier, Amsterdam, pp. 264-325.

Jovane, L., Florindo, F., Coccioni, R., Dinare's-Turell, J., Marsili, A., Monechi, S., Roberts, A.P., Sprovieri, M., 2007. The middle Eocene climatic optimum event in the Contessa Highway section, Umbrian Apennines, Italy. Geological Society of American Bulletin, 119, 413–427.

Jovane, L., Savian, J.F.,Coccioni, R., Frontalini, F., Bancalà, G., Catanzariti, R., Luciani, V., Bonhaty, S.M., Wilson, P.A., Florindo, F., 2013. Integrated magnetobiostratigraphy of the middle Eocene-lower Oligocene interval from the Monte Cagnero section, central Italy. Geolgical Society of London Special Publication, 373, http://dx.doi.org/10.1144/SP373.13.

Kaiho K., 1991. Global changes of Paleogene aerobic/anaerobic benthic foraminifera and deep-sea circulation. Palaeogeography, Palaeoclimatology, Palaeoecology 83 (1-3), 65-85.

Kaminski, M.A. 1984. Shape variation in Spiroplectammina spectabilis (Grzybowski). Acta Palaeontologica Polonica 29, 29-49.

Kaminski, M.A., Gradstein, F.M., 2005. Atlas of Paleogene Cosmopolitan Deep-water Agglutinated Foraminifera. Gryzbowski Foundation Special Publication, 10, pp. 547 + pp. vii.

Katz, M., Thunell, R., 1984. Benthic foraminiferal biofacies associated with middle Miocene to early Pliocene oxygen-deficient conditions in the eastern Mediterranean. Journal of Foraminiferal Research, 14 (3), 187-202.

Katz, E.M., Miller, K.J., 1989. Oligocene to Miocene benthic foraminiferal and abyssal circulation changes in the North Atlantic. Micropaleontology, 33, 97-149.

Katz, M.E., Tjalsma, R.C., Miller, K.G., 2003. Oligocene bathyal to abyssal benthic foraminifera of the Atlantic Ocean. Micropaleontology, 49 (2), 1–45.

Katz, M. E., Katz, D.R., Wright, J.D., Miller K.G., Pak, D.K., Shackleton, N.J., Thomas, E., 2003. Early Cenozoic benthic foraminiferal isotopes: Species reliability and interspecies correction factors. Paleoceanography, 18, doi:10.1029/2002PA00079.

Katz, M.E., Finkel, Z.V., Grzebyk, D., Knoll, A.H., Falkowski, P.G., 2004. Evolutionary trajectories and biogeochemical impacts of marine eukaryotic phytoplankton: Annual Reviews of Ecological and Evolutionary Systematics, 35, 523–526.

Katz M.E., Miller K.G., Wright J.D., Wade B.S., Browning J.V., Cramer B.S., Rosenthal Y., 2008. Stepwise transition from the Eocene greenhouse to the Oligocene icehouse. Nature Geosciences, 1, 329-334.

Kim, J.H., Meer, J.v.d., Schouten, S., Helmke, P., Willmott, V., Sangiorgi, F., Koç, N., Hopmans, E.C., Sinninghe Damsté, S., 2010. New indices and calibrations derived from the distribution of crenarchaeal isoprenoid tetraether lipids: Implications for past sea surface temperature reconstructions. Geochimica et Cosmochimica Acta, 74, 4639-4654.

Kitazato, H., Ohga, T., 1995. Seasonal changes in deep-sea benthic foraminiferal populations: results of long-term observations at Sagami Bay, Japan. In: Sakai, H., Nozaki, Y. (Eds.), Biogeochemical Processes and Ocean Flux Studies in the Western Pacific. Terra Scientific, Tokyo, 331-342.

Klaas, C., Archer, D.E., 2002, Association of sinking organic matter with various types of mineral ballast in the deep sea; implications for the rain ratio. Global Biogeochemical Cycles, 16, 1116, doi: 10.1029/ 2001GB001765.

Klevenz, V., Vance, D., Schmidt, D.N., Mezger, K., 2008. Neodymium isotopes in benthic foraminifera: Core-top systematics and a down-core record from the Neogene south Atlantic. Earth and Planetary Science Letters, 265, 571-587.

Koutsoukos, E.A.M., Leary, P.M., Hart, M.B., 1990. Latest Cenomanian–earliest Turonian low-oxygen tolerant benthonic foraminifera: a case study from the Sergipe Basin (N.E. Brazil) and the western Anglo-Paris Basin (southern England). Palaeogeography, Palaeoclimatology, Palaeoecology, 77, 145–177.

Kozdon, R., Kelly, D.C., Kita, N.T., Fournelle, J.H., Valley, J.W., 2011. Planktonic foraminiferal oxygen isotope analysis by ion microprobe technique suggests warm tropical sea surface temperatures during the Early Paleogene. Paleoceanography, 26, PA3206, doi:10.1029/2010PA002056.

Kuhnt, W., Wiedmann, J., 1995. Cenomanian-Turonian source rocks: Paleobiogeographic and paleoenvironmental aspects. In: Huc, A.Y. (Ed.), Paleogeography, paleoclimate and source rocks. American Association of Petroleum Geologists, Studies in Geology, 213–232.

Kumar, A., Perlwirz, J., Eischeid, J., Quan, X., Xu, T., Zhang, T., Hoerling, M., Jha, B., Wang, W., 2010. Contribution of sea ice loss to Arctic amplification. Geophysical Research Letters, 37, L21701, doi:10.1029/2010GL045022.

Kump, L.R., Arthur, M.A., 1999. Interpreting carbon-isotope excursions: Carbonates and organic matter. Chemical Geology, 161, 181–198.

Lear, C.H., Rosenthal, Y., Coxall, H.K., Wilson, P.A., 2004. Late Eocene to early Miocene ice sheet dynamics and the global carbon cycle. Paleoceanography, 19, PA4015, doi:10.1029/2004PA001039.

Lear, C.H., Bailey, T.R., Pearson, P.N., Coxall, H.K., Rosenthal, Y., 2008. Cooling and ice growth across the Eocene-Oligocene transition. Geology, 36 (3), 251–254.

Levin, L.A., Etter, R.J., Rex, M.A., Gooday, A.J., Smith, C.R., Pineda, J., Stuart, C.T., Hessler, R.R., Pawson, D., 2001. Environmental Influences on Regional Deep-Sea species diversity. Annual Review of Ecology and Systematics, 132, 51-93.

Levitus, S., Antonov, J., Boyer, T.P., 1994. Interannual variability of temperature at a depth of 125 m in the North Atlantic Ocean. Science, 266, 96–99.

Lirer, F., 2000. A new technique for retrieving calcareous microfossils from lithified lime deposits, Micropaleontology, 46, 365–369.

Liu, Z., Pagani, M., Zinniker, D., DeConto, R., Huber, M., Brinkhuis, H., Shah, S.R., Leckie, R.M., Pearson, A., 2009. Global cooling during the Eocene-Oligocene climate transition. Science, 323, 1187-1190.

Loeblich, A.R., Tappan, H., 1987. Foraminiferal genera and their classification, vol. 2. Van Nostrand Reinhold Company, New York, 1182 pp.

Lohmann, G.P., 1992. Increasing seasonal upwelling in the subtropical South Atlantic over the past 700,000 yrs: Evidence from deep-living planktonic foraminifera. Marine Micropaleontology, 19, 1-12.

Lopez-Urrutia, A., San Martin, E., Harris, R.P., Irigoien, X., 2006. Scaling the metabolic balance of the oceans. Proceedings of the National Academy of Science of the United States of America, 103, 8739–8744.

Loubere, P., 1991. Deep sea benthic foraminiferal assemblage response to a surface ocean productivity gradient: a test. Paleoceanography, 6, 193-204.

Loubere, P., 1996. The surface ocean productivity and bottom water oxygen signals in deep water benthic foraminiferal assemblages. Marine Micropaleontology, 28, 247-261.

Loubere, P., 1997. Benthic foraminiferal assemblage formation, organic carbon flux and oxygen concentrations on the outer continental shelf and slope. Journal of Foraminiferal Research, 27, 93–100.

Loubere, P., Fariduddin, M., 1999a. Quantitative estimation of global patterns of surface ocean biological productivity and its seasonal variation on timescales from centuries to millennia. Global Biogeochemical Cycles, 13, 115–133, doi: 10.1029/1998GB900001.

Loubere, P., Fariduddin, M., 1999b. Benthic foraminifera and the flux of organic carbon to the seabed. In: Sen Gupta, B.K., (Ed.), Modern foraminifera. Kluwer, Dordrecht, 181-199.

Lourens, L.J., Sluijs, A., Kroon, D., Zachos, J.C., Thomas, E., R□hl, U., Bowles, J., Raffi, I., 2005. Astronomical pacing of late Palaeocene to early Eocene global warming events. Nature, 435, 1083–1087.

Luciani, V., Giusberti, L., Agnini, C., Fornaciari, E., Rio, D., Spofforth, D.J.A., Pälike, H., 2010. Ecological and evolutionary response of Tethyan planktonic foraminifera to the middle Eocene climatic optimum (MECO) from the Alano section (NE Italy). Palaeogeography, Palaeoclimatology, Palaeoecology, 292, 82–95. doi:10.1016/j.palaeo.2010.03.029.

Lunt, D., Ridgwell, A., Sluijs, A., Zachos, J., Hunter, S., Haywood, A., 2011. A model for orbital pacing of methane hydrate destabilization during the Palaeogene. Nature Geosciences, 4, 775-778.

Lutze, G.F., Coulbourn, W.T., 1984. Recent benthic foraminifera from the continental margin of Northwest Africa; community structure and distribution. Marine Micropaleontology, 8, 361– 40.

Lyle, M., Lyle Olivarez, A., Backman, J., Tripati, A., 2005. Biogenic sedimentation in the Eocene equatorial Pacific — the stuttering greenhouse and Eocene carbonate compensation depth. In: Lyle, M., and Firth, (Eds.). Proceedings of the Ocean Drilling Program, Scientific results, 199, 1-35. Ocean Drilling Program, College Station, TX.

Lyle, M., Barron, J., Bralower, T.J., Huber, M., Olivarez Lyle, A., Ravelo, A.C., Rea, D.K, Wilson, P.A., 2008. Pacific Ocean and Cenozoic evolution of climate. Review of Geophysics, 46, RG2002.

Mackensen, A., Schmiedl, G., Harloff, J., Giese, M., 1995. Deep-sea foraminifera in the South Atlantic Ocean: Ecology and assemblage generation. Micropaleontology, 41, 342-358.

Mancin, N., Hayward, B.W., Trattenero, I., Cobianchi, M., Lupi, C., 2013. Can the morphology of deep-sea benthic foraminifera reveal what caused their extinction during the mid-Pleistocene Climate Transition? Marine Micropaleontology, 104, 53-70.

Marcott, S.A., Shakun, J.D., Clark, P.U., Mix, A.C., 2013. A Reconstruction of Regional and Global Temperature for the Past 11,300 Years. Science, 339, 1198-1201.

Martini, E., 1971, Standard Tertiary and Quaternary calcareous nannoplankton zonation. In: Farinacci, A. (Ed.), Proceedings of the 2nd Planktonic Conference, 2, Ed. Tecnoscienza, Roma, pp. 739–785.

Mathelin J.C. and Sztràkos K., 1993. L'Eocène de Biarritz (Pyrénées Atlantiques, SW France). Stratigraphie et paléoenvironment. Monographie des foraminifères. Cahiers de Micropaléontologie 8 (1/2), 5-182.

McCarren, H., Thomas, E., Hasegawa, T., R□hl, U., Zachos, J.C., 2008. Depth-dependency of the Paleocene-Eocene Carbon Isotope Excursion: paired benthic and terrestrial biomarker records (ODP Leg 208, Walvis Ridge). Geochemistry, Geophysics, Geosystem, 9, Q10008, doi: 10.1029/2008GC002116.

McGillicuddy, Jr. D.J., Anderson, L.A., Bates, N.R., Bibby, T., Buesseler, K.O., et al., 2007. Eddy/Wind Interactions Stimulate Extraordinary Mid-Ocean Plankton Blooms. Science, 316, 10121-1025.

McInerney, F.A., Wing S.L., 2011. The Paleocene-Eocene thermal maximum: a perturbation of carbon cycle, climate, and biosphere with implications for the future. Annual Review of Earth and Planetary Sciences, 39, 489–516.

Miller, C.B., Wheeler, P.A., 2012. Biological Oceanography, second edition. Willey-Blackwell, 464 pp.

Miller, K.G., Fairbanks, R.G., Mountain, G.S., 1987. Tertiary oxygen isotope synthesis, sea level history, and continental margin erosion. Paleoceanography, 2 (1), 1–19.

Miller, K. G., Wright, J. D., and Browning, J. V, 2005. Visions of ice sheets in a greenhouse world. Marine geology, 217, 215-231.

Moebius, I., Friedrich, O., Edgar, K.M., Scher, H.D., Sexton, P., 2013. Bottom water changes in the subtropical North Atlantic and the Southern Ocean associated to the Middle Eocene Climatic Optimum. AGU 2013 Fall Meeting Abstract (Control ID: 1805987), San Francisico 9-13 December 2013.

Moore, T.C., Rabinowitz, P.D., Borella, P.E., Shackleton, N.J., Boersma A., 1984. History of the Walvis Ridge. In: Moore, Jr. T.C., and Rabinowitz, P.D., (Eds.). Initial Reports of the Deep Sea Drilling Project, Washington, (U.S. Government Printing Office), 74, pp. 873-894.

Morigi, C., 2009. Benthic environmental changes in the Eastern Mediterranean Sea during sapropel S5 deposition. Palaeogeography, Palaeoclimatology, Palaeoecology, 273, 258–271.

Morigi, C., Jorissen, F.J., Gervais, A., Guichard, S., Borsetti, A.M., 2001. Benthic foraminiferal faunas in surface sediments off NWAfrica: relationship with organic flux to the ocean floor. Journal of Foraminiferal Research, 31, 350–368.

Muren, U., Berglund, J., Samuelsson, K., Andersson, A., 2005. Potential effects of elevated sea-water temperature on pelagic food webs. Hydrobiologia, 545, 153–166.

Murray, J.W., 2001. The niche of benthic foraminifera, critical thresholds and proxies. Marine Micropaleontology, 41, 1-7.

Murray, J.W., 2006. Ecology and applications of benthic foraminifera. Cambridge University Press, pp. 426 + pp. xi.

Murray, J.W., 2013. Living benthic foraminifera: biogeographic distributions and the significance of rare morphospecies. Journal of Micropalaeontology, 32, 1-58.

Nees, S., Altenbach, A.V., Kassens, H., Thiede, J., 1997. High resolution record of foraminiferal response to late Quaternary sea ice retreat in the Norwegian Greenland Sea. Geology 25, 659-662.

O'Connor, M., Piehler, M.F., Leech, D.M., Anton, A., Bruno, J.F., 2009. Warming and resource availability shift food web structure and metabolism. Plos Biology, 7-8, 1-6.

Ohkushi, K., Thomas, E., Kawahata, H., 2000. Abyssal benthic foraminifera from the northwestern Pacific (Shatsky Rise) during the last 298 kyr. Marine Micropaleontology, 38, 119–147.

Okada, H., Bukry, D., 1980. Supplementary modification and introduction of code numbers to the low-latitude coccolith biostratigraphic zonation (Bukry, 1973; 1975). Marine Micropaleontology, 5, 321–325.

Ortiz, S., and Thomas, E., 2012. Deep-sea turnover during the Ypresian-Lutetian transition, the inception of the Cenozoic global cooling trend. 34th IGC World Congress, Brisbane, Australia, 5-10 August 2012.

Olivarez Lyle, A., Lyle, M.W., 2006. Missing organic carbon in Eocene marine sediments: Is metabolism the biological feedback that maintains end-member climates? Paleoceanography, 21, PA2007, doi:10.1029/2005PA001230.

Ortiz, S., Thomas, E., 2006. Lower-middle Eocene benthic foraminifera from the Fortuna Section (Betic Cordillera, south-eastern Spain). Micropaleontology, 52 (2), 97-150.

Ortiz, S., Gonzalvo, C., Molina, E., Rodriguez-Tovar, F. J., Uchman, A., Vandenberghe, N., and Zeelmaekers, E., 2008. Palaeoenvironmental turnover across the Ypresian-Lutetian transition at the Agost section, Southeastern SpainL in search of a marker event to define the stratotype for the base of the Lutetian Stage. Marine Micropaleontology, 69, 297-313.

Pagani, M., Zachos, J.C., Freeman, K.H., Tipple, B., Bohaty S., 2005. Marked decline in atmospheric carbon dioxide concentrations during the Paleogene. Science, 309, 600–603.

Pagani, M., Liu, Z., LaRiviere, J., Ravelo, A.C., 2010. High Earth-system climate sensitivity determined from Pliocene carbon dioxide concentrations. Nature Geosciences, 3, 27-30.

Pagani, M., Pedentchouk, N., Huber, M., Sluijs, A., Schouten, S., Brinkhuis, H., Sinninghe Damsté, J.S., Dickens, G.R., and the Expedition 302 Scientists, 2006. Arctic hydrology during global warming at the Palaeocene/Eocene thermal maximum. Nature, 442, 671-675.

Pälike, H., Lyle, M.W, Nishi, H., Raffi, I., et al., 2012. A Cenozoic record of the equatorial Pacific carbonate compensation depth. Nature, 488, 609-615.

Parisi, G., Coccioni, R., 1988. Deep-water benthic foraminifera at the Eocene-Oligocene boundary in the Massignano section (Ancona, Italy). International Subcommission on Paleogene Stratigraphy, E/O Meeting (Ancona, October 1987) Special Publication II 3, pp. 97-109.

Passow, U., Carlson, C.A., 2012. The biological pump in a high CO_2 world. Marine Ecology Progress Series, 470, 249-271.

Paytan, A., Averyt, K., Faul, K., Gray, E., Thomas, E., 2007. Barite accumulation, ocean productivity, and Sr/Ba in barite across the Paleocene-Eocene Thermal Maximum. Geology, 35, 1139–1142.

Pawlowski, J., Holzmann, M., 2008. Diversity and geographic distribution of benthic foraminifera: a molecular perspective. Biodiversity and Conservation, 17, 317-328.

Pawlowski, J., Bowser, S.B., Gooday, A.J., 2007. A note on the genetic similarity between shallow- and deep-water *Epistominella vitrea* (Foraminifera) in the Antarctic. Deep Sea Research Part II: Topical Studies in Oceanography, 54, 1720-1726.

Pea, L., 2011. Eocene-Oligocene paleoceanography of the subantarctic South Atlantic: Calcareous Nannofossil reconstructions of temperature, nutrient, and dissolution history. Ph.D. thesis, pp. 205, Dottorato di Ricerca in Scienze della Terra XXIII° Ciclo, Università degli Studi di Parma (Italy).

Pearson, A., Ingalls, A.E., 2013. Assessing the Use of Archaeal Lipids as Marine Environmental Proxies. Annual Review of Earth and Planetary Sciences, 41, 359–384.

Pearson, P.N., Palmer, M.R., 2000. Atmospheric carbon dioxide concentrations over the past 60 million years. Nature, 406, 695–699.

Pearson, P.N., Shackleton, N.J., Hall, M.A., 1993. Stable isotope paleoecology of Middle Eocene planktonic foraminifera and multi-species isotope stratigraphy, DSDP Site 523, South Atlantic. Journal of Foraminiferal Research, 23, 123-140.

Pearson, P.N., Olsson, R.K., Hemblen, C., Huber, B.T., Berggren, W.A., 2006. Atlas of Eocene Planktonic Foraminifera. Cushman Special Publication, 41, 513 pp.

Pearson, P.N., Ditchfield, P.W., Singano, J., Harcourt-Brown, K.G., Nicholas, C.J., Olsson, R.K., Shackleton, N.J., Hallk, M.A., 2001. Warm tropical sea surface temperatures in the Late Cretaceous and Eocene epochs. Nature, 413, 481-488.

Pearson, P.N., van Dongen, B.E., Nicholas, C.J., Pancost, R.D., Schouten, S., Singano, J.M., Wade, B.S., 2007. Stable warm tropical climate through the Eocene Epoch. Geology, 35, 211-214.

Pearson, P.N., Nicholas, C.J., Singano, J.M., Bown, P.R., Coxal, H.K., van Dongen, B.E., Huber, B.T., Karega, A., Lees, J.A., Misaky, E., Pancost, R.D., Pearson, M., Roberts, A.P., 2004. Paleogene and Cretaceous sediment cores from the Kilwa and Lindi areas of coastal Tanzania. Tanzania Drilling Project Sites 1-5 . Journal of African Earth Sciences, 39, 25-62.

Peterson, L.C., Backman, J., 1990. Late Cenozoic carbonate accumulation and the history of the carbonate compensation depth in the western equatorial Indian Ocean. Proceedings of the Ocean Drilling Program Scientific Results, 115, 467– 507.

Phleger, F.B., Soutar, A., 1973. Production of benthic foraminifera in three east Pacific oxygen minima. Micropaleontology, 19, 110–115.

Pierrehumbert, R. T., 2002. The hydrologic cycle in deep-time climate problems. Nature, 419, 191-198.

Poore, R.Z., Brabb, E.E., 1977. Eocene and Oligocene planktonic foraminifera from the Upper Butano Sandstone and type San Lorenzo Formation, Santa Cruz Mountains, California. Journal of Foraminiferal Research, 7, 249-272.

Postuma, J.A, 1971. Manual of Planktonic Foraminifera, 422 pp.
Premoli Silva, I., Wade ,B., Pearson, P.N., 2006. Taxonomy, biostratigraphy, and phylogeny of *Globigerinatheka* and *Orbulinoides*. In: Pearson, P.N., Olsson, R.K., Huber, B.T., Hemleben, C., and Berggren W.A., (Eds). Atlas of Eocene planktonic foramifera. Cushman Foundation Special Publication, 41, p. 169-212.

Protodecima, F., Bolli, H.M., 1978. South East Atlantic DSDP Leg 40 Paleogene benthic foraminifers. In: Bolli, H.M., Ryan, W.B.F., et al., 1978. Initial Reports of the Deep Sea Drilling Project, vol. XL, Washington (U.S. Government Printing Office).

Richardson, A.J., Schoeman, D.S., 2004. Climate impacts on plankton ecosystems in the Northeast Atlantic. Science, 305, 1609–1613.

Ridgwell, A., Schmidt, D.N., 2010. Past constraints on the vulnerability of marine calcifiers to massive carbon dioxide release. Nature Geosciences, 3, 196-200.

Robert, C., Kennett, J.P., 1997. Antarctic continental weathering changes during Eocene/Oligocene cryosphere expansion: clay mineral and oxygen isotope expansion. Geology, 25, 587.

Sarmiento, J.L., Slater, R., Barber, R., Bopp, L., Doney, S.C., Hirst, A.C., Kleypas, J., Matear, R., Mikolajewicz, U., Monfray, P., Soldatov, V., Spall, S.A., Stouffe, R., 2004. Response of ocean ecosystems to climate warming. Global Biogeochemical Cycles, 18, GB3003.

Savian, J.F., Jovane, L., Trindade, R.I.F., Frontalini, F., Coccioni, R., Bohaty, S.M., Wilson, P.A., Florindo, F., Roberts, A., 2013. Middle Eocene Climatic Optimum (MECO) in the Monte Cagnero Section, Central Italy. Latinmag Letters, 3, Special Issue, PC02, 1-8. Proceedings Montevideo, Uruguay.

Shackleton, N.J., 1974. Attainment of isotopic equilibrium between ocean water and the benthonic foraminifera genus *Uvigerina*: Isotopic changes in the ocean during the last glacial, in Les Méthodes Quantitatives D'étude des Variations du Climat au Cours du Pléistocéne, Colloques internationaux Centre national de la recherche scientifique, 219, 203–209.

Schmiedl, G., Mackensen, A., Müller, P.J., 1997. Recent benthic foraminifera from the eastern South Atlantic Ocean. Dependence on food supply and water masses. Marine Micropaleontology, 32, 249-287

Schmiedl, G., Mitschele, A., Beck, S., Emeis, K.C., Hemleben, C., Schulz, H., Sperling, M., Weldeab, S., 2003. Benthic foraminiferal record of ecosystem variability in the eastern Mediterranean Sea during times of sapropel S5 and S6 deposition. Palaeogeography, Palaeoclimatology, Palaeoecology, 190,139-164.

Schouten, S., Hopmans, E.C., Schefuss, E., Sinninghe Damsté, J.S., 2002. Distributional variations in marine crenarchaeotal membrane lipids: a new tool for reconstructing ancient sea water temperatures? Earth and Planetary Science Letters, 204, 265-274.

Schouten, S., Hopmans, E.C., Rosell-Melé, A., Pearson, A., Adam, P., Bauersachs, T., Bard, E., Bernasconi, S.M., Bianchi, T.S., Brocks, J.J., et al., in press. An interlaboratory study of TEX_{86} and BIT analysis of sediments, extracts, and standard mixtures. Geochemistry, Geophysics, Geosystems, doi: 10.1002/2013GC004904.

Schrag, D.P., Depaolo, D.J., Richter, F.M., 1995. Reconstructing past sea surface temperatures: Correcting for diagenesis of bulk marine carbonate. Geochimica and Cosmochimica Acta, 59, 2265–2278.

Schroeder, C. J., Scott, D.B., Medioli, F.S., 1987. Can smaller benthic foraminifera be ignored in paleoenvironmental analyses? Journal of Foraminiferal Research, 17, 101-105.

Sen Gupta, B.K., Machain-Castillo, M.L., 1993. Benthic foraminifera in oxygen-poor habitats. Marine Micropaleontology, 20, 3-4.

Sexton, P.F., Wilson, P.A., Norris, R.D., 2006. Testing the Cenozoic multisite composite δ18O and δ13C curves: new monospecific Eocene records from a single locality, Demerara Rise (Ocean Drilling Program Leg 207). Paleoceanography, 21 (2), PA2019.

Sexton, P.F., Wilson, P.A., Pearson, P.N., 2006. Microstructural and geochemical perspectives on planktic foraminiferal preservation: ''Glassy'' versus ''Frosty''. Geochemistry, Geophysics, Geosystems, 7, Q12P19, doi:10.1029/2006GC001291.

Silva, K.A., Corliss, B.H., Rathburn, A.E., Thunell, R.C., 1996. Seasonality of living benthic foraminifera from the San Pedro basin, California borderland. Journal of Foraminiferal Research, 26, 71-93.

Singh, R.K., Gupta, A.K., 2010. Deep-sea benthic foraminiferal changes in the eastern Indian Ocean (ODP Hole 757B): Their links to deep Indonesian (Pacific) flow and high latitude glaciation during the Neogene. Episodes, 33-2, 73-82.

Slotnick, B.S., Dickens, G.R., Nicolo, M.J., Hollis, C.J., Crampton, J.S., Zachos, J.C., Sluijs, A., 2012. Large-Amplitude Variations in Carbon Cycling and Terrestrial Weathering during the Latest Paleocene and Earliest Eocene: The Record at Mead Stream, New Zealand. The Journal of Geology, 120, 487–505.

Sluijs, A., Bowen, G.J., Brinkhuis, H., Lourens, L.J., Thomas, E., 2007. The Paleocene-Eocene Thermal Maximum super greenhouse: biotic and geochemical signatures, age models and mechanisms of global change. In: Williams, M., Haywood, A.M., Gregory, F.J., Schmidt, D.N. (Eds.). Deep-Time Perspectives on Climate Change: Marrying the Signal from Computer Models and Biological Proxies. The Micropaleontological Society, Special Publication, pp. 323-349.

Sluijs, A., Zeebe, R.E., Bijl, P.K., Bohaty, S.M., 2013. A middle Eocene carbon cycle conundrum. Nature Geosciences, doi: 10.1038/NGEO1807.

Solomon, S., Qin, D., Manning, M., Marquis, M., Averyt, K., Tignor, M.M.B., LeRoy Miller, H., Jr., Chenet, Z., IPCC Climate Change 2007: The Physical Science Basis (Cambridge Univ. Press, 2007).

Smart, C.W., Thomas, E., Ramsay, A. T. S., 2007. Middle-late Miocene benthic foraminifera in a western equatorial Indian Ocean depth transect: Paleoceanographic implications. Palaeogeography, Palaoeclimatology, Palaeoecology 247, 402-420

Smart, C.W., King, S.C., Gooday, A., Murray, J.W., Thomas, E., 1994. A benthic foraminiferal proxy of pulsed organic matter paleofluxes. Marine Micropaleontology, 23, 89–99.

Smith R.W., Bianchi T.S., Li X., 2012. A re-evaluation of the use of branched GDGTs as terrestrial biomarkers: Implications for the BIT Index. Geochimica et Cosmochimica Acta, 80, 14–29.

Spofforth, D.J.A., Agnini, C., Pälike, H., Rio, D., Fornaciari, E., Giusberti, L., Luciani, V., Lanci, L., Muttoni, G., 2010. Organic carbon burial following the Middle Eocene Climatic Optimum (MECO) in the central-western Tethys. Paleoceanography, 25, PA3210.

Sprong, J., Kouwenhoven, T.J, Bornemann, A., Schulte, P., Stassen, P., Steurbaut, E., Youssef, M., Speijer, R.P., 2012. Characterization of the Latest Danian Event by means of benthic foraminiferal assemblages along a depth transect at the southern Tethyan margin (Nile Basin, Egypt). Marine Micropaleontology, 86–87, 15–31.

Stap, L., Lourens, L.J., Thomas, E., Sluijs, A., Bohaty, S., Zachos, J.C., 2009. High-resolution deep-sea carbon and oxygen isotope records of Eocene Thermal Maximum 2 and H2. Geology, 38, 208–210.

Stap, L., Lourens, L., van Dijk, A., Schouten, S., Thomas, E., 2010. Coherent pattern and timing of the carbon isotope excursion and warming during Eocene Thermal Maximum 2 as recorded in

planktic and benthic foraminifera. Geochemistry, Geophysics, Geosystems, 11, Q11011, doi:10.1029/2010GC003097.

Stap, L., Lourens, L. J., Thomas, E., Sluijs, A., Bohaty, S., Zachos, J. C., 2010. High-resolution deep-sea carbon and oxygen isotope records of Eocene Thermal Maximum 2 and H2. Geology, 38, 208-210.

Stassen, P., Thomas, E., Speijer, R.P., 2012. The progression of environmental changes during the onset of the Paleocene-Eocene thermal maximum (New Jersey Coastal Plain). Austrian Journal of Earth Sciences, 105/1, 154-160.

Stickley, C. E., St John, K., Koc, N., Jordan, R. W., Passchier, S., Pearce, R. B., and Learns, L. E., 2009. Evidence for middle Eocene Arctic sea ice from diatoms and ice-rafted debris. Nature, 460, 376-379

Stoll, H.M., 2005. Limited range of interspecific vital effects in coccolith stable isotopic records during the Paleocene-Eocene thermal maximum. Paleoceanography, 20, PA1007, doi:10.1029/2004PA001046.

Suhr, S.B., Pond, D.W., Gooday, A.J., Smith, C.R., 2003. Selective feeding by benthic foraminifera on phytodetritus on the western Antarctic peninsula: evidence from fatty biomarker analysis. Marine Ecology progress series 262, 153-162.

Sun, X., Corliss, B.H., Brown, C.W., Showers, W.J., 2006. The effect of primary productivity and seasonality on the distribution of deep-sea benthic foraminifera in the North Atlantic. Deep-Sea Research I, 53: 28-47

Stainforth, R.M., Lamb, J.L., Luterbacher, H.P., Beard, J.H, Jeffords, R.M. 1975. Cenozoic planktonic foraminiferal zonation and characteristics of index forms. Paleontological Contributions Article, 62, 425 pp.

Takeda, K., Kaiho, K., 2007. Faunal turnovers in central Pacific benthic foraminifera during the Paleocene–Eocene thermal maximum. Palaeogeography, Palaeoclimatology, Palaeoecology, 251, 175–197.

Takata, H., Nomura, R., Tsujimoto, A., Khim, B., Chung, I., 2013. Abyssal benthic foraminifera in the eastern equatorial Pacific (IODP exp 320) during the Middle Eocene. Journal of Paleontology, 87-6, 1160–1185.

Thomas, D.J., Via, R.K., 2007. Neogene evolution of Atlantic thermohaline circulation: Perspective from Walvis Ridge, southeastern Atlantic Ocean. Paleoceanography, 22, PA2212, doi:10.1029/2006PA001297.

Thomas, E., 1985. Late Eocene to Recent deep-sea benthic foraminifers from the central equatorial Pacific Ocean. In: Mayer, L., Theyer, F., et al., (Eds.). Initial Reports of the Deep Sea Drilling Project , Washington (U.S. Government Printing Office), 85, pp. 655 – 694.

Thomas, E., 1990. Late Cretaceous through Neogene deep-sea benthic foraminifers (Maud Rise, Weddell Sea, Antarctica): Proceedings of the Ocean Drilling Program, Scientific results, Volume 113: College Station, Texas, Ocean Drilling Program, 571–594.

Thomas, E., 1998. The biogeography of the late Paleocene benthic foraminiferal extinction, in Aubry, M.P., Lucas, S.G., and Berggren, W.A., (Eds.). Late Paleocene-early Eocene biotic and climatic events in the marine and terrestrial records. New York, Columbia University Press, pp. 214–243.

Thomas, E., 2003. Extinction and food at the seafloor: A high-resolution benthic foraminiferal record across the Initial Eocene Thermal Maximum, Southern Ocean Site 690. In: Wing, S.L., Gingerich, P.D., Schmitz, B., and Thomas, E., (Eds.). Causes and Consequences of Globally Warm Climates in the Early Paleogene. Boulder, Colorado, Geological Society of America Special Paper, 369, 319–332.

Thomas, E., 2007. Cenozoic mass extinctions in the deep sea: What perturbs the largest habitat on Earth? In: Monechi, S., Coccioni, R., and Rampino, M.R., (Eds.). Large Ecosystem Perturbations: Causes and Consequences. Geological Society of America Special Paper, 424, 1–23.

Thomas, E., 2008. Research Focus: Descent into the Icehouse, Geology, 36: 191-192.

Thomas, E., Gooday, A.J., 1996. Cenozoic deep-sea benthic foraminifers: Tracers for changes in oceanic productivity? Geology, 24, 355-358.

Thomas, E., Zachos, J.C., 2000. Was the late Paleocene thermal maximum a unique event? GFF, 122, 169-170.

Thomas, E., Booth, L., Maslin, M., Shackleton, N.J., 1995. Northeastern Atlantic benthic foraminifera during the last 45,000 years: changes in productivity seen from the bottom up. Paleoceanography, 10, 545–562, http://dx.doi.org/10.1029/94PA03056.

Thompson, J., Cook, G.T., Anderson, R., MacKenzie, A.B., Harkness, D.D., McCave, I.N., 1995. Radiocarbon age offsets in different-sized carbonate components of deep-sea sediments. Radiocarbon, 37, 91–101.

Tjalsma, R.C., Lohmann, G.P., 1983. Paleocene–Eocene bathyal and abyssal benthic foraminifera from the Atlantic Ocean. Micropaleontology, Special Publication, 4, 1–90.

Toffanin, F., Agnini, C., Fornaciari, E., Rio, D., Giusberti, L., Luciani, V., Spofforth, D.J.A., Pälike, H., 2011. Changes in calcareous nannofossil assemblages during the Middle Eocene Climatic Optimum: clues from the central-western Tethys (Alano section, NE Italy). Marine Micropaleontology, 81, 22–31.

Toffanin, F., Agnini, C., Rio, D., Acton, G., Westerhold, T., 2013. Middle Eocene to early Oligocene calcareous nannofossil biostratigraphy at IODP Site U1333 (equatorial Pacific). Micropaleontology, 59-1, 69-82.

Trevisani, E., 1997. Stratigrafia sequenziale e paleogeografia del margine orientale del Lessini Shelf durante l'Eocene superiore (Prealpi Venete, provincie di Vicenza e Treviso). Studi Trentini di Scienze Naturali, Acta Geologica 71 (1994), 145–168.

Tripati, A., Backman, J., Elderfield, H., Ferretti, P., 2005. Eocene bipolar glaciations associated with global carbon cycle changes. Nature, 436, 341–346.

Turich, C., Freeman, K.H., Bruns, M.A., Conte, M., Jones, A.D., Wakeham, S.G., 2007. Lipids of marine Archaea: Patterns and provenance in the water-column and sediments. Geochimica et Cosmochimica Acta, 71, 3272–3291.

Valiela, I., 1984. Marine Ecological Process. Springer, New York, 546 p.

Van der Zwaan, G.J., Jorissen, F.J., de Stigter, H.C., 1990. The depth dependency of planktonic/benthic foraminiferal ratios: constraints and applications. Marine Geology, 95, 1-16.

Van der Zwaan, G.J., Duijnstee I.A.P., Den Dulk M., Ernst S.R., Kouwenhoven, N.T., 1999. Benthic foraminifers: proxies or problems? A review of paleoecological concepts. Earth Sciences Reviews, 46, 213-236.

Van Morkhoven, F.P.C.M., Berggren, W.A., Edwards, A.S., 1986. Cenozoic Cosmopolitan deep-sea benthic foraminifera. Bullettin des Centres de Recherches Exploration-Production Elf-Aquitane, Mèmoire, 11, 11–421.

Via, R.K., Thomas, D.J., 2006. Evolution of Atlantic thermohaline circulation–Early Oligocene onset of deep-water production in the North Atlantic. Geology, 34, 441–444.

Villa, G., Fioroni, C., Pea, L., Bohaty, S.M., Persico, D., 2008. Middle Eocene–late Oligocene climate variability: Calcareous nannofossil response at Kerguelen Plateau, Site 748. Marine Micropaleontology, 69, 173 – 192.

Wade B.S., 2004. Planktonic foraminiferal biostratigraphy and mechanisms in the extinction of *Morozovella* in the late middle Eocene. Marine Micropaleontology, 51, 23–38.

Wade, B.S., Kroon, D., 2002. Middle Eocene regional climate instability: Evidence from the western North Atlantic. Geology, 30, 1011–1014.

Watanabe, S., 1989. New genus and five new species in order foraminiferida. Revista Española de Micropaleontologìa, XXI-2, 265-272.

Weijers, J.W.H., Schouten S., Spaargaren, O.C., Sinninghe Damsté, J.S., 2006. Occurrence and distribution of tetraether membrane lipids in soils: implications for the use of the TEX_{86} proxy and the BIT index. Organic Geochemistry, 37, 1680–1693.

Westerhold, T., R□hl, U., 2013. Orbital pacing of Eocene climate during the Middle Eocene Climate Optimum and the chron C19r event–missing link found in the tropical western Atlantic. Geochemistry, Geophysics, Geosystems, 14, 4811-4825.

Winguth, A.M.E., Thomas, E., Winguth, C., 2012. Global decline in ocean ventilation, oxygenation, and productivity during the Paleocene-Eocene Thermal Maximum: Implications for the benthic extinction. Geology, 40, 263–266.

Winterer, E.L., Bosellini, A., 1981. Subsidence and sedimentation on Jurassic passive continental margin, Southern Alps, Italy. American Association of Petroleum Geologists Bulletin, 65, 394–421.

Witkowski, J., Bohaty, S.M., McCartney, K., Harwood, D.M., 2012. Enhanced siliceous plankton productivity in response to middle Eocene warming at Southern Ocean ODP Sites 748 and 749. Palaeogeography, Palaeoclimatology, Palaeoecology, 326–328, 78–94.

Witkowski J., Bohaty S.M., Edgar K.M., Harwood D.M., in press. Rapid fluctuations in mid-latitude siliceous plankton production during the Middle Eocene Climatic Optimum (ODP Site 1051, western North Atlantic). Marine Micropaleontolgy, in press.

Zachos, J.C., Stott, L.D., Lohmann, K.C., 1994. Evolution of early Cenozoic marine temperatures. Paleoceanography, 9, 353-387.

Zachos, J.C., Quinn, T.M., Salamy, K.A. 1996. High resolution (104 years) deep sea foraminiferal stable isotope records of the Eocene-Oligocene climate transition. Paleoceanography, 11 (3), 251–266.

Zachos, J.C., Dickens, G.R., Zeebe, R.E., 2008. An early Cenozoic perspective on greenhouse warming and carbon-cycle dynamics. Nature, 451, 279–283.

Zachos, J.C., McCarren, H.K., Murphy, B., Röhl, U., Westerhold, T., 2010. Tempo and scale of late Paleocene and early Eocene carbon isotope cycles: implications for the origin of hyperthermals. Earth and Planetary Science Letters, 299, 242–249.

Zachos, J.C., Pagani, M., Sloan, L.C., Thomas, E., Billups, K., 2001. Trends, rhythms, and aberrations in global climate 65 Ma to present. Science, 292, 686–693.

Zachos, J.C., Opdyke, B.N., Quinn, T.M., Jones, C.E., Halliday, A.N., 1999. Early cenozoic glaciation, antarctic weathering, and seawater $^{87}Sr/^{86}Sr$: is there a link? Chemical Geology, 161, 165–180

Zachos, J.C., Röhl, U., Schellenberg, S.A., Sluijs, A., Hodell, D.A., Kelly, D.C., Thomas, E., Nicolo, M., Raffi, I., Lourens, L.J., McCarren, H., Kroon, D., 2005. Rapid acidification of the ocean during the Paleocene–Eocene Thermal Maximum. Science, 308, 1611–1615.

Zachos, J.C., Kroon, D., Blum, P., et al., 2004. Proceedings of the Ocean Drilling Program, Initial Reports, 208. Ocean Drilling Program, College Station, TX, pp. 1–112.

Zeebe, R.E., Zachos, J.C., 2013. Long-term legacy of massive carbon input to the Earth system: Anthropocene vs. Eocene. Philosophic Transactions of the Royal Society of London A, 10.1098/rsta.2012.0006.

Zhang, Y., Pagani, M., Liu, Z., Bohaty, S.M., DeConto, R., 2013. A 40-million-year history of atmospheric CO_2. Philosophic Transactions of the Royal Society of London A, 0.1098/rsta.2013.0096.

APPENDICES

Appendix 2. Census data of benthic foramifera in the ≥63 ≤450 µm size fraction.

SAMPLES	THICKNESS (Cm)	*Ammobaculites agglutinans*	*Ammodiscus glabratus*	*Ammodiscus peruvianus*	*Ammodiscus* spp.	*Ammomarginulina aubertae*	*Ammosphaeroidina pseudopauciloculata*	*Arenobulimina* sp.	*Bathysiphon* spp.	*Bigenerina* spp.	*Clavulina* spp.	*Cylindroclavulina eocaena*	*Cylindroclavulina* spp.	Juvenile clavulinids	*Conotrochammina* cf. *wangaia*	*?Conotrochammina* sp.	*Dorothia* spp.	Juvenile *Dorothia* spp.	*Eobigenerina variabilis*	Eobigenerinid large-sized specimen	*Glomospira charoides*	*Glomospira* spp.	*Glomospirella* sp.	*Haplophragmoides walteri*
COL1000	1000	0	0	0	0	0	0	0	2	0	0	0	0	0	0	0	0	0	2	0	0	2	0	0
COL40A	1080	0	0	0	0	0	0	0	1	0	0	1	0	0	0	0	0	0	1	0	0	0	0	1
COL80A	1120	0	0	0	0	0	0	0	1	0	0	0	0	0	0	0	0	0	3	0	2	0	0	0
COL160A	1200	0	1	0	0	0	0	0	3	0	0	1	0	0	0	0	0	0	2	0	0	0	0	0
COL240A	1280	0	0	0	3	0	0	0	3	0	0	0	0	0	0	0	0	0	2	0	1	1	0	0
COL280A	1320	0	0	1	1	2	0	0	7	2	0	0	0	0	0	0	0	1	5	0	0	2	0	0
COL320A	1360	0	0	0	0	0	0	0	3	3	0	0	0	0	0	0	0	0	6	0	1	1	0	0
COL360A	1400	0	0	0	0	0	0	0	11	1	0	0	0	0	0	0	0	0	5	0	1	2	0	0
COL400A	1440	0	0	0	0	0	0	0	2	0	0	0	0	0	0	0	0	1	0	0	1	0	0	0
COL440A	1480	0	0	1	0	0	0	0	11	3	0	0	0	0	0	0	0	0	6	0	1	3	0	0
COL480A	1520	0	0	0	1	1	0	0	0	2	0	0	0	0	0	0	0	0	6	0	0	1	0	0
COL520A	1560	0	0	0	0	0	1	0	7	1	0	1	0	0	0	0	0	0	27	0	3	3	0	0
COL560A	1600	0	1	1	0	0	0	1	4	3	0	1	0	0	0	0	0	1	7	0	2	2	0	0
COL600A	1640	0	0	0	0	0	1	0	12	1	0	0	0	0	0	0	0	0	14	0	4	4	0	0
COL620A	1660	0	2	0	0	0	0	1	1	1	0	0	1	0	0	0	0	0	11	0	6	1	0	1
COL640A	1680	0	0	0	0	0	1	0	2	3	0	0	0	0	0	0	0	0	0	0	1	1	0	0
COL10B	1695	0	0	0	0	0	0	1	1	0	0	0	0	0	0	0	1	0	1	0	0	0	0	0
COL40B	1725	0	0	0	0	0	0	0	1	0	0	0	0	0	0	0	0	0	0	1	0	0	0	0
COL113B	1798	0	0	0	0	0	0	1	0	0	2	0	0	0	0	0	0	1	0	0	0	0	0	0
COL140B	1825	0	0	0	0	0	0	0	1	1	0	0	0	0	0	0	0	0	1	0	0	0	0	0
COL180B	1865	0	0	0	0	0	0	0	1	0	0	0	0	0	0	0	0	1	0	0	0	1	0	0
COL245B	1930	0	0	0	0	0	0	0	1	3	0	0	1	0	0	0	1	0	3	0	1	0	0	0
COL305B	1990	0	0	0	0	0	0	0	2	2	0	0	0	0	0	0	0	1	0	0	0	0	0	0
COL365B	2050	0	0	0	1	0	1	0	2	0	0	0	0	1	0	0	0	2	3	0	0	1	0	0
COL405B	2090	0	0	0	0	0	0	0	0	0	0	0	0	0	0	0	0	0	0	0	0	0	0	0
COL470B	2155	0	0	0	1	0	1	1	2	0	7	0	0	1	2	0	2	0	0	0	0	0	0	0
COL550B	2235	0	0	0	0	0	1	0	1	0	0	0	0	0	0	0	0	0	1	0	0	0	0	0
COL610B	2295	0	0	0	0	0	1	0	0	0	1	0	1	0	0	0	0	0	1	0	1	1	0	0
COL690B	2375	0	0	0	0	0	0	0	2	0	0	0	0	0	0	0	0	0	0	0	0	0	0	0
COL750B	2435	0	0	0	1	4	0	0	0	0	0	4	0	0	0	0	0	0	2	0	16	3	1	0
COL825B	2510	0	0	0	0	0	0	0	6	0	2	0	0	0	0	0	0	0	0	0	1	1	0	0
COL865B	2550	1	0	0	1	0	0	0	1	0	0	0	0	0	0	0	0	0	2	0	0	0	0	0
COL945B	2630	0	0	2	0	0	0	0	1	0	1	0	1	0	1	0	0	0	0	0	0	0	0	0
COL1065B	2750	0	0	0	0	0	0	0	1	0	1	0	0	0	0	1	0	0	1	0	1	0	0	0
COL1145B	2830	0	0	0	0	0	0	0	0	0	0	0	0	0	0	0	0	0	3	0	0	0	0	0
COL1265B	2950	0	0	0	0	0	0	0	0	0	0	0	0	0	0	0	0	0	1	0	0	0	0	0
COL1385B	3070	0	0	0	2	0	0	0	2	0	0	0	0	0	0	0	1	0	1	0	1	0	0	1
COL1485B	3170	0	0	0	0	0	0	1	1	0	0	0	0	0	0	0	0	0	3	0	1	1	0	1

Appendix 2. Census data of benthic foramifera in the ≥63 ≤450 µm size fraction.

SAMPLES	THICKNESS (Cm)	*Haplophragmoides* cf. *walteri*	*Haplophragmoides* spp.	*Haplophragmoides* spp. (coarsely agglutinated specimens)	*?Haplophragmoides*	*Hormosina trinitatensis*	*Karrierella chapapotensis*	*Karrierella chapapotensis (sensu Tjalsma & Lohmann, 1983)*	*Karrierella* cf. *cubensis*	*Karrierella hantkeniana*	*Karrierella subglabra*	*Karrierella* spp.	*Karrerulina coniformis*	*Karrerulina conversa*	*Karrerulina horrida*	*Karrerulina* spp.	*Lituotuba lituiformis*	*Marsonella traubi*	*Marsonella* spp.	*Plectina dalmatina*	*Plectina* spp.	*Psammosphera* sp.	Pseudobolivinids	?Pseudobolivinids	*Ramulina* spp.	*Recurvoides anormis*	*Recurvoides* spp.	*Reophax duplex*
COL1000	1000	1	0	1	0	0	0	0	0	0	0	1	1	0	0	0	0	0	0	1	1	0	0	0	0	1	1	0
COL40A	1080	0	0	0	0	0	0	0	0	0	0	0	0	0	2	0	0	0	0	1	0	0	0	0	0	1	1	0
COL80A	1120	0	1	1	0	0	0	0	0	0	0	0	0	0	2	0	0	0	0	0	0	0	0	1	0	0	0	0
COL160A	1200	0	0	0	0	0	0	0	0	0	0	2	0	0	0	0	0	0	0	0	0	0	0	0	0	0	0	0
COL240A	1280	0	2	0	0	0	0	0	1	0	0	0	0	0	1	1	0	0	0	1	0	0	0	0	0	1	2	0
COL280A	1320	0	0	0	0	0	1	1	6	0	2	4	0	0	1	0	0	0	0	3	0	0	0	0	0	0	0	0
COL320A	1360	2	0	0	0	0	0	0	1	0	1	0	2	0	1	0	0	1	0	3	0	0	1	0	0	0	0	0
COL360A	1400	0	0	0	0	0	0	0	1	0	0	1	0	0	0	0	0	0	0	3	0	0	1	0	1	0	0	0
COL400A	1440	0	0	0	0	0	0	0	1	0	0	0	0	0	0	0	0	0	0	0	0	0	0	0	0	0	0	0
COL440A	1480	0	0	0	0	0	2	0	0	0	0	0	0	0	0	0	0	0	0	2	0	0	2	0	0	0	0	0
COL480A	1520	2	0	0	0	0	0	0	0	0	3	0	0	1	4	1	0	1	0	5	0	0	0	1	0	0	0	0
COL520A	1560	0	0	0	0	0	1	0	0	0	3	1	2	0	2	2	0	0	0	7	0	0	0	4	0	0	0	0
COL560A	1600	2	2	0	0	0	0	0	1	0	1	1	0	0	0	0	1	1	0	3	0	0	0	1	0	2	2	0
COL600A	1640	7	1	0	0	0	0	0	0	0	0	0	0	0	5	2	0	0	2	3	0	0	3	3	1	0	5	0
COL620A	1660	0	1	0	0	0	0	0	0	2	0	2	0	0	1	3	0	0	0	0	0	0	0	0	0	0	5	0
COL640A	1680	0	0	0	0	0	0	0	0	0	2	0	0	0	0	0	0	0	0	2	0	0	0	0	0	0	0	0
COL10B	1695	0	0	0	0	0	0	0	0	0	0	0	0	0	0	0	0	0	0	11	7	0	0	0	0	0	0	0
COL40B	1725	0	0	0	0	0	0	0	0	0	0	2	0	0	2	0	0	0	0	2	4	0	0	0	0	0	1	0
COL113B	1798	0	0	0	0	0	0	0	1	0	0	1	0	0	0	0	0	0	0	1	0	0	0	0	0	0	0	0
COL140B	1825	0	1	2	0	0	0	0	0	0	0	0	0	0	0	5	0	0	0	9	4	0	0	0	0	0	1	0
COL180B	1865	0	0	1	0	0	0	0	0	0	0	0	0	1	0	2	0	1	0	4	7	0	0	1	0	0	0	0
COL245B	1930	0	0	1	0	0	0	0	0	0	0	3	0	1	0	1	0	0	0	10	2	0	0	0	0	0	0	0
COL305B	1990	0	0	0	0	0	0	0	2	0	0	0	0	0	0	2	0	0	0	5	0	0	0	0	0	0	1	0
COL365B	2050	0	0	0	0	0	0	0	0	0	0	0	0	0	0	0	0	0	0	1	0	0	0	0	0	0	0	0
COL405B	2090	0	0	1	0	0	0	0	0	0	0	0	0	1	0	0	0	0	0	12	1	0	0	0	0	0	1	0
COL470B	2155	1	0	2	1	0	0	1	2	0	0	1	3	3	1	2	0	1	0	44	7	0	0	0	0	3	0	0
COL550B	2235	0	1	6	1	0	0	0	0	0	0	0	0	0	0	0	0	0	0	8	9	0	0	0	0	0	6	0
COL610B	2295	0	2	0	0	0	0	0	1	0	0	0	0	0	0	0	0	0	0	2	2	0	0	2	0	0	0	0
COL690B	2375	0	2	2	0	0	0	0	0	0	0	0	0	0	0	0	0	1	0	0	0	0	0	0	0	0	0	0
COL750B	2435	0	13	7	0	0	0	0	0	1	0	2	1	0	1	3	2	1	0	6	14	0	0	1	0	0	17	1
COL825B	2510	0	2	2	0	0	0	0	0	0	0	0	0	0	0	0	0	0	0	1	2	0	0	0	0	0	1	0
COL865B	2550	0	0	0	0	0	0	0	0	0	0	0	0	0	0	0	0	0	0	0	0	0	0	0	0	0	0	0
COL945B	2630	0	0	0	0	0	0	0	4	0	0	2	0	0	0	0	0	0	0	1	0	0	0	0	0	0	0	0
COL1065B	2750	0	0	1	0	0	0	0	0	0	0	1	0	0	0	0	0	0	0	0	0	0	0	0	0	0	0	0
COL1145B	2830	0	0	0	0	0	0	0	1	1	0	0	1	0	0	0	0	0	0	0	0	0	0	0	0	0	0	0
COL1265B	2950	0	0	0	0	0	0	0	1	0	0	0	0	0	1	1	0	0	0	0	0	0	0	0	1	0	0	0
COL1385B	3070	1	0	1	0	1	0	0	0	0	0	0	0	0	1	0	0	0	0	0	0	1	0	0	0	0	1	0
COL1485B	3170	0	0	0	0	0	1	0	0	0	0	2	0	0	0	0	0	0	0	1	0	0	0	2	0	0	0	0

Appendix 2. Census data of benthic foramifera in the ≥63 ≤450 µm size fraction.

SAMPLES	THICKNESS (Cm)	Reophacids	*Reticulophragmium* cf. *acutidorsatum*	*Reticulophragmium* spp.	*Saccammina placenta*	*Saccammina grzybowsky*	*Spiroplectammina dalmatina -pectinata* group	*Spiroplectammina navarroana*	*Spiroplectammina spectabilis*	*Spiroplectammina* cf. *spectabilis*	*Spiroplectammina* spp.	*Subreophax* spp.	*Textularia* spp.	*?Textularia*	Textularidae indet.	*Tritaxia szaboi*	*Tritaxia szaboi* juvenile	*Tritaxilina pupa*	*?Trochammina* sp.	Trochamminids	*Trochamminoides* spp.	*Vulvulina haeringensis -eocaena* group	*Vulvulina* spp.	Indeterminate agglutinants	Agglutinat sp. A	Agglutinat sp. B	Agglutinant sp. C	Agglutinant sp. D	Astrorhizida
COL1000	1000	0	0	0	0	0	0	0	0	0	3	2	0	0	0	0	0	0	2	0	0	0	0	4	0	0	0	0	22
COL40A	1080	0	0	0	0	0	0	0	0	0	0	0	0	0	0	0	0	0	0	0	0	0	0	1	0	0	0	0	23
COL80A	1120	0	0	0	0	0	1	0	0	0	0	0	0	0	0	0	0	0	2	0	0	0	0	2	0	0	0	1	18
COL160A	1200	0	0	0	0	0	1	0	0	0	0	0	0	0	0	0	0	0	1	0	0	0	0	1	1	0	0	0	16
COL240A	1280	0	0	0	0	0	0	0	0	0	0	5	0	0	0	0	0	0	2	0	0	2	0	1	1	0	0	1	57
COL280A	1320	8	0	1	0	0	0	0	0	0	0	0	0	0	0	0	1	0	0	0	0	1	0	9	1	0	0	0	121
COL320A	1360	0	0	0	1	0	0	0	0	0	0	0	0	0	0	0	0	0	2	0	0	2	0	5	0	0	0	0	28
COL360A	1400	1	0	0	1	0	0	1	0	0	0	0	0	0	0	0	0	0	2	0	0	3	0	7	3	0	0	0	132
COL400A	1440	0	0	0	0	0	0	0	0	0	1	0	0	0	0	0	0	0	1	0	0	1	0	2	0	0	0	0	13
COL440A	1480	2	0	0	0	0	1	2	0	0	0	0	0	0	0	0	4	0	0	0	0	3	0	7	1	0	0	0	115
COL480A	1520	0	0	0	0	0	0	0	1	0	1	1	0	0	0	0	1	0	7	0	0	0	0	3	2	0	0	0	52
COL520A	1560	5	0	0	0	0	6	0	0	1	0	0	0	1	0	0	3	0	4	0	0	4	0	15	1	0	0	0	221
COL560A	1600	0	0	0	0	0	0	0	0	0	0	1	0	0	0	2	2	0	14	0	0	0	0	11	8	0	0	1	66
COL600A	1640	3	2	0	0	0	0	0	0	0	1	0	0	0	0	1	1	0	4	0	1	0	0	50	1	0	2	0	168
COL620A	1660	0	0	0	0	0	0	0	0	0	0	0	0	0	0	0	0	0	0	1	0	0	0	17	5	0	0	0	57
COL640A	1680	0	0	0	0	0	0	1	0	0	0	0	2	0	0	0	0	0	1	0	0	0	0	5	2	0	0	1	61
COL10B	1695	0	0	0	1	0	0	0	0	0	0	0	0	0	0	0	0	1	2	0	0	2	0	9	0	3	0	0	44
COL40B	1725	0	0	0	0	0	0	1	0	0	0	0	0	0	0	0	1	0	1	0	0	0	0	12	0	1	0	0	45
COL113B	1798	0	0	0	0	0	0	0	0	0	0	0	0	0	0	0	0	0	2	0	0	0	0	3	0	0	0	0	14
COL140B	1825	0	0	1	0	0	0	1	0	0	0	0	0	0	0	0	0	0	1	0	1	0	0	8	2	0	0	0	25
COL180B	1865	0	0	0	0	0	0	0	0	0	0	0	0	0	0	0	0	0	9	0	0	0	0	10	1	0	0	0	21
COL245B	1930	0	0	0	0	0	0	0	0	0	0	0	1	0	0	0	0	0	2	0	0	1	0	3	0	0	0	0	36
COL305B	1990	0	0	0	0	0	0	0	0	0	0	0	0	0	0	0	0	0	8	1	0	0	0	4	0	0	0	0	26
COL365B	2050	1	0	0	0	0	0	0	0	0	0	0	0	0	0	0	0	0	2	0	0	0	0	2	0	0	0	0	28
COL405B	2090	0	0	0	0	0	0	0	0	0	0	0	2	0	0	0	0	0	0	0	0	1	0	9	2	0	0	0	41
COL470B	2155	0	0	0	0	0	0	0	0	0	0	0	0	0	0	0	0	1	10	0	1	1	0	35	0	3	0	0	130
COL550B	2235	0	0	0	0	3	0	0	0	0	0	1	0	0	0	0	0	0	2	0	1	0	0	25	1	3	0	0	85
COL610B	2295	0	0	0	1	0	0	0	0	0	0	2	0	0	0	0	0	0	5	0	0	0	0	10	0	0	0	0	44
COL690B	2375	0	1	0	0	0	0	0	0	0	0	0	0	0	0	0	0	0	0	0	3	1	0	8	0	0	0	0	10
COL750B	2435	0	0	0	2	0	0	0	0	0	0	1	0	0	0	0	0	0	0	0	3	0	0	61	23	0	0	0	479
COL825B	2510	1	1	0	0	0	0	0	0	0	0	0	0	0	0	0	1	0	1	0	0	2	1	17	2	1	0	0	37
COL865B	2550	0	0	0	0	0	0	0	0	0	0	0	0	0	0	0	0	0	7	0	0	1	0	0	0	0	0	0	24
COL945B	2630	0	0	0	0	0	0	0	0	0	0	0	0	0	0	0	0	0	0	0	0	0	0	0	0	0	0	0	20
COL1065B	2750	0	0	0	0	0	0	0	0	0	0	0	0	0	0	0	0	0	1	0	0	0	0	1	0	0	0	0	39
COL1145B	2830	0	0	0	0	0	0	0	0	0	0	0	0	0	0	0	0	0	0	0	0	1	1	1	1	0	0	0	18
COL1265B	2950	0	0	0	0	0	0	0	0	0	0	0	0	0	0	0	1	0	0	0	0	0	0	3	0	0	0	0	23
COL1385B	3070	0	0	0	0	0	0	0	0	0	2	0	0	0	0	0	0	0	0	0	0	1	0	3	1	0	0	0	46
COL1485B	3170	0	0	0	0	0	0	0	0	0	0	0	0	0	0	0	0	0	3	0	0	0	0	0	1	0	0	0	25

Appendix 2. Census data of benthic foraminifera in the ≥63 ≤450 μm size fraction.

SAMPLES	THICKNESS (Cm)	*Allomorphina macrostoma*	*Anomalinoides alazanensis*	*Anomalinoides capitatus*	*?Anomalinoides capitatus* juvenil	*Anomalinoides spissiformis*	*Anomalinoides* spp.	*Angulogerina muralis*	*Angulogerina* sp.	*Aragonia aragonensis*	*Astacolus* spp.	Bagginids	*Bolivina antegressa*	Bolivina spp.	*Bolivinoides crenulata*	*Bulimina alazanensis*	*Bulimina alazanensis* trans. to *B. truncana*	*Bulimina* cf. *alazanensis*	*Bulimina* cf. *elongata* group	*Bulimina midwayensis*	*Bulimina sculptilis*	*Bulimina sculptilis* var. *laciniata*	*Bulimina* cf. *semicostata*	*Bulimina stalacta*	*Bulimina* sp. with thin costae	*Bulimina trinitatensis -impendens* group	*Bulimina tuxpamensis*	*Bulimina* spp.	*Buliminella* spp.
COL1000	1000	0	0	0	0	2	7	1	0	0	1	0	3	21	47	2	0	13	3	3	0	0	0	3	0	1	1	8	5
COL40A	1080	0	0	1	0	0	2	0	1	0	0	0	2	31	56	3	0	9	5	2	0	0	0	1	0	1	1	9	2
COL80A	1120	0	0	0	0	0	5	1	0	1	0	0	4	35	41	0	0	12	9	5	0	0	0	1	0	2	1	11	4
COL160A	1200	0	0	0	2	2	1	0	0	0	0	0	5	36	27	0	0	11	3	0	0	0	0	2	0	2	2	7	4
COL240A	1280	0	0	0	0	2	5	1	0	0	0	0	2	40	56	0	0	8	10	2	0	0	1	3	0	4	4	10	4
COL280A	1320	0	0	1	0	2	6	0	0	0	0	0	31	51	90	3	0	28	14	0	0	0	0	1	0	3	2	12	1
COL320A	1360	0	0	1	1	1	1	1	0	1	0	0	7	18	21	2	0	13	25	12	0	0	0	7	0	1	6	16	5
COL360A	1400	0	0	0	0	1	5	0	0	0	0	0	29	37	50	16	0	19	19	1	0	0	1	9	0	3	6	19	9
COL400A	1440	0	0	0	0	1	3	1	1	0	0	0	7	25	30	0	0	8	13	3	0	0	3	0	0	1	3	17	3
COL440A	1480	0	0	0	1	1	0	3	0	0	0	0	11	22	42	2	0	15	11	5	0	0	2	6	0	4	0	16	9
COL480A	1520	0	0	0	0	0	15	15	0	1	0	0	11	122	49	2	0	14	18	5	1	0	0	1	0	6	1	25	12
COL520A	1560	0	0	1	1	4	12	3	0	1	1	0	29	114	139	10	1	21	27	11	0	0	21	11	1	5	3	10	15
COL560A	1600	0	0	0	1	1	6	0	0	0	0	0	6	51	63	2	0	13	23	7	0	0	10	5	0	7	1	24	0
COL600A	1640	0	0	0	0	2	13	1	0	0	0	0	0	27	5	4	0	15	0	20	0	0	0	2	0	5	1	1	7
COL620A	1660	1	1	0	0	1	7	1	0	0	0	0	2	41	37	1	0	6	5	17	0	1	3	4	0	0	2	9	3
COL640A	1680	0	0	0	1	1	4	0	0	0	0	0	6	23	39	1	0	18	9	3	0	0	0	4	0	1	1	5	1
COL10B	1695	0	0	0	0	0	4	0	0	0	0	0	138	68	37	30	1	2	3	2	4	15	1	0	9	0	0	8	0
COL40B	1725	0	0	0	0	0	2	7	0	0	0	0	34	287	157	22	0	73	0	6	0	8	10	0	4	2	1	12	11
COL113B	1798	0	0	0	0	0	5	1	0	0	0	0	34	37	31	1	0	4	9	1	0	0	2	0	0	4	3	14	5
COL140B	1825	0	0	0	0	0	3	0	0	0	0	0	3	17	7	12	0	0	16	5	0	0	131	0	1	4	12	154	0
COL180B	1865	0	0	0	0	0	0	0	0	0	0	0	10	40	9	18	0	0	0	2	0	1	129	0	2	7	0	57	1
COL245B	1930	0	0	0	0	2	1	0	0	0	0	0	14	60	35	8	0	7	4	2	0	1	1	0	0	9	1	10	8
COL305B	1990	0	0	0	0	2	3	0	0	0	0	0	30	38	56	1	0	7	14	0	0	0	0	0	0	4	1	5	1
COL365B	2050	0	0	1	0	1	5	2	0	0	0	0	15	42	54	0	0	11	2	1	0	0	3	2	0	0	3	8	1
COL405B	2090	0	0	0	0	0	2	0	0	2	0	0	9	21	13	87	0	3	0	0	0	0	1	0	0	7	0	8	1
COL470B	2155	0	0	0	0	0	1	0	0	0	0	0	13	7	4	11	0	2	0	0	0	0	2	0	1	54	0	4	3
COL550B	2235	0	0	0	0	0	0	0	0	0	0	2	155	12	2	11	0	0	0	1	0	0	1	0	0	22	0	2	2
COL610B	2295	0	1	0	0	1	1	0	0	0	0	0	4	21	24	1	0	0	0	0	0	0	1	2	0	3	0	3	4
COL690B	2375	2	0	0	0	0	2	0	0	0	0	0	10	86	6	15	0	0	0	0	1	0	2	0	0	0	0	16	0
COL750B	2435	0	0	0	0	0	4	0	0	0	0	1	459	43	5	5	0	1	0	8	0	10	1	0	0	0	0	25	2
COL825B	2510	0	0	0	0	0	0	0	0	0	0	0	75	13	0	1	0	0	0	3	0	0	0	0	1	0	0	3	1
COL865B	2550	0	0	0	0	0	1	1	0	0	0	0	11	50	43	0	0	3	33	0	0	0	1	1	0	2	0	4	7
COL945B	2630	0	0	0	0	0	1	2	0	0	0	0	3	26	81	0	0	4	60	1	0	0	1	0	0	2	0	18	2
COL1065B	2750	0	0	0	0	1	1	0	0	0	0	0	10	17	77	1	0	3	36	1	0	0	0	0	0	1	0	9	2
COL1145B	2830	0	1	0	0	2	1	2	0	0	1	0	6	46	106	1	0	10	14	1	0	0	3	0	0	2	1	11	10
COL1265B	2950	0	0	0	0	1	2	2	0	0	0	0	1	19	84	1	0	20	9	0	0	0	0	1	0	1	0	10	2
COL1385B	3070	0	0	0	0	6	10	0	1	0	0	0	3	26	113	0	0	4	12	1	0	0	0	0	0	1	0	10	3
COL1485B	3170	0	0	1	0	3	4	2	0	0	0	0	0	38	72	1	0	5	5	1	0	0	0	0	0	1	0	12	2

Appendix 2. Census data of benthic foraminifera in the ≥63 ≤450 µm size fraction.

SAMPLES	THICKNESS (Cm)	Buliminids	?*Cassidulina* cf. *ammosa* + *Cassidulina* spp.	*Caucasina* sp.	*Cibicides* cf. *westi*	*Cibicides westi* var. *arguta*	*Cibicides* spp.	*Cibicidoides barnetti*	*Cibicidoides barnett* i sapropel morphotype	*Cibicidoides cocaenus*	*Cibicidoides grimsdalei*	*Cibicidoides hettneri*	*Cibicidoides mexicanus*	*Cibicidoides micrus*	*Cibicidoides* cf. *r obertsonianus*	*Cibicidoides* cf. *subspiratus*	*Cibicidoides ungerianus*	?*Cibicidoide* s sp. A	?*Cibicidoides* spp.small?	*Cibicidoides* spp.	?*Coryphostoma* spp.	*Ellipsoglandulina* sp.	*Ellipsoidella* sp.	*Epistominella* spp.	*Eponides abatissae* var. *multicameratus*	*Eponides* cf. *abatissae* var. *multicameratus*	*Eponides* spp.	*Fursenkoina* spp.	?*Fursenkoina* spp.	*Globobulimina* spp.
COL1000	1000	2	1	12	0	0	3	2	0	0	0	1	0	1	0	0	0	2	0	1	0	0	0	0	1	0	5	0	1	0
COL40A	1080	1	2	13	0	0	9	1	0	0	2	1	0	0	0	1	1	2	0	2	1	0	0	0	2	0	3	2	0	0
COL80A	1120	0	8	18	0	0	4	0	0	0	0	4	0	2	0	1	0	8	0	5	1	1	0	1	0	4	3	0	1	0
COL160A	1200	5	1	18	0	0	5	0	0	0	5	0	0	0	0	0	0	1	0	0	0	0	0	0	0	0	2	0	0	0
COL240A	1280	0	3	16	0	0	10	2	0	1	4	1	0	2	0	1	1	1	2	1	0	0	0	0	0	0	5	0	0	0
COL280A	1320	0	0	47	1	0	12	0	0	2	2	0	0	0	0	1	0	3	6	10	0	0	0	0	3	0	2	0	1	0
COL320A	1360	1	7	18	0	0	5	1	0	0	0	1	0	2	0	0	0	3	5	7	0	0	0	0	2	1	5	0	0	0
COL360A	1400	0	0	17	0	0	10	2	0	0	5	0	0	3	0	4	0	0	3	1	0	0	0	0	1	1	4	0	2	0
COL400A	1440	3	0	16	0	0	3	1	0	0	2	0	1	2	0	0	0	0	7	1	1	0	0	1	1	0	1	0	1	0
COL440A	1480	0	0	8	0	0	10	2	0	0	5	0	0	5	0	0	1	11	0	9	0	0	0	0	1	2	4	0	0	0
COL480A	1520	4	3	9	0	0	74	3	0	0	6	2	1	2	0	0	1	2	6	11	1	0	0	0	0	1	12	0	0	0
COL520A	1560	0	0	21	0	0	19	9	0	2	16	3	3	12	0	1	1	14	0	11	0	0	1	0	6	8	6	1	1	1
COL560A	1600	3	1	1	0	0	2	13	2	0	10	5	0	6	0	2	0	0	10	8	0	0	0	0	1	0	7	0	0	0
COL600A	1640	1	0	24	0	1	4	8	0	1	5	1	0	5	0	0	1	9	27	0	0	0	0	0	4	2	8	0	0	0
COL620A	1660	4	3	20	0	0	1	3	6	0	12	0	0	15	0	0	0	0	27	13	0	0	0	0	2	2	5	0	0	0
COL640A	1680	1	0	14	0	1	6	0	0	2	6	0	0	1	0	0	0	4	3	0	0	0	0	0	2	1	4	0	0	0
COL10B	1695	4	0	8	0	0	7	0	3	0	0	0	0	2	2	0	0	4	15	0	0	0	0	0	0	1	0	0	1	2
COL40B	1725	3	0	24	0	0	50	0	0	0	0	0	0	5	0	0	0	6	25	0	4	0	0	2	0	0	4	0	0	1
COL113B	1798	3	1	37	2	0	13	0	0	1	3	1	0	7	0	0	0	4	0	13	0	0	0	0	1	2	9	0	0	0
COL140B	1825	1	1	34	0	0	1	0	7	0	0	1	0	2	0	0	0	3	2	0	1	0	0	1	1	1	1	1	0	0
COL180B	1865	1	0	44	0	0	2	0	0	0	0	0	0	6	0	0	0	6	37	0	0	0	0	0	1	0	1	2	0	0
COL245B	1930	7	8	23	0	0	8	4	4	0	9	0	0	5	0	0	0	0	22	0	0	0	0	0	1	0	3	0	0	3
COL305B	1990	3	3	13	0	0	14	2	0	0	2	0	0	2	0	0	0	3	2	12	0	0	0	0	4	3	4	0	0	0
COL365B	2050	2	3	12	0	0	12	2	0	0	3	0	0	2	0	1	0	5	0	4	0	0	0	0	2	0	0	0	0	0
COL405B	2090	3	11	35	0	0	1	1	9	0	0	0	0	8	0	0	0	0	22	2	0	0	0	0	0	0	0	1	0	13
COL470B	2155	11	25	30	0	0	0	13	20	0	2	0	0	12	0	0	0	16	18	2	0	0	0	0	0	0	3	0	1	0
COL550B	2235	1	21	2	0	0	0	4	7	0	1	0	0	6	0	0	0	10	10	0	0	0	0	0	0	0	0	0	0	1
COL610B	2295	8	5	35	0	0	3	2	0	0	0	2	0	9	0	2	1	3	5	7	0	0	0	0	2	0	4	0	0	0
COL690B	2375	1	1	6	0	0	0	0	0	0	0	0	0	2	0	0	0	0	15	0	0	0	0	0	0	0	7	0	0	0
COL750B	2435	15	11	18	0	0	0	0	17	0	1	0	0	5	0	0	0	0	11	4	0	0	0	0	0	0	1	0	0	3
COL825B	2510	2	2	1	0	0	1	0	15	0	1	0	0	5	0	0	0	0	7	0	0	0	0	0	1	0	4	0	0	0
COL865B	2550	0	2	14	0	1	13	0	0	0	1	1	0	2	0	0	0	5	2	1	2	0	0	0	1	1	7	0	0	0
COL945B	2630	2	4	17	0	0	7	1	0	0	4	0	1	1	0	1	0	3	1	1	1	0	0	0	4	1	6	1	0	0
COL1065B	2750	2	2	14	0	0	16	0	0	0	4	0	0	1	0	3	0	5	3	0	0	0	0	1	5	1	9	0	0	0
COL1145B	2830	0	22	38	1	0	40	1	0	0	1	2	0	3	0	3	0	5	10	1	0	0	0	3	2	0	6	0	0	0
COL1265B	2950	2	3	1	0	0	3	1	0	0	1	1	0	1	0	1	1	6	1	2	0	0	0	1	3	1	5	0	1	0
COL1385B	3070	2	5	4	0	0	3	3	0	0	9	3	0	0	0	1	0	4	0	3	0	0	0	0	4	1	2	1	0	0
COL1485B	3170	4	3	2	0	0	19	1	0	0	7	1	0	0	0	0	0	0	3	4	0	0	0	0	0	0	1	0	0	0

Appendix 2. Census data of benthic foramifera in the ≥63 ≤450 μm size fraction.

SAMPLES	THICKNESS (Cm)	*Nonionella* spp.	Nonionids	*?Nuttallides decorata*	*Nuttallides truempyi*	*Nuttallides umbonifera*	*Nuttallides* spp.	*Oridorsalis umbonatus*	*Oridorsalis* spp.	*Osangularia pteromphalia-mexicana group*	*Osangularia pteromphalia-mexicana* group sapropel morphotype	Osangularia cf. plummerae	*Osangularia* spp.	*Paleopolymorphina* sp.	*Parafrondicularia* spp.	*Planularia* spp.	*Planulina* spp.	*Plectofrondicularia* spp.	*Pleurostomella* spp.	Indeterminate pleurostomellids	Polymorphinids	*?Praebulimina* sp.	*Praeglobulimina pupoides*	*Pullenia cretacea*	*Pullenia eocaena*	*Pullenia quinqueloba*	*Pullenia* spp.	*Rectouvigerina mexicana*	*?Rectouvigerina ?mexicana*
COL1000	1000	7	0	9	5	69	5	1	4	7	0	0	0	0	0	0	0	0	8	0	1	0	0	0	0	0	2	0	0
COL40A	1080	2	0	14	3	112	6	1	4	3	0	0	0	0	0	0	0	0	6	0	0	1	0	0	0	0	0	0	0
COL80A	1120	1	0	19	6	90	10	1	2	13	0	0	0	0	0	0	0	0	9	0	2	2	0	0	0	0	2	0	1
COL160A	1200	3	0	9	5	50	3	4	11	10	0	0	5	0	0	0	0	0	3	0	2	0	0	0	0	0	1	0	0
COL240A	1280	3	0	14	10	37	6	2	7	17	0	0	2	0	0	1	0	0	12	0	0	0	0	0	0	0	2	0	0
COL280A	1320	1	0	48	17	44	15	1	8	1	0	2	11	0	0	0	0	0	24	0	9	0	0	0	0	1	2	1	0
COL320A	1360	2	0	12	12	15	18	3	1	10	0	0	8	0	0	0	0	0	8	0	1	0	0	0	0	2	6	1	0
COL360A	1400	2	0	22	11	38	2	2	7	5	0	0	4	0	0	1	0	0	18	0	2	0	0	0	1	1	1	1	2
COL400A	1440	2	0	4	1	34	4	1	5	11	0	0	1	0	0	0	0	0	5	0	0	0	0	0	0	0	1	0	2
COL440A	1480	1	1	12	8	33	11	2	6	6	0	2	11	0	0	0	0	0	10	0	6	1	0	0	0	1	3	0	1
COL480A	1520	2	0	8	13	56	3	3	5	6	0	0	2	0	0	0	1	0	7	0	2	7	0	0	0	0	3	1	2
COL520A	1560	2	0	45	27	34	0	13	13	9	0	0	10	0	0	0	0	0	21	0	3	3	0	0	0	1	3	1	2
COL560A	1600	3	1	16	11	27	13	7	8	13	0	1	5	1	0	0	0	0	17	0	1	0	0	0	0	1	3	0	1
COL600A	1640	2	1	36	13	6	0	1	6	0	0	0	8	0	0	0	0	0	4	0	1	0	0	0	0	0	1	0	0
COL620A	1660	7	0	7	14	11	25	6	2	0	1	0	1	0	0	0	0	0	9	0	0	1	0	0	0	0	1	0	0
COL640A	1680	1	2	18	4	16	2	2	1	7	0	1	5	0	0	0	0	0	9	0	1	0	0	0	0	0	1	1	0
COL10B	1695	1	0	0	5	1	0	58	12	0	0	0	46	0	0	0	0	0	13	1	0	0	2	0	0	0	0	2	3
COL40B	1725	1	1	0	6	7	0	29	17	0	0	0	39	0	0	0	0	0	5	0	0	0	0	0	0	1	1	4	2
COL113B	1798	1	0	1	15	126	0	5	10	0	0	0	3	0	0	0	0	0	6	0	0	0	0	0	1	0	1	1	2
COL140B	1825	1	0	0	4	11	0	13	11	3	0	0	19	0	0	0	0	0	1	0	0	0	3	0	0	0	0	0	0
COL180B	1865	0	0	0	1	3	0	43	15	0	0	0	16	0	0	0	0	0	3	0	1	0	9	0	0	0	2	3	2
COL245B	1930	1	0	4	2	15	2	14	8	0	0	0	0	0	0	0	0	0	8	0	0	0	0	0	0	0	1	2	2
COL305B	1990	2	0	8	17	167	3	4	9	2	0	0	1	0	0	1	0	0	6	0	5	0	0	1	0	4	0	0	0
COL365B	2050	3	0	8	3	148	2	0	1	1	0	0	1	0	0	0	0	0	8	0	1	0	0	0	1	0	0	0	0
COL405B	2090	1	0	0	13	6	0	38	12	0	0	0	14	0	0	0	0	0	0	0	0	0	20	0	0	0	7	3	0
COL470B	2155	0	0	3	13	4	7	30	33	1	0	1	27	0	0	0	0	0	4	0	1	0	0	0	0	1	1	1	5
COL550B	2235	0	0	0	7	2	1	36	22	0	1	0	11	0	0	0	0	0	1	0	0	0	1	0	0	0	0	7	6
COL610B	2295	1	0	15	7	24	5	17	10	1	1	0	13	0	0	0	0	0	5	3	0	0	0	0	1	1	1	2	1
COL690B	2375	2	0	0	8	6	12	2	9	0	0	0	52	0	0	0	0	0	2	0	0	0	12	0	0	0	0	4	2
COL750B	2435	2	0	0	39	8	1	127	19	2	14	0	6	0	0	0	0	0	2	0	0	0	13	0	0	0	5	18	0
COL825B	2510	0	0	0	6	8	1	37	27	0	0	0	28	0	0	0	0	0	1	0	0	0	3	0	0	0	1	1	4
COL865B	2550	5	0	19	6	335	3	2	6	0	0	1	1	0	0	0	0	0	2	1	3	0	0	0	0	0	1	1	0
COL945B	2630	1	0	20	11	135	0	3	10	1	0	0	0	0	0	0	0	0	4	0	0	0	0	0	0	0	0	1	0
COL1065B	2750	2	0	14	16	289	0	4	8	1	0	0	2	0	1	0	0	0	2	0	4	0	0	0	0	1	3	0	0
COL1145B	2830	2	0	19	20	287	0	5	20	2	0	0	2	0	0	0	0	1	3	0	1	0	0	0	0	1	2	0	1
COL1265B	2950	9	0	11	7	473	0	4	9	1	0	0	0	0	0	0	0	0	5	0	0	0	0	0	1	1	1	0	0
COL1385B	3070	6	0	18	30	256	7	8	1	2	0	0	0	0	0	0	0	0	5	0	1	2	0	0	0	1	5	0	1
COL1485B	3170	0	0	10	10	152	11	3	6	5	0	0	1	0	0	0	0	0	11	0	3	1	0	0	0	0	2	0	1

Appendix 2. Census data of benthic foraminifera in the ≥63 ≤450 µm size fraction.

SAMPLES	THICKNESS (Cm)	*?Rectouvigerina* sp.	*?Sporobulimmella* sp.	*Saracenaria* spp.	*Siphogenerinoides* cf. *eleganta*	*Siphonella* sp.	*Spiroloculina* sp.A	STH	Stilostomellids	*Tappanina selmensis*	*Trifarina* sp.A	*Trifarina* sp.B	*Trifarina* sp.C	*Turrilina* sp.	Unilocular hyalineous	Uniserial hyalineous	*Uvigerina chirana*	*Uvigerina farinosa*	*Uvigerina gracilis*	*Uvigerina* cf. *hourcqi*	*Uvigerina* sp.A	*Uvigerina* sp.B	*Uvigerina* sp.C	*Uvigerina* spp. with costae	*Uvigerina* spp.	*?Uvigerina*	Small indeterminated uvigerinids	*Valvulineria filiaeprincipis*	*Valvulineria wiltpuyti*	*Valvulineria* spp.	Valvulinerids	TOTAL	N/g > 63 um
COL1000	1000	0	0	1	0	0	0	0	5	0	1	0	0	0	2	16	0	2	2	0	0	0	0	0	0	0	1	0	0	0	1	319	371,41
COL40A	1080	0	0	0	0	1	0	0	1	0	0	0	0	0	2	15	0	3	1	0	0	0	0	0	0	0	1	0	0	0	0	310	348,98
COL80A	1120	0	0	4	0	0	0	0	3	0	0	0	0	0	2	11	0	4	5	0	1	0	0	3	1	0	0	0	0	0	0	366	439,11
COL160A	1200		0	1	0	1	0	0	2	0	0	0	0	0	7	10	0	9	2	0	0	0	0	0	0	0	0	0	0	0	0	285	340,30
COL240A	1280	0	0	0	0	0	2	2	1	0	1	2	0	0	4	14	6	6	6	0	0	0	0	0	0	0	0	0	0	0	0	453	252,90
COL280A	1320	9	0	0	0	14	4	45	7	0	7	0	0	0	7	24	0	33	0	0	0	0	0	0	0	0	9	0	0	0	0	877	454,75
COL320A	1360	0	0	0	0	2	0	0	2	0	6	4	0	0	2	13	0	13	5	0	0	0	0	4	0	0	0	0	0	0	0	480	282,33
COL360A	1400	2	0	0	0	5	2	19	8	0	4	0	0	0	2	23	0	24	0	0	0	0	0	0	0	0	2	0	0	0	0	691	341,85
COL400A	1440	0	0	2	0	3	0	0	2	0	1	0	1	0	1	16	2	11	4	0	0	0	0	0	0	0	0	0	0	0	0	287	392,16
COL440A	1480	0	0	0	0	17	0	15	4	0	3	2	0	0	2	21	0	43	0	0	0	0	0	1	4	0	0	1	0	0	0	607	302,45
COL480A	1520	0	0	1	0	10	1	0	4	0	4	1	0	0	5	25	0	22	7	0	0	0	0	12	0	0	0	0	0	0	0	758	868,25
COL520A	1560	0	0	2	0	3	7	22	11	0	5	0	1	0	7	43	0	36	16	0	0	0	0	0	0	0	0	1	0	0	0	1294	713,93
COL560A	1600	0	0	0	1	2	0	0	1	0	5	3	1	0	1	9	0	8	5	0	0	0	0	0	0	0	0	0	0	0	0	639	356,63
COL600A	1640	0	0	0	0	0	2	23	1	0	0	0	3	0	1	20	0	0	3	0	0	0	0	0	0	0	0	0	0	0	0	712	101,56
COL620A	1660	0	0	3	0	3	3	9	0	0	3	0	7	0	1	36	0	5	0	0	0	0	0	0	1	0	0	2	0	1	0	617	83,65
COL640A	1680	0	0	0	0	2	0	6	4	0	1	0	0	0	1	18	0	4	3	0	0	0	0	0	0	0	0	0	0	0	0	388	229,09
COL10B	1695	0	0	1	1	0	1	52	20	0	0	0	0	0	0	49	82	0	0	0	17	21	5	11	17	5	0	0	0	0	0	1045	353,93
COL40B	1725	0	0	0	0	0	0	44	10	1	5	0	0	0	2	55	9	6	5	0	0	2	1	8	2	0	0	0	0	0	0	1246	788,23
COL113B	1798	0	0	0	0	0	2	21	1	0	0	0	0	0	3	14	0	1	2	0	0	0	0	1	0	0	0	0	0	0	0	457	546,62
COL140B	1825	0	0	0	0	0	0	16	2	0	0	0	0	0	1	33	27	0	0	0	0	0	2	18	3	0	0	3	3	0	0	746	442,38
COL180B	1865	0	0	0	0	0	1	18	7	1	0	0	0	0	0	24	5	0	0	0	0	0	0	3	0	0	0	6	0	0	0	714	444,04
COL245B	1930	0	0	2	0	0	10	22	2	0	1	0	0	0	1	16	0	1	0	0	0	0	0	9	1	0	0	1	1	1	0	509	517,07
COL305B	1990	6	0	0	0	1	2	3	3	0	1	7	0	0	2	22	0	2	1	0	0	0	0	1	0	0	6	0	0	0	0	449	581,31
COL365B	2050	4	0	1	0	3	1	10	2	0	2	1	0	1	4	12	0	6	0	0	0	0	0	0	0	0	4	0	0	0	0	358	331,54
COL405B	2090	0	0	0	0	0	0	84	3	0	0	0	0	0	0	48	0	0	0	0	0	0	0	0	2	0	0	0	0	1	0	691	392,28
COL470B	2155	0	1	0	0	0	0	59	9	0	0	0	1	0	7	69	0	1	0	0	0	0	0	4	0	0	0	0	0	3	0	995	118,70
COL550B	2235	0	0	0	0	0	0	61	11	0	0	0	0	0	0	30	0	0	0	0	0	0	0	2	0	0	0	0	0	0	1	785	220,66
COL610B	2295	1	0	0	0	0	6	47	3	0	0	0	0	0	4	34	0	0	0	0	0	0	0	2	0	0	1	0	0	0	0	489	251,57
COL690B	2375	0	1	0	0	0	0	20	4	0	0	0	0	0	0	27	6	0	0	3	4	0	0	0	0	1	0	0	0	2	0	455	279,74
COL750B	2435	0	0	0	0	0	0	168	0	0	0	0	0	0	0	77	59	0	2	0	0	0	38	19	6	0	0	0	0	0	0	2310	143,73
COL825B	2510	0	0	0	0	0	0	33	5	0	0	0	0	0	0	26	12	0	0	4	3	0	0	12	0	0	0	0	0	1	0	518	131,65
COL865B	2550	1	0	0	0	1	0	8	6	0	0	1	0	0	7	10	0	2	4	0	0	0	0	3	0	0	1	0	0	0	0	375	563,53
COL945B	2630	0	0	0	0	0	1	6	6	0	0	0	0	0	3	8	0	10	3	0	0	0	0	1	0	0	0	0	0	0	0	418	569,70
COL1065B	2750	2	0	3	0	2	0	7	5	0	1	0	0	0	1	19	0	4	0	0	0	0	0	2	0	0	2	1	0	0	0	433	547,95
COL1145B	2830	0	0	0	0	0	2	5	3	0	4	0	1	0	5	20	0	3	0	0	0	0	0	1	0	0	0	0	0	1	0	583	721,48
COL1265B	2950	0	0	0	0	0	0	7	2	0	0	0	1	0	3	18	0	3	0	0	0	0	0	0	0	0	0	0	0	0	0	331	372,23
COL1385B	3070	0	0	0	0	0	1	0	1	0	0	1	0	0	7	32	0	2	1	0	0	0	0	0	1	0	0	0	0	0	0	495	561,76
COL1485B	3170	0	0	2	0	2	0	0	1	0	0	0	0	0	5	16	0	10	0	0	0	0	0	0	0	0	0	0	0	0	0	377	459,73

Appendix 2.1. Census data of benthic foramifera in the ≥450 μm size fraction.

SAMPLES	THICKNESS (cm)	*Ammodiscus cretaceus*	*Ammodiscus glabratus*	*Ammodiscus peruvianus*	*Ammodiscus tenuissimus*	*Ammosphaeroidina pseudopauciloculata*	*Clavulina parisiensis* auct.	*?Cribrostomoides trinitatensis*	*Haplophragmoides horridus*	*Haplophragmoides c* oarsely agglutinated	*Haplophragmoides* spp.	*?Haplophragmoides*	*Karrierella subglabra*	*Lituotuba lituiformis*	*Marsonella traubi*	*Paratrochamminoides* spp.	*Plectina dalmatina*	*Plectina* sp. coarsely agglutinated	*?Plectina* colapsed	*Recurvoides anormis*	*Recurvoides* spp.	*Reophax* sp.	*Reticulophragmium acutidorsatum*	*?Textularia*	*Trifaxia szaboi*	*Tritaxilina pupa*	*Tritaxilina* sp.
COL1000	1000	0	0	0	0	0	0	0	1	0	0	0	0	1	3	0	19	0	0	0	0	0	0	0	2	1	0
COL40A	1080	0	1	1	0	0	0	1	1	0	0	0	0	0	3	0	30	0	0	0	0	0	0	0	2	0	0
COL80A	1120	0	0	0	0	0	0	0	0	0	0	1	0	0	2	1	27	0	0	0	0	0	0	1	3	0	0
COL160A	1200	1	0	0	0	0	0	1	0	0	0	0	0	0	1	1	24	0	0	0	0	0	0	0	4	0	0
COL240A	1280	1	0	0	0	1	0	0	0	0	0	0	1	0	0	0	9	0	0	0	0	0	0	0	5	0	0
COL280A	1320	0	0	0	0	0	0	0	0	0	0	0	0	0	1	1	4	0	0	1	0	0	0	0	15	0	0
COL320A	1360	0	0	1	0	0	0	0	0	0	0	0	0	0	0	0	10	0	0	0	0	0	0	0	14	0	0
COL360A	1400	0	0	0	0	0	0	0	0	0	0	0	0	0	0	0	5	0	0	0	1	0	0	0	3	0	0
COL400A	1440	0	0	0	0	0	0	0	0	0	0	0	0	0	3	0	20	0	0	0	0	0	0	0	3	0	0
COL440A	1480	0	0	0	0	0	0	0	0	0	0	0	0	0	0	1	7	1	0	0	0	0	0	0	48	0	0
COL480A	1520	0	1	0	0	0	0	0	0	0	0	0	0	0	5	0	21	0	0	1	0	0	0	0	30	0	0
COL520A	1560	0	0	0	0	0	0	0	0	0	0	0	0	0	1	1	11	1	0	0	1	0	0	0	45	0	0
COL560A	1600	0	0	0	0	0	0	0	0	0	0	0	0	0	0	0	16	2	0	0	0	0	0	0	37	0	0
COL600A	1640	0	0	0	0	0	0	0	0	0	0	0	0	0	0	1	1	0	0	0	0	0	0	0	8	0	0
COL620A	1660	0	0	0	0	0	0	0	0	0	0	0	0	0	0	0	2	0	0	0	0	0	0	0	0	0	0
COL640A	1680	0	0	0	0	0	0	0	0	0	0	0	0	0	1	0	1	0	0	0	1	0	0	0	3	0	0
COL10B	1695	0	0	0	0	0	0	0	0	0	0	0	0	0	1	0	1	0	0	0	0	0	0	0	0	0	0
COL40B	1725	0	0	0	0	0	0	0	0	0	0	0	0	0	0	0	0	0	0	0	0	0	1	0	0	1	0
COL113B	1798	0	0	0	0	0	0	0	0	0	0	0	0	0	6	0	9	0	0	0	0	0	0	0	0	0	0
COL140B	1825	0	0	0	0	0	0	0	0	0	0	0	0	0	0	0	0	0	0	0	1	0	0	0	0	0	0
COL180B	1865	0	0	0	0	0	0	0	0	0	0	0	0	0	0	0	2	0	0	0	0	0	0	0	0	0	0
COL245B	1930	0	0	1	0	0	0	0	0	0	1	0	0	0	0	0	43	0	0	0	0	0	1	0	1	1	1
COL305B	1990	0	0	0	0	0	0	0	0	0	1	0	0	0	4	0	52	0	0	0	0	0	0	0	0	2	0
COL365B	2050	1	1	0	0	0	0	0	1	3	1	0	0	0	2	0	46	0	0	0	0	0	0	0	0	2	0
COL405B	2090	0	0	0	0	0	0	0	0	0	0	0	0	0	0	0	2	0	0	0	0	0	0	0	0	0	0
COL470B	2155	0	0	0	0	0	0	0	0	0	0	0	0	0	0	0	3	4	0	0	0	0	0	0	0	0	0
COL550B	2235	0	0	0	0	0	0	0	0	0	0	0	0	0	0	0	2	0	0	0	0	0	0	0	0	0	0
COL610B	2295	0	0	0	0	0	0	0	0	0	0	0	0	0	6	0	35	0	0	0	0	0	0	0	0	4	0
COL690B	2375	0	0	0	0	0	0	0	0	0	0	0	0	0	0	0	1	0	0	0	0	0	1	0	0	0	0
COL750B	2435	0	0	0	0	0	0	0	0	0	0	0	0	0	0	0	0	0	0	0	1	0	0	0	0	0	0
COL825B	2510	0	0	0	0	0	0	0	0	0	0	0	0	0	0	0	0	0	0	0	0	0	0	0	0	1	0
COL865B	2550	1	0	0	0	0	0	0	0	0	0	0	0	0	3	1	97	0	0	1	0	0	0	0	0	0	0
COL945B	2630	0	0	0	0	0	0	0	0	0	0	0	0	0	7	0	44	0	0	0	0	0	0	0	0	1	0
COL1065B	2750	1	1	0	0	0	0	0	0	0	1	0	0	0	2	0	63	0	0	0	0	0	0	0	0	4	0
COL1145B	2830	0	0	0	1	0	0	0	0	1	0	0	0	0	2	0	60	0	0	0	3	0	0	0	2	4	0
COL1265B	2950	0	0	0	0	0	1	0	0	0	0	0	0	0	0	0	20	0	1	1	1	0	0	0	0	2	0
COL1385B	3070	3	3	3	2	0	0	0	0	5	0	0	0	0	0	1	16	0	0	0	0	0	0	0	0	3	0
COL1485B	3170	0	2	0	0	0	1	0	0	0	0	0	0	0	10	0	27	0	1	1	0	0	0	0	0	8	0

Appendix 2.1. Census data of benthic foramifera in the ≥450 μm size fraction.

SAMPLES	THICKNESS (cm)	*?Trochammina* sp. (sensu Grünig, 1985)	*Trochammina* sp.	*?Trochammina*	*Trochamminoides subcoronatus*	*Trochamminoides* spp.	*Vulvulina haeringensis-eocaena* group	Indeterminate agglutinants	Astrorhizida	*Anomalinoides capitatus*	*Baggina* cf. *marielina*	*Cibicidoides barnetti*	*Cibicidoides eoceanus*	*Cibicidoides grimsdalei*	*Cibicidoides havanensis*	*Cibicidoides ungerianus*	*Cibicidoides* spp.	*Chilostomella* sp.	Dentalinid	*Gyroidinoides soldanii*	*Hanzawaia ammophila*	*Lenticulina granulata*	smooth *Lenticulina* spp.	*Marginulinopsis fragaria*	*Marginulinopsis* sp.	*Nodosarella* spp.	*Nodosaria-Chrysalogonium* group
COL1000	1000	0	0	1	0	3	0	0	2	1	0	0	12	0	0	0	1	0	0	0	0	0	8	0	0	0	0
COL40A	1080	1	0	0	0	0	0	0	1	6	0	0	24	0	0	0	0	0	0	0	0	0	6	6	0	0	0
COL80A	1120	0	0	0	0	1	0	0	0	1	0	0	10	0	0	0	0	0	0	0	0	0	5	1	0	0	0
COL160A	1200	0	0	0	0	0	0	0	1	1	0	0	13	0	0	0	0	0	0	0	0	1	13	0	0	0	0
COL240A	1280	0	0	0	1	0	0	0	1	2	0	1	14	0	1	0	0	0	0	0	0	1	2	0	0	1	0
COL280A	1320	0	0	0	0	0	0	0	0	4	0	0	11	0	0	0	0	0	0	0	0	0	2	1	0	0	0
COL320A	1360	0	0	0	0	0	0	0	0	5	0	0	6	0	0	0	0	0	0	0	0	0	4	1	0	0	1
COL360A	1400	0	0	0	0	0	0	0	0	2	0	0	9	0	0	0	0	0	0	0	0	1	1	0	0	2	0
COL400A	1440	0	0	0	0	1	0	0	0	1	0	0	5	0	0	0	0	0	0	0	0	0	4	2	0	0	1
COL440A	1480	0	0	0	0	0	0	0	0	1	0	0	7	0	0	0	0	0	1	0	0	0	4	3	0	0	1
COL480A	1520	0	0	0	0	0	0	0	0	2	0	1	36	0	0	0	0	0	1	0	0	3	6	2	0	1	1
COL520A	1560	0	0	0	0	2	0	0	0	4	0	0	6	0	0	0	0	0	0	0	0	0	5	1	0	0	0
COL560A	1600	0	0	0	0	1	0	0	2	2	0	0	11	0	0	0	0	0	0	0	0	0	2	0	0	1	1
COL600A	1640	0	0	0	0	0	0	0	3	0	0	0	1	0	0	0	0	0	0	0	0	0	0	0	0	0	0
COL620A	1660	0	0	0	0	1	0	0	3	0	0	0	0	0	0	0	0	0	0	0	0	0	2	0	0	0	0
COL640A	1680	0	0	0	0	0	0	1	0	1	0	1	7	0	0	0	0	0	0	0	0	0	0	0	0	0	0
COL10B	1695	0	0	0	0	0	0	0	0	0	0	0	0	0	0	0	0	0	0	0	0	0	8	0	0	0	0
COL40B	1725	0	0	0	0	0	0	0	0	0	0	0	0	0	0	0	0	0	0	0	0	0	4	0	0	0	0
COL113B	1798	0	0	0	0	0	0	0	0	1	0	0	0	0	0	0	0	0	0	0	1	1	18	1	0	0	0
COL140B	1825	0	0	0	0	0	0	0	1	0	0	0	0	0	0	0	0	1	0	0	0	3	24	0	0	0	0
COL180B	1865	0	0	0	0	0	0	0	0	0	0	0	0	0	0	0	0	1	0	0	1	0	11	0	0	0	0
COL245B	1930	0	0	0	0	0	0	0	4	0	0	0	0	0	0	0	0	2	3	0	14	1	13	1	1	0	2
COL305B	1990	0	0	0	0	0	0	0	0	4	0	0	13	0	0	1	1	0	0	0	1	1	15	0	0	0	1
COL365B	2050	2	0	0	0	0	0	0	1	6	0	0	4	0	0	2	0	0	1	0	1	0	12	0	0	0	2
COL405B	2090	0	0	0	0	0	0	0	0	0	0	0	0	0	0	0	0	0	0	0	3	0	2	0	0	0	0
COL470B	2155	0	0	0	0	0	0	0	6	0	0	0	0	0	0	0	0	0	0	0	3	0	7	0	0	0	0
COL550B	2235	0	0	0	0	0	0	0	0	0	10	0	0	0	0	0	0	0	0	0	3	1	16	0	0	0	2
COL610B	2295	0	0	0	0	0	0	0	0	12	1	0	16	0	0	0	0	0	0	0	2	0	11	0	2	0	1
COL690B	2375	0	0	0	0	0	1	0	0	0	0	0	0	0	0	0	0	0	0	0	0	0	6	0	0	0	0
COL750B	2435	0	0	0	0	0	0	0	0	0	0	0	0	0	0	0	0	0	0	0	0	0	2	0	0	0	0
COL825B	2510	0	0	0	0	0	0	0	0	0	0	0	0	0	0	0	0	0	0	0	3	1	11	1	0	0	0
COL865B	2550	0	0	0	0	1	0	0	3	18	0	0	3	2	0	0	0	0	0	1	4	1	3	0	0	0	0
COL945B	2630	0	0	0	0	0	0	0	5	4	0	0	5	4	0	0	0	0	0	1	0	1	8	1	0	0	1
COL1065B	2750	0	1	0	0	0	0	0	10	3	0	0	0	2	0	0	0	0	0	0	1	0	16	1	4	0	0
COL1145B	2830	0	0	0	0	1	0	0	7	2	0	0	2	3	0	1	0	0	0	0	1	0	16	0	0	0	0
COL1265B	2950	0	0	0	0	0	1	0	12	2	0	0	6	3	0	0	0	0	0	0	0	0	10	1	0	0	0
COL1385B	3070	0	1	0	0	0	0	0	7	1	0	0	5	11	0	0	0	0	0	0	0	0	30	2	5	1	4
COL1485B	3170	0	0	0	0	1	0	0	7	8	0	0	7	5	1	0	0	0	0	1	2	0	14	3	0	0	3

Appendix 2.1. Census data of benthic foramifera in the ≥450 µm size fraction.

SAMPLES	THICKNESS (cm)	*Nonionella* spp.	*Oridorsalis umbonatus*	*Osangularia pteromphalia-mexicana group*	*Parafrondicularia* spp.	Polymorphinids	*Planularia* sp.	*Planulina* spp.	*Pleurostomella* spp.	*Pullenia quinqueloba*	*Pullenia* sp.	*Saracenaria* spp.	Stilostomellids	*Uvigerina* big costae spp.	*?Vaginulina* sp.	*Valvulineria filiaeprincipis*	*Valvulineria* sp.	Total	N/g > 450 um
COL1000	1000	0	0	1	0	0	0	0	0	0	0	0	1	0	0	0	0	57	0,5722892
COL40A	1080	0	0	0	0	0	0	0	0	0	0	0	0	0	0	0	0	83	0,8081792
COL80A	1120	0	0	1	0	0	0	0	1	0	0	0	0	0	0	0	0	55	0,5533199
COL160A	1200	0	0	0	0	0	0	0	0	0	0	0	0	0	0	0	0	61	0,6143001
COL240A	1280	0	0	0	0	0	0	0	0	0	0	0	0	0	0	0	0	41	0,4133065
COL280A	1320	0	0	0	0	0	0	0	0	0	0	0	0	0	0	1	0	41	0,4120603
COL320A	1360	0	0	0	0	0	0	0	0	0	0	0	0	0	0	0	0	42	0,4154303
COL360A	1400	0	0	0	0	0	0	0	0	0	0	0	0	0	0	0	0	24	0,2409639
COL400A	1440	0	0	0	0	0	0	0	0	0	0	0	0	0	0	0	0	40	0,4555809
COL440A	1480	0	0	0	0	0	0	0	0	0	0	0	0	0	0	0	0	74	0,7377866
COL480A	1520	0	0	1	0	0	0	0	0	0	0	0	0	0	0	0	0	112	1,1188811
COL520A	1560	0	0	0	0	1	0	0	0	0	0	0	0	0	0	0	0	79	0,8449198
COL560A	1600	0	0	0	0	0	0	0	0	0	0	0	0	0	0	0	0	75	0,753012
COL600A	1640	0	0	0	0	0	0	0	0	0	0	0	0	0	0	0	0	14	0,1787995
COL620A	1660	0	0	0	0	0	0	0	0	0	0	0	0	0	0	0	0	8	0,0812183
COL640A	1680	0	0	0	0	0	0	0	0	1	0	0	0	0	0	1	0	18	0,4090909
COL10B	1695	0	0	0	0	0	0	0	0	0	0	0	0	0	0	0	0	10	0,1204819
COL40B	1725	0	0	0	0	0	0	1	0	0	0	0	0	1	0	0	0	8	0,0878156
COL113B	1798	0	1	0	0	0	0	0	0	0	0	0	0	0	0	0	0	38	0,4046858
COL140B	1825	0	0	0	0	0	0	0	0	0	0	0	0	0	0	1	0	31	0,3128153
COL180B	1865	0	0	0	0	0	0	0	0	0	0	0	0	0	0	0	0	15	0,1628664
COL245B	1930	0	0	0	0	0	0	0	0	0	0	0	0	66	0	0	0	156	2,9175238
COL305B	1990	0	0	0	0	0	0	0	0	0	0	0	0	0	0	0	0	96	1,0480349
COL365B	2050	0	0	1	1	0	0	0	0	0	0	1	0	0	0	1	0	92	1,5081967
COL405B	2090	0	0	0	0	0	0	0	0	0	0	0	0	0	0	1	0	8	0,1882353
COL470B	2155	0	0	0	0	0	0	0	0	0	0	0	0	0	0	0	0	23	0,2327935
COL550B	2235	0	0	0	0	0	0	0	0	0	0	0	0	0	0	0	0	34	0,3894616
COL610B	2295	0	0	0	0	0	0	0	0	0	0	0	0	0	0	0	0	90	0,9164969
COL690B	2375	1	0	0	0	0	0	0	0	0	0	0	0	14	0	0	0	24	0,2649007
COL750B	2435	0	0	0	0	0	0	0	0	0	0	0	0	11	0	0	0	14	0,1581921
COL825B	2510	0	0	0	0	0	0	0	0	0	0	0	0	15	0	0	0	32	0,3149606
COL865B	2550	0	0	0	0	0	0	0	0	0	0	0	0	2	0	0	0	141	1,8311688
COL945B	2630	0	0	0	0	0	1	0	0	0	2	1	0	0	0	2	0	88	1,006865
COL1065B	2750	0	0	0	0	0	0	0	1	0	0	0	0	0	0	0	0	111	1,2570781
COL1145B	2830	0	0	0	0	0	0	0	0	0	0	0	0	0	0	0	1	107	1,0985626
COL1265B	2950	0	0	0	0	0	0	0	0	0	0	0	0	0	1	0	0	62	0,6231454
COL1385B	3070	0	0	0	0	0	0	0	0	0	0	0	0	0	0	0	0	103	1,0320641
COL1485B	3170	0	1	0	0	0	0	0	0	0	0	0	0	0	0	0	0	103	1,078534

Appendix 3. Site 1263 geochemical, fine fraction and foraminiferal accumulation rates data.

Leg	Site	H	Core	Sc	Top	Bot	mcd	mbsf	S_ID	BFAR	CFAR	FFAR	TEX_{86}	cren/gr	BIT	CaCO3-bulk δ13C	CaCO3-bulk δ18O	*Acarinina* δ13C	*Acarinina* δ18O	*Globigerinatheka* δ13C	*Globigerinatheka* δ18O	*Nuttallides truempyi* δ13C	*Nuttallides truempyi* δ18O
208	1263	B	8	1	76	78	131,6	113,26	4438709							2,36	0,34						
208	1263	B	8	1	97	99	131,81	113,47	4438710									3,16	0,28			1,24	0,39
208	1263	B	8	1	116	118	132	113,66	4438711							2,51	0,50						
208	1263	B	8	1	118	120	132,02	113,68	4794865														
208	1263	B	8	1	136	138	132,2	113,86	4438712	130,2322	0,012117	122,4287						3,10	0,45			1,08	0,68
208	1263	B	8	2	7	9	132,41	114,07	4438724					5120,434	0,605116	2,44	1,00						
208	1263	B	8	2	9	11	132,43	114,09	4794866														
208	1263	B	8	2	26	28	132,6	114,26	4438725	116,1547	0,013591	137,3212						3,17	0,42			1,10	0,50
208	1263	B	8	2	46	48	132,8	114,46	4438726					9592,359	0,301272	2,45	0,78						
208	1263	B	8	2	48	50	132,82	114,48	4794867														
208	1263	B	8	2	67	69	133,01	114,67	4438727	111,0884	0,011317	114,3421						3,11	0,38			1,13	0,59
208	1263	B	8	2	86	88	133,2	114,86	4438728														
208	1263	B	8	2	88	90	133,22	114,88	4794868							2,50	1,06						
208	1263	B	8	2	106	108	133,4	115,06	4438729	171,316	0,016226	163,9508						3,16	0,20			1,12	0,54
208	1263	B	8	2	127	129	133,61	115,27	4438730				0,723631	63976,59	0,521888	2,40	0,88						
208	1263	B	8	2	146	148	133,8	115,46	4438731	171,1245	0,017722	179,0617						3,25	0,32			0,84	0,20
208	1263	B	8	3	16	18	134	115,66	4438747							2,38	0,49						
208	1263	B	8	3	18	20	134,02	115,68	4794869														
208	1263	B	8	3	37	39	134,21	115,87	4438748	88,95519	0,012957	130,9175						3,49	0,38			1,28	0,58
208	1263	B	8	3	56	58	134,4	116,06	4438749				0,738546	26587,67	0,414372	2,62	0,99						
208	1263	B	8	3	58	60	134,42	116,08	4794870														
208	1263	B	8	3	76	78	134,6	116,26	4438750	198,4652	0,017082	172,5926						3,10	0,34			1,21	0,55
208	1263	B	8	3	97	99	134,81	116,47	4438751							2,58	0,78						
208	1263	B	8	3	99	102	134,83	116,49	4794871														
208	1263	B	8	3	116	118	135	116,66	4438752	134,6765	0,01949	196,9231						2,97	0,24			1,32	0,51
208	1263	B	8	3	136	138	135,2	116,86	4438753							2,53	0,81						
208	1263	B	8	3	138	140	135,22	116,88	4794918														
208	1263	B	8	4	7	9	135,41	117,07	4438754	108,7894	0,01235	124,7832						2,96	0,31			1,33	0,52

Appendix 3. Site 1263 geochemical, fine fraction and foraminiferal accumulation rates data.

Leg	Site	H	Core	Sc	Top	Bot	mcd	mbsf	S_ID	BFAR	CFAR	FFAR	TEX_{86}	cren/gr	BIT	CaCO3-bulk δ13C	CaCO3-bulk δ18O	*Acarinina* δ13C	*Acarinina* δ18O	*Globigerinatheka* δ13C	*Globigerinatheka* δ18O	*Nuttallides truempyi* δ13C	*Nuttallides truempyi* δ18O
208	1263	B	8	4	26	28	135,6	117,26	4438755							2,44	0,47						
208	1263	B	8	4	28	30	135,62	117,28	4794872														
208	1263	B	8	4	46	48	135,8	117,46	4438756	167,1226	0,022499	227,3335						2,75	-0,07			1,09	0,19
208	1263	B	8	4	67	69	136,01	117,67	4438757														
208	1263	B	8	4	69	71	136,03	117,69	4794873														
208	1263	B	8	4	86	88	136,2	117,86	4438758	121,8583	0,023291	235,3278						3,27	0,16			0,90	0,58
208	1263	B	8	4	106	108	136,4	118,06	4438759														
208	1263	B	8	4	108	110	136,42	118,08	4794874														
208	1263	B	8	4	127	129	136,61	118,27	4438760	109,8459	0,023169	234,1023						3,21	0,29	2,74	0,149351	1,21	0,40
208	1263	B	8	4	146	148	136,8	118,46	4438761							2,46	0,45						
208	1263	B	8	5	0	3,5	136,84	118,5	4794875					11197,35	0,785641	2,66	0,33						
208	1263	B	8	5	16	18	137	118,66	4438762	109,2617	0,022446	226,7944						3,17	0,14	2,75	0,104543	1,11	0,20
208	1263	B	8	5	37	39	137,21	118,87	4438763							2,44	0,59						
208	1263	B	8	5	39	42,5	137,23	118,89	4794876				0,847537	7939,853	0,373998								
208	1263	B	8	5	56	58	137,4	119,06	4438764	149,8814	0,024386	246,3969						3,34	0,15	2,71	0,531003	1,31	0,26
208	1263	B	8	5	76	78	137,6	119,26	4438765							2,36	0,25						
208	1263	B	8	5	78	83	137,62	119,28	4794879				0,801394	7845,73	0,457079	2,32	0,12						
208	1263	B	8	5	97	99	137,81	119,47	4438766	82,03979	0,020424	206,3606						3,26	0,01	2,82	0,536059	0,88	0,15
208	1263	B	8	5	116	118	138	119,66	4438767							2,22	0,02						
208	1263	B	8	5	118	121,5	138,02	119,68	4794880				0,847352	9995,457	0,909184	2,18	-0,14						
208	1263	B	8	5	136	138	138,2	119,86	4438768	148,942	0,019627	198,3102			0,431057			3,21	0,31	2,81	0,422209	0,83	-0,25
208	1263	B	8	5	138	143	138,22	119,88	4794881				0,831471	26672,29		2,11	-0,26						
208	1263	B	8	6	6	8	138,4	120,06	4438769				0,893254	17438,8	0,636516	2,07	-0,39						
208	1263	B	8	6	9	11,5	138,43	120,09	4794882														
208	1263	B	8	6	26	28	138,6	120,26	4438770	81,94204	0,011652	117,7289				2,09		3,04	0,13	2,90	-0,22132	0,98	-0,05
208	1263	B	8	6	28	32	138,62	120,28	4794883				0,874793	18426,99	0,561138		-0,31						
208	1263	B	8	6	46	48	138,8	120,46	4438771							2,27	0,03						

Appendix 3. Site 1263 geochemical, fine fraction and foraminiferal accumulation rates data.

Leg	Site	H	Core	Sc	Top	Bot	mcd	mbsf	S_ID	BFAR	CFAR	FFAR	TEX_{86}	cren/gr	BIT	CaCO3-bulk δ13C	CaCO3-bulk δ18O	*Acarinina* δ13C	*Acarinina* δ18O	*Globigerinatheka* δ13C	*Globigerinatheka* δ18O	*Nuttallides truempyi* δ13C	*Nuttallides truempyi* δ18O
208	1263	A	14	7	14	16	141,78	124,03	4438804	264,8566	0,03253	328,6866						2,83	-0,21	2,35	0,070893	0,662	0,778
208	1263	B	9	1	5	7	142	122,05	4438780				0,825	5141,5	0,782167	2,18	0,46						
208	1263	B	9	1	7	9	142,02	122,07	4794903														
208	1263	B	9	1	25	27	142,2	122,25	4438781	235,5768	0,040634	410,5634						3,01	0,14	2,55	0,494215	0,637	0,756
208	1263	B	9	1	45	47	142,4	122,45	4438782							2,04	0,55						
208	1263	B	9	1	47	50,5	142,42	122,47	4794904							2,00	0,54						
208	1263	B	9	1	65	67	142,6	122,65	4438783	165,8186	0,04308	435,2779						2,97	0,13	2,48	0,302256	0,478	0,781
208	1263	B	9	1	85	87	142,8	122,85	4438784							2,27	0,65						
208	1263	B	9	1	87	90,5	142,82	122,87	4794905					2004,687	0,689797	2,23	0,82						
208	1263	B	9	1	105	107	143	123,05	4438785	134,0483	0,025448	257,1289						2,87	0,35	2,52	0,522983	0,633	0,729
208	1263	B	9	1	125	127	143,2	123,25	4438786					5758,183	0,705263	2,16	0,61						
208	1263	B	9	1	127	129	143,22	123,27	4794906														
208	1263	B	9	1	145	147	143,4	123,45	4438787	216,51	0,031048	313,7092						2,77	0,11	2,28	0,229552	0,361	0,595
208	1263	B	9	2	15	17	143,6	123,65	4438788							2,11	0,60						
208	1263	B	9	2	17	20,5	143,62	123,67	4794907				0,814768	7522,065	0,670934	2,09	0,67						
208	1263	B	9	2	35	37	143,8	123,85	4438789	171,7388	0,0393	397,0847						3,09	0,10	2,77	0,31045	0,511	0,697
208	1263	B	9	2	55	57	144	124,05	4438790							2,30	0,84						
208	1263	B	9	2	57	60,5	144,02	124,07	4794908							2,23	0,93						
208	1263	B	9	2	75	77	144,2	124,25	4438791	105,7391	0,032158	324,9256						3,14	-0,09	2,38	0,376878	0,697	0,771
208	1263	B	9	2	95	97	144,4	124,45	4438792							2,18	0,63						
208	1263	B	9	2	97	100,5	144,42	124,47	4794909				0,807611			2,33	0,56						
208	1263	B	9	2	115	117	144,6	124,65	4438793	122,9022	0,030927	312,4901						2,82	0,03	2,49	0,435808	0,565	0,538
208	1263	B	9	2	135	137	144,8	124,85	4438794							2,45	0,58						
208	1263	B	9	2	137	139	144,82	124,87	4794910														
208	1263	B	9	3	5	7	145	125,05	4438795	55,70774	0,032011	323,4376						2,87	0,37	2,45	0,531875	0,792	0,633
208	1263	B	9	3	27	30,5	145,22	125,27	4794911				0,768945	9264,937	0,877252	2,19	0,61						
208	1263	B	9	3	67	70,5	145,62	125,67	4794912				0,804388	6397,652	0,597084	2,18	0,52						
208	1263	B	9	3	107	110,5	146,02	126,07	4794913				0,759626	8017,296	0	2,25	0,65						
208	1263	B	9	4	0	3,5	146,45	126,5	4794914				0,75937	7693,528	0,665734	2,15	0,53						
208	1263	B	9	4	40	43,5	146,85	126,9	4794915				0,764008	5974,766	0,479122	2,27	0,64						
208	1263	B	9	4	80	83,5	147,25	127,3	4794915					3952,682	0,491639	2,22	0,57						

Appendix 4. Census data of benthic foramifera in the ≥63 ≤500 µm size fraction.

Leg	Site	H	Core	Sc	Top	Bot	mcd	mbsf	S_ID	*?Ammodiscus?*	*Arenobulimina* sp.	*Dorothia* sp.	*Eggerella bradyi*	*Karrerierella chapapotensis*	*Karrerierella chilostoma*	*Karrerierella subglabra*	*Karrerierella* cf. *cubensis*	*Karrerierella* sp. deformed	*Karrerierella* spp.	*Plectina dalmatina*	*Spiroplectammina spectabilis*	*Subreophax sp.*	*Vulvulina haeringensis-eocaena group*	*Quinqueloculina* sp.	*Spiroloculina* sp.	*Abyssammina incisa*	*Alabamina weddelensis*
208	1263	B	8	1	136	138	132,2	113,86	4438712	0	0	0	4	0	0	0	4	0	0	0	0	0	0	0	1	0	23
208	1263	B	8	2	26	28	132,6	114,26	4438725	0	0	0	0	0	3	0	0	0	0	0	0	0	0	0	0	0	16
208	1263	B	8	2	67	69	133,01	114,67	4438727	0	0	0	2	2	1	0	0	0	0	0	0	0	0	0	0	0	67
208	1263	B	8	2	106	108	133,4	115,06	4438729	0	0	0	0	1	1	0	2	0	0	0	0	0	0	0	0	0	25
208	1263	B	8	2	146	148	133,8	115,46	4438731	0	0	0	0	0	3	0	0	0	0	0	0	0	0	0	0	0	51
208	1263	B	8	3	37	39	134,21	115,87	4438748	0	0	0	0	2	1	0	1	0	0	0	0	0	0	0	0	0	16
208	1263	B	8	3	76	78	134,6	116,26	4438750	0	0	0	0	1	0	0	0	0	0	0	0	0	0	0	0	0	122
208	1263	B	8	3	116	118	135	116,66	4438752	0	0	0	0	1	0	0	0	0	0	0	0	0	0	0	0	0	36
208	1263	B	8	4	7	9	135,41	117,07	4438754	0	0	0	3	1	1	0	0	0	0	0	0	0	0	0	0	0	10
208	1263	B	8	4	46	48	135,8	117,46	4438756	0	0	0	5	1	1	0	0	0	0	0	0	1	0	0	1	0	16
208	1263	B	8	4	86	88	136,2	117,86	4438758	0	0	0	1	1	1	0	0	0	0	0	0	0	0	0	0	0	12
208	1263	B	8	4	127	129	136,61	118,27	4438760	0	0	0	0	1	0	0	0	0	0	0	0	0	0	0	0	0	29
208	1263	B	8	5	16	18	137	118,66	4438762	0	0	0	1	0	0	0	0	0	0	0	0	0	0	0	1	0	44
208	1263	B	8	5	56	58	137,4	119,06	4438764	0	0	0	3	0	2	0	1	0	0	0	0	0	0	0	0	0	29
208	1263	B	8	5	97	99	137,81	119,47	4438766	0	0	0	1	1	1	0	0	0	0	0	0	0	0	0	1	0	15
208	1263	B	8	5	136	138	138,2	119,86	4438768	0	1	0	0	2	2	0	0	0	0	0	0	0	0	1	0	0	31
208	1263	B	8	6	26	28	138,6	120,26	4438770	0	0	0	3	3	0	0	0	0	2	0	0	0	0	0	1	0	11
208	1263	B	8	6	66	68	139	120,66	4438772	0	0	1	0	2	0	0	0	0	0	0	0	0	0	0	1	0	18
208	1263	B	8	6	106	108	139,4	121,06	4438774	0	0	0	0	0	0	0	0	0	0	0	0	0	0	0	0	0	9
208	1263	B	8	6	146	148	139,8	121,46	4438776	0	0	0	1	1	0	0	0	0	0	0	0	0	0	0	0	0	48
208	1263	B	8	7	36	38	140,2	121,86	4438778	0	0	0	1	0	2	0	0	0	0	0	0	0	0	0	1	0	26
208	1263	A	14	6	45	47	140,59	122,84	4438796	0	0	0	1	2	0	0	0	0	0	0	0	0	0	0	1	0	21
208	1263	A	14	6	85	87	140,99	123,24	4438798	0	0	0	4	6	1	0	0	0	0	0	0	0	0	0	0	0	18
208	1263	A	14	6	125	127	141,39	123,64	4438800	0	0	0	3	3	3	0	0	0	0	0	0	0	0	0	0	0	8
208	1263	A	14	7	14	16	141,78	124,03	4438804	0	0	0	0	1	2	0	0	0	0	0	0	0	0	0	0	0	10
208	1263	B	9	1	25	27	142,2	122,25	4438781	0	0	0	1	0	0	1	0	0	0	0	0	0	0	0	0	0	11
208	1263	B	9	1	65	67	142,6	122,65	4438783	0	0	0	0	3	1	1	0	0	0	0	0	0	0	0	0	0	15
208	1263	B	9	1	105	107	143	123,05	4438785	1	0	0	1	2	1	0	0	0	0	0	0	0	1	2	0	0	21
208	1263	B	9	1	145	147	143,4	123,45	4438787	0	0	0	0	0	1	0	0	0	0	0	0	0	0	0	0	0	43
208	1263	B	9	2	35	37	143,8	123,85	4438789	0	0	0	2	3	2	0	0	0	0	0	0	0	0	0	0	0	21
208	1263	B	9	2	75	77	144,2	124,25	4438791	0	0	0	1	3	0	0	0	0	1	0	0	0	0	0	1	0	15
208	1263	B	9	2	115	117	144,6	124,65	4438793	0	0	0	1	4	1	0	0	0	0	1	2	0	0	0	1	0	52
208	1263	B	9	3	5	7	145	125,05	4438795	0	0	0	0	2	1	0	0	1	0	0	1	0	2	0	0	1	14

Appendix 4. Census data of benthic foramifera in the ≥63 ≤500 µm size fraction.

Leg	Site	H	Core	Sc	Top	Bot	mcd	mbsf	S_ID	*Alabamina* sp.	*Angulogerina muralis*	*Anomalinoides capitatus*	*Anomalinoides glabratus*	*Anomalinoides semicribratus*	*Anomalinoides spissiformis*	*Anomalinoides* spp.	*Aragonia aragonensis*	*Astacolus* sp.	*Bolivinoides crenulata*	*Bolivinoides huneri*	*Bolivina malovensis*	*Bolivina* spp.	*Bulimina alazanensis*	*Bulimina* cf. *alazanensis*	*Bulimina glomarchallengeri*	*Bulimina impedens*	*Bulimina semicostata*	*Bulimina simplex*	*Bulimina stalacta*	*Bulimina thriedra*	*Bulimina tuxpamensis*
208	1263	B	8	1	136	138	132,2	113,86	4438712	0	0	0	2	0	2	0	0	1	0	59	0	0	2	0	3	4	0	0	0	0	0
208	1263	B	8	2	26	28	132,6	114,26	4438725	0	0	0	3	0	1	0	0	1	0	95	6	0	6	0	5	6	3	0	1	0	8
208	1263	B	8	2	67	69	133,01	114,67	4438727	1	0	0	11	0	5	1	0	3	0	41	0	0	12	0	1	8	5	0	0	0	10
208	1263	B	8	2	106	108	133,4	115,06	4438729	0	0	0	6	0	4	1	0	0	0	22	0	1	2	0	4	4	3	0	0	0	1
208	1263	B	8	2	146	148	133,8	115,46	4438731	1	0	0	8	0	2	2	0	0	0	31	0	0	4	0	1	7	2	0	0	0	4
208	1263	B	8	3	37	39	134,21	115,87	4438748	0	0	0	2	0	1	2	0	1	0	40	0	0	1	1	7	2	0	1	0	0	4
208	1263	B	8	3	76	78	134,6	116,26	4438750	0	0	0	3	0	1	0	0	0	0	9	0	0	0	0	0	3	2	0	0	0	5
208	1263	B	8	3	116	118	135	116,66	4438752	0	0	0	0	1	2	2	0	1	0	6	0	3	1	1	3	1	3	1	0	0	4
208	1263	B	8	4	7	9	135,41	117,07	4438754	0	0	0	3	0	6	1	0	0	0	101	9	1	0	0	1	1	2	0	2	0	0
208	1263	B	8	4	46	48	135,8	117,46	4438756	0	0	0	4	0	0	0	0	1	0	67	2	0	1	0	0	2	0	0	0	0	4
208	1263	B	8	4	86	88	136,2	117,86	4438758	0	0	0	0	0	1	0	0	2	0	47	2	0	0	0	2	6	1	0	0	0	5
208	1263	B	8	4	127	129	136,61	118,27	4438760	0	0	0	3	0	6	0	0	0	0	57	2	0	2	0	4	11	5	0	0	0	3
208	1263	B	8	5	16	18	137	118,66	4438762	0	0	0	1	0	4	0	1	2	0	53	2	0	11	0	3	6	4	1	0	0	7
208	1263	B	8	5	56	58	137,4	119,06	4438764	0	0	0	3	0	3	0	0	1	0	17	0	0	9	0	1	4	2	0	0	1	7
208	1263	B	8	5	97	99	137,81	119,47	4438766	0	0	0	3	0	6	2	4	1	0	55	1	0	6	0	1	5	5	1	0	0	16
208	1263	B	8	5	136	138	138,2	119,86	4438768	0	0	0	0	0	1	2	2	0	0	32	0	0	1	0	0	9	1	2	0	0	9
208	1263	B	8	6	26	28	138,6	120,26	4438770	0	0	0	8	0	3	2	4	0	0	37	0	1	3	0	1	9	2	0	0	0	9
208	1263	B	8	6	66	68	139	120,66	4438772	0	0	0	0	0	3	23	1	0	1	20	0	0	0	0	0	1	5	0	0	0	7
208	1263	B	8	6	106	108	139,4	121,06	4438774	0	0	0	1	0	1	0	1	0	0	95	1	0	0	0	1	0	0	0	0	0	6
208	1263	B	8	6	146	148	139,8	121,46	4438776	0	0	0	2	0	2	0	2	1	0	91	2	0	2	0	0	0	1	0	0	0	5
208	1263	B	8	7	36	38	140,2	121,86	4438778	0	0	0	0	0	6	0	1	0	0	47	0	0	0	0	1	1	0	0	0	0	5
208	1263	A	14	6	45	47	140,59	122,84	4438796	0	0	1	3	0	7	3	1	0	0	38	0	0	0	0	3	0	0	3	0	0	6
208	1263	A	14	6	85	87	140,99	123,24	4438798	0	0	0	6	0	3	5	0	1	0	40	1	0	1	0	1	2	1	3	0	0	17
208	1263	A	14	6	125	127	141,39	123,64	4438800	0	0	1	8	0	4	2	0	2	0	14	0	0	5	2	0	0	2	7	1	0	9
208	1263	A	14	7	14	16	141,78	124,03	4438804	1	0	0	3	0	4	0	0	0	0	31	0	0	5	1	2	0	0	2	0	0	10
208	1263	B	9	1	25	27	142,2	122,25	4438781	0	0	0	5	0	4	2	0	0	0	30	1	0	2	0	1	0	0	3	0	0	11
208	1263	B	9	1	65	67	142,6	122,65	4438783	0	0	0	6	0	7	1	0	1	0	41	1	0	3	0	1	4	0	1	0	0	4
208	1263	B	9	1	105	107	143	123,05	4438785	1	0	2	7	0	7	2	0	6	0	81	0	3	12	0	1	2	2	2	0	0	15
208	1263	B	9	1	145	147	143,4	123,45	4438787	0	0	0	7	0	2	1	1	0	0	64	1	0	6	0	2	2	1	1	0	0	5
208	1263	B	9	2	35	37	143,8	123,85	4438789	0	1	0	2	0	5	1	1	0	2	49	0	0	5	0	0	3	2	0	0	0	6
208	1263	B	9	2	75	77	144,2	124,25	4438791	0	0	0	0	0	4	2	2	0	0	121	0	0	5	0	2	1	3	0	0	0	15
208	1263	B	9	2	115	117	144,6	124,65	4438793	0	0	0	4	0	16	1	0	0	0	13	0	0	0	0	1	2	2	0	0	0	9
208	1263	B	9	3	5	7	145	125,05	4438795	0	0	0	6	0	7	1	0	0	0	13	1	0	0	0	2	4	0	0	0	0	1

Appendix 4. Census data of benthic foramifera in the ≥63 ≤500 µm size fraction.

Leg	Site	H	Core	Sc	Top	Bot	mcd	mbsf	S_ID	*Bulimina* cf. *elongata*	*Bulimina* spp.	*Buliminella grata-Buliminella beaumonti*	Undetermined buliminids	*Caucasina schischkinskye*	*Caucasina* sp.	*Cassidulina* sp.	*Cibicides* spp.	*Cibicidoides barnetti*	*Cibicidoides eocaenus*	*Cibicidoides grimsdalei*	*Cibicidoides havanensis*	*Cibicidoides lamontdohertyi*	*Cibicidoides perlucidus*	*Cibicidoides praemundulus*	*Cibicidoides praemundulus* juvenile	*Cibicidoides proprius*	*Cibicidoides ungerianus*
208	1263	B	8	1	136	138	132,2	113,86	4438712	10	2	2	0	0	13	0	0	0	0	0	0	33	0	0	0	0	1
208	1263	B	8	2	26	28	132,6	114,26	4438725	8	0	5	0	0	29	0	0	0	1	0	0	20	0	0	3	0	0
208	1263	B	8	2	67	69	133,01	114,67	4438727	21	2	8	0	0	13	0	0	0	0	0	0	44	0	0	0	0	0
208	1263	B	8	2	106	108	133,4	115,06	4438729	12	2	13	1	0	20	0	0	0	0	0	0	28	0	0	1	0	0
208	1263	B	8	2	146	148	133,8	115,46	4438731	8	0	7	1	0	11	0	0	0	0	0	0	11	0	0	1	0	0
208	1263	B	8	3	37	39	134,21	115,87	4438748	7	1	4	0	0	4	0	0	0	0	0	0	14	0	0	0	0	0
208	1263	B	8	3	76	78	134,6	116,26	4438750	4	0	15	0	0	13	0	0	0	0	0	0	28	0	0	0	0	0
208	1263	B	8	3	116	118	135	116,66	4438752	6	0	1	0	0	5	0	1	0	0	1	0	20	0	1	0	2	0
208	1263	B	8	4	7	9	135,41	117,07	4438754	6	1	3	1	0	7	0	1	0	0	0	0	12	0	0	1	0	0
208	1263	B	8	4	46	48	135,8	117,46	4438756	10	0	5	0	0	22	0	0	0	0	0	0	23	0	0	0	0	0
208	1263	B	8	4	86	88	136,2	117,86	4438758	12	0	2	0	0	8	0	0	1	0	0	0	10	0	0	0	0	1
208	1263	B	8	4	127	129	136,61	118,27	4438760	10	0	9	0	0	19	0	0	0	0	0	0	26	0	0	0	0	0
208	1263	B	8	5	16	18	137	118,66	4438762	6	0	4	0	0	15	0	0	0	0	0	0	9	0	0	0	0	0
208	1263	B	8	5	56	58	137,4	119,06	4438764	1	0	5	0	0	9	0	0	1	1	0	0	11	0	0	1	0	0
208	1263	B	8	5	97	99	137,81	119,47	4438766	14	0	0	0	0	15	0	0	0	1	0	0	11	0	0	0	0	0
208	1263	B	8	5	136	138	138,2	119,86	4438768	13	0	1	0	0	21	0	0	0	1	0	0	0	0	1	0	0	0
208	1263	B	8	6	26	28	138,6	120,26	4438770	13	0	1	0	0	10	0	0	1	0	0	0	4	0	0	1	0	0
208	1263	B	8	6	66	68	139	120,66	4438772	4	1	0	0	0	25	1	1	0	0	0	0	1	0	1	0	0	0
208	1263	B	8	6	106	108	139,4	121,06	4438774	15	0	1	0	0	20	0	0	1	0	0	0	22	0	0	0	0	0
208	1263	B	8	6	146	148	139,8	121,46	4438776	14	1	4	1	0	15	0	1	0	0	0	0	29	0	0	0	0	1
208	1263	B	8	7	36	38	140,2	121,86	4438778	16	1	5	0	0	13	0	0	1	1	0	0	34	0	0	0	0	0
208	1263	A	14	6	45	47	140,59	122,84	4438796	17	2	3	0	0	7	0	0	1	0	0	0	10	0	0	1	0	1
208	1263	A	14	6	85	87	140,99	123,24	4438798	20	3	2	1	0	18	0	0	0	1	0	0	19	0	0	2	0	0
208	1263	A	14	6	125	127	141,39	123,64	4438800	12	0	6	0	0	8	0	0	0	0	0	0	9	0	0	0	0	0
208	1263	A	14	7	14	16	141,78	124,03	4438804	12	2	5	0	0	7	0	0	0	0	0	1	15	0	0	0	0	0
208	1263	B	9	1	25	27	142,2	122,25	4438781	3	0	3	0	0	4	0	0	0	1	0	0	22	0	3	0	0	0
208	1263	B	9	1	65	67	142,6	122,65	4438783	19	0	2	0	0	23	0	0	0	0	0	0	13	0	1	2	0	0
208	1263	B	9	1	105	107	143	123,05	4438785	31	0	6	0	1	25	0	0	2	1	2	0	7	0	0	3	0	1
208	1263	B	9	1	145	147	143,4	123,45	4438787	14	0	2	0	0	2	0	0	0	0	0	0	24	0	0	1	0	0
208	1263	B	9	2	35	37	143,8	123,85	4438789	8	0	4	0	0	2	2	0	0	0	1	0	16	0	0	0	0	0
208	1263	B	9	2	75	77	144,2	124,25	4438791	11	0	10	1	0	1	0	1	0	0	1	0	31	0	0	0	0	0
208	1263	B	9	2	115	117	144,6	124,65	4438793	33	0	7	0	5	5	0	0	0	2	2	0	14	0	0	0	0	0
208	1263	B	9	3	5	7	145	125,05	4438795	16	0	5	0	0	1	0	0	0	0	1	0	3	1	0	0	0	0

Appendix 4. Census data of benthic foramifera in the ≥63 ≤500 µm size fraction.

Leg	Site	H	Core	Sc	Top	Bot	mcd	mbsf	S_ID	*Globobulimina* spp.	*Globocassidulina crassa*	*Globocassidulina subglobosa*	*Gyroidinoides danvillensis*	*Gyroidinoides depresuss*	*Gyroidinoides gyrardanus*	*Gyroidinoides mediceus*	*Gyroidinoides planulatus*	*Gyroidinoides subangulatus*	*Gyroidinoides* spp.	*Hanzawaia ammophila*	*Hemirobulina* sp.	*Heronallenia pusilla*	*Heronallenia* sp.	*Laevidentalina* spp.	*Lagena* spp.	*Lenticulina* spp.	low trochospiral hyalineous
208	1263	B	8	1	136	138	132,2	113,86	4438712	2	0	29	0	1	0	19	2	3	0	0	0	3	1	4	1	0	0
208	1263	B	8	2	26	28	132,6	114,26	4438725	0	0	37	0	1	0	7	3	2	1	0	0	2	0	2	1	1	0
208	1263	B	8	2	67	69	133,01	114,67	4438727	1	0	83	0	4	0	18	8	2	1	0	0	1	8	3	2	3	0
208	1263	B	8	2	106	108	133,4	115,06	4438729	3	1	58	0	0	0	24	5	8	2	0	0	8	4	6	4	1	0
208	1263	B	8	2	146	148	133,8	115,46	4438731	3	3	48	0	1	0	20	6	7	1	0	0	4	1	2	2	1	0
208	1263	B	8	3	37	39	134,21	115,87	4438748	0	0	36	2	2	1	14	2	4	1	0	0	3	1	1	3	1	0
208	1263	B	8	3	76	78	134,6	116,26	4438750	0	0	65	1	2	0	28	8	4	1	0	0	9	2	1	2	1	0
208	1263	B	8	3	116	118	135	116,66	4438752	8	0	47	2	3	0	16	2	6	0	0	0	8	0	3	2	2	0
208	1263	B	8	4	7	9	135,41	117,07	4438754	0	0	40	0	0	0	10	0	3	0	0	0	3	0	0	1	0	0
208	1263	B	8	4	46	48	135,8	117,46	4438756	1	0	82	0	1	0	15	4	3	0	0	1	9	1	5	0	1	0
208	1263	B	8	4	86	88	136,2	117,86	4438758	3	0	24	0	1	1	8	0	1	0	0	0	3	0	5	2	0	0
208	1263	B	8	4	127	129	136,61	118,27	4438760	1	0	66	0	2	0	12	5	4	3	0	0	9	5	5	3	0	0
208	1263	B	8	5	16	18	137	118,66	4438762	2	0	20	0	3	1	19	3	4	0	0	0	9	1	7	4	3	0
208	1263	B	8	5	56	58	137,4	119,06	4438764	0	1	47	0	10	1	1	0	3	19	0	0	4	1	2	2	0	0
208	1263	B	8	5	97	99	137,81	119,47	4438766	3	0	70	0	1	0	11	8	6	1	0	0	6	0	9	0	7	0
208	1263	B	8	5	136	138	138,2	119,86	4438768	2	2	76	0	2	1	7	0	8	8	0	0	7	0	4	3	3	0
208	1263	B	8	6	26	28	138,6	120,26	4438770	0	0	45	1	0	0	3	7	4	1	0	0	8	1	1	4	0	0
208	1263	B	8	6	66	68	139	120,66	4438772	0	0	27	0	4	0	0	0	5	2	0	0	5	1	10	3	2	0
208	1263	B	8	6	106	108	139,4	121,06	4438774	0	0	4	0	2	0	3	1	3	1	0	0	4	1	1	3	3	0
208	1263	B	8	6	146	148	139,8	121,46	4438776	2	0	30	5	0	0	9	3	7	4	0	0	5	2	6	5	4	0
208	1263	B	8	7	36	38	140,2	121,86	4438778	5	1	36	2	4	2	5	0	4	7	0	0	7	0	6	8	1	0
208	1263	A	14	6	45	47	140,59	122,84	4438796	3	0	56	0	2	0	17	4	6	1	0	1	3	5	6	5	1	0
208	1263	A	14	6	85	87	140,99	123,24	4438798	1	0	57	1	1	0	23	4	5	0	0	0	16	2	8	3	1	0
208	1263	A	14	6	125	127	141,39	123,64	4438800	2	0	65	1	0	0	19	1	1	1	1	0	10	3	7	6	1	0
208	1263	A	14	7	14	16	141,78	124,03	4438804	2	0	47	0	0	0	13	1	1	0	0	0	4	1	0	1	0	0
208	1263	B	9	1	25	27	142,2	122,25	4438781	8	0	72	0	4	2	1	0	4	9	0	0	0	0	7	1	0	0
208	1263	B	9	1	65	67	142,6	122,65	4438783	0	0	26	0	1	3	7	0	1	0	0	0	5	1	3	2	0	0
208	1263	B	9	1	105	107	143	123,05	4438785	1	0	61	3	1	1	12	5	4	2	0	0	7	0	10	3	1	1
208	1263	B	9	1	145	147	143,4	123,45	4438787	2	0	55	0	2	1	12	5	1	3	0	0	8	2	3	6	3	0
208	1263	B	9	2	35	37	143,8	123,85	4438789	1	1	62	0	2	0	14	6	1	2	0	0	7	0	0	0	2	0
208	1263	B	9	2	75	77	144,2	124,25	4438791	6	0	52	1	6	1	8	0	2	9	0	0	3	1	3	2	0	0
208	1263	B	9	2	115	117	144,6	124,65	4438793	9	0	65	0	4	0	23	8	1	3	0	0	14	4	9	1	0	0
208	1263	B	9	3	5	7	145	125,05	4438795	3	1	31	1	4	0	0	0	0	8	0	0	3	0	3	0	2	0

Appendix 4. Census data of benthic foramifera in the ≥63 ≤500 µm size fraction.

Leg	Site	H	Core	Sc	Top	Bot	mcd	mbsf	S_ID	*Neoconorbina* sp.	*Nodosarella* spp.	*Nodosaria* spp.	*Nonion havanense*	*Nonion* spp.	*Nonionella longicamerata*	*Nonionella robusta*	*Nonionella* spp.	*Nuttallides truempyi*	*Nuttallides umbonifera*	*Oridorsalis plummerae*	*Oridorsalis umbonatus*	*Oridorsalis* spp.	*Ortomorphina* spp.	*Osangularia* cf. *plummerae*	*Paleopolymorphina* sp.	*Pleurostomella* spp.	Polymorphinids
208	1263	B	8	1	136	138	132,2	113,86	4438712	0	0	0	0	0	0	1	0	70	48	2	12	1	0	0	1	5	1
208	1263	B	8	2	26	28	132,6	114,26	4438725	0	0	0	1	0	0	0	0	62	50	6	16	1	0	0	0	7	2
208	1263	B	8	2	67	69	133,01	114,67	4438727	1	1	1	4	0	1	1	1	108	108	2	11	0	2	0	0	11	4
208	1263	B	8	2	106	108	133,4	115,06	4438729	0	0	0	2	1	0	1	2	105	94	1	4	1	0	0	0	18	5
208	1263	B	8	2	146	148	133,8	115,46	4438731	0	0	0	3	0	0	0	0	68	51	1	3	1	1	0	1	9	2
208	1263	B	8	3	37	39	134,21	115,87	4438748	1	0	0	1	0	0	2	0	57	60	1	3	2	2	1	0	9	0
208	1263	B	8	3	76	78	134,6	116,26	4438750	0	2	0	0	0	0	2	0	209	41	3	9	0	0	0	0	8	2
208	1263	B	8	3	116	118	135	116,66	4438752	0	0	0	2	0	0	1	1	97	40	2	5	0	0	0	0	6	3
208	1263	B	8	4	7	9	135,41	117,07	4438754	0	1	0	4	0	0	1	0	54	34	1	2	0	0	0	0	5	2
208	1263	B	8	4	46	48	135,8	117,46	4438756	6	1	1	5	0	0	3	1	86	67	0	1	1	1	0	0	8	4
208	1263	B	8	4	86	88	136,2	117,86	4438758	4	1	0	9	0	0	1	0	82	74	1	2	0	1	1	0	3	2
208	1263	B	8	4	127	129	136,61	118,27	4438760	4	2	0	7	3	0	7	1	114	123	1	1	0	0	1	0	8	3
208	1263	B	8	5	16	18	137	118,66	4438762	2	1	1	3	0	0	1	1	117	118	0	4	0	1	1	0	16	2
208	1263	B	8	5	56	58	137,4	119,06	4438764	1	0	2	1	1	1	6	0	67	87	1	6	0	0	6	0	14	3
208	1263	B	8	5	97	99	137,81	119,47	4438766	7	1	0	4	0	0	12	0	89	101	2	13	0	1	0	0	15	4
208	1263	B	8	5	136	138	138,2	119,86	4438768	0	2	0	5	2	0	7	0	97	60	2	5	0	0	0	0	18	2
208	1263	B	8	6	26	28	138,6	120,26	4438770	5	1	1	6	1	0	4	1	81	43	1	6	0	2	0	0	15	0
208	1263	B	8	6	66	68	139	120,66	4438772	2	0	1	2	0	0	2	1	93	33	0	5	0	1	0	1	0	2
208	1263	B	8	6	106	108	139,4	121,06	4438774	5	0	0	9	0	0	4	0	76	43	0	4	0	2	1	0	3	1
208	1263	B	8	6	146	148	139,8	121,46	4438776	9	2	0	4	0	1	6	5	115	98	5	15	0	0	3	0	19	1
208	1263	B	8	7	36	38	140,2	121,86	4438778	1	1	0	6	0	0	11	0	117	62	5	2	0	0	0	0	8	1
208	1263	A	14	6	45	47	140,59	122,84	4438796	5	1	1	5	1	0	5	4	132	87	0	2	0	2	0	0	18	1
208	1263	A	14	6	85	87	140,99	123,24	4438798	4	0	0	6	0	0	13	2	141	136	4	8	0	5	0	0	15	1
208	1263	A	14	6	125	127	141,39	123,64	4438800	3	4	1	6	1	0	7	2	173	122	1	5	0	1	1	0	14	4
208	1263	A	14	7	14	16	141,78	124,03	4438804	0	0	0	3	0	0	6	0	91	67	1	4	0	3	0	0	9	2
208	1263	B	9	1	25	27	142,2	122,25	4438781	0	1	0	2	0	0	4	1	76	86	2	7	0	1	0	0	14	0
208	1263	B	9	1	65	67	142,6	122,65	4438783	0	2	0	5	0	0	6	1	65	35	0	7	0	1	0	0	7	1
208	1263	B	9	1	105	107	143	123,05	4438785	1	1	2	3	4	0	6	0	89	122	3	26	0	3	0	0	15	3
208	1263	B	9	1	145	147	143,4	123,45	4438787	0	3	0	12	1	0	14	1	118	57	0	3	0	1	6	0	16	4
208	1263	B	9	2	35	37	143,8	123,85	4438789	0	2	0	8	0	0	3	1	73	26	1	1	0	0	0	0	11	5
208	1263	B	9	2	75	77	144,2	124,25	4438791	0	2	0	4	0	0	2	1	102	30	4	9	1	5	0	0	12	2
208	1263	B	9	2	115	117	144,6	124,65	4438793	0	2	1	19	1	0	2	3	115	86	7	15	0	4	1	1	20	5
208	1263	B	9	3	5	7	145	125,05	4438795	0	2	0	5	0	4	5	1	90	15	7	12	0	4	0	0	16	2

Appendix 4. Census data of benthic foramifera in the ≥63 ≤500 μm size fraction.

Praeglobobulimina	*Pullenia eocaena*	*Pullenia quinqueloba*	*Pullenia salisburyi*	*Pullenia* sp.	*Pseudopolymorphina* sp.	*Pseudouvigerina semilabiata*	*?Pseudouvigerina* sp.	*Pyrulina extensa*	*Quadrimorphina profunda*	*Resigia westcotti*	*Reussella* sp.	*Saracenaria* spp.	*Seabrookia rugosa*	*Siphonodosaria* spp.	*?Sporobulimina eocaena?*	*Stetsonia minuta*	*Stilostomella* spp.	*Turrilina* sp.	unilocular hyalineous	uniserial hyalineous	*Uvigerina chirana*	*?Valvulineria?*	**TOTALE**	N/gr
0	0	0	0	0	0	0	0	0	0	0	0	1	9	1	0	7	0	0	1	0	0	0	458	134,6069
0	0	0	1	0	0	0	0	0	1	0	0	2	3	7	0	7	0	2	0	0	0	0	505	126,8203
0	0	0	0	0	1	0	0	1	0	1	0	1	10	27	2	21	1	2	3	0	0	0	789	116,37
0	0	0	0	0	0	0	2	0	0	0	0	4	8	22	0	17	2	0	0	0	0	0	686	179,46
0	0	0	1	0	0	0	0	0	1	0	0	0	10	6	0	18	2	0	1	0	0	0	523	179,26
0	0	1	0	0	1	0	0	0	0	0	0	0	5	10	0	5	1	0	1	0	0	0	403	94,46
0	0	0	0	0	0	0	0	0	0	0	0	2	5	28	4	5	3	2	0	0	0	0	751	197,24
0	0	0	0	0	0	0	0	0	1	0	0	0	4	17	0	1	4	3	0	0	0	0	525	141,08
0	0	0	0	0	1	0	0	0	0	0	0	3	10	3	0	0	1	0	0	0	0	0	404	113,96
0	0	0	0	0	1	1	0	0	7	3	0	0	20	12	0	2	1	1	3	0	0	0	618	175,07
0	0	0	1	0	0	0	0	0	7	2	0	1	8	11	0	14	1	4	0	0	0	0	472	127,65
0	0	0	0	0	2	1	0	2	2	4	0	4	14	12	0	22	2	0	0	0	0	0	762	109,17
0	0	1	1	0	4	0	0	1	3	3	0	10	10	35	0	3	4	3	1	0	1	0	727	108,59
0	0	0	0	0	0	1	0	0	2	0	0	4	6	8	0	3	2	0	0	1	0	0	494	163,64
0	1	1	0	0	0	5	0	0	2	1	0	3	5	18	0	6	0	0	0	0	1	0	713	89,57
0	0	0	2	0	1	1	2	0	2	0	0	6	2	1	0	2	3	4	1	0	0	0	559	162,62
0	0	0	0	0	1	1	0	0	1	0	0	2	5	6	0	2	2	1	2	1	0	0	442	81,44
0	0	0	0	0	0	1	0	0	5	0	0	5	4	24	0	5	5	0	0	0	0	0	404	140,64
0	0	0	0	0	1	0	0	0	0	0	0	1	4	14	0	8	7	0	0	0	0	0	411	134,98
0	0	0	1	0	0	0	0	0	2	4	0	1	2	18	0	6	3	2	0	0	0	0	669	219,34
0	0	0	2	0	1	0	2	0	3	4	0	7	1	5	0	9	2	0	0	0	1	0	562	161,26
0	0	0	1	0	1	0	0	0	3	0	0	3	6	11	0	5	1	2	0	0	0	0	602	188,71
0	0	0	1	2	0	0	0	0	4	1	0	2	4	20	1	5	2	2	1	0	0	1	753	231,47
0	0	0	3	0	1	0	0	1	3	0	0	0	15	28	0	4	2	0	2	0	0	0	759	208,66
0	0	0	0	0	0	0	0	0	0	0	0	1	4	15	1	2	1	1	0	0	0	0	531	289,18
0	0	0	0	1	0	1	1	1	1	1	0	3	0	16	0	5	1	5	0	0	0	0	542	234,13
0	0	0	0	2	1	0	1	0	1	0	0	1	2	12	3	3	0	1	4	0	0	0	426	164,80
0	0	0	1	0	0	0	0	0	0	1	0	0	3	13	3	15	0	0	2	0	0	0	800	133,22
0	1	0	2	0	0	0	0	0	5	9	0	3	2	24	0	17	13	0	2	0	0	0	701	223,78
1	2	0	0	0	0	0	0	1	5	3	0	0	1	21	0	0	1	2	2	0	0	0	489	170,68
0	0	0	0	0	0	0	4	0	7	5	0	1	1	19	0	4	6	1	1	0	0	0	630	105,09
0	0	0	2	0	2	1	15	0	13	3	1	4	4	11	0	6	4	1	0	0	0	0	746	122,14
0	0	1	4	0	0	0	1	0	3	2	0	2	0	23	0	0	1	1	0	0	0	0	396	57,58

Appendix 5. Alano section foraminiferal isotopic results.

Sample ID	Depth (cm)	δ13C *Acarinina*	δ18O *Acarinina*	δ13C *Subbotina*	δ18O *Subbotina*	δ13C *Planorotalites capdevilensis*	δ18O *Planorotalites capdevilensis*	δ13C *Nuttallides truempyi*	δ18O *Nuttallides truempyi*
COL1265 B	2950,00	1,32	-1,86	0,08	-1,15	0,93	-1,67	0,00	-0,55
COL865 B	2550,00	1,63	-2,98	0,56	-3,09	1,19	-3,19	0,24	-0,85
COL865 B	2550,00								-1,17
COL365 B	2050,00	0,78	-2,56	0,16	-2,26	0,59	-2,34	-0,09	-1,17
COL 40A	1080,00	1,34	-1,98	0,11	-1,22	1,06	-1,91	-0,05	-1,10
COL40A	1080,00	1,24	-1,33						
COL1385B	3070,00					0,91	-2,76		

Appendix 5. Monte Cagnero section foraminiferal isotopic results.

Sample ID	Depth (m)	δ13C *Nuttallides truempyi*	δ18O *Nuttallides truempyi*	δ13C *Planorotalites capdevilensis*	δ18O *Planorotalites capdevilensis*	δ13C *Planorotalites capdevilensis*	δ18O *Planorotalites capdevilensis*	δ13C *Subbotina*	δ18O *Subbotina*	δ13C *Acarinina*	δ18O *Acarinina*
CAG 61	61,00	1,06	-1,34	2,06	-1,89	2,16	-1,76	1,61	-2,59	2,13	-2,27
CAG 62	62,00							1,67	-1,64		
CAG 62	62,00	1,03	-1,12	1,99	-2,19	1,95	-1,66	1,61	-2,47	2,32	-3,79
CAG 62,55	62,55			1,98	-1,85	2,04	-1,84	1,66	-2,73	2,27	-2,39
CAG 62,55	62,55	0,97	-0,91								
CAG 63,00	63,00	0,86	-0,70	2,08	-1,80			1,65	-2,25	2,38	-2,44
CAG 63,00	63,00					2,07	-1,79			2,36	-2,22
CAG 65,40	65,40	1,10	-1,65	2,02	-1,96	2,10	-2,29	1,71	-2,41	2,34	-2,58
CAG 65,40	65,40					2,12	-1,81				

Appendix 5.1 Monte Cagnero section census of *Planorotalites capdevilensis* (≥ 63 μm size fraction)

CAMPIONE	Depth (m)	*Planorotalites capdevilensis*	N/g *Planorotalites capdevilensis*
CAG 61.00	61	126	157
CAG 61.20	61,2	121	31
CAG 61.60	61,6	338	160
CAG 62.00	62	392	137
CAG 62.40	62,4	175	217
CAG 62.55	62,55	442	550
CAG 63.00	63	507	316
CAG 63.40	63,4	20	5
CAG 63.55	63,55	8	25
CAG 64.00	64	174	191
CAG 65	65	376	119
CAG 65.20	65,2	111	113
CAG 65.40	65,4	542	879
CAG 66	66	7	2
CAG 67.00	67	331	213

Appendix 5.1 Alano section census of *Planorotalites capdevilensis* (≥ 63 µm size fraction)

S_ID	Depth (Cm)	*Planorotalites capdevilensis*	N/g *Planorotalites capdevilensis*
COL1000	1000	69	88,6747
COL40A	1080	112	139,591
COL80A	1120	90	115,8954
COL160A	1200	50	64,45116
COL240A	1280	37	23,87097
COL280A	1320	44	28,30151
COL320A	1360	15	9,495549
COL360A	1400	38	24,41767
COL400A	1440	34	49,5672
COL440A	1480	33	21,05683
COL480A	1520	56	71,60839
COL520A	1560	34	23,27273
COL560A	1600	27	17,3494
COL600A	1640	6	1,226054
COL620A	1660	11	1,786802
COL640A	1680	16	11,63636
COL10B	1695	1	0,385542
COL40B	1725	7	4,917673
COL113B	1798	126	171,7572
COL140B	1825	11	7,103935
COL180B	1865	3	2,084691
COL245B	1930	15	17,95399
COL305B	1990	167	233,3624
COL365B	2050	148	155,2787
COL405B	2090	6	4,517647
COL470B	2155	4	0,647773
COL550B	2235	2	0,733104
COL610B	2295	24	15,64155
COL690B	2375	6	4,238411
COL750B	2435	8	0,723164
COL825B	2510	8	2,519685
COL865B	2550	335	556,8831
COL945B	2630	135	197,7117
COL1065E	2750	289	418,9354
COL1145E	2830	287	377,1663
COL1265E	2950	473	598,8526
COL1385E	3070	256	328,3367
COL1485E	3170	152	203,7277